

STARS and NEBULA - New Generations of Hydroprocessing Catalysts for the Production of Ultra Low Sulfur Diesel

Sonja Eijsbouts, Frans Plantenga, Bob Leliveld, Yoshimasa Inoue* and Katsuhisa Fujita*

Akzo Nobel Catalysts B.V., Research Centre Amsterdam, P.O.Box 37650, 1030 BE Amsterdam, The Netherlands and

*Nippon Ketjen Co., Ltd., R&D Center, 17-4, Isoura-cho, Niihama, Ehime, Japan

Introduction

EU, Japan and US have decided to lower sulfur in diesel to the 10 – 15 ppm level in very near future. This means that refiners have to apply more and more severe hydroprocessing (more reactor volume, higher pressure and temperature), i.e. have to invest heavily in new hydrodesulfurization (HDS) capacity and start desulfurizing streams that were not treated before. To do this in the most efficient and economic way is a major challenge for the refiners, catalyst and process designers.

Type 2 Active Sites

The last few hundred ppm sulfur leftover after “normal” hydrotreating is present in much less reactive molecules: alkyl-substituted dibenzothiophenes. These molecules not only react slower but their reaction mechanism is also different, involving first a hydrogenation of the aromatic part of the molecule followed by a desulfurization step (rather than direct hydrogenolysis). This hydrogenation pathway has led to the development of a new generation of catalysts, whereby another type of active sites, Type 2, was maximized. Type 2 sites are generated by careful tuning of the metal-support interaction and are thought to be more effective for hydrogenation reactions. Two Type 2 catalysts, Ni-Mo KF848-STARS and Co-Mo KF757-STARS are commercially available.

Special Features of Type 2 Catalysts. The lower metal-support interaction leads to a different sulfidation behavior of the Type 2 catalysts. The sulfidation is complete at lower temperature (Figures 1 and 2) and proceeds through a different Mo intermediate (Mo^{5+}) (Figure 2) in Type 2 catalysts compared to conventional catalysts, containing typically a mixture of Type 1 and 2 sites.

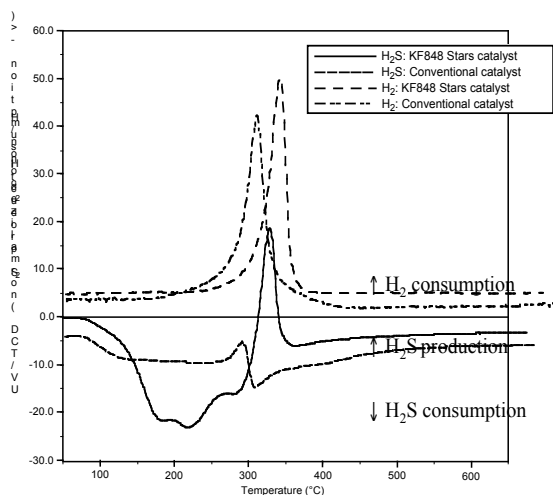


Figure 1. Temperature Programmed Sulfidation (TPS) patterns of conventional Ni-Mo KF843 and Ni-Mo KF848-STARS catalysts.

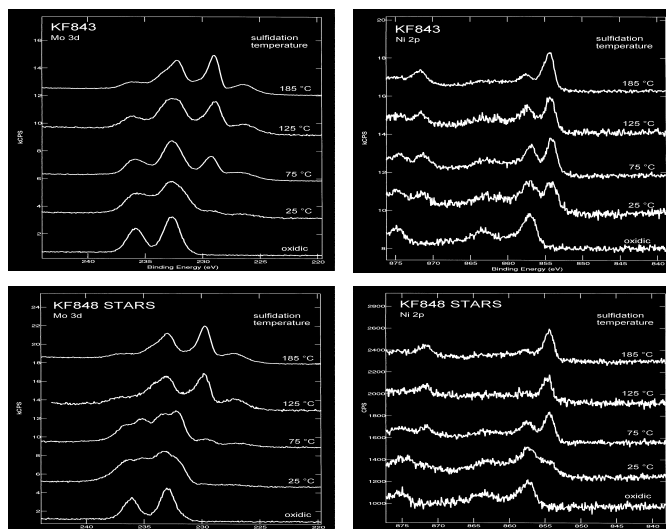


Figure 2. X-ray Photoelectron Spectroscopy (XPS) spectra of conventional Ni-Mo KF843 and Ni-Mo KF848-STARS catalysts.

Performance of Type 2 Catalysts. The incorporation of Type 2 sites leads to a higher activity of Ni-Mo (Figure 3) and Co-Mo catalysts. While traditionally Co-Mo catalysts were used for HDS, Ni-Mo catalysts are applied for some process conditions (higher pressure) nowadays. The reason is that the activity ranking of a Ni-Mo Type 2 changes compared to a Co-Mo Type 2 catalyst as a function of the hydrogen pressure and operating severity (Figure 4).

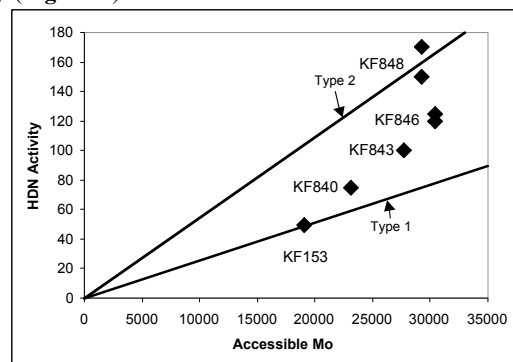


Figure 3. HDN activity (VGO) of conventional Ni-Mo (KF153, KF840, KF843 and KF846) and Ni-Mo KF848-STARS Catalysts.

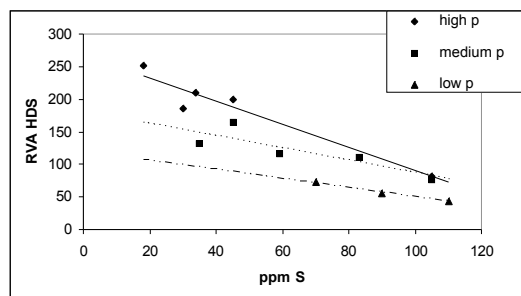


Figure 4. Changing activity ranking of Ni-Mo versus Co-Mo catalysts due to changing reaction mechanism in diesel HDS at different reaction pressures. Relative volume activity (RVA) HDS of KF848 is calculated versus the KF757 reference.

NEBULA Catalyst

The opportunities are even bigger with the NEBULA catalyst¹⁾, a joint development of Akzo Nobel with ExxonMobil, which is a totally novel hydroprocessing catalyst not made according to today's technology of alumina carriers with impregnated metals. NEBULA is such an improvement in activity, that it enables refiners to produce ultra low sulfur diesel in most high-pressure units that have been designed for the production of 500 ppm S (Figure 5).

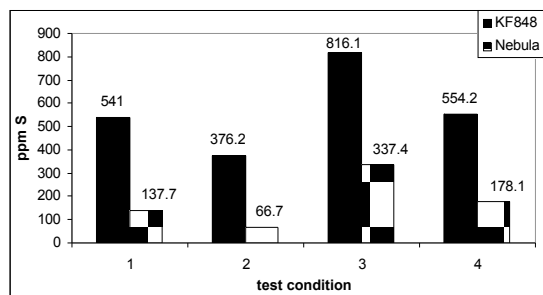


Figure 5. HDS performance of NEBULA and KF848 in diesel HDS.

Besides using NEBULA for treating the diesel fractions, NEBULA can contribute to the production of low S diesel when used in VGO pretreatment, preceding the hydrocracking and FCC units (Figures 6-8). Just like in diesel HDS, KF757 has a good performance at higher product S levels. KF848 and especially NEBULA outperform KF757 at low product S levels. As really low product S levels can be obtained only at low product N levels (Figure 9), not only the HDS but also the hydrodenitrogenation (HDN) and hydrogenation (HDA) activities are improved.

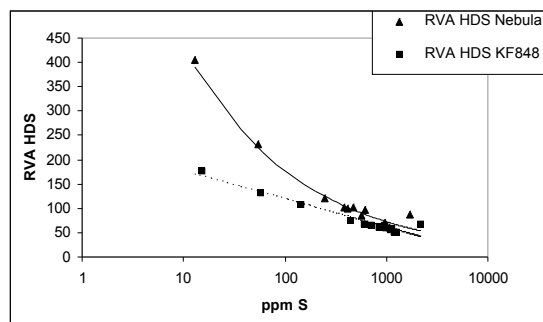


Figure 6. HDS performance of NEBULA and KF848 in VGO hydrotreating. RVA HDS is calculated versus the KF757 reference.

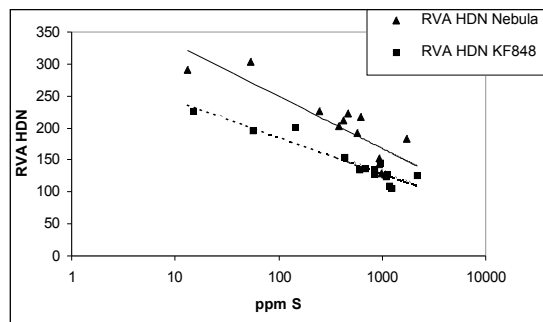


Figure 7. HDN performance of NEBULA and KF848 in VGO hydrotreating. RVA HDN is calculated versus the KF757 reference.

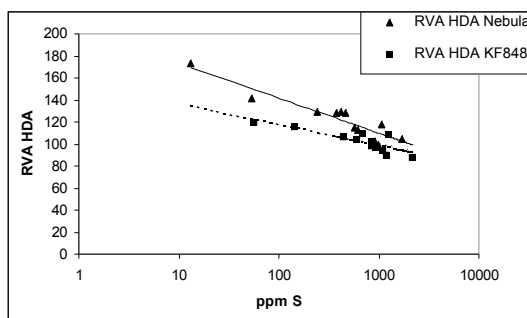


Figure 8. HDA performance of NEBULA and KF848 in VGO hydrotreating. RVA HDA is calculated versus the KF757 reference.

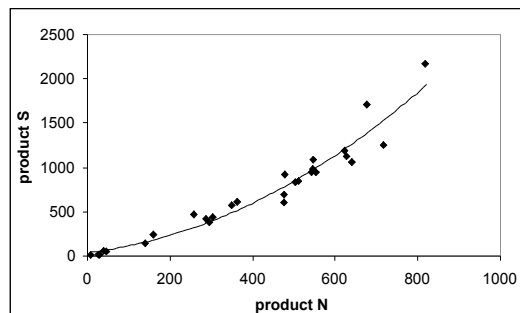


Figure 9. Product S and N level of hydrotreated VGO corresponding to Figures 6 – 8.

Summary Catalyst Development

Figure 10 shows the development of the “traditional” hydroprocessing catalysts and the new catalyst generations, “STARS and NEBULA technology”.

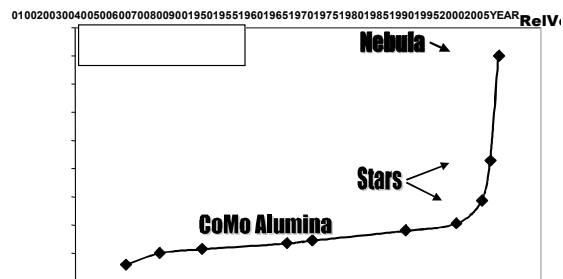


Figure 10. Development of hydrotreating catalyst in past 50 years.

Already with the move to STARS, a new development S-curve was started. At present, the end point of the graph is NEBULA, a catalyst with breakthrough activity that reaches four times the activity of the conventional catalysts. Nowadays, NEBULA is finding its place in the refinery processes. NEBULA catalyst not only helps to use the existing units to meet the future product specifications. It also helps to maintain the product specifications while increasing the cycle length by running the units at less severe conditions (e.g. lower temperature) or while increasing the unit throughput at normal operating conditions.

References

1. D. Pappal; NPRA Annual meeting, March 23-25, 2003, AM-03-59.

CHARACTERISTICS OF NOVEL TITANIA CATALYST PREPARED BY MULTI-GELATION METHOD IN DEEP-DESULFURIZATION CONDITION

Shinichi Inoue^{*1}, Akihiro Muto^{*1}, Hidehiko Kudou^{*1},
Takeo Ono^{*2}

*1: PEC Chiyoda Laboratory
(Research & Development Center, Chiyoda Corporation)
1-1 Minamiwatarida-cho, Kawasaki-ku, Kawasaki, 210-0855, Japan
E-mail : sinoue@ykh.chiyoda.co.jp

*2 : Ono Professional Engineer Office
1-38 Furuichiba, Saiwai-ku, Kawasaki 211-0952, Japan

Introduction

Japanese refiners started providing cleaner diesel fuel of 50ppm sulfur content in the spring 2003. Furthermore, the movement of new regulation reinforcement is anticipated to reduce sulfur content in diesel oil under 10 or 15ppm by 2008. Thus, excellent hydrodesulfurization catalyst is so desired. During the last decade, titania supported molybdena catalysts have attracted increasing attention. Several articles dealing with titania outlined a higher intrinsic activities than on the conventional alumina support. However, titania catalyst was not commercially used because TiO₂ is regarded having a small specific surface area less than 50-60m²/g and poor thermal stability.

The novel manufacturing technology of structure controlled titania support catalyst was proposed for the further improvement of diesel fuel in ultra deep hydrodesulfurization¹⁾. The multi-gelation method has a good performance for controlling pore structures, i.e., pore size distributions as shown in Figure 1.

In this study, we investigated the denitrogenation activities of controlled meso-porous titania catalyst prepared by the multi-gelation method.

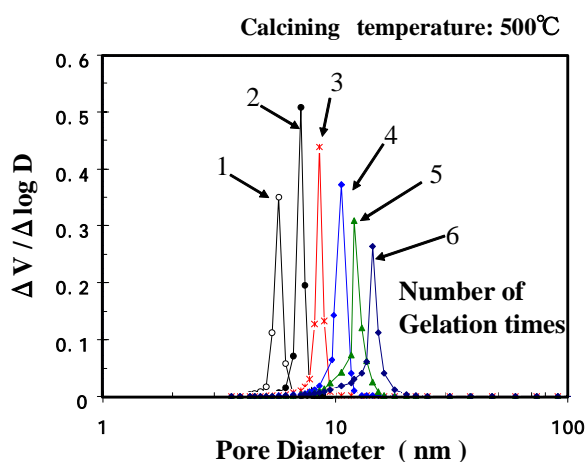


Figure 1. Pore Distributions of TiO₂ Controlled by Multi-Gelation Method

Experimental

1) Preparation Method of TiO₂ Support

Multi-gelation method is the procedure to produce the inorganic oxides gel by swinging of pH of solution dexterously several times. This method can be employed in preparation of hydrous titanium. It can control a particle size of TiO₂ uniformly with a designed pore size. Figure 2 shows the preparation flow diagram of the multi-gelation method to synthesize TiO₂. The raw materials are acidic TiCl₄ and basic ammonia solutions. Hydroxyl gel of TiO₂ was synthesized by swinging pH from TiCl₄ and ammonia solutions. TiCl₄ and ammonia solutions were supplied to the gelation vessel alternately, and hydrous titanium was synthesized. Particles of hydrous titanium were controlled in desirable particle size by alternately supplying TiCl₄ or ammonia solution. And hydrous titanium was washed by water to remove ammonium chloride. After filtration, TiO₂ as a catalyst or a catalyst carrier was molded to cylindrical shapes by the extruder, for example. And it was dried at 120 °C and is calcined at 500 °C in the standard procedure.

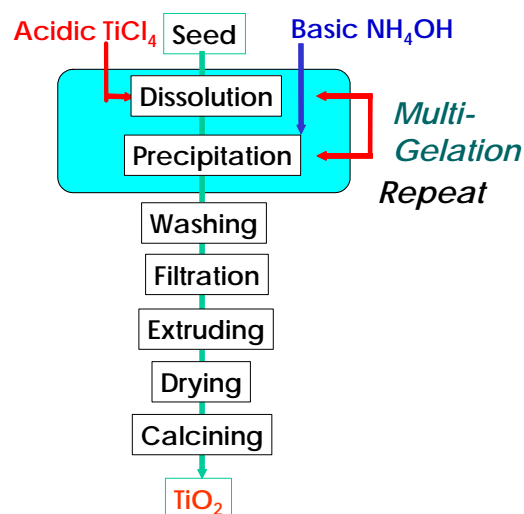


Figure 2. Preparation Flow Diagram of TiO₂ by Multi-Gelation Method

2) Catalysts

TiO₂ supports properties used in this study are as follows: Specific surface area is 162m²/g, average pore diameter is 9nm whose pH swing number is 3 times. The CoMo/TiO₂ catalysts were prepared by gel impregnation method: TiO₂ gel was impregnated with ammonium heptamolybdate and Cobalt nitride as required. This was followed by drying at 120°C for 3h and calcination in air at 500°C for 3h.

3) Measurement of HDS and HDN activity

The HDS and HDN experiments were carried out with a fixed-bed reactor. The catalyst was presulfided with the feed oil spiked by DMDS. Typical reaction conditions were as follows: H₂/Oil ratio 250, LHSV 2 h⁻¹, reaction pressure 5 MPa, Reaction temperature 330 - 350°C. The Middle-East straight run gas oil with 1.3wt% sulfur was used as feed stock.

Results and Discussion

1) Hydrodesulfurization Activity

The activity of the proprietary TiO_2 catalyst compared with the conventional CoMo/alumina catalyst for 500 ppm HDS are shown in Figure 3. This Figure also shows the reactivity of CoMo/ TiO_2 catalyst prepared using conventional TiO_2 carrier with 60 m^2/g of surface area. It is important to mention that the catalytic activity of the TiO_2 supported prepared by multi-gelation method with high surface area and good pore distribution is much higher than that of the catalyst using conventional TiO_2 support with low surface area. Furthermore, it also shows that the new TiO_2 catalyst has 2 times higher hydrodesulfurization activity than that of the commercial alumina catalyst.

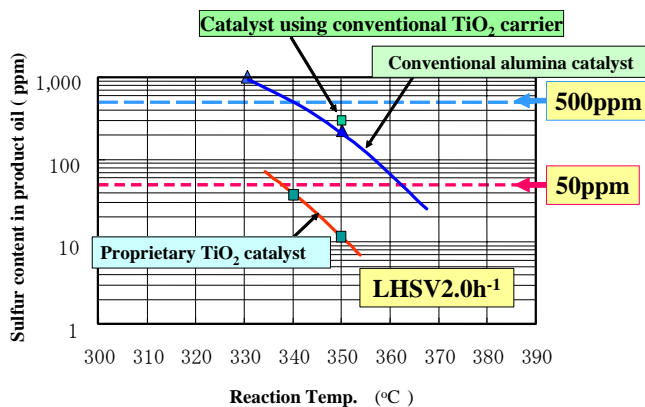


Figure 3. HDS Performance of Proprietary TiO_2 Catalyst

2) Characteristic of denitrogenation activities

It was found another remarkable characteristic of TiO_2 catalyst that the titania catalyst has high denitrogenation selectivity. Figure 4 shows the correlation between desulfurization rate and nitrogen removal rate of TiO_2 and commercial alumina catalysts. Comparing at the same decarburization rate, denitrogenation selectivity of CoMo/ TiO_2 catalyst is much higher than Commercial CoMo and NiMo alumina catalyst.

Figure 5 shows the correlation between nitrogen removal rate and chemical hydrogen consumption of titania and commercial alumina catalysts. In spite of high denitrogenation selectivity, it is clear that the hydrogen consumption of titania catalyst is about $10\text{Nm}^3/\text{kl}$ lower than the commercial CoMo and NiMo alumina catalysts at the range of high nitrogen conversion rate.

Generally, it is considered that denitrogenation reaction passed through a hydrogenation of aromatic ring with nitrogen. It is considered that the hydrogenation reaction rate of titania catalyst for the other aromatic compound is slower than that of alumina catalysts.

Accordingly, hydrogenation of aromatic is restrained as much as possible, and it may be said that CoMo/titania catalyst is more economic catalyst for desulfurization and denitrogenation.

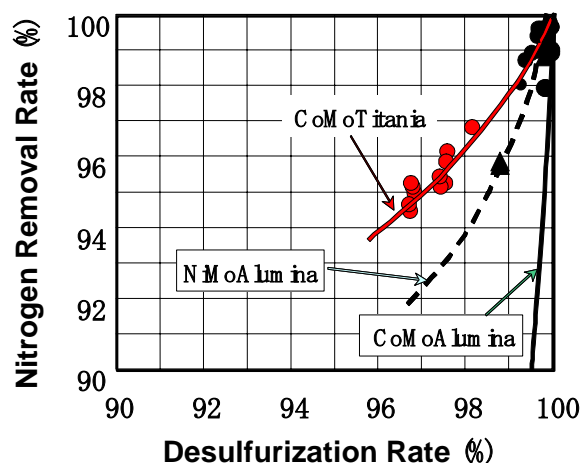


Figure 4. Correlation between desulfurization rate and nitrogen removal rate

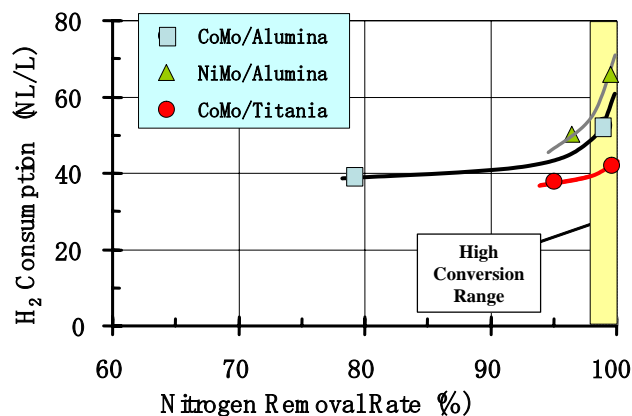


Figure 5. Correlation between nitrogen removal rate and H_2 consumption

Conclusions

It was confirmed that TiO_2 with high specific surface area by the novel multi-gelation method showed good performance of catalytic activity, especially denitrogenation activities, in ultra-deep hydrodesulfurization condition. Therefore, the proprietary TiO_2 catalyst is good candidates for the hydrodesulfurization or hydrotreating processes.

Acknowledgement. This work has been entrusted by the New Energy and Industrial Technology Development Organization under a subsidy of the Ministry of Economy, Trade and Industry of Japan.

Reference

- 1) Inoue, S., Kudou, H., Muto, A., Ono, T., The 255th ACS National Meeting in Fuel Symposia New Orleans, LA, March 23-27, 2003 Spring

CATALYTIC POTENTIAL OF CARBON-SUPPORTED NiMo-SULFIDE FOR ULTRA-DEEP HYDRODESULFURIZATION OF DIESEL FUEL

Masato Kouzu, Yasunori Kuriki, Hamdy Farag, Kinya Sakanishi, Yosikazu Sugimoto, and Ikuo Saito

National Institute of Advanced Industrial Science and Technology (AIST), Tsukuba Center, Ibaraki 305-8565, Japan

Introduction

The regulation of sulfur content in diesel fuel to around 10 ppm is coming closer to the reality in a couple of years for the suppression of air pollution in urban areas. To achieve such ultra-deep hydrodesulfurization (HDS) of diesel fuel without new investment in petroleum refineries, further improvements in HDS catalytic performance are required in terms of the much higher activity and selectivity for HDS of refractory sulfur compounds such as 4,6-dimethyldibenzothiophene (4,6-DMDBT).

Enhancing dispersion of the active components is one of the approaches to modify the HDS catalyst. In the case of conventional alumina-supported CoMo and NiMo catalysts, the dispersion of the active components such as CoMoS and NiMoS phases is hardly enhanced due to the strong polarity and the limited surface area of the alumina support.¹ Carbon supports such as active carbons and carbon blacks have been reported to have the potentials for enhancing the dispersion of the active sulfides because of the weak polarity and the higher surface area.² Solar et al. quantitatively measured the surface functional groups of some active carbons to analyze the dispersion of the active component.³ It has been also reported that CoMo and NiMo sulfides on active carbons can be superior to the conventional alumina-supported ones in the activity and selectivity for HDS of DBT derivatives, suggesting that carbon-supported Mo sulfides may enhance hydrogenative HDS route.^{4,5}

The most important key for ultra-deep HDS of diesel fuel is to selectively desulfurize refractory alkyl-DBT derivatives through the hydrogenative HDS, because the hydrogenation of neighboring aromatic ring of alkyl-DBT derivatives accelerates C-S bond scission. Hence, it is expected that NiMo sulfide supported on active carbon with high surface area can be one of the potential catalysts for the achievement of ultra-deep HDS of diesel fuel.

In the present study, HDS reactions of 4,6-DMDBT as a model feedstock and real gas oil are performed over NiMo sulfide catalysts supported on a particular active carbon (NiMo/C) by using a micro-autoclave and a down-flow tubular reactor with fixed-bed, respectively, in order to clarify the catalytic potential of NiMo/C in comparison to a conventional NiMo/alumina catalyst.

Experimental

Catalyst preparation. A commercially available active carbon powder with the surface area of 3,000 m²/g was used as the support material of NiMo/C prepared. Ni and Mo were simultaneously impregnated on the active carbon by incipient wetness procedure using methanol solution of the organic salts, Ni acetate tetrahydrate and MoO₂ acetylacetonate. Ratio of Ni/Mo was kept constant at 0.2 on the basis of their weight. The impregnating procedures were repeated to the prescribed amount of the active components, followed by atmospheric drying at 80°C between the each step. Amounts of Ni and Mo impregnated were analyzed by ICP-AES measurement.

Prepared precursor of NiMo/C was sulfided at 400°C under atmospheric gas flow of H₂S/H₂ mixture in off-site, prior to the activity measurement. Both the porosity and the morphology were

measured by N₂ adsorption and TEM observation, respectively, in the final sulfide form of the catalyst.

Activity measurement. A micro-autoclave inserted into electric furnace of vertically shaking type was used for a reaction of the model feedstock. The model feedstock was composed of DBT (2.0%), 4,6-DMDBT (0.2%), 1-MN (5.0%) in decane solvent. After 5 ml of the model feedstock, 30 mg of the catalyst and 3 MPa of H₂ gas were charged into the autoclave, the reaction was conducted at 320°C. The processed model feedstock was subjected to GC-FID and GC-MS to calculate the conversion ratio and the product yield.

Following the above activity measurement, a reaction of the real feedstock was carried out in a down-flow tubular reactor. The real gas oil feedstock contained 12,300 ppm-S and 120 ppm-N. 4 ml of the catalyst was packed into the reactor with silicon carbide of the diluent. After set-up of the reactor unit, the temperature was made to increase from ambient to 330°C for 16 h in the flow of the real feedstock with 2% dimethyldisulfide. Then, the HDS reaction was operated at 330-350°C with LHSV of 1.5-3.0 h⁻¹. The hydrogen gas pressure and the volumetric hydrogen gas/oil ratio were kept at 5 MPa and 250 Ni/l, respectively. The HDS rate constant was analyzed using 1.3th order kinetics.

A commercially available NiMo catalyst supported on alumina (NiMo/Al) was subjected to these activity measurements as the reference to evaluate the catalytic potential of NiMo/C.

Results and Discussion

A variety of NiMo/C catalysts were prepared to analyze the dispersion of the active component on the active carbon. **Table 1** summarizes effect of the amounts of the active components on the conversion of 4,6-DMDBT in the reaction of the model feedstock.

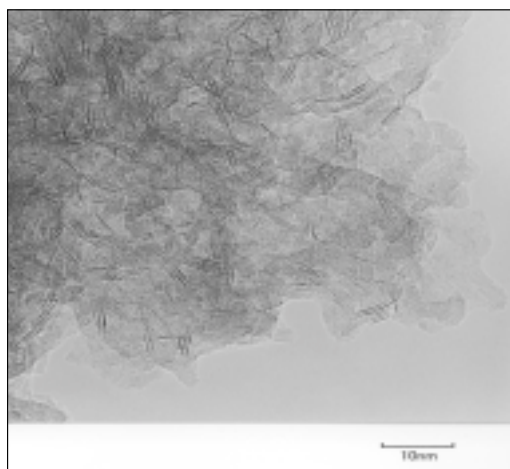
Table 1. Conversion of 4,6-DMDBT and DBT in the reaction of the model feedstock at 320°C for 1.0h

Catalyst	NiMo/C		(NiMo/Al)			
	Ni [wt%]	Mo [wt%]	2	3	5	3
4,6-DMDBT	2	10	3	4	5	3
Converting ratio [%]	30.7	37.1	49.3	53.6	17.9	0.22
Rate Const. [h ⁻¹]	0.42	0.59	0.82	0.78	0.22	0.6
C ₂ BP [%]	2.1	1.6	2.1	2.3	1.6	1.6
C ₂ CHB [%]	11.7	15.8	30.3	30.7	5.1	5.1
C ₂ BCH [%]	2.9	6.3	6.3	10.2	1.2	1.2
DBT	71.5	78.9	91.1	90.2	43.8	0.63
Converting ratio [%]	71.5	78.9	91.1	90.2	43.8	0.63
Rate Const. [h ⁻¹]	1.45	1.76	2.50	2.15	0.63	0.6
BP [%]	41.0	43.4	49.7	45.7	26.8	26.8
CHB [%]	26.6	30.8	37.7	40.6	14.0	14.0
BCH [%]	1.8	3.2	3.1	3.3	0.4	0.4

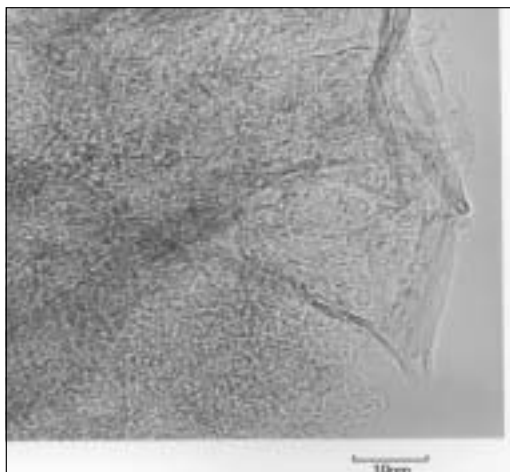
The conversion of 4,6-DMDBT was enhanced with the increase of the amount of the active component, although the converting ratio reached the peak at 20%-Mo. 4,6-DMDBT was mainly converted into C₂-CHB via the hydrogenative HDS route. Except for 25%-Mo, the reaction rate constant on 1st order kinetics increased in proportion to the amount of the active component. The maximum reaction rate constant, at 20%-Mo, was above 4 times as large as NiMo/Al. It is supposed that the enhanced dispersion was kept constant until the amount of impregnated Mo reached at 20%

The positive effect of the amount of the active component was evident, also, in the conversion of DBT. 60-70% of DBT was converted into CHB via the hydrogenative HDS route.

TEM images gave the evident information on the enhanced dispersion of the active component in NiMo/C, as shown in **Figure 1**. Layered structure of the active component was visible in NiMo/Al, whereas not visible in NiMo/C, indicating the higher dispersion of the active component in NiMo/C. A small portion of layered structure of NiMo/C may be formed at the external slit on the active carbon. Although the active component was not appreciable in TEM image, Ni and Mo were detected in EDX spectrum at the same measuring field. It is an evidence that the higher dispersion of the active phases may be achieved on NiMo/C catalyst. The invisible active component on the active carbon was independent of the amount impregnated, which was consistent with the reaction rate constant for converting 4,6-DMDBT mentioned above.



(a) NiMo/Al



(b) NiMo/C, 4%Ni-20%Mo

Figure 1. TEM images of NiMo/Al and NiMo/C catalysts (1.5million magnification)

The reaction of the real gas oil feedstock was carried out over the best NiMo/C that contained 4%Ni and 20%Mo. **Figure 2** shows the reaction temperature versus the residual sulfur content.

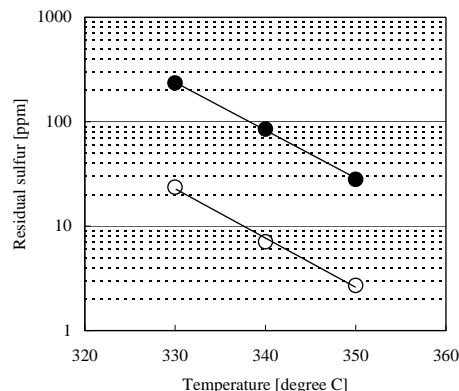


Figure 2. Reaction temperature vs. residual sulfur content in the reaction of the real feedstock under hydrogen pressure of 5MPa with LHSV of $1.5h^{-1}$. ○, NiMo/C ($k_{HDS}@330^{\circ}C$: $1.59h^{-1}$); ●, NiMo/Al ($k_{HDS}@330^{\circ}C$: $0.68h^{-1}$)

NiMo/C achieved 10ppm-S level at $337^{\circ}C$, whereas not completed over NiMo/Al under the present operating conditions. It is revealed that NiMo/C can be also advantageous catalyst for the ultra-deep HDS of real diesel fuel. The HDS rate constant over NiMo/C was above 2 times higher than that over NiMo/Al. This was consistent with the reaction rate constant for converting 4,6-DMDBT in the reaction of the model feedstock, taking into difference in the bulk density consideration.

Conclusions

Catalytic potential of NiMo/C prepared using an active carbon powder with the surface area of $3,000 m^2/g$ was evaluated in order to achieve the ultra-deep HDS of diesel oil. The reaction rate constant for converting 4,6-DMDBT was enhanced in proportion to the amount of the active component in a reaction of model feedstock at $320^{\circ}C$, although the reaction rate constant reached the peak at 20%-Mo. The maximum rate constant over NiMo/C was 4 times larger than that over NiMo/Al. TEM observation showed the much higher dispersion of the active species on NiMo/C. The best NiMo/C containing 4%Ni and 20%Mo achieved 10ppm-S at $337^{\circ}C$ in a reaction of the real gas oil feedstock using a down-flow tubular reactor, whereas was not completed over NiMo/Al under the same condition. The HDS rate constant over NiMo/C was above 2 times higher than that over NiMo/Al. Hence, NiMo/C can be a candidate for the innovative catalyst for the ultra-deep HDS.

Acknowledgement. The work has been entrusted by the New Energy and Industrial Technology Development Organization under a subsidy of the Ministry of Economy, Trade and Industry.

References

1. Grange, P., *Catal. Rev-Sci. Eng.*, **1980**, 21, 135
2. Rodriguez-Reinoso, F., *Carbon*, **1998**, 36, 3, 159
3. Solar, J. M., Derbyshire, F. J., DeBeer, V. H., Randvic, L. R., *J. Catal.*, **1991**, 129, 330
4. Hamdy, F., Whitehurst, D. D., Sakanishi, K., Mochida, I., *Catal. Today*, **1999**, 50, 9
5. Sakanishi, K., Nagamatsu, T., Mochida, I., Whitehurst, D.D., *J. Mol.Catal. A:Chemical*, **2000**, 155, 101.

SONO-SYNTHESIS AND CHARACTERIZATION OF NANOPHASE HYDRODESULFURIZATION CATALYSTS

Christopher L. Marshall¹, Devinder Mahajan², A. Jeremy Kropf¹,
Manuela Serban¹, Norma B. Castagnola¹, and Jonathan C. Hanson³

¹Chemical Technology Division, Argonne National Laboratory,
Argonne, Illinois 60439-4837

²Energy Sciences and Technology Department, Brookhaven National
Laboratory, Upton, New York 11973-5000 USA and Department of
Materials Science and Engineering, Stony Brook University, Stony
Brook, New York 11794-2275 USA

³Department of Chemistry, Brookhaven National Laboratory, Upton,
New York 11973-5000 USA

Introduction

The generation of microporous and small-particle chalcogenides for catalytic hydrodesulfurization (HDS) of transportation fuels and heavy crude is of interest. However, currently employed commercial wet chemical synthesis techniques result in large sheets of MoS₂. A few recent reports include preparation of supported MoS₂ on alumina catalyst with a Co promoter, sonolysis of Mo(CO)₆/Co(CO)₃NO/wide-pore Al-MCM-41 in decalin to produce nano particles of Mo and Co oxides on an alumina support that was further treated to form the HDS catalyst, and sonochemical preparation of supported nano HDS catalysts, Co-Mo-S/ Al₂O₃, Ni-Mo-S/ Al₂O₃, and Co-Ni-Mo-S/ Al₂O₃. These catalysts were shown to exhibit several-fold higher HDS activity than comparable micrometer-sized commercial catalysts.

Results and Discussion

A convenient synthesis of nano-size HDS catalytic materials in several-gram quantities is the main focus of the present activity at Brookhaven National Laboratory (BNL) and Argonne National Laboratory (ANL). Several hydrocarbon solvents have been evaluated to optimize "cavitation" that is critical to produce nano Mo metal particles by decomposition of molybdenum hexacarbonyl. Further in situ complexation of nano Mo with elemental sulfur yields nano MoS₂. With a known ratio of Co₂(CO)₈/Mo(CO)₆, the method produces nano Co/MoS₂. Sonolysis of Mo(CO)₆ in the presence of γ -Al₂O₃ produced supported nano Mo, i.e., nano MoS₂/ γ -Al₂O₃. The yields of all three nano-sized materials are >90% based on the starting Mo(CO)₆.

The prepared samples are being characterized at the National Synchrotron Light Source (NSLS) at BNL and the Advanced Photon Source (APS) at ANL. The measurement of these materials is a challenge. Preliminary x-ray diffraction (XRD) data show that the prepared materials indeed are nano-size. Transmission electron microscopy (TEM) (with a resolution of 0.16 nm) is being used to measure the morphology and particle size of the samples.

The nano-scale materials exhibit temperature-programmed reduction (TPR) profiles that are about 75°C higher than the commercially available catalyst. Adding cobalt to the molybdenum has no effect on the temperature of the reduction but does lower the overall amount of hydrogen adsorption. The MoS₂ nanophase materials are highly reactive and susceptible to oxidation in air. Running x-ray adsorption near edge spectroscopy (XANES) at the APS in

temperature-programmed oxidation (TPO) mode (**Figure 1**) shows that the native material oxidizes at the relatively low temperature of 365°C. The addition of Co to the nanophase MoS₂ material

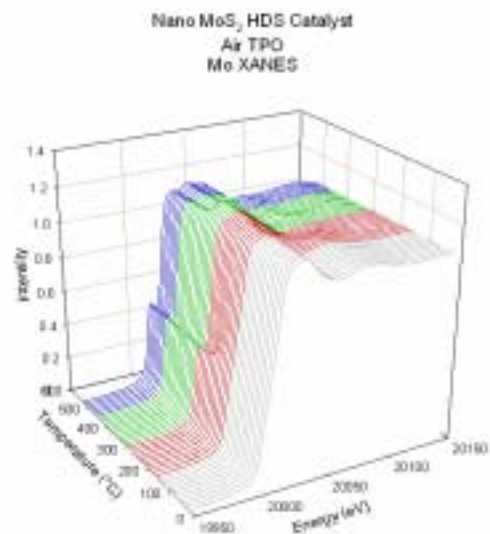


Figure 1 – Temperature programmed oxidation followed by Mo XANES.

(necessary for HDS catalytic activity) removes some of this oxidation instability. Principle component analysis (PCA) (**Figure 2**) provides us with an estimate of the amount of a specific component at any given temperature.

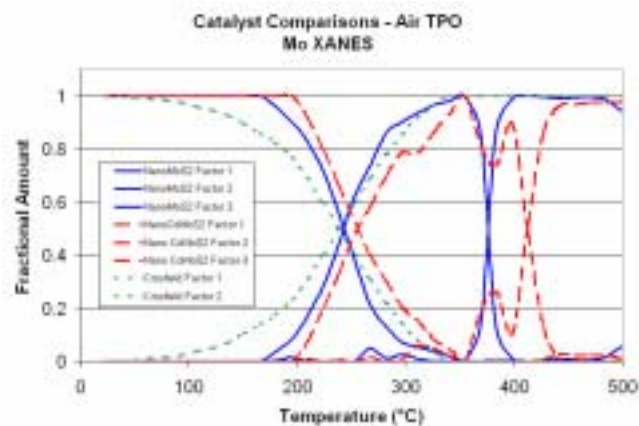


Figure 2. Principle Component Analysis of the types of Mo during TPO of commercial and nano-phase MoS₂.

HDS activity of several supported metals has been correlated with the temperature programmed reduction (TPR) peak. The TPR for the nano-MoS₂ and nano-Co/MoS₂ materials is significantly higher than that of the supported materials. The fact that the temperature of the TPR reduction peak was almost the same as nano-MoS₂ implies that there was not a combination of these two phases. In addition, the width of the TPR peak for the nano-sized materials (nano-MoS₂ and nano-Co/MoS₂) is significantly broader than the commercial catalyst. The wider TPR peak for the sonochemically-generated materials implies that there is a much broader distribution of active sites in the nanophase materials versus the commercially prepared catalyst. This would result in a wider variety of active sites and is probably the

reason for the lower activity for the sonochemically prepared materials.

Preliminary HDS activity evaluation studies show lower activity for the nano-CoS-MoS₂ compared to the nano-MoS₂. This was surprising but is mirrored in the TPR data. The activity of the unsupported nanosized catalysts, however, is much higher than the commercial micron-sized counterparts. This enhancement comes from the increased surface area of the nanoparticles. In the micron-sized catalysts, diffusion in between the long rafts of MoS₂ is mass transport limited, so it is expected that most of the activity comes from the 'rims' and 'edges.' Incorporation of Co to MoS₂ increases the activity of the catalyst. In preliminary studies, the catalytic activities are compared at commercially operated temperature that may not be the optimized temperature for nanosized MoS₂-based catalysts.

A major problem with hydrodesulfurization is the hydrogenation of olefins, which leads to loss of research octane number (RON). The rate of olefin hydrogenation is much faster than HDS, but competitive adsorption of S at the active site strongly inhibits the hydrogenation reaction. At low S levels, olefin hydrogenation takes over. To model these olefins in our HDS runs, 1-octene (1 wt.%) was added to the liquid feed and the HDS tests were run again. Interestingly, the sonochemically synthesized nanophase catalysts are less active for olefin hydrogenation than their commercial counterparts. This observation contrasts the expected result that the hydrogenation function in nanosized catalysts should increase because nanosizing increases the number of edge sites. Work is in progress to further decrease the hydrogenation function with concomitant increase in the HDS activity of the synthesized nanophase materials.

Acknowledgement. This work was performed under the auspices of the U. S. Department of Energy, under contract number W-31-109-ENG-38.

ZEOLETIC SUPPORT OF HDS CATALYSTS FOR DEEP HYDRODESULFURIZATION TO ACHIEVE 10PPM SULFUR LEVEL

Naoyuki Kunisada, Ki-Hyouk Choi, Yo-ozo Korai, Isao Mochida*, and K. Nakano[†]

*Institute of Material Chemistry and Engineering, Kyushu University,

Kasuga-Koen, Kasuga, Fukuoka 816-8580, JAPAN

[†]Catalysts & Chemicals Ind. Co. Ltd, JAPAN

*e-mail: mochida@cm.kyushu-u.ac.jp

INTRODUCTION

NO_x, SO_x and particulate matters exhausted from diesel engine which combusts gas oil as fuel has provided a sincere social problem all over the world. The drastic reduction of sulfur in gas oil is expected to reduce those environmental pollutants and burden for diesel engines. Removing sulfur species deeply from gas oil has two difficulties; the first one is very low reactivity of some refractory sulfur species in gas oil such as 4,6-dimethyldibenzothiophene (4,6-DMDBT), 4,6,x-trimethyldibenzothiophene (4,6,x-TMDBT) having methyl group at 4 and 6 positions, the second is the strong inhibitors in feed oil and the products such as H₂S, NH₃, nitrogen species and aromatic compounds^{1,2}. Hence deep HDS of these refractory sulfur species in gas oil can be achieved rather easily by the first and second stages of the catalysts when H₂S removal is performed between stages. Another approach is to develop catalysts of higher activity. Larger amount or better dispersion of sulfides have potential possibility for higher activity. Nevertheless severe conditions appear necessary.

The present authors prepared a two layer catalyst bed to achieve desulfurization without H₂S (NH₃) removal between layers. The functions of the catalysts in each layer are defined as follows. 1st layer : complete removal of reactive sulfur species and 95% removal of refractory sulfur species. 2nd layers : remaining refractory sulfur species (around 400-500ppm) must be removed to less than 10ppm in the presence of H₂S and NH₃. In the present study, several types of zeolite containing supports for HDS catalysts are prepared to be examined in the first and second layers.

Zeolite support has been reported to provide high HDS activity and resistivity against H₂S. However it loses activity and accelerates the cracking of paraffin substrate. Hence, it is the present target to reduce the deactivation and cracking activity with maintain HDS activity and resistivity.

EXPERIMENTALS

a, Gas oil samples

Straight Run Gas Oil (SRGO) and Hydrodesulfurized Straight Run Gas Oil (HSRGO) were used as typical feedstocks for the first and second layer catalysts, respectively in this study. The SRGO contains 11780ppm while the HSRGO contains 340ppm of sulfur. Furthermore, the SRGO contains 155ppm while the HSRGO contains 20ppm of nitrogen.

b, Catalysts

The catalysts used in this study were CoMo and NiMo supported on alumina(-A), silica-alumina(-SA), alumina-zeolite composite(-AZ, -ACZ), silica-alumina-zeolite composite(-SAZ), modified zeolite alumina(-ACZ) which were manufactured by a commercial catalyst

vendor. **Table 1** shows their surface area, average pore size measured by BET and NH₃ desorbed amount measured by NH₃-TPD.

c, Hydrotreatment

SRGO and HSRGO were hydrotreated over the catalyst at 340°C under 50kg/cm² of H₂ for first layer, 50 kg/cm² H₂ with H₂S (1.67%) and 50 kg/cm² H₂ with H₂S (1.67%) added ethylenediamine (15ul) for second layer in a 100ml autoclave.

The ratio of catalyst to feed was 1g/10g. Catalyst was presulfided at 360°C under the stream of H₂S(5%)/H₂ mixture for 2hr before the catalytic reaction.

Table.1 Catalysts properties

	Surface area (m ² /g)	Pore volume (cm ³ /g)	NH ₃ -Desorbed area (mmol/g-cat.)
CoMoA	191	0.41	0.48
NiMoA	175	0.34	0.62
CoMoSA	221	0.41	0.56
NiMoSA	242	0.39	0.49
CoMoAZ	265	0.34	0.81
NiMoAZ	262	0.35	0.66
NiMoSAZ	271	0.33	0.85
CoMoSAZ	274	0.32	0.82
NiMoACZ	129	0.36	0.58

RESULTS

a, HDS of SRGO

Figure 1 shows remaining sulfur chromatograms of SRGO after HDS over NiMo- and CoMo-A, NiMo- and CoMo-SA, NiMo- and CoMo-AZ, NiMo- and CoMo-SAZ, and NiMo-ACZ catalysts at 340°C under 50 kg/cm² H₂. NiMo-AZ shows the highest activity among nine catalysts, and its remaining sulfur content is less than 300ppmS. Although NiMo-ACZ, having smaller surface area, shows low activity, zeolite containing catalysts having larger surface area except for NiMo-ACZ tend to show higher activity than SA- and A-series catalysts for HDS of SRGO that contained major reactive sulfur species. The HDS at this stage removed all reactive sulfur species and about 95% of refractory sulfur species to achieve sulfur level of 500ppm.

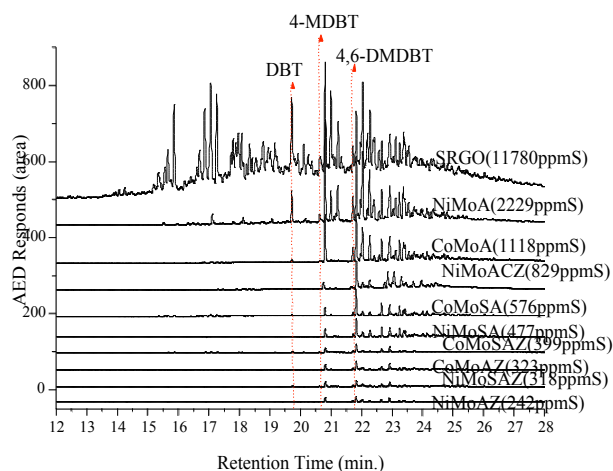


Figure 1. HDS of SRGO over several NiMo and CoMo catalysts

d, HDS of HSRGO in the presence of H₂S and NH₃

Figure 2 shows HDS of H-SRGO in the presence of both H₂S and NH₃. **Figure 3** shows GC-AED carbon chromatograms after HDS of HSRGO in the presence of both H₂S and NH₃. NiMo-A of large pore was found very active for HDS of refractory sulfur species in the presence of H₂S and NH₃ to achieve less than 6ppmS. In contrast, CoMo-A, NiMo-SA and CoMo-SA were less active. NiMo-AZ and CoMo-AZ were much inhibited by addition H₂S and NH₃. NiMo-ACZ, NiMo-SAZ and CoMo-SAZ having strong acidity were found very active as a second layer catalyst.

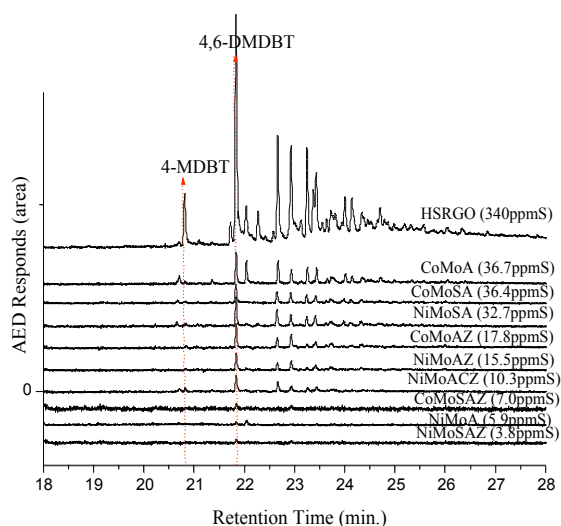


Figure 2. GC-AED sulfur chromatograms on HDS of H-SRGO in the presence of H₂S and NH₃

Acidic catalyst can crack and isomerize hydrocarbons. As can be seen in **Figure 3**, a number of products were found at a range of shorter retention time as a result of hydrocracking. Such products were the most remarkable on alumina-zeolite supported catalysts. In contrast NiMo-ACZ containing zeolite catalyst showed higher activity didn't crack for isomerize hydrocarbons at all. Although the strength of acidity of NiMo-ACZ can be demonstrated, cracking of hydrocarbons is not distinct.

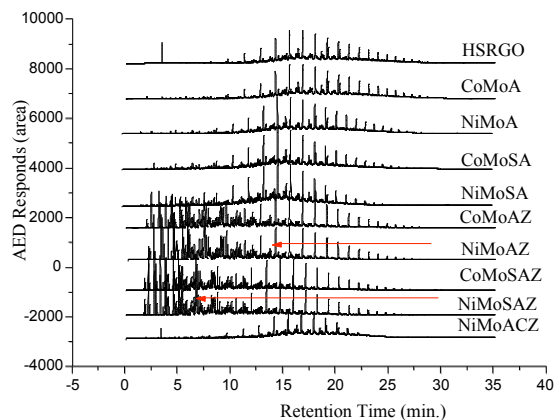


Figure 3. AED Carbon Chromatograms of HDS over some Acidic Catalysts

DISCUSSIONS

The present study revealed that the two layers of the best HDS catalysts with appropriate activity under respective conditions can be a logical approach to achieve deep HDS of gas oil.

The first layer catalyst must eliminate 100% of reactive sulfur species, first of all. Hence, the catalyst must have larger surface area, slightly smaller pore being allowed for the larger surface area. Acidity helps higher activity. 95% of refractory sulfur species must be also eliminated. Its content is still in relatively large range, being less influenced by inhibitors. Moderate acidity is helpful for the hydrogenative HDS.

The second layer catalyst eliminates the refractory sulfur species of 100-500ppm to less than 10ppm in the presence of H₂S and NH₃. The catalyst must have larger pores to accept the refractory sulfur species of tri aromatic rings with methyl groups more than di aromatic rings. Acidity is important to enhance HDS of the refractory sulfur species in the hydrogenation route by moderate H₂S inhibition. Zeolite containing CoMo and NiMo showed higher activity in SRGO, HSRGO+H₂S+NH₃. On the other hand, zeolite having strong acidity is easily deactivated and can crack and isomerizes hydrocarbons. ACZ catalyst showed very high activity in HDS of HSRGO, while it didn't crack the substrate so much. Therefore, modified zeolite-alumina catalyst may have longer life time than any other zeolite containing catalyst, with have high cracking activity.

Appropriate sets of two catalysts with successive layers are very active to achieve regulated Sulfur level of gas oil. It is always discussed whether CoMo or NiMo is better catalyst for the first and second layers. The support and supporting procedure appear very influential and hence we can not tell which is better at this stage. Nevertheless high dispersion in designed shape of the sulfides must be practiced in any supports.

ACKNOWLEDGEMENT

This work has been entrusted by the New Energy and Industrial Technology Development Organization under a subsidy of the Ministry of Economy, Trade and Industry of Japan.

REFERENCE

1. Isoda, T.; Ma, X.; Mochida, I. *Sekiyu Gakkaishi*, **1994**, *37*, 506.
2. Whitehurst, D. D.; Isoda, T.; Mochida, I. *Adv. Catal.*, **1998**, *42*, 345.
3. Isoda, T.; Ma, X.; Mochida, I. *Sekiyu Gakkaishi*, **1995**, *25*, 38.

DIBENZOTHIOPHENE HYDRODESULFURIZATION OVER BULK UNPROMOTED AND COBALT PROMOTED MoS₂ CATALYSTS

Hamdy Farag; Kinya Sakanishi; Masato Kouzu; Akimitsu Matsumura; Yoshikazu Sugimoto and Ikuo Saito

Institute for Energy Utilization, AIST
Tsukuba West 16-1 Onogawa, Ibaraki 305-8569, Japan

Introduction

Environmental concerns are the driving force behind the growing interest of removing sulfur compounds from middle distillate fuels. To encounter the strict of nowadays regulation of sulfur content superior, catalyst is needed. Polyaromatic sulfur compounds are confirmed to be the real obstacle for deep hydrodesulfurization (HDS) reaction. They are the leftover species after deep HDS. These species react through consecutive and sequence reaction in which the selectivity plays a role in the reaction mechanism. In respect to this, catalyst designers encounter two options; one is to search for a catalyst in which the hydrogenation is the pioneer feature of its activity and the other is an ascertained catalyst for the hydrogenolysis of C-S bond. MoS₂ based catalysts are widely applied for HDS reactions. The role of cobalt in promoting MoS₂ supported catalysts has been extensively studied and the synergetic effect is well established.^{1,2} Nevertheless, the impact of cobalt addition to bulk MoS₂ on the selectivity trend of HDS is not clear yet. A better understanding how cobalt may modify the bulk MoS₂ catalyst will provide researchers with fruitful information about how such inclusions promote the HDS activity in case of supported Mo-catalysts. In this piece of work we address some experimental insight work on the comparison between behavior of bulk and supported Mo-catalysts. In addition, it may contribute the linkage between the catalytic activity and selectivity in HDS reaction. Kinetic treatments that focus on the selectivity change of HDS of dibenzothiophene (DBT) are prescribed.

Experimental

Bulk MoS₂ was synthesized through heat annealing in presence of continuous flow of 10v/v% H₂S/H₂ gas mixture. Detail of preparation and characterization of this catalyst is stated elsewhere³. The obtained highly crystalline MoS₂ phase was further ground fine particle around nanometer sizes. This form of MoS₂ was applied to be a primary support for cobalt addition. Alcoholic solution of cobalt (II) acetate was impregnated to MoS₂ at ambient temperature. This mixture was exposed to ultrasonic for 10min. Then the sample was dried at 80°C under vacuum condition. Thereafter, the catalyst was pre-sulfided at 400°C by flow of 10v/v H₂S/H₂ gas mixture. CoS phase synthesized via heat annealing of cobalt (II) acetate with gas flow of 10v/v% H₂S/H₂.

The HDS catalytic activity of DBT was investigated through the use of a batch magnetically stirrer micro-autoclave reactor. All reaction runs were examined at 340°C and 3MPa H₂. Some reaction runs were carried out after addition of copper powder which serves as a scrubber of the continuous production of H₂S during HDS. Reaction products were tracked by the aid of GC-FID and GC-MS.

Results and Discussion

The main HDS products from DBT obtained over the studied catalysts are biphenyl (BP) and Phenylcyclohexane (PC) in addition to the well-known intermediate of H4-DBT. However, it is unique of the MoS₂ and/or Co-promoted bulk MoS₂ catalysts that traces of

fragmented products like alkylated derivatives of benzene or even naphthalene is formed. The presence of these species could be explained due to a series of consecutive hydrogenation reactions that takes place over this kind of catalysts. Table 1 shows the catalysts characterization and the product distribution of DBT HDS at ca. 50% conversion level. Fixed conversion level was adopted because the selectivity of these consecutive and parallel reactions varies with the conversion level.

Table 1. Activity of Bulk MoS₂ Promoted Cobalt Catalysts for DBT HDS.

Catalyst	Co wt%	Level of H ₂ S ^a	HDS*	Selectivity at 50% conv. level		
				BP	PC	H4-DBT
CoS	100	High	2	24.4	21.6	3.9
MoS ₂	0	Low	24	22.3	25.3	2.4
MoS ₂	0	High	83	8.2	28.5	13.3
MCS-I	2	High	38	28.5	16.4	5.1
MCS-II	10	High	33	28.5	16.3	5
MCS-III	16	Low	17	43.2	6.2	0.7
MCS-III	16	High	33	28.6	16.7	5.2

*s⁻¹.g.cat.⁻¹.10⁻⁴, (340°C & 3MPa H₂), ± 3%

The HDS activity of CoS is very low compared with MoS₂ catalyst. One may notice the sharp decrease in activity for Co-promoted MoS₂ catalysts. Unlike the supported CoMo catalysts, Co addition to bulk MoS₂ has a negative effect on the HDS activity. In addition the selectivity of DBT HDS was changed dramatically based on the level of H₂S in the reaction medium. **Figures 1,2 and 3** show the activity and selectivity behavior of the MoS₂ and Co-promoted MoS₂ catalysts. To explain the connection between cobalt inclusions and the changes in HDS activity, one must look at their impact on the selectivity trend.

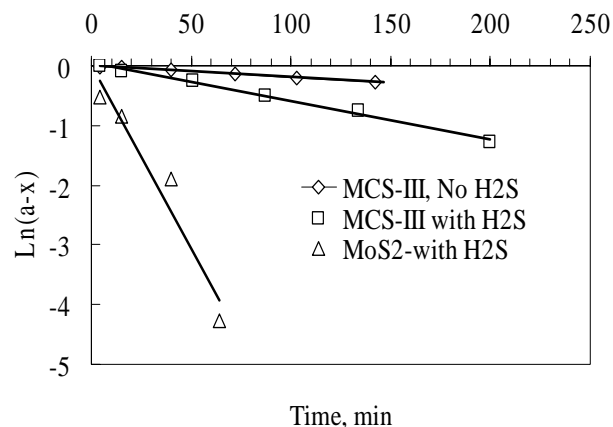


Figure 1. Pseudo-first order plots of DBT HDS over MoS₂ and MCS-III catalysts with or without copper addition.

It is interesting to note the drastic change in selectivity in presence or absence of Co. The obvious decrease of activity with Co inclusions to MoS_2 is markedly linked in a direct proportion relation with the change made on the selectivity behavior. This raises the consolidation between selectivity and activity in HDS reaction. Another interesting feature of the present results is the effect of H_2S on the selectivity and activity of DBT HDS. Figures 3 and 4 show the effect of H_2S level on the HDS selectivity of DBT over MCS-III catalyst. H_2S level is defined as whether copper are included or not into the reaction medium. It is evident that H_2S promote the reaction via the acceleration of the hydrogenation route. Nevertheless, the contribution from the direct hydrogenolysis route is still significant. DBT HDS showed pseudo-first order behavior and the influence of H_2S on the activity is clarified on Figure 1. Figures 2 and 3 illustrate the selectivity changes over MoS_2 and MSC-III catalyst. The hydrocracked fragments products were assumed to result from PC.

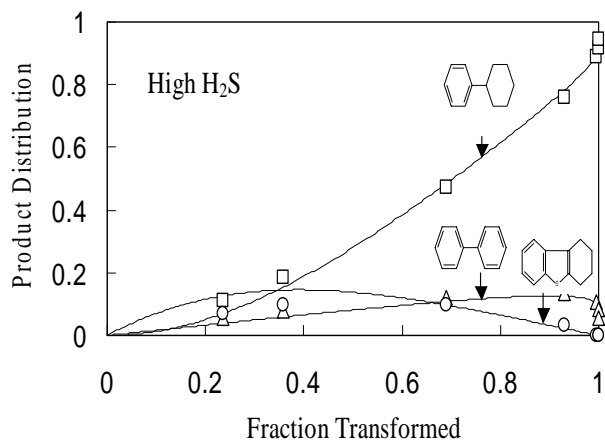


Figure 2. HDS selectivity Curves of DBT (MoS_2 , 340 °C & 3MPa H_2).

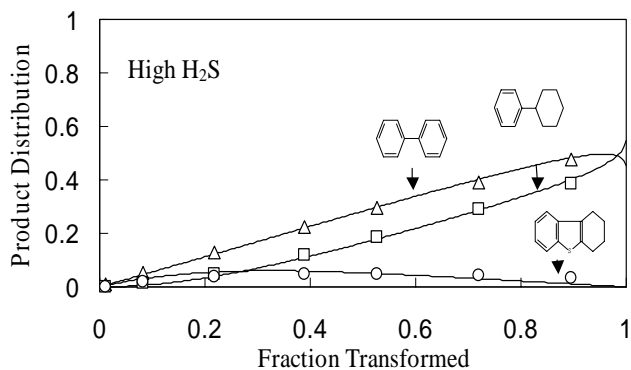


Figure 3. HDS selectivity Curves of DBT (MCS-III, 340 °C & 3MPa H_2).

The decrease in activity of MoS_2 after inclusion of Co is suggested to be due to the negative synergetic effect that has been widely known for these supported catalysts. In other words, the synergy in the present bulk sulfides is not helpful for HDS activity. It

seems that this synergy rule the HDS reaction via more contribution of the direct desulfurization route leading to BP species. The reaction through this route is reported to undergo geometrical difficulty to reach the prospected catalytic active sites. In this respect, it is suggested that the catalytic activity is linked with two distinct active sites. The inclusions of Co to the MoS_2 catalyst replaced some of the usable hydrogenation sites in MoS_2 catalyst. Consequently, these sites will no longer be active for hydrogenation. The obtained new sites forward the reaction to the direct desulfurization route.

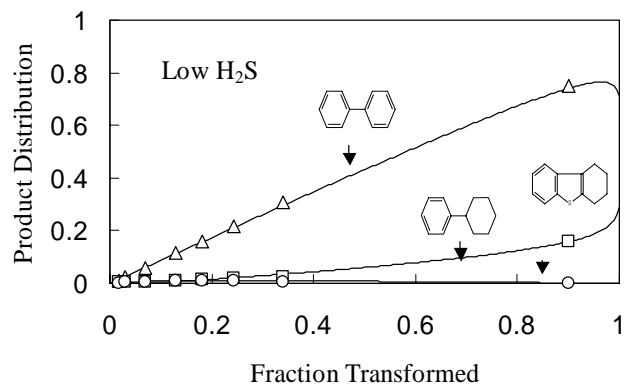


Figure 4. HDS product distribution curves of DBT over MCS-III catalyst, the run with added copper powder. (340°C & 3MPa H_2)

In summary, the results show the close correlation between activity and selectivity in HDS reaction and how cobalt modified the HDS reaction mechanism occurred over MoS_2 catalyst.

Acknowledgment. This work has been entrusted by the New Energy and Industrial Technology Development organization under a subsidy of the Ministry of Economy, Trade and Industry.

References

1. Prins, R., *Adv.Catal.* **2002**, 46, 399.
2. Rossini, S., *Catalysis Today* **2003**, 77, 467.
3. Farag, H., *Energy & Fuel* **2002**, 16, 944.
4. Nava, H.; Ornelas, C.; Aguilar, A.; Berhault, G.; Fuentes, S.; Alonso, G., *Catal.Lett.* **2003**, 86(4), 257.

IN SITU FT-IR STUDY OF CO HYDROGENATION ON A MOLYBDENUM NITRIDE CATALYST

Dong Liu, Yunqi Liu, Tao Zhou, Chenguan Liu, Guohe Que

INTRODUCTION

Free ammonia had been replaced with N_2/H_2 gases, the production of molybdenum nitride and Co-promoted molybdenum nitride, which had more sufficient specific surface area, had been obtained from the two-stage temperature-programmed reduction of molybdenum oxides with the mixture of N_2/H_2 gases. The new synthetic molybdenum nitride and co-promoted molybdenum nitride is very sensitive to air, so it should be pre-treated in the cell—namely the new synthetic molybdenum nitride should be retarded-oxidized by oxygenic inert gas on their surface and a thin layer of $CoMoN_x$ will be formed on their surface. $CoMoN_x$ on surface layer will invert to molybdenum nitride due to hydrogenation at 673K, and will improve their hydrodesulfurization activity. Because hydrofining catalysts will be influenced by H_2S in the hydrodesulfurization process, they should possess high activity and cracking activity (desulfurization activity). It is difficult to distinguish which is better between hydrogenation activity and cracking activity for molybdenum nitride catalysts when organosulfur is adopted to evaluate activity, because H_2S in production will bring some disturbance on surface structure of catalysts. The CO hydrogenation activity was measured by FT-IR in-situ method. Mo_2N and $CoMoN_x$ were prepared and used in the experiment, and compared their effect on CO hydrogenation activity with MoS_2 .

EXPERIMENTAL

Catalysts preparation

The production of molybdenum nitride and co-promoted molybdenum nitride were obtained from the two-stage temperature-programmed reduction of molybdenum oxides with the mixture of N_2/H_2 gases. The BET specific surface areas of molybdenum nitride and Co-promoted molybdenum nitride (atomic ratio of Co and Co+Mo is 0.25) are 165 and 158 m^2/g respectively. MoS_2 (99.9%) was produce by Beijing chemical reagent company.

Method of in situ FT-IR study on CO hydrogenation

CO hydrogenation was carried out in a self-designed IR cell described as Figure 1. The IR cell was made of quartz, the length and high of optical path were ascertained by Magna-750 Fourier Transform Infrared spectrometer. The IR cell (a hollow cell) adding with water inlet and outlet tube were constituted into a whole circular cooling system to protect windows. Heating zone, made up to groove shape to keep insulation of resistance heater, was situated in the middle of the cell. Heating power was 350W. A self-supporting disc (13mm diameter) was prepared by compressing the powder obtained by Catalysts (1% Mo_2N , MoS_2 or $CoMoN_x$ mixed with 99% $\gamma-Al_2O_3$). This disc was mounted in a self-designed IR quartz cell described as Figure 1. A thermocouple well was indwelled in the middle of the IR cell around the catalysts disc. Actual temperature about catalysts (reaction temperature) was measured by the thermocouple. Programmed temperature control instrument, joined with all heating zone and temperature detector in the IR cell, will control the temperature. Air inlet and air outlet were installed on two end of the cell that were adopted with KBr plate and were connected with air inlet channel and outlet channel of in-situ systems by vacuum silicone grease.

Partial pressure of CO, H_2 are 1.01×10^4 and $2.02 \times 10^4 Pa$ respectively in the CO hydrogenation experiment, reaction temperature is 673K unless otherwise stated.

The catalyst disc was degassed under vacuum for 1hr at 673 K, then was pre-reduced in-situ in high-purity H_2 at $2 \times 10^3 Pa$ for

2hr. In-situ IR spectra of the disc in CO, H_2 at the quoted temperatures and pressures were recorded with a Nicolet Magna-750 Fourier Transform Infrared spectrometer. The resolution was $4cm^{-1}$, the scanning area was $4000-400 cm^{-1}$, the scanning frequency was 256.

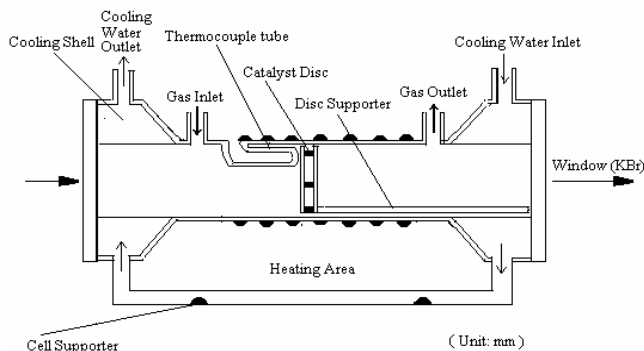


Figure 1. In-situ FT-IR Quartz Cell



Figure 1b. Disc Quartz Supporter

RESULTS AND DISCUSSION

CONFIRMATION OF REACTION PRODUCT

It was confirmed by IR spectrum of methane standard gas (99.99%) that there was methane in the reaction product. Figure 2 shows the IR spectrum of methane standard gas and the reaction product of CO and H_2 . There were two broad infrared bands at 3020 and $1310 cm^{-1}$ emerged on the IR spectrum of methane standard gas, which were coincided with two infrared bands on the IR spectrum of reaction products of CO and H_2 . It showed that there might be methane existed in the reaction products of CO and H_2 . It means that gaseous CO_2 in the IR cell might cause the bands at $2200-2400 cm^{-1}$ and the band at $1400-1600 cm^{-1}$ may be due to H_2O , H_2O is one of the reaction products of CO hydrogenation. On the existing of H_2 , the main reaction is hydrogenation, but the disproportionation of CO may have occurred (to form CO_2 and C). This experiment mainly observes and studies the hydrogenation activity about molybdenum nitride catalyst. CH_4 is main hydrogenation product in the reaction of CO probe molecule hydrogenation and CH_4 did not react to form C_2 further, which showed the high selectivity of CO hydrogenation on the surface of molybdenum nitride catalyst.

Figure 3 shows the effect on the IR spectra about reaction products that are formed by CO hydrogenation reaction on the surface of molybdenum nitride catalyst different time. It shows obviously that methane IR spectra peak area will increase while the reaction time increasing when we compare IR spectra peak area on different time. The peak area will characterize the hydrogenation activity of catalysts instead of the concentration of reaction products because it is proportionate with concentration of reaction products, when we deal with the experimental data.

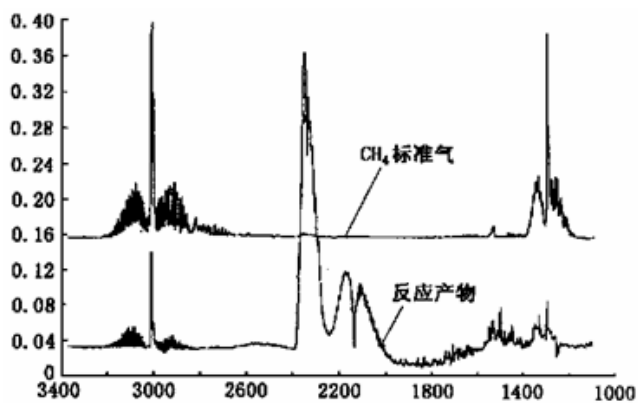


Figure 2. Spectra of the production of CO hydrogenation and pure methane

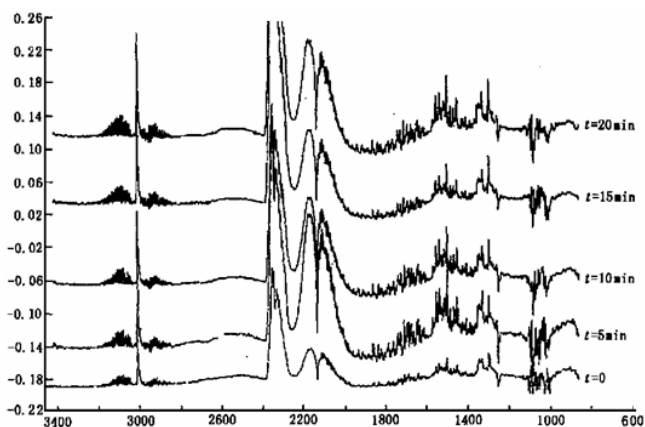


Figure 3. Spectra of the production of CO hydrogenation on Mo₂N

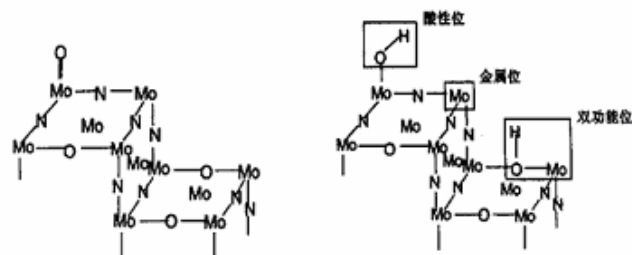
INFLUENCE FACTORS OF HYDROGENATION ACTIVITY ON THE (Co-PROMOTED) MOLYBDENUM NITRIDE CATALYST

H₂-reduction pretreatment

In order to find the influence factors of CO hydrogenation activity about molybdenum nitride catalyst, we compared CO hydrogenation activity on different time about Mo₂N and CoMoN_x catalysts before H₂-reduction pretreatment with after H₂-reduction pretreatment, and compared them with CO hydrogenation activity of MoS₂ catalysts. The result shows in the table1. Table1 shows: ① It is the same result to Mo₂N and CoMoN_x catalysts that CO hydrogenation activity will be reduced after catalysts were hydrogenation reduction; ② CO hydrogenation activity will be increased by adding Co into molybdenum nitride catalyst; ③ Hydrogenation activity of passivated molybdenum nitride catalysts is lower than that of MoS₂ catalysts. The reason is the surface structure of passivated molybdenum nitride catalysts is high dispersing molybdenum nitride oxide due to introduce O₂ after molybdenum nitride catalysts were passivated (figure 4-a). Oxides atom and hydrogen atom dissociated from hydrogen molecule formed to -OH, which improve the acidity of catalysts and reduce the metallic property of catalysts (hydrogenation activity) (figure4 (b)). Catalytic hydrogenation promoter of Co is mainly depended on its the ability of high-activated hydrogen, and at the same time its lower hydrogen adsorptivity improve hydrogenation activity of catalysts, because Co addition improve the quantity of hydrogen fugacity.

Reaction temperature

Figure2 shows CO hydrogenation activity of Mo₂N and CoMoN_x catalysts on different reaction temperature and reaction time (showed by CH₄ peak area). While reaction temperature increasing, CO hydrogenation activity increases obviously. In the proper temperature range, addition of Co will improve hydrogenation activity.



(1) passivated molybdenum (2) reduced molybdenum

Figure 4. The surface layer structure of Mo₂N

CONCLUSIONS

The production of molybdenum nitride and Co-promoted molybdenum nitride has been obtained from the temperature-programmed reduction of molybdenum oxides with the mixture of N₂-H₂ gases. The BET surface areas of molybdenum nitride and Co-promoted molybdenum nitride are 165 and 158m²/g respectively. The CO hydrogenation activity was measured by FT-IR in-situ method. It is showed high activity and selectivity of methane formation. It is the same result to Mo₂N and CoMoN_x catalysts that CO hydrogenation activity will be reduced after catalysts were hydrogenation reduction. Addition of Co will improve hydrogenation activity; Hydrogenation activity of passivated molybdenum nitride catalysts is lower than that of MoS₂ catalysts.

REFERENCE

- (1) OYAMAST, Preparation and catalytic properties of transition metal carbides and nitrides[J]. Catalysis Today, 1992, 15:179-200
- (2) M. Lin, Practical FT-IR Spectroscopy, Publishing House of Chinese Environment, Beijing, 1991.
- (3) A. Jayasooriya, M.A. Chesters, M.W. Howard, et al., Surf.Sci. 93 (1980) 526.
- (4) W.M. Mandy and H.R. Colin, J. Catal. 141 (1993) 355.
- (5) M.R. Prairie, J.G. Highfield and A. Renken. Chemical Engineering Science, 46 (1991) 113
- (6) B. Robert and C. Sophia, Surf. Sci, 87 (1991) 1791

CHEMISTRY-AIDED DESIGN OF FUTURE CLEAN FUELS

Edward L. Sughrue and Uday T. Turaga

Bartlesville Technology Center, ConocoPhillips Company,
Bartlesville, OK 74004

Introduction

During most of the last century, refining research focused on maximizing the production of fuels and petrochemicals from a barrel of petroleum and improving the properties of fuels to meet the demands of the automakers' newer engines. This produced a number of processes such as catalytic cracking, alkylation, and catalytic naphtha reforming [1]. Societal demands for a cleaner environment and the resulting Clean Air Act in 1970 shifted the focus of refining research and catalyzed the advent of clean fuels, which first appeared in the form of lead-free gasoline.

The Increasing Stringency of the Regulatory Ladder

Lead removal was the first in a series of developments influencing the evolution of gasoline. These developments are described in the regulatory ladder shown in Figure 1. Lead removal is at the foot of the ladder followed by reformulated gasoline (RFG) with lower vapor pressure and the addition of oxygenates. We are currently at the step mandating gasoline sulfur content less than 30 ppm. At higher steps in the ladder, even lower sulfur levels such as 10 ppm or less could be mandated. The elimination of benzene and methyl *tertiary*-butyl ether (MTBE) from gasoline will likely be formalized in the near future. Similarly, addition of renewable fuels such as ethanol is anticipated. At the top of the ladder is the Driveability Index (DI), which is being discussed increasingly in the context of a more consistent fuel.

The arrows at the top of the ladder in Figure 1 imply that new clean fuels regulations will continue beyond those discussed here which are critical but not exhaustive. The ladder represents the increasing difficulty of producing clean fuels that meet increasingly stringent regulations. Each new regulation places a new constraint on the properties of allowable fuels. The property constraints in turn limit what can be blended into the gasoline pool thus defining what refining processes can produce. For example, the loss in octane because of the phase-out of lead was offset by catalytic naphtha reforming, alkylation, and the addition of MTBE.

Clean Fuels from Fuel Composition and Properties

Relating the properties of a fuel to its composition reveals the impact that regulations have on both fuel and refinery process chemistry. For example, reducing fuel vapor pressure impacts the amount of C₄ and C₅ hydrocarbons allowed in the fuel. Similarly, any reductions in DI reduce the permissible amounts of C₉ and C₁₀ aromatics in gasoline. Removing these light hydrocarbons or heavy aromatics reduces gasoline's octane and also demands a home for the now orphan streams. While C₉ aromatics have high octane numbers, they have poor cetane values and make inferior quality diesel. Therefore, after removal from gasoline, their alternative use is as fuel gas and fuel oil, both of which are not high-value markets.

Fuel composition and properties also enable insight for the design of tools and techniques to produce clean fuels. One such example relates to hydrodesulfurization of diesel fuels. Analytical methods were developed in the early 1990s to routinely identify—accurately and quantitatively—the types of sulfur molecules present at ppm levels. Concurrently reaction kinetics for different sulfur

compounds had been accurately described [2]. Combining analytical measurements with fundamental kinetics led to the development of sophisticated reactor and process models. Currently, at ConocoPhillips, catalyst hydrodesulfurization activity data from a standardized laboratory reactor test is combined with the feed sulfur distributions and other compositional properties in a reactor model to predict product sulfur concentrations, hydrogen consumption, and catalyst life for new and existing hydrodesulfurization units. This approach facilitates the determination of optimal solutions for low-sulfur diesel at each of our 15 different refineries.

Low-Sulfur Gasoline Without Octane Loss

Detailed compositional analyses combined with reaction kinetics have also proven useful in the production of low-sulfur gasoline. Regulations mandating low-sulfur gasoline raised the issue of removing sulfur without losing octane. Most of the sulfur in gasoline is associated with the gasoline produced in the catalytic cracker. This gasoline also contains 20-30% olefins, which contribute to the fuel's octane. Attempts to reduce sulfur through hydrodesulfurization of gasoline results in the hydrogenation of olefins to paraffins causing significant loss of octane. A comparison of the distribution of sulfur and olefins by boiling points shows that a higher percentage of the olefins boil below 180 °F while most of the sulfur compounds boil above 250 °F. This led some to fractionate the light end off gasoline feedstocks followed by hydrotreatment of only the heavy fraction.

While such a strategy might work for sulfur specifications of 30 ppm, the prospect of intensifying regulations specifying sulfur content to levels as low as 10 ppm calls for a greater understanding of the olefin-sulfur interactions. It is interesting to note that although 50% of the olefins in gasoline are in the C₅ fraction, the hydrogenation of olefins in the C₆ and C₇ fraction results in greater octane loss (Figure 2). For example the hydrogenation of methyl-2-butene to iso-pentane actually increases road octane from 90 to 91.5, while the hydrogenation of 2-methyl-2-hexene reduces octane from 87 to 44. It may also be noted that thiophene boils very near the C₇ olefins. Furthermore, at high olefin concentrations, Langmuir-Hinshelwood kinetics of olefin hydrogenation predict a rate dependence on olefins closer to zero than one. This implies that leaving the C₅ olefins in the feed to compete with the C₇ olefins for hydrogenation sites will actually reduce octane loss.

It is therefore clear that desulfurization through separation or fractionation has limited potential for effective desulfurization. In light of this, a different set of investigations were begun to answer the question, "Is it possible to remove sulfur without significant hydrogenation?" These investigations resulted in ConocoPhillips' proprietary S Zorb Sulfur Removal Technology, which uses certain metal combinations capable of adsorbing and decomposing thiophenic sulfur with only minimal olefin saturation and without forming any hydrogen sulfide. The ability to accomplish desulfurization without the formation of hydrogen sulfide is a critical advantage of the S Zorb Sulfur Removal Technology over hydrotreating. Hydrogen sulfide, produced during hydrotreating, is known to react with olefins and form mercaptans, thereby enhancing product sulfur.

The Utility of Olefins Beyond Octane Loss

While retention of olefins for the sake of gasoline octane is good, future clean fuel issues demand increased understanding and value for olefins. Of the different types of hydrocarbons available to petroleum and fuel chemists, olefins are the most reactive and undergo a suite of reactions including alkylation, dimerization, and

cracking at conditions much milder than demanded by corresponding paraffins, aromatics, and naphthenes. For example, C₉ and C₁₀ aromatics can be alkylated with C₅ and C₇ olefins to produce diesel-range material with acceptable cetane numbers. Similarly, dimerization of C₅ olefins could reduce vapor pressure. Olefins offer such versatility and flexibility, which need better understanding and creative utilization to unlock issues that will dominate the future of clean fuels.

Conclusions

The future of clean fuels will continue to be both challenging and full of opportunities for creative chemists and chemical engineers. A critical tool toward the development of processes and products for producing clean fuels will be a strong understanding of the fundamentals of fuel chemistry. Recent advances in analytical techniques, kinetic modeling of fuel components, catalysis and materials, and reactor engineering will enable the production of a new generation of clean fuels.

References

1. Martino, G.; Courty, P.; and Marcilly, C. In *Handbook of Heterogeneous Catalysis*; Ertl, G.; Knozinger, H.; and Weitkamp, J.; Eds.; VCH: Berlin, Germany, **1997**; pp. 1801-1818.
2. Girgis, M. J. and Gates, B. C. *Ind. Eng. Chem. Res.* **1991**, *30*, 2021-2058.

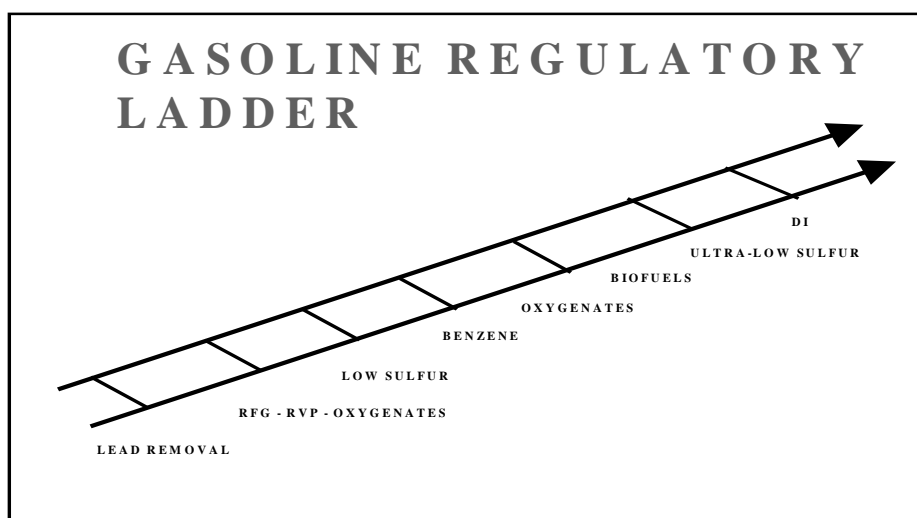


Figure 1. The issues that constitute the increasingly stringent regulatory ladder.

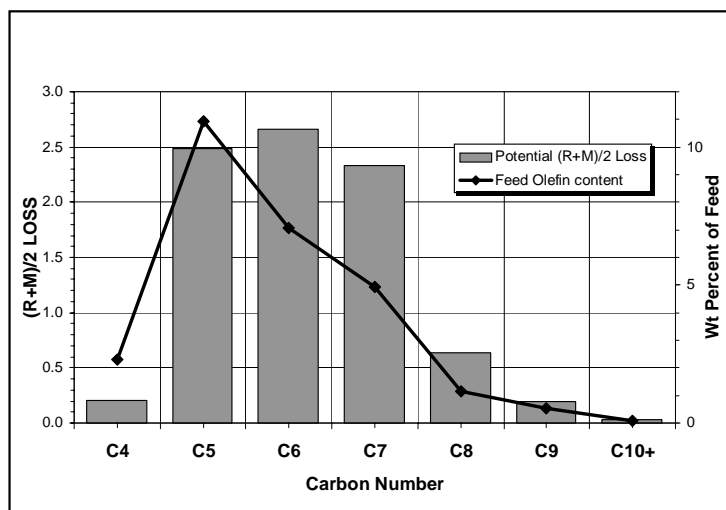


Figure 2. Olefins distribution and potential octane loss for gasoline.

ADSORPTIVE DESULFURIZATION OF DIESEL FUEL OVER A METAL SULFIDE-BASED ADSORBENT

Xiaoliang Ma, Lu Sun, and Chunshan Song*

Clean Fuels and Catalysis Program, The Energy Institute and
Department of Energy and Geo-Environmental Engineering,
The Pennsylvania State University, 209 Academic Projects Building,
University Park, PA 16802
*E-mail: csong@psu.edu

Introduction

Ultra-deep removal of sulfur from diesel fuel is important for environmental protection and fuel cell applications (1,2). The current hydrodesulfurization technology is difficult to reduce the sulfur content in diesel fuel to less than 10 ppmw, because the remaining sulfur compounds in the current commercial diesel fuel are the refractory sulfur compounds, the alkyl dibenzothiophenes with one and/or two alkyl groups at the 4- and/or 6-positions (1,3,4). On the other hand, the conventional hydrodesulfurization technology has to be operated at high temperature and high pressure with hydrogen, resulting in high cost for the ultra-deep hydrodesulfurization. Selective adsorption desulfurization is a promising technology for the ultra-deep desulfurization of diesel fuel. We are exploring a new approach at Penn State called selective adsorption for removing sulfur (PSU-SARS), for ultra-deep removal of sulfur from liquid hydrocarbon fuels (1, 2, 5-11).

The major challenge to our proposed approach is to selectively adsorb sulfur compounds onto the surface of the solid adsorbent but leave the coexisting hydrocarbons including aromatic and olefinic hydrocarbons as well as saturated hydrocarbons, untouched. On the other hand, for the industrial applications one of the key points in the adsorptive desulfurization process is to develop the adsorbent that can be regenerated easily. We envision that the interaction between the sulfur compounds and the adsorption sites on the adsorbent should be selective and suitable in strength. The too strong interaction between them will cause a difficulty in the subsequent regeneration process, while the too weak interaction probably results in a low adsorption selectivity and low capacity. In the present approaches we attempted to develop a metal-sulfide-based adsorbent that not only can selectively adsorb the sulfur compounds but also can be easily regenerated without using hydrogen gas.

Experimental

Two model diesel fuels (MD-1 and MD-2) were used in the present study. MD-1 contains the same molar concentration (3.9 mmol/L) of dibenzothiophene (DBT), 4-methyldibenzothiophene (4-MDBT) and dimethyldibenzothiophene (4,6-DMDBT), and 1-methylnaphalene (1-MNA). MD-2 contains only one sulfur compound, DBT. The total sulfur concentration in MD-1 and MD-2 is 486 and 200 ppmw, respectively. MD-1 and MD-2 also contain 10 wt% of n-butylbenzene for mimicking the aromatics in the real diesel. The detailed composition of the model diesel fuels is listed in Table 1 and 2. The sulfur compounds and hydrocarbons contained in the fuels were purchased from Aldrich without further treatment before use.

The adsorbent used in the present study was Adsorbent-6, which was prepared from CoMo oxides supported on γ -alumina (CoMo/ γ -Al₂O₃; CoO: 3wt%; MoO₃: 14wt%; Surface area: 183 m²/g; Pore volume: 0.4755 ml/g; Average pore size: 102 Å). CoMo/ γ -Al₂O₃ was sulfided at 350 °C with 10 vol % H₂S in H₂ at a flow rate of 200 ml/min for 4 h. The sulfided CoMo/ γ -Al₂O₃ was cooled to room temperature under the same atmosphere, and then, kept into hexane before use. Adsorbent-6 was obtained by treating the sulfide CoMo/ γ -Al₂O₃ with H₂ at 300 °C for 60 min. About 2 g of the sulfided

CoMo/ γ -Al₂O₃ was parked into a stainless steel column with internal diameter of 4.6 mm and length of 150 mm. The adsorbent bed volume was 2.49 ml. H₂ gas was passed through the column at ambient pressure and a flow rate of 20 ml/min. After the treatment, the column temperature was reduced to the assigned temperatures for the adsorption.

The adsorption experiments were performed at ambient pressure without using H₂ gas. The model diesel fuel was fed into the column and flowed up through the adsorption bed. The flow rate was 0.2 ml/min, corresponding to a LHSV of 4.8 h⁻¹. The treated model fuel was collected for analysis. The regeneration of the spent adsorbents was accomplished by washing the adsorbent with a polar solvent followed by heating the adsorbent to remove the remaining solvent. The polar solvent was pumped through the adsorbent bed at 60 °C and a LHSV of 4.8 h⁻¹. After washing, the adsorbent bed was heated to 300 °C under a nitrogen flow at 20 ml/min for 1 h, and then, was cooled to the assigned temperature for the subsequent adsorptive desulfurization.

Analysis of concentration of sulfur compounds in the treated MD-1 was performed by using GC with a capillary column, XTI-5 (Restek) 30 m x 0.25 mm x 0.25 μ m, and a flame ionization detector (FID). An Antek 9000 Series Sulfur Analyzer (detection limit 0.5 ppmw) was used for determining sulfur concentration in the treated MD-2.

Results and Discussion

Figure 1 shows the molar concentration of sulfur compounds and 1-MNA at the outlet as a function of the effluent amount for the adsorptive desulfurization of MD-1 over Adsorbent-6 at 50 °C. The first break-through compound was 1-MNA with a break-through point at 0.2 g/g (gram of MD-1 per gram of adsorbent) and a saturation point at 1.6 g/g. The second one was 4,6-DMDBT with a break-through point at 0.4 g/g. The concentration of 4,6-DMDBT was kept below 0.2 mmol/l before the effluent amount reached 2.5 g/g, and then, increased quickly to the saturation point at 4.4 g/g. Break-through point of 4-MDBT was at 2.5 g/g with a saturation point at 5.0 g/g. The last break-through compound was DBT with a break-through point at 3.5 g/g and a saturation point at > 5.5 g/g. It is clear that Adsorbent-6 has much higher selectivity to adsorb DBTs compared to aromatics represented by 1-MNA. As is well known, 1-MNA has a higher π -electron density on its aromatic ring than that of DBTs (9), although the aromatic ring size of the former is smaller than that of the latter. It is clear that interaction between the S atom and the adsorption sites plays an important role in the competitive adsorption between DBTs and 1-MNA. From a comparison of DBT, 4-MDBT and 4,6-DMDBT, the adsorption selectivity increases in the order of 4,6-DMDBT < 4-MDBT < DBT, implying that the methyl groups at the 4 and 6-positions inhibit the interaction between the S atom and the adsorptive sites on the adsorbent, which results in the decrease in the adsorption capacities of 4,6-DMDBT and 4-MDBT.

It should be noted the system we used is based on selective adsorption, not reaction. No detectable biphenyls and cyclohexylbenzenes type products were found in the effluent, indicating that no HDS reaction takes place at such conditions.

Adsorption desulfurization of MD-2 over Adsorbent-6 was conducted at 50 °C under ambient pressure. The total sulfur concentration at outlet as a function of the treated MD-2 amount is shown in Figure 2. When the treated MD-2 amount was less than 2.5 g/g, the sulfur concentration at outlet was less than 10 ppmw. After 2.5 g/g of the effluent amount, the sulfur concentration increased sharply with increasing the effluent amount. Adsorbent-6 was saturated when the effluent amount reached about 8 g/g. The adsorptive capacity corresponding to the break-through point at 10 ppmw sulfur level and the saturation point was 0.65 and 0.77

milligram of sulfur per gram of adsorbent (mg-S/g-A), respectively. Adsorption desulfurization of MD-2 over Adsorbent-6 at 150 °C was also conducted, but the performance was poorer than that at 50 °C. This indicates that lower temperature is better for the adsorptive desulfurization over this type of adsorbents, in contrast to the nickel-based adsorbents (12).

After regeneration of the spent adsorbent, the adsorption performance of the regenerated adsorbents was tested. The adsorption break-through curves for the regenerated adsorbents are shown in Figure 2 in comparison with the curve for the fresh adsorbent. It shows clearly that the break-through curves for the 1st regenerated adsorbent and the 2nd regenerated adsorbent coincide well with that for the fresh adsorbent, especially when the treated MD-2 amount is less than 4 g/g. The adsorption capacity corresponding the break-through point at 10 ppmw sulfur level for the 1st regenerated adsorbent and the 2nd regenerated adsorbent is 0.65 and 0.66 mg-S/g-A, respectively. It implies that the spent adsorbent can be regenerable, and almost all adsorption capacity in the adsorbent can be recovered by our developed method.

Acknowledgments. We gratefully acknowledge the financial support by US Department of Energy and US Department of Defense.

References

1. Song, C., Ma, X., *Appl. Catal. B.*, 41 (1-2), 207-238 (2003).
2. Song, C. *Catalysis Today.*, 77 (1), 17-50 (2002).
3. Ma, X., Sakanishi, K., Mochida, I., *Ind. Eng. Chem. Res.* 33, 218 (1994).
4. Gates, B.C., Topsoe, H., *Polyhedron* 16, 3213 (1997).
5. Ma, X, Sun, L., and Song, C., *Catal. Today*, 77, 107-116 (2002).
6. Velu, S., Ma, X., and Song, C., *Am. Chem. Soc. Div. Petr. Chem. Prepr.*, 48 (2), 58-59 (2003).
7. Velu, S., Watanabe, S., Ma, X., and Song, C., *Am. Chem. Soc. Div. Petr. Chem. Prepr.*, 48 (2), 56-57 (2003).
8. Ma, X., Sprague, M., Sun, L., and Song, C., Ultra-Deep Desulfurization of Gasoline and Diesel for Fuel Cell Applications by SARS Adsorbent and Process. Materials Research Society Fall 2002 National Meeting, Boston, Dec. 2-6, 2002
9. Ma, X., Sprague, M., Sun, L., and Song, C., *Am. Chem. Soc. Div. Fuel Chem. Prepr.*, 47, 452 (2002).
10. Velu, S., Ma, X., and Song, C., Zeolite-Based Adsorbents for Desulfurization of Jet Fuel by Selective Adsorption. *Am. Chem. Soc. Div. Fuel Chem. Prepr.*, 47, 457 (2002).
11. Ma, X., Sun, L., Yin, Z. and Song, C., *Am. Chem. Soc. Div. Fuel Chem. Prepr.*, 46 (2), 648-649 (2001).
12. Ma, X., Velu, S., Sun, L., and Song, C., *Am. Chem. Soc. Div. Fuel Chem. Prepr.*, 48, (2003), in submission.

Table 1 Composition of MD-1

No.	Name	Concentration		
		wt %	mmol/l	ppmw
Sulfur compounds				
1	DBT	0.095	3.93	165
2	4-MDBT	0.099	3.81	160
3	4,6-DMDBT	0.107	3.85	162
Total Sulfur			11.59	486
4	Naphthalene (99%)	0.067		
5	2-methylnaphthalene (98%)	0.074	3.85	
6	n-Hexadecane(99+%)	39.97		
7	n-Dodecane(99+%)	39.50		
8	n-Tetradecane (99+%)	0.109		
9	Decalin(99+%)	9.988		
10	t-Butylbenzene(99%)	9.988		

Table 2 Composition of MD-2

No.	Name	Concentration		
		wt %	mmol/l	ppmw
1	DBT (99+%)	0.115	4.84	200
2	1-Methylnaphthalene(97%)	0.090	4.89	
3	n-Hexadecane(99+%)	88.67		
4	n-Tetradecane (99+%)	0.122		
5	n-Butylbenzene(99%)	10.01		
Others		1.00		

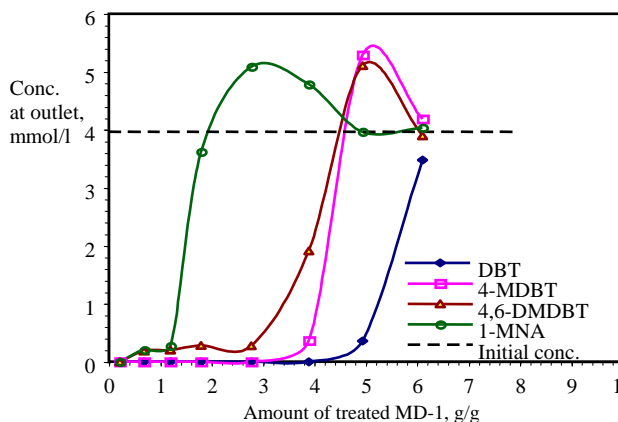


Figure 1. Break-through curves of MD-1 over Adsorbent-6

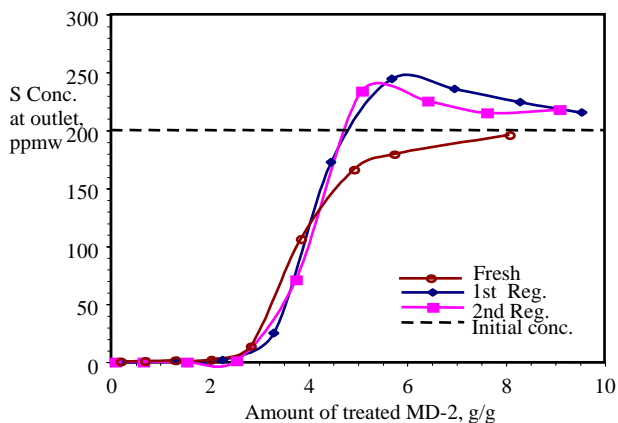


Figure 2. Break-through curves of MD-2 over fresh and regenerated adsorbents at 50°C

ADSORPTIVE REMOVAL OF SULFUR COMPOUNDS FROM NAPHTHA FRACTIONS BY USING CARBON ADSORBENTS

Kinya Sakanishi*, Hamdy Farag, Shinya Sato, Akimitsu Matsumura, and Ikuo Saito

National Institute of Advanced Industrial Science and Technology (AIST), Tsukuba West, Ibaraki 305-8569, Japan

Introduction

Ultra-deep desulfurization of gasoline and diesel fuels is aimed to produce sulfur-free fuels or their sulfur contents below 10 ppm for the environmental protection in urban areas. To develop fuel cell vehicles in the future, olefin and aromatic compounds as well as sulfur compounds are to be removed to extremely low levels of less than percent levels of the former two compounds and tens of ppb levels of sulfur compounds.¹⁻³

Hydrodesulfurization(HDS) of gasoline and diesel fuels has been widely applied in petroleum refineries for the production of such sulfur-free fuels, however, reduction of sulfur levels below 10 ppm is hardly achieved by conventional catalysts under HDS process conditions.⁴ Much higher activity and selectivity of HDS catalysts should be designed for the removal of refractory sulfur compounds in petroleum light products.

Adsorptive removal processes of sulfur compounds from petroleum distillates have been also developing for the complete capture to achieve the sulfur levels below ppm order. Some of such adsorptive sulfur removal procedures are expected to produce sulfur-free gasoline and diesel fuels because of their simple and energy-saving manner without hydrogen consumption. Although variable kinds of adsorbents have been screened for the achievement of sulfur-free fuel production, effects of coexisting aromatic compounds on the adsorption selectivity of sulfur compounds are not fully elucidated.

Carbon adsorbents such as active carbon and active carbon fiber are one of the most promising materials for the selective removal of sulfur compounds at relatively low temperatures around room temperatures due to their extremely high surface area and very uniform pore size distribution with weak polarity.⁵

In the present study, some of mesoporous carbon adsorbents are investigated to estimate their adsorption capacity and selectivity for sulfur compounds such as benzothiophene(BT) and 2-methyl-benzothiophene(2MBT) and in their mixture with some aromatic compounds as model feedstocks. In addition, a real naphtha fraction is also treated with active carbons of different surface areas and particle sizes with or without dilution with n-hexane solvent. Mesoporous active carbons of finer particles are revealed to be preferable for the selective adsorption of two-ring sulfur compounds such as BT and 2MBT.

Experimental

Some properties of carbon adsorbents used in the present study are summarized in Table 1. Three types of active carbons(MaxSorb, Diahope, and Alkali-activated carbon prepared from Marlim Brazilian vacuum residue: MarVR-AC) and a carbon black(Ketjen Black) are selected for the comparison of adsorption capacity and selectivity. All of the active carbons were ground to < 60 mesh and dried at 333 K under vacuum prior to the adsorption experiment.

A simple model feedstock of BT(0.05 g) in 10 cc n-heptane was prepared for the evaluation of adsorption capacity. A series of model solutions of toluene(T), naphthalene(N), 1-methylnaphthalene(1MN),

and 2-methylbenzothiophene(2MBT) were prepared for the evaluation of adsorption selectivity. These solutions were mixed with 0.5 g of carbon adsorbent and stirred for 1 h at room temperature.

10 g of a real naphtha fraction supplied from Japan Energy Co.(sulfur content: ca.300 ppm; b.p. range: 70-151°C) and its 10 wt% solution diluted with n-hexane were also treated with 0.1 g of active carbon for checking the adsorption ability of carbon adsorbents.

Model solutions and real naphtha fractions were analyzed by GC-AED before and after the adsorption treatment.

Results and Discussion

First of all, detection limit of sulfur compounds by GC-AED was examined by changing the measurement conditions such as split ratios, injection amounts, and gas flow rates with a series of standard BT solutions in their concentrations of 87.2 ppm, 7.44 ppm, 0.84 ppm, 0.071 ppm, and 8.7 ppb. It is revealed that about 0.05 ppm(50 ppb) of BT can be detected by GC-AED measurement by adjusting the split ratio to 1:1 and the injection amount to 2 ul. GC-AED can be a powerful tool for the detection of tens ppb level of sulfur compounds, enabling us to check the quality of nearly sulfur-free fuels.

Adsorption capacity of carbon adsorbents for BT is summarized in Table 1. Among the carbon adsorbents examined in the present study, the adsorption capacity was in the order of Diahope [0.083 (g-BT / g-adsorbent)] > Ketjen Black [0.062] > MaxSorb [0.056] > MarVR-AC [0.041]. It seems that relatively mesoporous active carbons may be preferable for the selective adsorption of BT.

Table 1
Some properties of carbon adsorbents and their adsorption capacity for benzothiophene (BT) *

Carbons	S.A. (m ² /g)	Av.pore dia. (nm)	Pore vol. (ml/g)	Ads. for BT (g / g)
MaxSorb (active carbon)	3370	0.37	1.88	0.056
Diahope (active carbon)	1150	1.2	0.70	0.083
Ketjen Black (carbon black)	1270	< 0.3	1.39	0.062
MarVR-AC (active carbon)	2150	1.9	1.05	0.041

* BT 0.05 g in 10cc n-heptane with 0.5 g carbon at r.t for 1 h

Adsorption selectivity of each model compound on Diahope powder was summarized in Table 2. Roughly speaking, adsorption ratio of each substrate increase with its molecular weight or molecular size, however, it is suggested that sulfur compounds may be more selectively adsorbed on Diahope powder.

Table 2 Adsorption selectivity of each model compound*

	Adsorption (%)
Toluene	10
Naphthalene (Np)	31
1-methylnaphthalene(1MN)	25
Benzothiophene (BT)	83
2-methylbenzothiophene(2MBT)	89

* 0.05 g of each substrate in 10 cc n-heptane with 0.5 g

Diahope(< 60 mesh) at r.t. for 1h

Adsorption selectivity of mixed model compounds on Diahope powder was summarized in Table 3. Adsorption ratios of sulfur compounds decreased significantly with increased adsorption ratios of two-ring aromatic compounds, indicating large interference of similar-sized aromatic compounds against sulfur compounds. It is noted that a single ring aromatic compound of toluene may not be adsorbed so much as two-ring aromatic compounds, suggesting that a majority of one-ring aromatic compounds in gasoline and naphtha fractions may not interfere with the adsorption of sulfur compounds.

Table 3 Adsorption selectivity of mixed model compounds*

	Adsorption (%)
Toluene	8.5
Naphthalene (Np)	39
1-methylnaphthalene(1MN)	35
Benzothiophene (BT)	54
2-methylbenzothiophene(2MBT)	62

* 20% of five model solutions mixed and treated with 0.5 g Diahope(< 60 mesh) at r.t. for 1h

According to the sulfur-chromatograms of the naphtha feedstock analyzed by GC-AED before and after the adsorption treatment, the original naphtha fraction mainly consisted of alkylated thiophene derivatives with a small amount of benzothiophene and its alkylated derivatives, and the benzothiophene derivatives were selectively removed by the adsorption treatment, although such two-ring aromatic sulfur compounds are relatively minor components.

Table 4 compares the adsorption behaviors of two active carbons of Diahope and MaxSorb with two levels of particle sizes of < 60 mesh and 60-100 mesh for neat naphtha fraction. It is revealed that a very small amount of sulfur compounds as low as a few percents were adsorbed in all the cases examined in the present study regardless of the carbon types and particle sizes. The recovery yield of the naphtha feedstock was also as low as 80%, indicating the difficulty in the selective adsorption of sulfur compounds and in the effective recovery of non-adsorbed species from the carbon adsorbents.

Table 4 Adsorption treatment of neat naphtha fraction using active carbon powders*

Adsorbent	Adsorbed S(%)	Recovery(%)
Diahope (< 60 mesh)	2.8	79
Diahope (60 - 100 mesh)	1.9	83
Maxsorb (< 60 mesh)	3.5	78
Maxsorb (60 – 100 mesh)	2.1	81

* 10 g of neat naphtha solution was stirred with 0.1 g active carbon at r.t. for 1h

Table 5 summarizes the adsorption amount of sulfur compounds from real naphtha fraction when it was diluted with n-hexane to 10wt% before the adsorption treatment. Although the adsorbed amount of sulfur compounds remained low even if the naphtha fraction was diluted to 10%, finer particles of the active carbons gave slightly higher adsorption capacity. MaxSorb gave the larger adsorption capacity for sulfur compounds in real naphtha feedstock in comparison to Diahope, probably due to its higher surface area and pore volume regardless of their particle sizes.

In addition, recovery yields of the naphtha fraction after the adsorption treatment were always above 90 %, suggesting that n-hexane solvent may not only improve the adsorption efficiency of sulfur compounds by enhancing the diffusion into the pore structure

of the carbon adsorbent, but also facilitate the separation and recovery of non-adsorbed species from the carbon adsorbent.

Table 5 Adsorption treatment of 10wt% naphtha fraction diluted with n-hexane by using active carbon powders*

Adsorbent	Adsorbed S(%)	Recovery(%)
Diahope (< 60 mesh)	11	95
Diahope (60 - 100 mesh)	9.5	97
Maxsorb (< 60 mesh)	21	92
Maxsorb (60 – 100 mesh)	16	93

* 10 g of naphtha solution(10wt%) was stirred with 0.1 g active carbon at r.t. for 1h

Table 6 summarizes the adsorption behaviors of mixed sulfur compounds which consists of each 1wt% of 2-methylthiophene (2MT), ethylphenylsulfide(EPS), benzothiophene(BT), and 2-methylbenzo-thiophene(2MBT), and diphenylsulfide(DPS) dissolved in n-hexane solvent. Two-ring aromatic sulfur compounds were more selectively adsorbed on Diahope powder, reflecting from their molecular sizes in the order of BT < 2MBT < DPS. It is suggested that microporous carbon adsorbents may be favorable for the removal of one-ring sulfur compounds such as 2MT and EPS. Otherwise, the conventional catalytic hydrodesulfurization treatments are preferable for the removal of such one-ring aromatic sulfur compounds because of their much higher reactivity under the milder conditions compared to two-ring and three-ring aromatic sulfur compounds.

Table 6 Adsorption selectivity of mixed sulfur model compounds *

	Adsorption (%)
2-methylthiophene(2MT)	21
Ethylphenylsulfide (EPS)	33
Benzothiophene (BT)	52
2-methylbenzothiophene(2MBT)	59
Diphenylsulfide(DPS)	68

* 1wt % of five model sulfur compounds dissolved in n-hexane solvent mixed with 0.5 g Diahope(< 60 mesh) at r.t. for 1h

Conclusion

The present study revealed that relatively mesoporous active carbons with finer particle size may be preferable for the selective adsorption of two-ring sulfur compounds such as BT and 2MBT contained in the naphtha fraction. Hydrogenative removal of one-ring sulfur compounds with the adsorption treatment had better be combined for the more effective and optimized desulfurization procedures.

Acknowledgment

The work has been entrusted by the New Energy and Industrial Technology Development Organization under a subsidy of the Ministry of Economy, Trade and Industry.

References

- Song, C., *Prepr. ACS Div. Fuel Chem.*, **2002**, 47(2), 438.
- Ma, X., Sun, L., Song, C., *Catalysis Today*, **2002**, 77(1), 107.
- Ma, X., Sprague, M., Sun, L., Song, C., *Prepr. ACS Div. Petrol. Chem.*, **2002**, 47(1), 48.
- Whitehurst, D.D., Isoda, T., Mochida, I., *Advan. Catal.*, **1998**, 42, 345
- Sano, Y., Choi, K., Korai, Y., Mochida, I., *Prepr. ACS Div. Fuel Chem.*, **2003**, 48(1), 138

REGENERABLE ADSORBENTS FOR THE ADSORPTIVE DESULFURIZATION OF TRANSPORTATION FUELS FOR FUEL CELL APPLICATIONS

S. Velu, Shingo Watanabe, Xiaoliang Ma, and Chunshan Song*

Clean Fuels and Catalysis Program, The Energy Institute, and
Department of Energy and Geo-Environmental Engineering
The Pennsylvania State University
209 Academic Project Building, University Park, PA 16802
*E-mail: csong@psu.edu

Introduction

The requirement of ultra-clean transportation fuels, particularly, gasoline and diesel, has resulted in a continuing worldwide effort to dramatically reduce the sulfur levels in them. The presence of sulfur in these fuels is a very serious environmental concern because on combustion in the internal combustion engines, the sulfur is converted into toxic SO_x. The Government agencies in various countries have implemented more stringent regulations for refineries to produce gasoline and diesel fuels with reduced sulfur content. For instance, the U.S EPA recently issued a new Tier II regulation that mandates refineries to reduce the sulfur content of gasoline from the current average of 300 ppmw to 30 ppmw by 2005-2006 and to cut down the sulfur content of highway diesel fuel from the current limit of 500 ppmw to 15 ppmw by 2006. Lowering the sulfur content in transportation fuels not only reduces the SO_x emission, but it also contributes to reducing the emissions of other noxious gases such as NO_x and hydrocarbons by allowing the automotive catalytic converters to work better.

The need for the production of ultra-clean gasoline and diesel fuel is further motivated by the rapid development of fuel cells for mobile, stationary and portable power application for which the sulfur levels need to be further reduced down to 1 ppmw. Hydrodesulfurization (HDS) using sulfided Ni-Mo or Co-Mo catalyst at high temperature and high pressure is a conventional method being employed by the refineries to produce low sulfur gasoline and diesel in order to meet the environmental regulations.^{1,2} However, the process is inefficient to produce ultra-clean transportation fuels, particularly for fuel cell applications. Alternative methods such as adsorptive desulfurization, oxidative and extractive desulfurization, biodesulfurization, etc. are being developed in recent years to produce ultra-low-sulfur gasoline and diesel fuels.

Among the alternative methods, adsorptive desulfurization is a promising approach and several new processes, such as IRVAD and Philips S-Zorb processes have been reported recently.^{3,4} The challenges in the adsorptive desulfurization include the following: (i) the adsorbent should be selective to remove only sulfur compounds without adsorbing the aromatics and olefins present the fuel; (ii) for on-board or on-site fuel cell applications, the adsorptive desulfurization should be performed at close to the ambient temperature; and (iii) the adsorbent should be regenerable for subsequent use.

A new process concept is being developed in our laboratory at PSU known as selective adsorption for removing sulfur (PSU-SARS) for the adsorptive desulfurization of gasoline, diesel and jet fuel.^{1,2,5,6} Here we report what may be characterized as the "sense and grab" and "sense and shoot" approaches employed for selectively removing organic sulfur compounds present in these fuels. In the former approach, the sulfur compounds are selectively adsorbed onto certain adsorbents. The adsorbed sulfur compounds are recovered and the adsorbents are

regenerated either by solvent washing or by oxidative regeneration. In the "sense and shoot approach", the sulfur compounds adsorbed onto the adsorbents are decomposed because of the occurrence of surface reactions with adsorbents. The sulfur is retained on the surface of the adsorbent and the remaining organic moiety is added to the fuel. The performance of the adsorbents is regained by reductive regeneration or a combined oxidative and reductive regeneration. In this communication we show few examples for our approaches for the desulfurization of diesel fuels and regeneration of adsorbents by solvent washing and reductive regeneration methods.

Experimental

A wide variety of materials, including metal ions loaded on zeolites or mesoporous materials, mixed metal oxides, hydrotalcite-like anionic clays, metal modified activated carbon, supported metals, etc were tested as adsorbents. Most of these materials were synthesized in our laboratory as described elsewhere.^{1,2,5,6} Either a model fuel containing thiophene (as representative for gasoline) or 4,6-Dimethyldibenzothiophene (4,6-DMDBT; as representative for diesel fuel) or commercial real gasoline / diesel fuels were used as a feedstock. The adsorbent was packed in a stainless steel column with an internal diameter of 4.6 mm and length of 150 mm. The adsorbent bed volume was 2.49 ml. Adsorbents such as zeolite-based, activated carbon and mixed oxides were initially activated at 200°C in N₂ flow to remove any adsorbed gases and then cooled down to the adsorption temperature (60°C). Sulfur-free n-decane was fed into the column using a HPLC pump at a rate of 0.2 ml/min. (LHSV = 4.8 h⁻¹) for about 10 min to remove entrapped gases and then switched to the sulfur containing feed with the same space velocity. Samples were collected periodically and their total sulfur contents were determined using an Antek 9000 Series Sulfur Analyzer (detection limit 0.5 ppmw). A GC equipped with a sulfur selective pulsed flame photometric detector (PFPD) was used to identify the nature of sulfur compounds present in the feed and effluent.

Regeneration of spent adsorbent was performed by solvent washing, oxidative or reductive regeneration. In the solvent washing method, a 1:1 mixture of methanol and toluene was flowed through the adsorbent bed at 70°C until the sulfur in the washing solvent became undetectable. The oxidative regeneration was effected by treating the spent adsorbent by flowing air at 300°C for 2-3 h while the reductive regeneration was performed by flushing the adsorbent with H₂ gas at 500°C for 2-3 h.

Result and Discussion

The sulfur compounds present in gasoline, jet fuel and diesel are derivatives of thiophene (T), benzothiophene (BT) and dibenzothiophene (DBT), respectively. The reactivity of these sulfur compounds in the HDS reaction decreases in the order; thiophene (100) > benzothiophene (30) ≥ dibenzothiophene (30) > MDBT (5) > DMDBT (1).^{7,8} The GC chromatograms obtained using a sulfur selective PFPD for two kinds of low sulfur diesel received from commercial sources are shown in Fig. 1. As can be seen, the 4,6-DMDBT is present as a major sulfur compound even in the diesel fuel containing below 10 ppmw of sulfur. This is the most refractory sulfur compound and is very difficult to remove by the existing the HDS process because of the steric hindrance exerted by the presence of methyl groups at the 4 and 6 positions.

In order to develop regenerable adsorbents for the desulfurization of diesel fuels, a wide variety of new adsorbents based on zeolites, mixed metal oxides, activated carbon and supported metal compounds have been tested using a model diesel fuel containing 220 ppmw of sulfur as 4,6-DMDBT in a

mixture of decane and hexadecane solvents. The breakthrough curves for the adsorptive removal of 4,6-DMDBT from the model diesel fuel at 60°C over transition metal oxides supported on MCM-41 mesoporous material and activated carbon are shown in Fig. 2. It is interesting to note that in both cases, the 4,6-DMDBT has been completely removed. The MCM-41-based adsorbent exhibits a breakthrough capacity of 3.5 mg of sulfur per g of adsorbent while the transition metal supported on activated carbon shows very high breakthrough capacity of 12.6 mg/g of adsorbent.

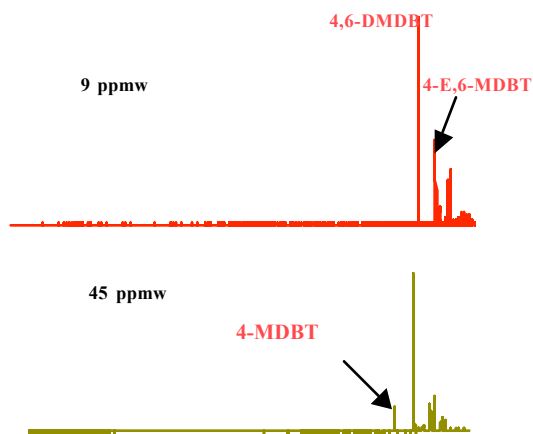


Fig. 1. Sulfur selective GC PFPD Chromatogram of low sulfur diesel fuels containing 9 ppmw and 45 ppmw sulfur

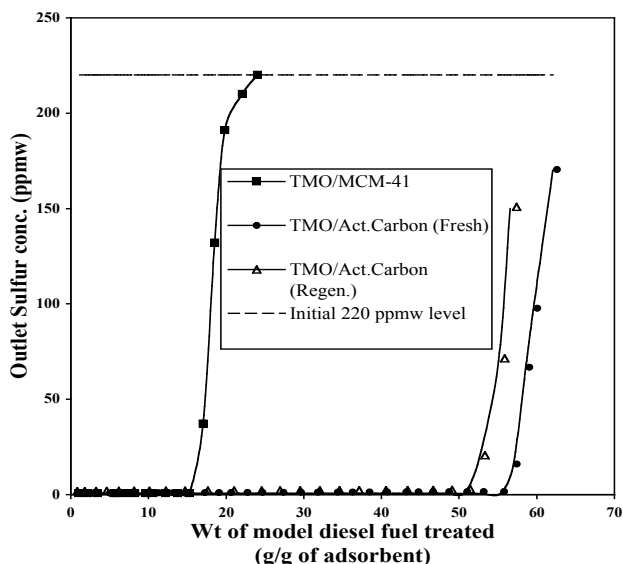


Fig. 2. Breakthrough curves for the adsorptive desulfurization of a model diesel fuel containing 4,6-DMDBT at 60°C over Transition metal oxides supported on MCM-41 and activated carbon. LHSV = 4.8 h⁻¹

Attempt has been made to regenerate these adsorbents by flushing with a 1:1 mixture of methanol and toluene at 70°C. In order to estimate the amount of solvent required to completely recover the 4,6-DMDBT and to regenerate the adsorbent for subsequent use, the fractions of the solvent have been collected and analyzed using the total sulfur analyzer. The profile for recovering the 4,6-DMDBT by solvent washing from the spent

activated carbon-based adsorbent is shown in Fig.3. The sulfur content in the initial few fractions exceeded 1000 ppmw and then decreases exponentially. The results indicate that most of the sulfur compounds could be recovered using 20 cc of the solvent per g of adsorbent. However, about 100 cc of the solvent is required under the present experimental condition for the complete removal of all the sulfur compounds adsorbed on this particular adsorbent.

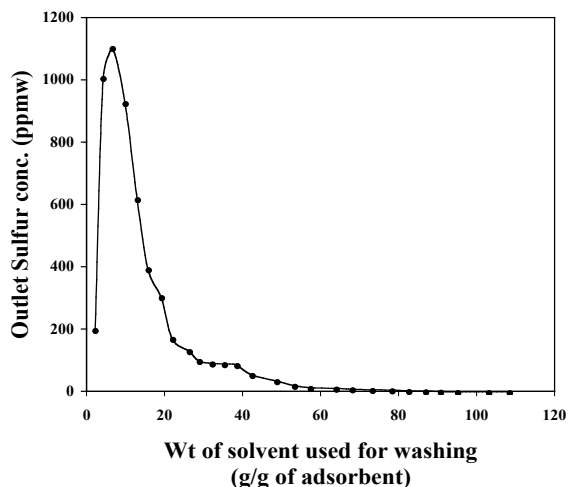


Fig.3. Profile for recovering the adsorbed 4,6-DMDBT by solvent washing from the spent activated carbon-based adsorbent at 70°C

After the solvent washing, the regenerated adsorbent has been flushed with N₂ gas (40 ml/min) for about 1 h at 300°C in order to remove any adsorbed solvent molecules. Desulfurization of model diesel fuel over regenerated adsorbent has been performed under the same experimental condition as that of fresh sample and the sulfur breakthrough curve obtained on the regenerated sample is shown in Fig. 2 itself along with that of fresh samples. The breakthrough curves of fresh and regenerated samples are close to coincidence and this indicates that solvent washing can regenerate the adsorbent almost completely. This observation infers that the adsorbent simply grabs the sulfur sulfur compound (4,6-DMDBT) from the fuel and holds it by some weak interactions without destroying. Flushing with solvent is sufficient to break such weak interactions.

There are several advantages of solvent washing for the regeneration of spent adsorbent. For instance, the organic sulfur compounds can be recovered by separating them from the solvent and the concentrated sulfur compounds can be treated in small HDS reactors to remove sulfur and the remaining organic moiety can be blended with the fuel.^{1,2} Regeneration by solvent washing is an environmentally benign method because it avoids the emissions of SO_x generated by oxidative regeneration or H₂S generated in the reductive regeneration.

In the "sense and shoot" approach, model and real diesel fuels have been treated over adsorbents such as Ni supported on SiO₂-Al₂O₃, and nano-composite materials derived from hydrotalcite-like anionic clays. These materials exhibit better adsorption performance at relatively elevated temperature of around 200°C. This indicated that the sulfur compounds over these adsorbents are removed by surface reactions rather than weak interactions. Experiments using model fuels revealed that the sulfur compounds are destroyed and converted into

corresponding organic moiety although no hydrogen gas has been used during the adsorption.

Fig.4 shows the breakthrough curves for the adsorptive desulfurization of a low sulfur diesel fuel containing 45 ppmw of sulfur shown in Fig. 1. (bottom panel). In addition to the 4,6-DMDBT, the fuel contained 4-ethyl-6methyl dibenzothiophene (4-E,6-MDBT) which is even more refractory than the 4,6-DMDBT because of the presence of ethyl group instead of methyl group in the 4th position. The results indicate that the adsorbent is capable of sensing the sulfur compounds from this very dilute feed (feed containing only 45 ppmw of sulfur) and removing them completely (below 1 ppmw) by the surface reaction. The adsorbent has been regenerated by treating with H₂ gas at 500°C for 1-2 h and then reused for the subsequent run. The breakthrough curves of the regenerated adsorbent in two cycles, also shown in Fig.4, indicate that the adsorption performance can be completely regained by the reductive regeneration.

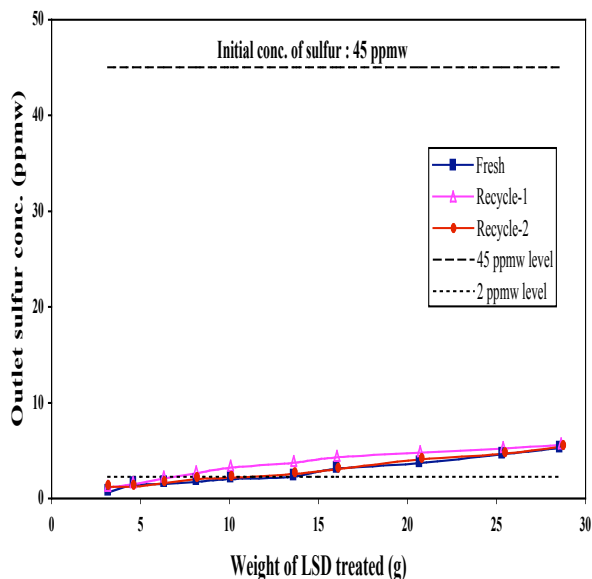


Fig. 4. Breakthrough curves for the adsorptive desulfurization of low sulfur diesel containing 45 ppmw of sulfur over a Ni-based adsorbent at 200°C. LHSV = 4.8 h⁻¹

Several other adsorbents are currently being evaluated using the "sense and grab" and "sense and shoot" approaches in order to develop highly efficient and regenerable adsorbents for the production of ultra-clean gasoline, diesel and jet fuel for refinery and fuel cell applications and the detailed results will be reported.

Conclusions

New regenerable adsorbents based on zeolites, mesoporous materials, activated carbon, supported metal, etc, are being developed for the selective removal of organic sulfur compounds present in gasoline, diesel and jet fuels using "sense and grab" and "sense and shoot" approaches. In the former approach, certain adsorbents such as metal oxide supported on activated carbon simply grabs the 4,6-DMDBT present in the model diesel fuel at 60°C and hold it by some weak interactions without chemical reaction. The adsorbed sulfur compound could

be recovered by solvent washing and the adsorbent could be completely regenerated for subsequent use. On the other hand, in the sense and shoot approach, the adsorbent such as supported Ni metal, adsorbs the sulfur compounds at elevated temperature. The adsorbed sulfur compounds are decomposed and the remaining organic moiety is added to the fuel. The adsorbent could be regenerated by reductive regeneration at 500°C using hydrogen gas.

Acknowledgements

This work was supported in part by the US department of Energy and in part by the US department of Defense.

References

- (1) Song, C.; Ma, X. *Applied Catalysis B: Environmental*, **2003**, 41, 207; Song, C., *Catalysis Today*, **2002**, 77 (1), 17.
- (2) Ma, X.; Sun, L.; Song, C. *Catal.Today*, **2002**, 77, 107.
- (3) Irvin R.L. Process for Desulfurizing gasoline and hydrocarbon Feedstocks, U.S. Patent 5730860, 1998
- (4) For Philips S-Zorb process, see <http://www.fuelstechnology.com/szorbgas.htm>
- (5) S. Velu, Xiaoliang Ma and Chunshan Song, *Preprint Paper – American Chemical Society, Division Fuel Chemistry* **2002**, 47(2), 447-448.
- (6) Xiaoliang Ma, Michael Sprague, Lu Sun and Chunshan Song, *Preprint Paper – American Chemical Society, Division Fuel Chemistry* **2002**, 47(2), 452-453.
- (7) Gates, B. C.; H. Topsøe, *Polyhedron*. **1997**, 16, 3213.
- (8) Ma, X.; Sakanishi, K.; Mochida, I. *Ind. Eng. Chem. Res.* **1996**, 35, 2487.

SYNTHESIS OF HIGH-PERFORMANCE NAPHTHENIC KEROSENE FROM SELECTED REFINERY NAPHTHA FEEDSTOCKS

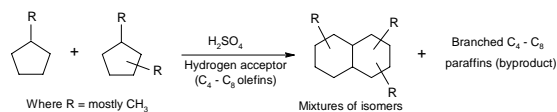
F.V. Hanson, R. Aggrawal, D. Bhat, J.V. Fletcher, and W. Zmierzczak

Department of Chemical & Fuels Engineering, University of Utah
Salt Lake City, Utah 84112

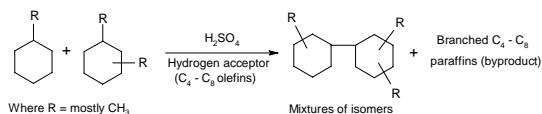
Introduction

A recently developed process for the synthesis of naphthenic kerosene (NK) from selected refinery naphtha feedstocks can provide an opportunity to produce high-performance jet fuel/rocket propellant compositions accommodating the next generation of aircraft, and reusable space access vehicles, which must use the high-temperature performance fuel to cool critical engine components.¹ The process is based on newly elucidated chemistry of naphthenes (alkylated cyclopentanes and cyclohexanes), which embraces several types of the following simultaneously occurring catalytic reactions.²

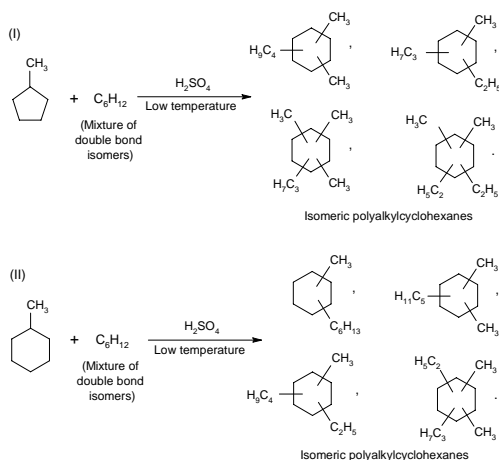
1. Self-condensation (dehydrodimerization and dehydrotrimerization) of alkylcyclopentanes to alkylsubstituted decalins and some alkylsubstituted tricyclic naphthenes, *e.g.*,



2. Self-condensation (dehydrodimerization) of alkylcyclohexanes to alkylsubstituted bicyclohexyls (dodecahydrobiphenyls), *e.g.*,



3. Dispersive alkylation of monocyclic naphthenes by C₄ - C₈ olefins to polyalkylcyclohexanes, *e.g.*,



The reactions occur at low temperatures in the presence of concentrated H₂SO₄ as a catalyst and reaction medium. The product obtained contains alkylated bicyclic (and some tricyclic) naphthenes, *i.e.*, alkylated decalins, some alkylated bicyclohexyls, alkylated perhydrophenanthrenes, alkylated hydrindanes, and polyalkylated cyclohexanes. Olefins and sulfur-containing compounds present in the naphthenic reaction mixtures act as hydrogen acceptors. It results in production of highly-branched paraffinic gasoline components as a byproduct and exhaustive hydrodesulfurization.

Experimental

Semi-batch experimental process runs to produce naphthenic kerosene were performed using:

- (a) mixtures of two naphthenic model compounds, *i.e.*, methyl cyclopentane (MCP) and methylcyclohexane (MCH) of variable composition, with 1-hexene as olefinic hydrogen acceptor (initial temperature, 7 °C, increasing to 12 °C; olefin addition rate, 0.3 g/min; molecular naphthenes/olefin ratio, 2.0; total reaction time, 120 minutes; and, H₂SO₄/naphthenes wt ratio, 4); and
- (b) refinery naphthene-rich naphthas *i.e.*, heavy virgin naphtha (HVN) and intermediate virgin naphtha (IVN) with olefinic light catalytically cracked naphtha (LCCN) (initial temperature, 7 °C, increasing to 12 °C during the run; LCCN addition rate, 1g/min; calculated molecular naphthenes/olefins ratio, 2.0; total reaction time, 77 minutes; and, H₂SO₄/naphthenes wt ratio, 4).

The reaction runs were performed in a semi-batch stirred tank reactor system (a three-neck flask), equipped with a mechanical stirrer, a reflux condenser, and a metering pump for introducing the reactants and a remote temperature controlled water bath. A mixture of a liquid catalyst (concentrated H₂SO₄) and the naphthenic component was placed in the reactor, and the olefinic component was added dropwise to the reaction mixture. Contact between the acid phase and the hydrocarbon phase was maintained by vigorous stirring.

Reaction feeds and products obtained were analyzed using a HP-6890 gas chromatograph equipped with an HP-1 capillary column, flame ionization and mass spectrometer detectors. Sulfur analysis was also carried out to determine the feeds and products sulfur content using Horiba sulfur analyzer, SLFA-800.

Results and Discussion

Results of conversions to NK products for relevant model naphthenes (MCP + MCH variable mixtures) and 1-hexene as a hydrogen acceptor in the initial reaction runs are summarized in **Figure 1**.³

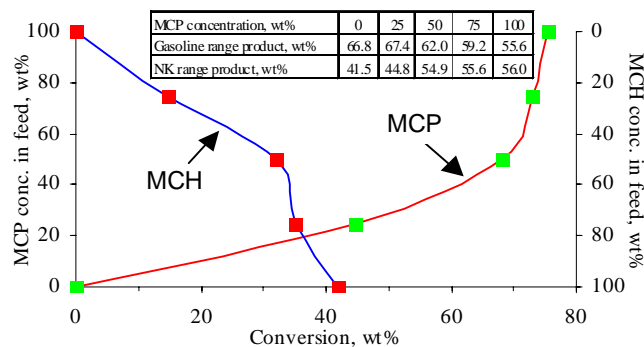


Figure 1. Conversion of MCP and MCH (variable compositions) to naphthenic kerosene range components.

In addition, the table in the figure shows the contents of gasoline and NK fractions (overlapped) in products obtained during the model compounds reaction runs.

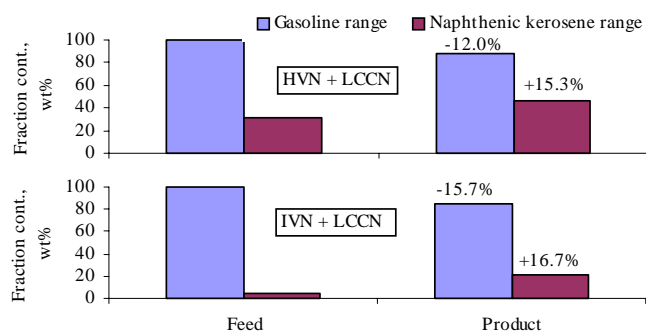
Similar (not optimized) runs were performed with refinery naphtha feeds under similar process conditions.^{3,4} The chemical type composition of the naphthas, summarized in **Table 1**, in general, indicated their potential suitability for use as feed in the NK process. The only undesirable components were arenes, which undergo undesirable reactions of sulfonation, and alkylation with olefins.

Table 1. Distribution of naphtha components by chemical type

Component type	HVN, wt%	IVN, wt%	LCCN, wt%
Olefins	00.0	00.1	39.2
n-Paraffins	19.6	33.6	01.6
Isoparaffins	19.5	32.5	33.5
Naphthenes	35.6	20.0	09.0
Arenes	25.2	13.2	16.6
Unidentified	00.1	00.6	00.1

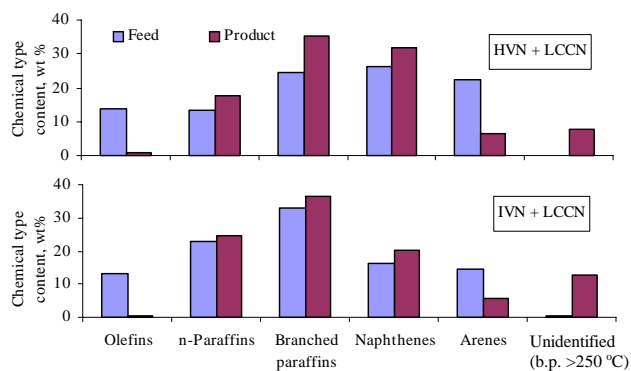
Two reaction runs were carried out with the use of naphthene-rich intermediate virgin (HVN) and heavy virgin (IVN) naphthas in combination with olefinic (hydrogen acceptor) light catalytically cracked naphtha (LCCN). The stoichiometric naphthenes/olefins ratio for dehydrodimerization (DHD) reactions in the reaction mixture was determined on the basis of detailed GC/MS analysis of these feeds. The obtained conversions of the naphthenic components in naphtha feeds to NK products, *i.e.*, 25.3 wt% for HVN, and 14.9 wt% for IVN were considerably lower as compared to the model compound runs. Also, reduction in sulfur concentration by ~ 80 wt% was found.³

The comparison of the compositions of feeds and reaction products obtained in these runs is summarized in **Figures 2 and 3**.⁴ **Figure 2** shows the changes in (overlapped) gasoline (b.p. < 225 °C) and naphthenic kerosene (b.p. > 150 °C) range product distributions relative to the feed. The increase in the content of NK range products obtained in the runs with HVN and IVN was 15.3 wt%, and 16.7 wt% respectively. It was mostly due to dehydrodimerization (DHD), dehydrotrimerization (DHT), and dispersive alkylation of naphthenes, and alkylation of arenes.

**Figure 2.** Comparison of the change of gasoline and naphthenic kerosene range fraction distributions in feeds and reaction products obtained in the refinery naphtha runs.

The comparison of feeds and products from the refinery naphtha runs, in terms of chemical type distribution, were obtained by using PIONA (n-paraffins, isoparaffins, olefins, naphthenes and arenes distribution) analysis techniques.⁴ The results obtained demonstrated in **Figure 3** show that the olefinic component of LCCN is highly reactive under the process conditions as reflected by the high conversion of olefins in the feed (92 wt% with HVN and 97 wt% with IVN) in DHD, dispersive alkylation of naphthenes, alkylation of arenes, and dimerization.

The total increase in naphthenes was a result of their dispersive alkylation, whereas the increase in branched paraffins was related to hydrogen transfer to LCCN-derived olefin molecules and their concurrent skeletal isomerization. The lower then expected

**Figure 3.** Comparison of the change in different chemical type component distributions in feeds and reaction products obtained in the refinery naphtha runs.

conversions of the naphthenic components in these reaction runs in combination with almost complete conversion of olefins can be ascribed to the competitive reactions of alkylation of arenes and dimerization of olefins, which resulted in reduction of olefinic hydrogen acceptors.

Reduction in concentration of arenes in the reaction mixture was caused by their retention in the sulfuric acid phase.

Conclusions

Studies using model compounds and refinery naphthas have shown the significant conversion of naphthenes to the naphthenic kerosene type compounds simultaneously with an improvement in desirable gasoline fraction properties.

Manipulation of process conditions, *i.e.*, feed to olefin ratios, and H₂SO₄ concentration, temperature, contacting time, *etc.*, and feed composition *via* cut selection and feed pretreatment, can be used to control the conversion of naphthenes and the selectivity of the process toward maximizing high performance naphthenic kerosene products. Virgin naphthas high in naphthenes and low in aromatics are the preferred feedstocks. Cracked naphthas high in olefins are the preferred hydrogen acceptors.

Sulfuric acid is suitable as a catalyst and as a reaction medium provided that aromatics in the feed are low. The sulfur content of the refinery naphthas can be dramatically reduced under the process conditions studied.

Acknowledgements

The authors acknowledge the financial support of BP Air and the Petroleum Research Center at the University of Utah. Professor Joseph S. Shabtai is thanked for many stimulating discussions related to the chemistry of the process.

References

- Lander, H.R., Maurice, L.Q., Harrison, W.E. III, and Edwards, T., Proc. of XIV Int. Symp. on Air Breathing Engines (ISABE), Paper IS-253, Florence, Italy, **1999**.
- Shabtai, J., Zmierczak, W., and Tsai, C.H., Proc. of XIV Int. Symp. on Air Breathing Engines (ISABE), Paper IS-7070, Florence, Italy, **1999**.
- Aggrawal, R., M.S. Thesis, University of Utah, **2003**.
- Bhat, D., M.S. Thesis, University of Utah, **2003**.

OXIDATIVE DESULFURIZATION OF DIESEL FUELS BY MOLECULAR OXYGEN

Satoru Murata, Kazutaka Murata, Koh Kidena,
and Masakatsu Nomura

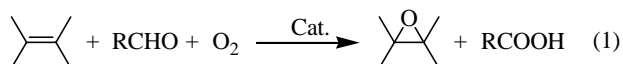
Department of Applied Chemistry, Faculty of Engineering, Osaka
University, 2-1 Yamada-oka, Suita, Osaka 565-0871, Japan

Introduction

Deep desulfurization of petroleum-derived fuels is nowadays the most important technology in petroleum industry. Sulfur-containing compounds in the fuels are converted to sulfur oxide, *i.e.* SO_x, during their combustion. Therefore, amounts of *S*-compounds were strictly limited. For example, regulation of sulfur amounts in diesel fuels in Japan is 500 wtppm, and the value will be reduced to 50 wtppm in 2005 and 10 wtppm in 2008. Petroleum-refining and catalyst-making companies, therefore, are trying to develop new and efficient desulfurization processes and highly active catalysts.

In 1990s, an epoch making process was proposed, *so-called*, oxidative desulfurization (ODS). ODS consists of two processes: the former one is oxidation of sulfur-containing compounds in feeds and the latter is removal of oxidized *S*-compounds from the feeds. ODS has several advantages compared with a classical hydrodesulfurization process: (1) reaction conditions are very mild such as ambient pressures and temperatures, (2) there are high potentials for desulfurization of sterically hindered thiophene derivatives, and (3) expensive hydrogen is not required. Oxidants examined were peroxyacetic acid, hydrogen peroxide-acetic or formic acids, hydrogen peroxide-polyoxometalate, etc.¹ Photoreduction of DBT in the presence of sensitizer or catalyst under molecular oxygen was also examined.² The authors are very interested in oxidation with peroxy carboxylic acids, because reaction proceeds rapidly and selectively. However, large scale-storage and usage of peroxide are somewhat dangerous.

Transition metal-catalyzed co-oxidation of aldehydes and organic substrates with molecular oxygen may solve the above problems. Co-oxidation of aldehydes and alkenes are well known, and extensively studied by several authors. The reaction is believed to proceed *via* two steps, autoxidation of aldehydes to peroxy acids and oxidation of alkenes to oxiranes by peroxy acids produced *in situ* (eq. 1).³



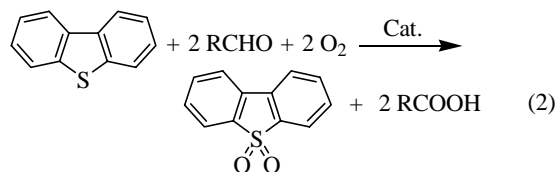
Therefore, the authors examined the co-oxidation of aldehydes and *S*-containing compounds such as dibenzothiophene (DBT) by molecular oxygen to develop a new system for deep desulfurization of petroleum-derived fuels.

Experimental

Typical procedure for oxidation of model compounds was as follows: A mixture of cobalt(II) acetate (0.05 mmol), *n*-octanal (4 mmol), DBT (1 mmol), and benzene (10 mL) was stirred at 40 °C under ambient pressure of oxygen. Time-profiles of DBT conversion was monitored by gas chromatographic analysis.

Results and Discussion

A benzene solution of DBT was employed for model of diesel fuels. A mixture of benzene, cobalt acetate, DBT, and *n*-octanal was stirred at 40 °C for 15 min under ambient pressure of oxygen, DBT being oxidized to the corresponding sulfone in an almost quantitative yield (eq. 2, R=*n*-C₇H₁₅).



In order to check the stoichiometry of this reaction, the following experiments were conducted: A benzene solution containing cobalt acetate (0.05 mmol), DBT (1 mmol), and *n*-octanal (1 mmol) was stirred at 40 °C for 15 min under oxygen, GC-analysis of the products indicating formation of 1 mmol of *n*-octanoic acid and 0.5 mmol of DBT sulfone, and recovery of 0.5 mmol of DBT. In the absence of either cobalt catalyst or aldehyde, the reaction did not proceed and DBT was recovered almost quantitatively. These results indicate that the stoichiometry of the reaction obey the **equation 2**.

Several metal salts and aldehydes were examined as catalysts and sacrificial materials for this reaction, respectively, the results being summarized in **Table 1**. This indicates that both cobalt(II) acetate and chloride are the most suitable catalysts among the metal salts employed and aliphatic aldehydes with 6-10 carbons and benzaldehyde could be used instead of *n*-octanal.

Table 1. Oxidation of DBT with molecular oxygen in the presence of several transition metal salts and aldehydes.

Metal salt	Aldehyde	Conv. of DBT (mol%)
Co(OAc) ₂	<i>n</i> -octanal	> 99
CoCl ₂	<i>n</i> -octanal	> 99
Mn(OAc) ₂	<i>n</i> -octanal	> 99
Ni(OAc) ₂	<i>n</i> -octanal	54
CuCl	<i>n</i> -octanal	35
<i>none</i>	<i>n</i> -octanal	0
Co(OAc) ₂	<i>none</i>	0
Co(OAc) ₂	<i>n</i> -hexanal	> 99
Co(OAc) ₂	<i>n</i> -decanal	96
Co(OAc) ₂	benzaldehyde	93
Co(OAc) ₂	cinnamaldehyde	0

Then, the authors tried to desulfurization of commercial diesel oil by this method. The commercial oil (100 mL) was treated with cobalt acetate (0.1 mmol) and *n*-octanal (16 mmol) at 40 °C for 16 h under oxygen. Oxidized *S*-compounds were removed from the feed by adsorption with alumina. Concentration of sulfur could be reduced from 193 wtppm (in the original feed) to <5 wtppm by these treatments. The results may indicate that this brand-new ODS process has a potential to meet a future regulation of sulfur in the diesel fuel.

Acknowledgements. The authors thank Dr. Ikushima (Petroleum Energy Center, Japan) and Mr. Nagai (Taiyo Oil Co., Ltd.) for their helps concerning analysis of sulfur contents in the oils.

References.

- (1) Aida, T. Yamamoto, D. *Prepr. Pap.-Am. Chem. Soc., Div. Fuel Chem.* **1994**, 39, 623; Babich, I. V.; Moulijn, J. A. *Fuel* **2003**, 82, 607.
- (2) Hirai, T.; Ogawa, K.; Komasa, I. *Ind. Eng. Chem. Res.* **1996**, 35, 586; Matsuzawa, S.; Tanaka, J.; Sato, S.; Ibusuki, T. *J. Photochem. Photobiol.* **2002**, 149, 183.
- (3) Kholdeeva, O. A.; Grigoriev, V. A.; Maksimov, G. M.; Fedotov, M. A.; Golovin, A. V.; Zamaraev, K. I. *J. Mol. Catal. A*, **1996**, 114, 123; Nam, W.; Kim, H. J.; Kim, S. H.; Ho, R. Y. N.; Valentine, J. S. *Inorg. Chem.* **1996**, 35, 1045; Komiya, N.; Naota, T.; Oda, Y.; Murahashi, S.-I. *J. Mol. Catal. A*, **1997**, 117, 21.

NOVOZYM435 -CATALYZED TRANSESTERIFICATION OF SOYBEAN OIL FOR BIODIESEL PRODUCTION IN A SOLVENT-FREE MEDIUM

Wei Du*, Yuan-yuan Xu, De-hua Liu

Department of Chemical Engineering, Tsinghua University, Beijing
100084, P. R. China

Biodiesel, generally classified as fatty acid alkyl esters, has become more attractive recently because of its environmental benefits. Although biodiesel has been successfully produced chemically at present, there are several associated problems to restrict its development, such as glycerol recovery and removal of inorganic salt. The disadvantages caused by chemical catalysts are largely prevented by using lipases as the catalysts and enzymatic production of biodiesel fuel has drawn considerable attention in recent years.

For large-scale production of biodiesel, the repeated use of lipase is one of the major issues. In this paper, effects of some key issues (such as temperature, alcohol/oil ratio, glycerol removal etc.) on the enzymatic reaction during biodiesel production have been studied and within the optimized conditions, lipase expressed good stability in continuous batch operation in the production of biodiesel.

Effect of temperature, oil/alcohol molar ratio and by-product glycerol were studied during Lipozyme TL IM-catalyzed continuous batch operation when short chain alcohols used as the acyl acceptor. In non-continuous batch operation, the optimal oil/alcohol ratio and temperature were 1:4 and 40°C-50°C; however, during the continuous batch operation, the optimal oil/alcohol ratio and temperature were 1:1 and 30°C respectively; 95% of enzymatic activity remained after 10 batches when iso-propanol adopted to remove by-product glycerol during repeated use of the lipase.

Effect of glycerol

Enzymatic transesterification of renewable oil with short chain alcohols as acyl acceptor for biodiesel production has been studied extensively in recent years. However, with these short chain alcohols as the acyl acceptor, glycerol, as one of the major by-products, has been demonstrated to have some serious negative effect on enzymatic activity. During the repeated use, lipase lost its activity dramatically which mainly due to the negative effect of glycerol.

Some hydrophilic organic (propanol, iso-propanol, butanol, tert-butanol) have been tried to remove glycerol during the repeated use of lipase and iso-propanol has been found to be the most effective for glycerol removal.

Operational stability with glycerol removal by iso-propanol

The operational stability of lipase with glycerol removal by iso-propanol has been studied further in this paper and lipase expressed good operational stability. There was no observable loss of lipase activity after 10 batches of continuous operation.

Effect of molar ratio of methanol / oil

It is well known that excessive short-chain alcohols such as methanol might inactivate lipase seriously. However, at least three molar equivalents of methanol are required for the complete conversion of the oil to its corresponding ME and effect of molar ratio of oil/methanol has been studied comparatively during batch and continuous batch operation.

In batch operation the highest ME yield (92 %) could be obtained at methanol/oil molar ratio 4:1. Either higher methanol concentration (5:1) or lower methanol concentration (3:1) would decrease ME yield to some degree.

However, it has been demonstrated that during the continuous process, lipase lost its activity dramatically at methanol/oil molar ratio 4:1 and effect of methanol/oil ratio on enzymatic activity was studied further in continuous batch operation. The optimal molar ratio of methanol/oil was 1:1 in continuous batch operation, at which lipase remained relatively high activity.

Effect of temperature

Effect of temperature on enzymatic transesterification of soybean oil was examined at the range from 30°C to 50°C in batch operation and high temperature resulted in relatively high ester yield. However, it has also been found that when temperature is above 50°C, enzyme loses its activity dramatically. So in batch process, 40-50°C is optimal for enzymatic biodiesel production.

However, in continuous batch operation, it has been demonstrated that higher temperature resulted in larger loss of lipase activity and 30°C is optimal by taking into lipase stability and activity into consideration.

It has been demonstrated that temperature, methanol/oil molar ratio and glycerol have varied effect on lipase-catalyzed transesterification of soybean oil during batch and continuous batch operation of biodiesel production. Within the optimized conditions, lipase remained high activity after continuous batch operation which demonstrates that enzymatic transesterification of renewable oil is very promising for large-scale production of biodiesel.

ENZYMATIC CONVERSION OF WASTE OIL TO BIODIESEL IN A SOLVENT-FREE SYSTEM

Hong Wu, Min-hua Zong*, Qian Luo, and Hua-chang Wu

Biotechnology Department, South China University of Technology, Guangzhou 510640, P. R. China

*Author for correspondence (Fax: 86-20-87112979; E-mail: btmhzong@scut.edu.cn)

Introduction

Production of biodiesel from vegetable oil and animal fats has drawn more and more attention because of the increasing awareness of environmental pollution and short supply of fossil fuels. Presently, the industrial-scale production of biodiesel is performed chemically, using alkali as catalyst. However, there are several problems with this process, such as excessive methanol requirement, high energy demanding, difficulties in glycerol recovery, disposal of fatty acid alkaline salts (soaps) creating other environmental concerns. Thus enzymatic alcoholysis of triacylglycerols (TAG) seems to be a promising alternative because of its mild reaction conditions, easy recovery of glycerol and being free of chemical wastes.

Several studies on lipase-catalyzed alcoholysis of vegetable oils and animal fats with primary and secondary alcohols in a solvent or a solvent-free system have been reported.¹⁻³ Owing to the toxicity and flammability of organic solvents, and the easiness of product recovery, enzymatic alcoholysis in a solvent-free system is preferable.

Immobilized *Candida Antarctica* lipase was found to be the most effective for the methanolysis of oil and fats.^{4,5} However, its cost is prohibitively high for this purpose. In this paper, some efforts have been made to explore the possibility to use a relatively cheap lipase from *Thermomyces lanuginosus*, commercially called Lipozyme TL IM for biodiesel production.

Experimental

Materials. Waste oil was provided by restaurant in South China University of Technology, CRL (lipase from *Candida Rugosa*), myristic acid methyl ester, palmitic acid methyl ester, steric acid methyl ester, oleic acid methyl ester, linoleic acid methyl ester, linolenic acid methyl ester and heptadecanoic acid methyl ester were purchased from Sigma (USA), Novozym 435 (lipase from *Candida Antarctica*), Lipozyme TL IM (lipase from *Thermomyces lanuginosus*) and Lipozyme RM IM (lipase from *Rhizomucor miehei*) were kindly donated by Novo Nordisk Co. (Denmark). All other chemicals were obtained commercially and of analytical grade.

Reaction. The methanolysis of waste oil was carried out at 35°C, 130rpm using 10% immobilized lipase based on oil weight. The four-step reaction was conducted as follows. The mixture of the first-step reaction contained 10g of oil and 1:1 molar equivalent of methanol. The second-, third- and fourth-step reactions were initiated by adding 0.8:1 molar equivalent of methanol upon 90% conversion of methanol to methyl esters.

Analysis. The methyl ester (ME) content in the reaction mixture was assayed with a HP4890 gas chromatography equipped with a HP-5 capillary column (0.53mm×15m) using heptadecanoic acid methyl ester as an internal standard. The column temperature was hold at 180°C for 1 min, raised to 186°C at 0.8°C/min and kept for 1 min, then upgraded to 280°C at the rate of 20°C/min.

Results and Discussion

As shown in **Table 1**, Novozym 435, Lipozyme TL IM and

Lipozyme RM IM could all catalyze the reaction effectively. Lipozyme TL IM is the cheapest among them and was used for further study.

Table 1 Effect of different lipases on methanolysis of waste oil

Enzyme	ME content(%)	Methanol conversion(%)
Lipozyme TL IM	32.2	96.7
Lipozyme RM IM	32.4	97.3
Novozym 435	33.1	99.4
CRL	1.2	3.5

10g waste oil, methanol/oil molar ratio1:1, 10% lipase based on oil weight, 130rpm, 40°C, 24h.

As can be seen in **Figure 1**, the conversion dropped sharply when more than 1.5 molar equivalents of methanol were present initially in the oil mixture, suggesting the severe inactivation of the enzyme. The lipase has been proved to be irreversibly inactivated by transferring it into the fresh substrates (methanol/oil 1:1,mol/mol) and following the methanolysis course, which was in good agreement with Shimada's report.⁶

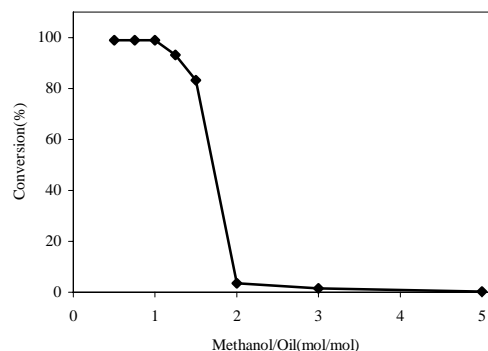


Figure 1. Effect of methanol/oil molar ratio on methanolysis of waste oil. 10g waste oil, 10% Lipozyme TL IM based on oil weight, 130rpm, 40°C, 30h. The conversion was expressed as the percentage of methanol consumed for the formation of ester (when the molar ratio of methanol /oil was less than 3), and as the ratio of methyl ester to the oil (when the molar ratio of methanol /oil was more than 3).

The influence of enzyme quantity on the methanolysis of waste oil was presented in **Figure 2**. It has been found that ME content was increased by increasing lipase quantity up to 10% based on oil weight. The conversion reached 24.7% after 12h reaction with 10% of the lipase. Interestingly, only 22.7% of waste oil was converted to its corresponding methyl esters in 12h in spite of the highest initial reaction rate with 12% enzyme. This may be explained by the observable aggregation of the immobilized enzyme at high concentration (>10% based on oil weight), which led to a lower enzymatic activity due to a higher mass transfer limitation.

Figure 3 shows temperature effect on the reaction. When the temperature was below 40°C, the reaction could be improved by raising temperature. Further increase in temperature, however, resulted in a lower ME content in the reaction mixture, indicating the inactivation of the enzyme by high temperature, which was confirmed by the low conversion of waste oil to methyl ester in the case of reusing the enzyme for the conversion of fresh substrates (methanol/oil 0.75:1, mol/mol) at 35°C.

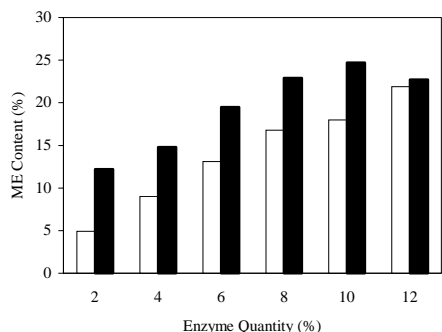


Figure 2. Effect of enzyme quantity on methanolysis of waste oil. 10g waste oil, methanol/oil molar ratio 0.75:1, 130rpm, 40°C. □, ester content upon 1h incubation; ■, ester content upon 12h incubation.

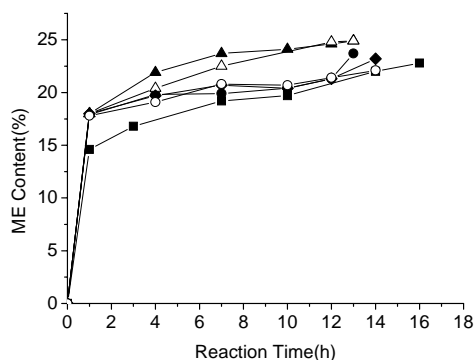


Figure 3. Effect of temperature on methanolysis of waste oil. 10g waste oil, methanol/oil molar ratio 0.75:1, 10% Lipozyme TL IM based on oil weight, 130rpm. ■, 25°C; ●, 30°C; ▲, 35°C; △, 40°C; ◆, 45°C; ○, 50°C.

Enzymatic methanolysis of waste oil at different shaking speed ranging from 100 to 220rpm was performed and the result showed that there was no observable difference in ME content and methanol was nearly completely converted to esters in 12h over the range from 130 to 180rpm. However, above 180rpm, little increase in reaction rate was observed with further increase in shake speed, but less ME was formed (only 22.1% in 12h at 220rpm). This was due to enzyme inactivation by higher shearing stress as indicated by the low ME content when the enzyme was reused for the methanolysis of fresh substrates (methanol/oil 0.75:1, mol/mol) at 130rpm.

At least 3 molar equivalents of methanol are required for the complete conversion of waste oil to its corresponding ME. The lipase, however, will be significantly inactivated in a mixture with more than 1 molar equivalent of methanol. Hence, a stepwise adding of methanol is necessary. The optimum substrate molar ratio (methanol/oil) was found to be 3.4:1 (data not shown). The typical reaction time course was shown in **Figure 4** (with total methanol/oil molar ratio being 3.4:1). For the first-step reaction, 12h incubation (methanol/oil 1:1, mol/mol) gave a 31.9% ME content. The second step was initiated by adding methanol (with methanol/oil molar ratio being 0.8:1) into the reaction system when the incubation has lasted for 24h. The ME content reached 52.4% in 12h (total 36h). Then followed by the addition of the third batch of methanol (with methanol/oil molar ratio being 0.8:1) at the end of the second step

which proceeded for 24h. The ME content reached 71.1% after incubation for another 14h (total 62h). The fourth batch of methanol (with methanol/oil molar ratio being 0.8:1) was added 10h later. The conversion of waste oil to its corresponding ME was as high as 90.2% when the incubation went on for 96h, demonstrating the effectiveness of Lipozyme TL IM, a lipase with 1,3-specificity, for biodiesel production. Acyl migration from *sn*-2 to *sn*-1 or *sn*-3 position might account for this. The similar phenomenon has also been observed by some other researchers.⁷ To shorten the reaction time, the four-step procedure was modified as follows: the reaction was initiated by adding 10% immobilized enzyme (based on oil weight) into a mixture of methanol and oil (1:1, mol/mol), followed by feeding methanol three times (methanol/oil 0.8:1, mol/mol) at 12h, 24h and 38h, respectively. This four-step process converted more than 90% of the oil to its corresponding methyl esters.

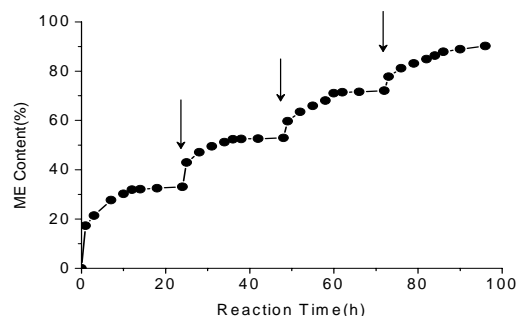


Figure 4. Reaction time course for methanolysis of waste oil. 10g waste oil, 0.38g methanol (methanol/oil molar ratio 1:1), 10% Lipozyme TL IM based on oil weight, 130rpm, 35°C. Methanol was fed three times (0.30g each) upon incubation for 24, 48 and 72h as indicated with arrows.

Conclusion

Immobilized enzyme from *Thermomyces lanuginosus*, commercially called Lipozyme TL IM showed high activity in methanolysis of waste oil. A four-step process with stepwise feeding of methanol was efficient for the conversion of waste oil to its corresponding methyl esters and so are potential for biodiesel production from waste oil.

References

- Steinke, G.; Kirchhoff, R.; Muknerjee, K. D., *J. Am. Oil Chem. Soc.*, **2000**, *77*, 361-366
- Watanabe, Y.; Shimada, Y.; Sugihara, A.; Tominaga, Y., *J. Am. Oil Chem. Soc.*, **2001**, *78*, 703-707
- Watanabe, Y.; Shimada, Y.; Sugihara, A.; Noda, H.; Fukuda, H.; Tominaga, Y., *J. Am. Oil Chem. Soc.*, **2000**, *77*, 355-360
- Shimada, Y.; Watanabe, Y.; Sugihara, A.; Tominaga, Y., *J. Mol. Catal. B: Enzym.*, **2002**, *17*, 133-142
- Köse, Ö.; Tüter, M.; Aksoy, H. A., *Bioresour. Technol.*, **2002**, *83*, 125-129
- Shimada, Y.; Watanabe, Y.; Samukawa, T.; Sugihara, A.; Noda, H.; Fukuda, H.; Tominaga, Y., *J. Am. Oil Chem. Soc.*, **1999**, *76*, 789-792
- Kaieda, M.; Samukaw, T.; Matsumoto, T.; Ban, K.; Kondo, A.; Shimada, Y.; Noda, H.; Nomoto, F.; Ohtsuka, K.; Izumoto, E.; Fukuda, H., *J. Biosci. Bioeng.*, **1999**, *88*, 627-631

ACTIVE SITES AND ACTIVITY IN HDS CATALYSIS: THE EFFECT OF H₂ AND H₂S PARTIAL PRESSURE

Bas M. Vogelaar, Narinobu Kagami¹, A. Dick van Langeveld^{*2},
Sonja Eijsbouts³ and Jacob A. Moulijn

Reactor & Catalysis Engineering Group, Faculty of Applied Sciences, Delft University of Technology, Julianalaan 136, 2628 BL Delft, The Netherlands.

¹Idemitsu Kosan Co. Ltd. 26 Anesakikaigan Ichihara-city, Chiba, 229-0107, Japan.

²Particle Optics Group, Faculty of Applied Sciences, Delft University of Technology, Lorentzweg 1, 2628 CJ Delft, The Netherlands.

³Akzo Nobel Chemicals B.V., P.O. Box 37650, 1030 BE Amsterdam, The Netherlands.

Introduction

We recently reported some extraordinary results in the hydrodesulfurization of a light gas oil (LGO) [1]: At low conversion (around 50% sulfur removal) the catalyst activity appeared to be independent of the H₂ pressure. This is very uncommon, as most studies in fixed bed systems at high conversion (>95%) or in autoclave reactors report a first order dependency between activity and H₂ pressure. To understand the behavior at low conversion we must realize that in a flow reactor, the partial pressure of gas-phase inhibitors (like H₂S) scales linearly with the total pressure according to Eq. 1. Here, V_m is the molar volume at standard conditions (0.024 m³/mol), M_S the molar mass of sulfur (0.032 kg/mol), p the total pressure, HTO the hydrogen-to-oil ratio, ρ_L the liquid feed density (kg/m³), $[S_0]$ the mass fraction of sulfur in the feed, and X the level of sulfur conversion.

$$p_{H_2S} = \frac{V_m}{M_S} \frac{p}{HTO} \rho_L [S_0] X \quad (\text{Eq. 1})$$

This means that when the total pressure in the trickle bed reactor is increased and the conversion level remains the same (as in the LGO case) the H₂S partial pressure increases correspondingly. When the inhibiting effect of H₂S is of the same magnitude as the accelerating effect of the H₂ pressure, both effects will cancel out, and the reaction rate does not change. Obviously the temperature has no effect as both total pressure and “dilution rate” (HTO) do not change.

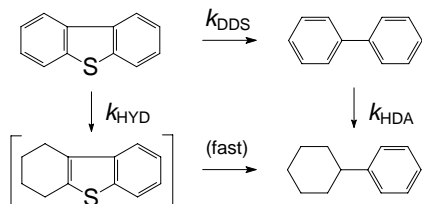


Figure 1. Simplified reaction network for the hydrodesulfurization of dibenzothiophene, adapted from [2].

The question remains why this strong H₂S inhibition only manifests itself at low conversion. A logical explanation may be found in the composition of the LGO feed: It contains a relatively high amount of sulfur (8445 ppmw), of which a large fraction consists of dibenzothiophene (DBT) and its mono-substituted analogues. These components exhibit low steric hindrance and are easily converted, mainly by the direct desulfurization route (DDS,

see Fig. 1). At high conversion levels (>95%) the rate is fully controlled by the desulfurization of di-substituted DBTs [3]. These compounds are essentially converted by the prehydrogenation route (HYD), as the DDS route is retarded due to steric hindrance. The fact that H₂S inhibits the DDS route much stronger than the HYD route completes our hypothesis for the LGO HDS pressure independence at low conversion. In order to test this hypothesis we have performed several DBT HDS experiments under various process conditions upon different catalyst pretreatments.

Experimental

A model NiMo catalyst supported on γ -Al₂O₃ containing 10 wt% MoO₃ and 2.5 wt% NiO was prepared by pore volume impregnation. The catalyst was calcined, then crushed and sieved before testing. Steady state experiments were performed in a microflow trickle bed reactor using 4 grams of catalyst (250 – 500 μ m) diluted with SiC particles (200 μ m) to ensure proper hydrodynamic behavior. The catalyst was sulfided *in-situ* in the gas phase using 10 vol% H₂S in H₂ at 60 ml/min, 400°C and 1 atm. during 2 hours. The feed consisted of 0.2 wt% DBT and 0.2 wt% n-C₁₈ (internal standard) in n-C₁₆. Samples were taken after 5 hours stabilization time and one hour later (as duplo). Batch experiments were done in a 200 ml swinging-capillary autoclave reactor using 200 mg of catalyst (150 – 250 μ m). The same sulfiding procedure and feed composition as in the flow reactor was used. In one experiment 700 mg of copper powder was added as H₂S scavenger. This is a proven method to remove all H₂S produced during the reaction [2]. A blank run (without catalyst) confirmed that copper alone had negligible catalytic activity. Samples were analyzed using a GC with FID detector.

Results and Discussion

The effect of H₂ pressure on the DBT HDS activity is shown in Figure 2. The overall HDS rate constant shows a very weak dependency on H₂ pressure, just like in the LGO case we reported previously. Moreover, when we decompose the total activity into the specific rate constants for the DDS and HYD route (assuming constant selectivity, *i.e.* $k_{HDA} \approx 0$) we clearly see that the DDS rate is zero-order in pressure, whereas the HYD rate is perfectly first order. This implies that the DDS route is strongly inhibited by self-produced H₂S, and the HYD route shows no measurable inhibition.

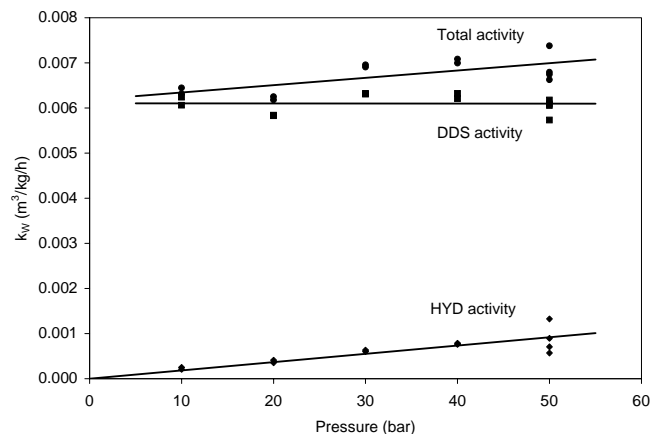


Figure 2. Effect of H₂ pressure on DBT HDS (microflow reactor, 225°C, LHSV = 2.4 h⁻¹, HTO = 588 nl/l).

At a constant H₂S partial pressure (0.2 bar) the picture changes dramatically (Fig. 3). The DDS route now shows a perfect first order fit, as well as the HYD route. Both rates are lower due to inhibition

* Corresponding author, email: A.D.vanLangeveld@tnw.tudelft.nl

by H₂S. Taking into account that this experiment was conducted at a 50°C higher temperature and the activation energy was found to be about 75 kJ/mol, the DDS rate constant at 30 bar decreased by a factor of 10 and the HYD rate constant by a factor of 2. This proves that indeed the DDS route is much more sensitive to H₂S inhibition than the HYD route.

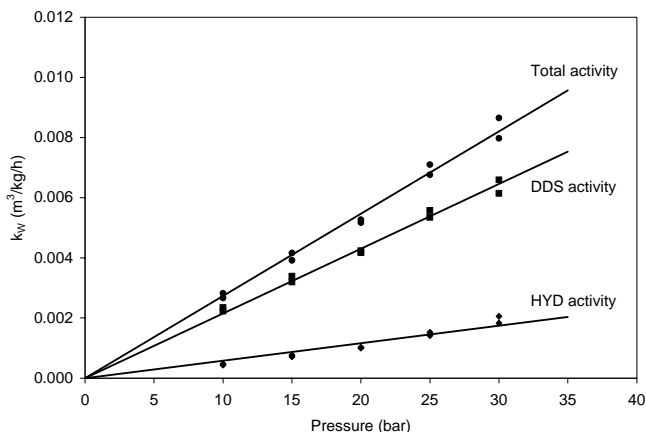


Figure 3. Effect of H₂ pressure on DBT HDS at constant (0.2 bar) H₂S partial pressure (microflow reactor, 275°C, LHSV = 2.4 h⁻¹, HTO = 588 nl/l).

In a previous paper [4] we have shown that during the HDS of thiophene in the gas phase, the state of the catalyst active phase, *viz.* the number of exposed Mo or Ni atoms (;sulfur vacancies;) changes as a result of the different conditions during presulfiding and reaction. When we look at the effect of catalyst pretreatment on the liquid phase DBT HDS (Fig. 4) we see that the total HDS activity ($k_{\text{DDS}} + k_{\text{HYD}}$) does not change, but the selectivity (HYD to DDS) does change. Apparently a H₂ treatment before reaction reduces the number of HYD sites and evenly increases the number of DDS sites. This can be explained when a H₂ treatment, analogous to gas phase thiophene HDS, creates sulfur vacancies on the catalyst active surface by removing sulfur and/or SH groups. These acidic groups are involved in the HYD reaction pathway, and the sulfur vacancies are responsible for the direct sulfur abstraction (DDS).

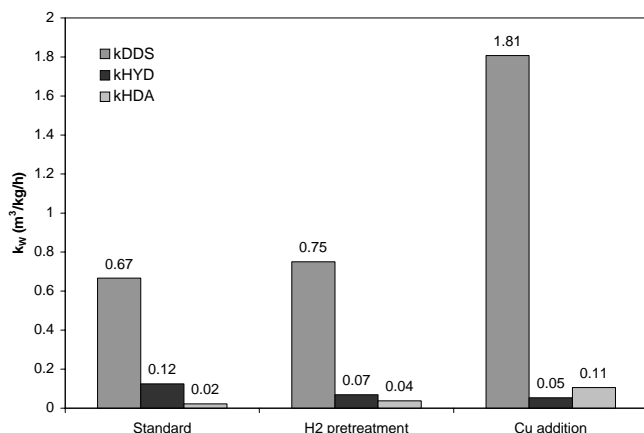


Figure 4. Effect of H₂ pretreatment and H₂S removal on the DBT HDS rate constants (batch autoclave, 350°C, 50 bar).

When all self-produced H₂S is removed from the system by copper powder, we observe a tremendous increase in DDS activity. This again proves the high sensitivity of the DDS sites to sulfur

inhibition. The rate of HDA increases accordingly, so it appears that the same type of sites catalyzes the HDA reaction. The reactants and H₂S are competitive adsorbents on the vacant sites, which can also explain the perfect first-order fit in DBT conversion when self-produced H₂S is not removed. Apparently the adsorption effects normally observed (Langmuir-Hinshelwood kinetics) cancel out. Based on our observations we propose the following rate equation for the DDS route (Eq. 2).

$$r_{\text{DDS}} = \frac{k_{\text{HDS}} C_{\text{DBT}} p_{\text{H}_2}}{1 + K_{\text{DBT}} C_{\text{DBT}} + K_{\text{H}_2\text{S}} p_{\text{H}_2\text{S}} + K_{\text{H}_2} p_{\text{H}_2}} \quad (\text{Eq. 2})$$

Here we assume that H₂ dissociation occurs on the same sites as the DDS reaction, which is not unlikely as these sites (vacant Mo or Ni atoms) apparently catalyze the HDA reaction as well. When the adsorption constants K_{DBT} and $K_{\text{H}_2\text{S}}$ are approximately equal, the number of vacant sites does not change during reaction and pseudo first-order kinetics are observed. When H₂S is removed, the adsorption of DBT becomes significant and the reaction rate will deviate from the first order model (as was the case in the experiment with Cu addition). Furthermore, when K_{H_2} is small compared to K_{DBT} and $K_{\text{H}_2\text{S}}$ the reaction also becomes first order in hydrogen pressure, as was observed in our microflow experiments. Also the apparent order in $p_{\text{H}_2\text{S}}$ becomes -1, which cancels out against the first order in p_{H_2} in a flow reactor (without H₂S addition), in full agreement with our DBT and LGO HDS results. The HYD route shows very little inhibition, which implies the role of H₂S as competitive adsorbent is small. Possibly, at high H₂S concentrations, the HDS of the prehydrogenated DBT molecules becomes a limiting factor.

Conclusions

In the hydrodesulfurization of high sulfur-containing oil streams (*e.g.* LGO) inhibition by self-produced H₂S plays an important role. The major fraction of sulfur compounds in these streams consists of dibenzothiophene and its mono-substituted analogues, which are mainly converted by the direct desulfurization (DDS) route. At low conversion this leads to a zero-order behavior in hydrogen pressure, because in a flow reactor the partial pressure of gaseous reaction products (in particular H₂S) scales linearly with the total pressure, and the DDS route exhibits a very strong inhibition by H₂S.

The effect of H₂S partial pressure on the catalytic performance is two-fold: The H₂S/H₂ ratio may alter the balance between DDS sites (sulfur vacancies) and HYD sites (SH groups) on the catalyst active phase. Secondly, H₂S competes very strongly with reactants for adsorption on vacant sites, thus inhibiting the DDS reaction. The effect on HYD activity is much smaller, and may be due to inhibition of the second step in this pathway; the HDS of prehydrogenated species. All experimental observations can be explained by a Langmuir-Hinshelwood kinetic model in which $K_{\text{H}_2} \ll K_{\text{DBT}} \approx K_{\text{H}_2\text{S}}$.

Acknowledgement. AKZO Nobel Chemicals, the Netherlands, and the Dutch Organization for Scientific Research (NWO) are gratefully acknowledged for financial support.

References

- [1] Vogelaar, B.M.; Gast, J.; van Langeveld, A.D.; Eijsbouts, S.; and Moulijn, J.A. Prepr. Pap. - *Am. Chem. Soc., Div. Petr. Chem.*, **2002**, 47 (1).
- [2] Farag, H.; Mochida, I.; and Sakanishi, K. *Appl. Catal. A - Gen.*, **2000**, 194-195, 147-157.
- [3] Vradman, L.; Landau, M.V.; and Herskowitz, M. *Catal. Today* **1999**, 48, 41-48.
- [4] Vogelaar, B.M.; Steiner, P.; van Langeveld, A.D.; Eijsbouts, S.; and Moulijn, J.A. Prepr. Pap. - *Am. Chem. Soc., Div. Petr. Chem.*, **2002**, 47 (1).

INHIBITING EFFECTS OF BASIC NITROGEN ON DEEP HYDRODESULFURIZATION OF DIESEL

Uday T. Turaga, Gang Wang, Xiaoliang Ma, and Chunshan Song*

Clean Fuels and Catalysis Program, The Energy Institute and Department of Energy and Geo-Environmental Engineering, The Pennsylvania State University, University Park, PA 16802

*Corresponding author. E-Mail: csong@psu.edu

Introduction

The subject of inhibition of hydrodesulfurization (HDS) activity has been studied extensively [1] and some of the key inhibitors include aromatics, nitrogen-containing compounds, hydrogen sulfide, saturated hydrocarbon solvents, ammonia, and even water. Of these, nitrogen-containing compounds were identified as having the most severe inhibiting effect [2]. Atmospheric gas oil, which is frequently used as a diesel feedstock, typically, contains nitrogen compounds 70% of which are non-basic (e.g., carbazole type) while the rest are basic (e.g., quinoline type). Light cycle oil, a feedstock used for diesel and thermally stable naphthenic jet fuels [3, 4], contains much higher nitrogen, predominantly non-basic in nature [5]. Diesel and some jet fuel feedstocks, therefore, have enough nitrogen species to significantly influence deep HDS.

Nitrogen's effects on HDS catalytic activity could become all the more important because the U.S. Environmental Protection Agency requires that diesel in 2006 have sulfur content no more than 15 wppm [6]. Sulfur removal to such depths will require knowledge of the influence of non-sulfur diesel fuel components on deep hydrodesulfurization. Furthermore, the reactivity of nitrogen-containing heterocompounds is much lower than those of polyaromatic sulfur compounds (PASCs) [7]. Therefore, nitrogen compounds will be present in appreciable quantities even at very low sulfur levels and could significantly influence the deep HDS of PASCs.

Several researchers have clearly established the inhibiting effect of basic nitrogen compounds on the HDS of thiophene and dibenzothiophene (DBT) [8, 9]. However, there is little literature on the effects of quinoline and tetrahydroquinoline (THQ) specifically on the HDS of DBT and 4,6-dimethyldibenzothiophene (4,6-DMDBT). The present work evaluates the inhibiting effects of THQ and quinoline on a commercial Co-Mo/ γ -Al₂O₃ hydrodesulfurization catalyst. This extends our previously reported studies on novel HDS catalysts [3, 10-13].

Experimental

All catalysts were evaluated in a laboratory-scale fixed-bed flow reactor which has been described elsewhere [12]. The catalyst evaluation conditions used in this project are summarized in Table 1. All catalysts were sulfided *in situ* at uniform conditions. A typical model compound feedstock contained 1500-2000 wppm of sulfur in the form of 4,6-DMDBT and DBT dissolved in hydrocarbon solvents such as *n*-dodecane (*n*-C₁₂) or *n*-tridecane (*n*-C₁₃). These feeds were spiked with either quinoline or THQ in amounts such that the total nitrogen content was 250 ppm. The liquid reaction products were characterized using a Hewlett Packard 5890 Series II gas chromatograph coupled with flame ionization (FID) and flame photometric detectors (FPD).

A Co-Mo/ γ -Al₂O₃ commercial catalyst supplied by Criterion Catalyst Corporation, Houston, TX, was used for this study. This

catalyst is referred to in this study by its trade name, C-344. A typical catalyst evaluation experiment used 1 g of the catalyst. All catalysts evaluated in the flow reactor were particles of 0.5-1.0 mm in diameter.

Table 1. Flow Reactor Experimental Conditions.

Catalyst Sulfidation	
Temperature	350 °C
10% H ₂ S in H ₂ (vol.%) flow rate	200 ml/min
Time	4 hours
Deep HDS Reaction	
Temperature	240-350 °C
Pressure	660 psi
Weight Hourly Space Velocity	1-8 h ⁻¹
Hydrogen/Hydrocarbon	300 ml/ml
Catalyst particle size	0.5-1.0 mm (18-35 mesh)
Catalyst weight	1 g

Results and Discussion

Figure 1 shows the conversion of 4,6-DMDBT with and without the presence of quinoline and THQ. Similarly, Figure 2 presents conversion data for DBT. It is clear in both cases that the conversion of the PASCs is inhibited by both quinoline and THQ. However, inhibition by THQ is significantly more in comparison to that by quinoline. At higher temperatures, the inhibiting effects of quinoline on the HDS of 4,6-DMDBT are magnified. Nevertheless, quinoline continues to be weaker inhibitor in comparison to THQ.

A potential explanation for the differences in inhibiting effects shown by quinoline and THQ lies in their basicities. The aqueous phase pK_a values of quinoline and THQ are 4.9 and 5.0, respectively [13]. The pK_a values provide an indicator of the proton affinity tendencies of these molecules. Clearly, THQ has a marginally higher proton affinity than quinoline. Therefore, THQ could be expected to have a stronger tendency to adsorb and deactivate adsorption sites on the commercial catalyst surface. Although it is recognized that under the conditions in which HDS occurs, the molecules might be in gas phase, it is instructive in evaluating the aqueous phase to draw preliminary trends.

Determining the influence of quinoline and THQ on the HDS of PASCs is an important problem because of the characteristics of the hydrodenitrogenation of quinoline, which might be present in significant quantities at the low sulfur levels required by new specifications. The hydrodenitrogenation of quinoline takes place through one of two pathways. The first produces decahydroquinoline and propylcyclohexylamine as intermediates, while the second results in THQ and *o*-propylaniline. Both pathways lead to propylcyclohexane, which is the main product of the hydrodenitrogenation of quinoline.

Earlier studies on quinoline hydrodenitrogenation had suggested that the pathway forming THQ and *o*-propylaniline was negligible [13]. However, over phosphided Ni-Mo catalysts, Jian and Prins [14] have shown that this is not the case. They found that in the temperature range of 350-370 °C, about 35-40% of the hydrodenitrogenation of quinoline occurs through the pathway forming THQ and *o*-propylaniline as intermediates.

The results of the present paper suggest that if more of quinoline is converted through the pathway producing THQ as an intermediate, the THQ formed as an intermediate might further magnify the

inhibition of the overall HDS reaction. Therefore, the results presented in this paper quantifying the extent and difference of inhibition caused by quinoline and THQ are an important step towards further understanding of the inhibiting effects of nitrogen on deep hydrodesulfurization of diesel feedstocks. (9 pt)

Conclusions

The inhibiting effects of quinoline and THQ were evaluated for the HDS of PASCs, namely DBT and 4,6-DMDBT. Both forms of basic nitrogen were found to inhibit the HDS of both PASCs. THQ, however, had a larger inhibiting effect in comparison to quinoline. The origin of this higher inhibiting effect is tentatively attributed to the former's marginally higher proton affinity. The effect of nitrogen-containing compounds on the deep HDS of diesel feedstocks is a critical problem because with ultra-low sulfur specifications, the concentration of nitrogen will become high enough to influence the overall HDS reaction. Therefore, a better understanding of nitrogen compounds and the intermediates formed during their decomposition (e.g., THQ which is formed during the hydrodenitrogenation of quinoline) on HDS is required, towards which this paper makes an important contribution.

Acknowledgements. The authors are grateful to Professor Harold H. Schobert for useful discussions. The United States Air Force Office of Scientific Research and the United States Department of Energy supported this work.

References

1. Girgis, M. J. and Gates, B. C. *Ind. Eng. Chem. Res.* **1991**, *30*, 2021-2058.
2. Schulz, H.; Bohringer, W.; Waller, P.; Ousmanov, F. *Catal. Today*, **1999**, *49*, 87.
3. Turaga, U.T. and Song, C. *Am. Chem. Soc. Div. Pet. Chem. Prepr.*, **2002**, *47*, 97.
4. Song, C. In *Chemistry of diesel fuels* Song, C.; Hsu, C.S.; and Mochida, I. Eds. Taylor & Francis: New York, **2000**, pp 1-60.
5. Dorbon, M. and Bernasconi, C. *Fuel* **1989**, *68*, 1067.
6. EPA. *Federal Register* **1999**, *64*, 26142.
7. Zeuthen, P.; Knudsen, K.G.; Whitehurst, D.D. *Catal. Today* **2001**, *65*, 307-314.
8. Satterfield, C.N., M. Modell, and J.F. Mayer, "Interactions between catalytic hydrodesulfurization of thiophene and hydrodenitrogenation of pyridine." *AIChE Journal*, 1975. **21**: p. 1100-1197.
9. Satterfield, C.N.; Modell, M; Wilkens, J.A. *Ind. Eng. Chem. Proc. Des. Dev.* **1980**, *19*, 154.
10. Turaga, U.T. and Song, C. *Proc.16th Ann. Intl. Pitt. Coal Conf.* **1999**, Paper No. 20-25.
11. Turaga, U.T. and Song, C. *Am. Chem. Soc. Div. Pet. Chem. Prepr.*, **2001**, *46*, 275.
12. Turaga, U.T. and C. Song, "MCM-41-Supported Co-Mo catalysts for deep hydrodesulfurization of light cycle oil." *Submitted*, 2003.
13. Ho, T.C. *Catal. Rev.—Sci. & Eng.*, **1988**, *30*, 117.
14. Jian, M.; Prins, R. *J. Catal.*, **1998**, *179*, 18.

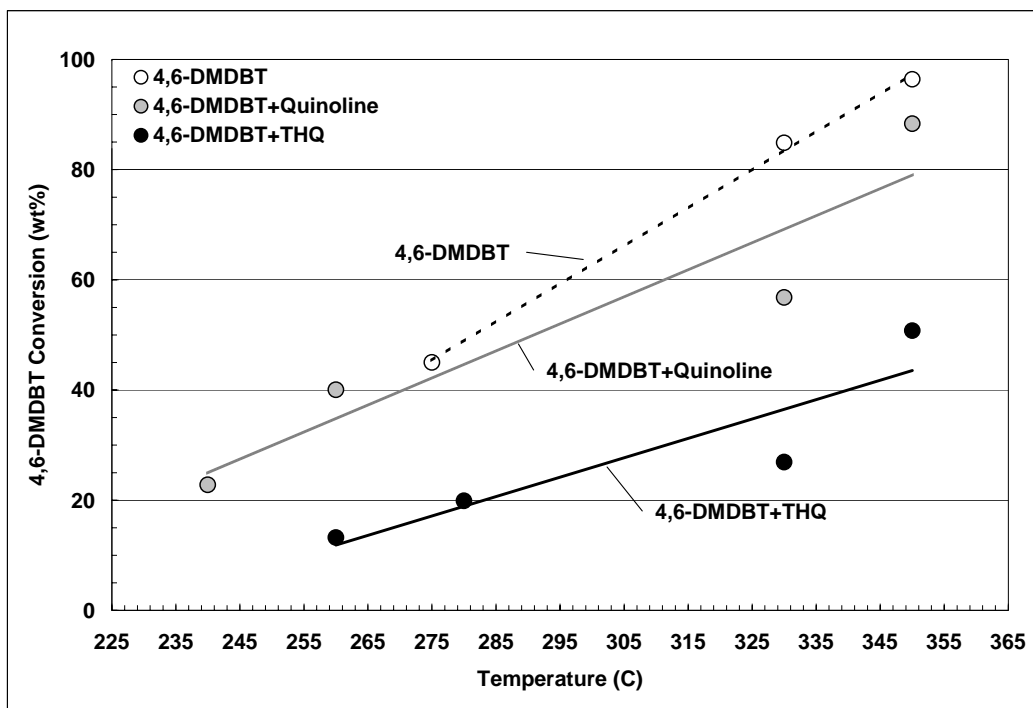


Figure 1. HDS of 4,6-DMDBT with and without basic nitrogen compounds.

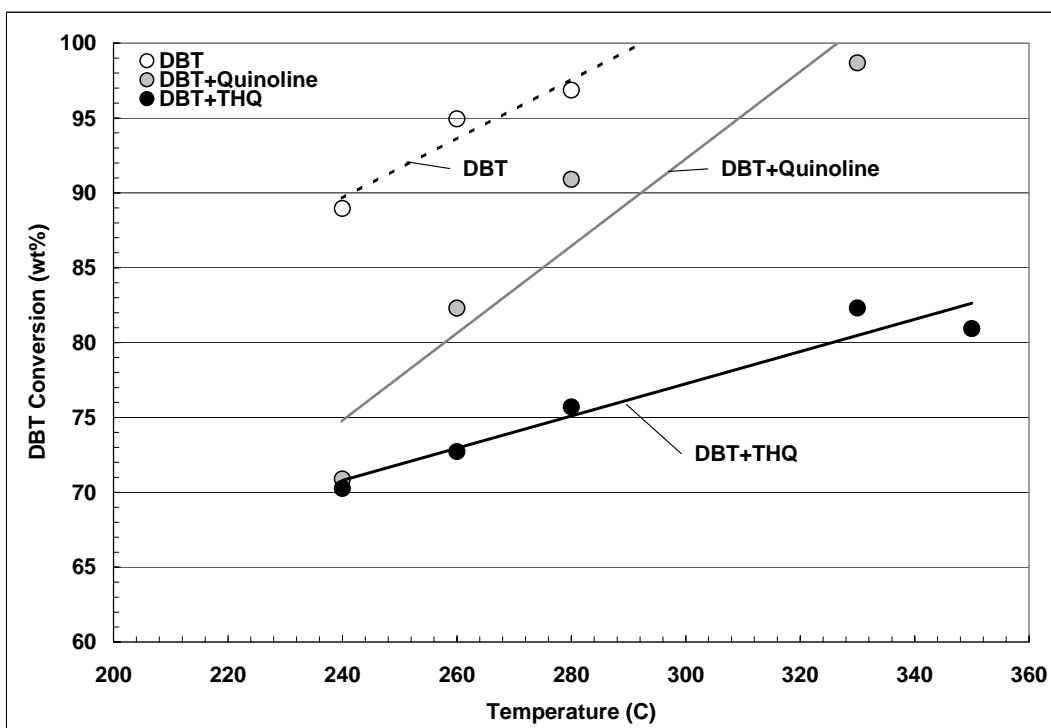


Figure 2. HDS of DBT with and without basic nitrogen compounds.

KINETIC STUDY OF EFFECTS OF AROMATIC COMPOUNDS ON DEEP HYDRODESULFURIZATION OF 4,6-DIMETHYLDIBENZOTHIOPHENE

Jae Hyung Kim, Xiaoliang Ma and Chunshan Song*

Clean Fuels and Catalysis Program, The Energy Institute and Department of Energy and Geo-Environmental Engineering, The Pennsylvania State University, 209 Academic Projects Building, University Park, PA 16802
*E-mail: csong@psu.edu

Introduction

Deep hydrodesulfurization (HDS) of diesel fuel is an important research area due to increasingly stringent environmental regulations for the sulfur content in fuel (1). The sulfur level in diesel fuel will have to be reduced from the present 500 ppmw to 15 ppmw by 2006. Therefore, the studies on deep hydrodesulfurization of diesel fuels are being conducted by many research groups with various methods (1-4).

Sulfur compounds remaining in the current commercial diesel fuel are alkyl dibenzothiophenes (DBTs), especially those with one or two alkyl groups at the 4- and 6-positions. These alkyl DBTs have been reported to be the refractory sulfur compounds in diesel fuel (2,3), in which 4,6-dimethyl-dibenzothiophene (4,6-DMDBT) is a typical refractory sulfur compound. HDS of DBTs generally proceeds through two reaction pathways, hydrogenation and hydrogenolysis pathways (4,5). In our previous study (6), we found that hydrogenation pathway was much more dominant than hydrogenolysis pathway in HDS of 4,6-DMDBT, and the reaction pathways of 4,6-DMDBT can be described as shown in Figure 1.

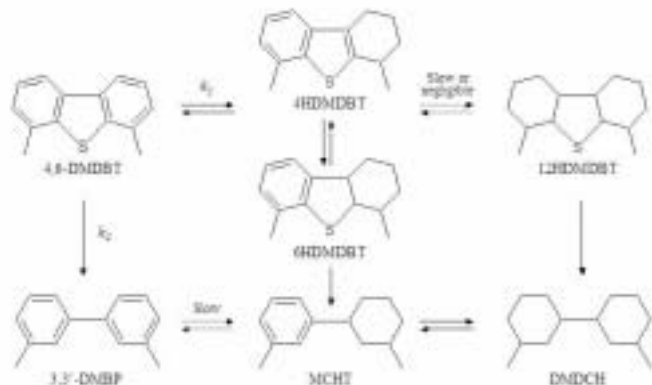


Figure 1. Schematic diagram of 4,6-DMDBT reaction pathways.

Diesel fuel and gas oil contain considerable amounts of aromatic and nitrogen compounds, which may affect the hydrodesulfurization reaction rate. The reported studies on effect of aromatic compounds on the reaction pathways of 4,6-DMDBT were limited in the literature and some previous results are still debated. Some researchers reported that the addition of aromatic compounds led to a significant negative effect on the rate of HDS, though others showed a slight inhibition of aromatics toward HDS (7). In this study, effect of aromatic compounds on HDS of 4,6-DMDBT were examined kinetically using the method that was developed in our previous study (6).

Experimental

4,6-DMDBT was used as the model sulfur compounds in the present study was used. The feed for each run contained 0.05g of 4,6-

DMDBT and 4.00g of decalin as solvent. In order to examine the effect of aromatic compounds on HDS of 4,6-DMDBT, an equimolar amount of 1-methylnaphthalene (1-MN) and 4,6-DMDBT (or 0.74 mol of fluorene and 1.00 mol of 4,6-DMDBT) were added into the feed. The reactions were carried out in 25-mL, horizontal micro-reactor agitated at 200 strokes/min in a fluidized sand bath at the reaction condition of 300°C and 300psi H₂ pressure. Gas chromatography with a FID detector was used for quantitative analysis of products. GC-MS and some standard samples were used for identification of products.

Two commercial catalysts from Criterion, Cr344 (CoMo/Al₂O₃) and Cr424 (NiMo/Al₂O₃), were used after presulfidation with 10 vol % H₂S in H₂ at a flow rate of 200 ml/min, 350°C for 4 h. After presulfidation, the catalysts were stored in decalin before use in order to minimize oxidation.

Results and Discussion

In order to get better kinetic data, the conversion of 4,6-DMDBT was kept below 20%. The main products from 4,6-DMDBT HDS were HDMDBT (hydrodimethyldibenzothiophene), MCHT (methyl cyclohexyltoluene). In addition, DMDC (dimethyldicyclohexyl) was also detected at high conversion. During HDS of 4,6-DMDBT, the main products from 1-methylnaphthalene (1-MN) hydrogenation were 1-methylalinalin (1-methyltetrahydronaphthalene) and 5-methylalinalin (5-methyltetrahydronaphthalene). Hexahydrofluorene was a dominant product from hydrogenation of fluorene.

In general, HDS of individual sulfur compound follows the pseudo-first-order kinetics, thus:

$$\ln(C_{DMDBT} / C_{DMDBT0}) = -(k_1 + k_2) \cdot t \quad (1)$$

where k_1 is the pseudo first-order rate constant for the hydrogenation pathway, and k_2 is the pseudo first-order rate constant for the hydrogenolysis pathway. The value of $(k_1 + k_2)$, the overall rate constant, can be calculated from experimental data. Figure 2 and 3 show the pseudo first order kinetic profiles of 4,6-DMDBT HDS in the presence and absence of aromatic compounds over CoMo and NiMo sulfide catalysts. The overall rate constants calculated on the basis of the experimental data are shown in Table 1.

Based on the results, the presence of 1-MN reduces significantly the HDS rate of 4,6-DMDBT. For the CoMo sulfide catalyst, the overall rate constant of 4,6-DMDBT decreases from $44.15 \times 10^{-5} \text{ s}^{-1} \text{ g} \cdot \text{cat}^{-1}$ in the absence of 1-MN to $33.90 \times 10^{-5} \text{ s}^{-1} \text{ g} \cdot \text{cat}^{-1}$ in the presence of 1-MN, and for NiMo sulfide catalyst, from $117.21 \times 10^{-5} \text{ s}^{-1} \text{ g} \cdot \text{cat}^{-1}$ to $76.22 \times 10^{-5} \text{ s}^{-1} \text{ g} \cdot \text{cat}^{-1}$. It was found that fluorene shows a much stronger effect on the overall rate constant than 1-MN. The overall rate constant in the presence of fluorene is 21.59×10^{-5} and $56.71 \times 10^{-5} \text{ s}^{-1} \text{ g} \cdot \text{cat}^{-1}$ for the CoMo catalyst and the NiMo catalysts, respectively. Koltai and coworkers reported the effects of aromatic compounds, including anthracene, phenanthrene and fluorene, on 4,6-DMDBT over NiMo sulfide catalyst at 300°C and 725 psi (7). They reported that there is no significant effect of the coexisting anthracene and dihydroanthracene on HDS of 4,6-DMDBT, even the concentration of anthracene and dihydroanthracene is 7 times higher than that of 4,6-DMDBT, while there is significant effect of the coexisting phenanthrene and fluorene on HDS of 4,6-DMDBT. Our result about the effect of fluorene is consistent with the result from Koltai and coworkers.

In this study, the individual rate constants for each reaction pathway were calculated by using the method suggested in our previous work (6). In this method, the ratio of k_1/k_2 was calculated by

the ratio of the initial selectivity of primary products, as shown below:

$$\frac{k_1}{k_2} = \frac{[\text{Initial Selectivity of HDMDBT}]}{[\text{Initial Selectivity of DMBP}]} \quad (2)$$

Individual rate constants were calculated in combination of k_1/k_2 and (k_1+k_2) values. Table 1 lists the calculated rate constants for each reaction pathway with and without the presence of aromatic compounds. For the CoMo catalyst, the presence of the aromatic compounds degrades the rates for both hydrogenation pathway and hydrogenolysis pathway. For the NiMo catalyst, the presence of the aromatic compounds degrades slightly the rate for hydrogenolysis pathway, but degrades strongly the rate for hydrogenation pathway. The decrease of k_1/k_2 in the presence of the aromatic compounds was observed, indicating that these aromatic compounds have more effect on hydrogenation pathway than on hydrogenolysis pathway. The different effects of the aromatic compounds on the two pathways, especially over the NiMo catalyst, imply that the hydrogenation and hydrogenolysis might occur at different active sites, and the decrease of the catalytic activity of the NiMo catalyst by the aromatic compounds is probably due to a competitive adsorption between the aromatic compounds and 4,6-DMDBT for the active sites of hydrogenation.

Conclusions

In this study, effects of the aromatic compounds on HDS of 4,6-DMDBT were investigated kinetically. The presence of 1-MN and fluorene affects significantly on HDS of 4,6-DMDBT at the reaction conditions of 300°C and 300 psi. The change in the ratio of k_1/k_2 indicates that the aromatic compounds have more negative impact on the hydrogenation pathway than on hydrogenolysis pathway. From a comparison of the two aromatic compounds, fluorene is a stronger inhibitor than 1-MN.

Acknowledgement. This work was supported in part by New Energy and Industrial Technology Development Organization, Japan, and by US Department of Energy, National Energy Technology Laboratory.

References

- (1) Song, C.; Ma, X. *Appl. Catal. B: Environ.*, **2003**, *41*, 207.
- (2) Ma, X.; Sakanishi, K.; Mochida, I. *Ind. Eng. Chem. Res.*, **1994**, *33*, 218.
- (3) Gates, B. C.; Topsoe, H. *Polyhedron*, **1997**, *16*, 3213.
- (4) Broderick, D. H.; Gates, B. C. *AIChE J.*, **1981**, *27*, 663.
- (5) Sakanishi, K.; Nagamatsu, T.; Mochida, I.; Whitehurst, D. J. *Mol. Cat. A*, **2000**, *155*, 101.
- (6) Kim, J. H.; Ma, X.; Song, C.; Oyama, T.; Lee, Y. K. Prepr. Pap. – *Am. Chem. Soc., Div. Fuel Chem.*, **2003**, *48* (1) 40.
- (7) Koltai, T.; Macaud, M.; Guevara, A.; Schulz, E.; Lemaire, M.; Baccard, R.; Vrinat, M. *Appl. Catal. A*, **2002**, *231*, 253.

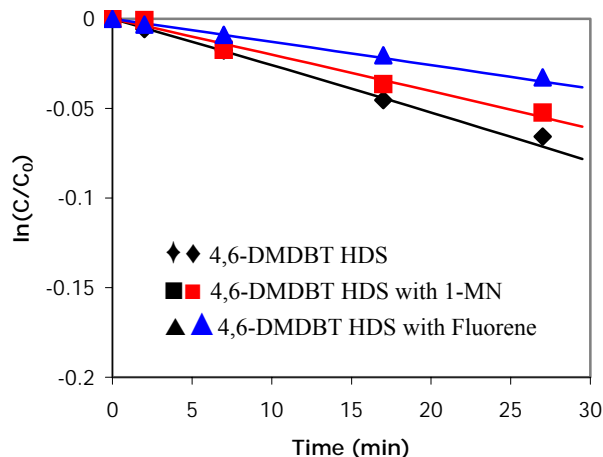


Figure 1. The effect of aromatic compounds on HDS of 4,6-DMDBT over CoMo sulfide catalyst.

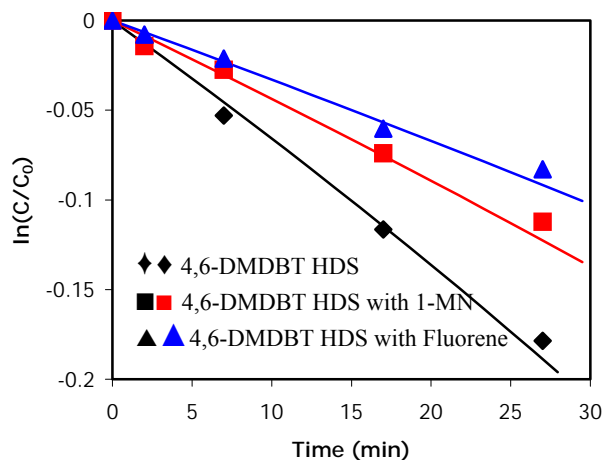


Figure 2. The effect of aromatic compounds on HDS of 4,6-DMDBT over NiMo sulfide catalyst.

Table 1. Kinetic Results for the Effect of Aromatic Compounds on Hydrodesulfurization of 4,6-DMDBT

Inhibitor		Rate constant ($10^{-5} \text{ s}^{-1} \text{ g}\cdot\text{cat}^{-1}$)		
		None	1-MN	Fluorene
CoMo Sulfide	k_1+k_2	44.15	33.90	21.59
	k_1/k_2^a	2.26	2.22	1.79
	k_1	30.60	23.38	13.85
	k_2	13.55	10.50	7.73
NiMo Sulfide	k_1+k_2	117.21	76.22	56.71
	k_1/k_2^1	5.36	3.66	2.65
	k_1	98.77	59.85	41.17
	k_2	18.44	16.37	15.54

^a $k_1/k_2 = [\text{Initial selectivity of HDMDBT}]/[\text{Initial selectivity of DMBP}]$

APPLICATION OF DATAMINING METHOD (ID3) TO CORRELATION OF FEED PROPERTIES AND REACTIVITY FOR HDS OF DIESEL FUEL

Narinobu Kagami, Ryuichiro Iwamoto, Masaru Amano, and Tetsuji Tani

Manufacturing Department, Idemitsu Kosan Co., Ltd.
26 Anesakikaigan Ichihara-city Chiba, 299-0107, Japan

Introduction

In recent years, much attention has been focused on the deep hydrodesulfurisation (HDS) of diesel fuel oil because environmental legislation has become more and more strict. Then it becomes more important to estimate the reaction temperature correctly to meet the target of sulfur at various conditions using various feedstocks. Because too deep desulfurisation makes the catalyst life shorter than producing correct target sulfur diesel¹⁾, determining the accurate corrected WAT (weight average temperature) is very important for the management of the diesel production and the catalyst life span.

It is well known that corrected WAT is used to evaluate the catalyst life. And WAT is a function of the operation condition factors such as temperature, LHSV, Hydrogen pressure, Hydrogen-oil ratio and of the feed properties. Operation condition factors can be normalized from the formula based on n-order (pseudo) reaction and Arrhenius plots through tuning the constant. These operation factors can be changed independently using pilot tests, however, it is almost impossible with a real feed to vary just one property independently. Therefore, the suitable selection of key factors of feed properties might be difficult using real feed.

The formula of the corrected WAT normalized to the standard from various feed properties was made by trial and error method somehow, using the factors chosen by the information of literature²⁾. However, we still need a convenient way to evaluate the validity of the chosen factors.

Recently, datamining methods tend to be used more commonly in data processing field. Datamining is one of the technologies for building knowledge-based systems by inductive inference from examples. Therefore, it can also be the method to search the valuable information from large data sets. In datamining methods, the classification analysis called ID3 (Iterative dichotomiser) is applicable.

ID3 algorithm was suggested by J.R Quinlan³⁾ and extended to deal with numerical values⁴⁾. Using entropy of information that shows the degree of chaotic state, ID3 establishes the importance of the factor automatically.

Then ID3 was applied to evaluate the validity of the chosen factors from various feed properties for the corrected WAT normalized to the standard.

Experimental

Catalyst and Pretreatment. 100cc of commercial catalyst of CoMo type catalyst was filled in a high-pressure micro-flow reactor. Before the evaluation of SRLGO, the catalyst was presulfided in situ at 250 °C for 2h and then 300 °C for 2h in stream of a dimethyl-disulfide/SRLGO/hydrogen mixture (sulfur content, adjusted as 2.5wt%).

Pilot Test. Pilot tests were carried out using high-pressure micro-flow reactor. The temperature of the catalyst bed was kept constant to avoid temperature difference over the catalyst bed by heater blocks. Thermocouples were located in the center of the catalyst beds. In these range of the operation conditions, the results of sulfur content of the product were from 500 to 5 ppm.

Analysis of feeds and products. Six kinds of straight run light gas oils (SRLGO) from Middle East crude were tested in high pressure flow reactor. The various properties of feedstocks were measured as shown in Table 1.

The sulfur content of product was also measured. The product oils were stripped by nitrogen to get rid of the H₂S in the liquid before the measurement.

ID3 data analysis. ID3 software package were used for the analysis of the data of pilot tests (XpertRule (Lascombe and Company, Ltd.)). Figure.1 shows the algorithm of ID3. A classification rule was expressed as a decision tree. The relationship between object Item A and attribute Items X, Y, Z were examined using the entropy of information. As step 0 shows, the entropy of the object item (I) was calculated. Next object item is divided according to the attribute items, and each entropy (E (X, Y, Z)) was calculated as step 1 shows. Then the subtract values of I - E (X, Y, Z) were information gains. And the largest information gain means that the information becomes less chaotic. Then, Item X was selected as first attribute and this routine was reiterated. In this way, ID3 can select the simplest decision tree.

Definition for entropy of information

$$\text{Entropy } E_n = \sum p_n (\sum -p_i \log_2 p_i)$$

p_n : Probability for all data, p_i : Probability for each case(i)

$$\text{At Step 0, } \sum p_n = 1, \quad E_n = I(i) = \sum -p_i \log_2 p_i$$

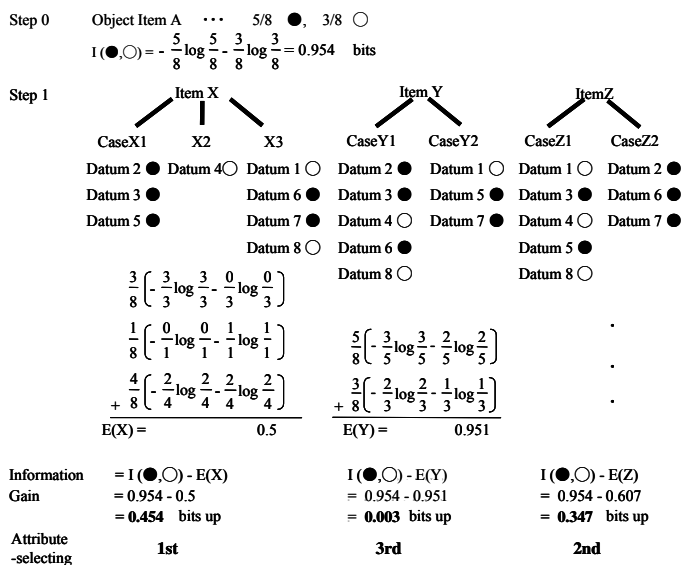


Figure 1. Outline algorithm of ID3(Iterative Dichotomiser).

Results and Discussion

Operation condition factors can be corrected independently, because each operation factor can be changed independently using the same feed stocks. It is well known that corrected WAT is used to evaluate the catalyst activity and its deactivation rate. The reaction temperature under the normalized conditions can be calculated as follows (Arrhenius eq.1, n-order reaction eq.2, hydrogen-oil ratio eq.3, hydrogen pressure eq.4).

$$\ln k = \ln A - \frac{Ea}{RT}, \ln k' = \ln A - \frac{Ea}{RT''} \quad (eq.1)$$

$$k = \frac{LHSV}{n-1} \times \left(\frac{1}{S_p^{n-1}} - \frac{1}{S_f^{n-1}} \right) \quad (eq.2)$$

$$k' = k \times \left(\frac{Hoil-Ratio_p}{Hoil-Ratio_s} \right)^a \quad (eq.3)$$

$$k' = \exp(\ln k') \times \left(\frac{HP_p}{HP_s} \right)^b \quad (eq.4)$$

In Fig.2, the actual WAT and corrected WAT standardized at a certain operation condition were shown. After the normalization of operation condition factors, the data scattering range becomes small. However, the scattering is still above 15 °C difference, depending on the properties on the kind of feed.

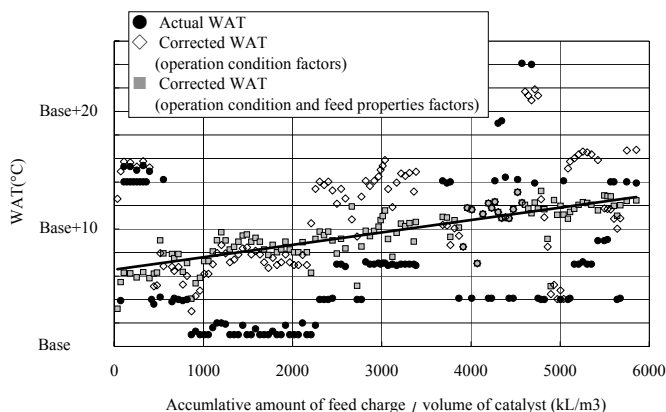


Figure 2. Actual and Corrected WAT for HDS reaction.

The WAT during the deep desulfurisation of the gas oil could be regarded to increase linearly with time on stream as shown in some literature⁵. When LHSV's were changed, accumulative amount of feed throughput per catalyst volume should be better to use instead of time on stream, to evaluate the deactivation pattern of catalyst.

Recently the inhibition of HDS reaction by nitrogen compounds was evaluated⁶. Especially the basic nitrogen compounds are thought to have the strongest effects to HDS reaction.

Moreover, it is well known that the heavier sulfur compounds (Dibenzothiophene (DBT) type sulfur compounds, especially 4,6-substituted DBT) has a lower activity than lighter sulfur compound such as benzothiophene type sulfur compounds.

Therefore, the following factors of feed properties were chosen for WAT normalized feed properties as eq.5 shows. "SpGr" is density of feed stocks and it is also used for residue hydrodesulfurization reaction. "Base N" is the content of basic nitrogen (Potentiometric titration). And "T90" is the temperature of 90% distillation (ASTM D-86), which means how heavy the feed is.

Then the trial and error method was used to determine the constant value of a, b, c (eq.5).

$$\ln A' = \ln A + a \cdot \ln \left(\frac{SpGr'}{SpGr} \right) + b \cdot \ln \left(\frac{BaseN'}{BaseN} \right) + c \cdot \ln \left(\frac{T90'}{T90} \right) \quad (eq.5)$$

As deactivation pattern was regarded to be linear line, the least square method was applied and the standard deviation of all data was minimized changing each constant values. In this way, the values of constants were determined, and the results of normalization of feed properties are shown in Fig.2 Then, the difference from the linear line calculated by the least square became around 4 °C and much smaller than the one normalized only operation condition factors.

As described above, corrected WAT for feed properties was obtained. However, there is still the question whether the factors of feed properties chosen for normalization of the WAT are the best or not. To evaluate the validity of the chosen factors, ID3 method was

used. Each difference between the data of corrected WAT normalized operation condition factors and the calculated deactivation line was examined.

Therefore, the data of subtraction from the diamond plot (◇) to the line in Fig.2 is the object item "A" and, "A" is examined by the feed properties factors, items "X, Y, Z". Operation factors are also used to convince that the normalization of them is. The one applied method is ID3, and the other is the correlation coefficient for the analysis. However, object item "A" should not be continuum but step number for the ID3 analysis. Then subtraction was classified per 2 °C.

Table 1 shows the results of the analysis. The effective factors for classification were arranged in order of increasing entropy (Class I to XII), using ID3 method. Clearly, the smaller the entropy, the more effective the factor is. However, in order to select the valid factors, they should be independent of each other. Therefore, the correlation coefficient analysis was also used, and the factors which have a coefficient above 0.8 are shown as the same pattern-code.

Table 1. The Results of ID3 and Correlation Coefficient.

Ranking of entropy (step 1, E(X,Y...))	Effective factor for classification					
I	Type of feed	-	-	-	-	-
II	Density	Nitrogen	Basic nitrogen	-	-	-
III	Saturate	1-ring Arom.	T50VOL%	T60VOL%	T70VOL%	Viscosity
IV	Feed Sulfur	T80VOL%...	T90VOL%...	T95VOL%...	EP.	-
V	-	?	?	?	?	?
VII	Accumulative amount of feed	-	-	-	-	-
VIII	WAT	-	-	-	-	-
IX	LHSV	-	-	-	-	-
X	Product Sulfur	-	-	-	-	-
XI	H2/Oil	-	-	-	-	-
XII	H2 Press.	-	-	-	-	-

The most effective factor is type of feed, and it means that the feed properties factors normalization should be done. The second ranking factors are density, and nitrogen, and basic nitrogen. The correlation coefficient of nitrogen and basic nitrogen is higher, then it means that they had a monotonic relation. Therefore, only the basic nitrogen was selected considering the information described above. The third effective ranking is saturate. It was examined in the same way (eq.5) to minimize the standard deviation. However, it has almost no effect to reduce the standard deviation. The forth are Feed sulfur, T90 vol%, T95vol%, and EP, then the feed sulfur has already been used to calculate the reaction rate constant. T90 vol%, T95vol%, and EP could be considered to be the same factor, then, T90vol% should be taken.

As described above, the factors determined by trial and error method are shown in the bold type, and these are validated by ID3 and correlation coefficient analysis.

Acknowledgment. We thank Prof. Jacob A. Moulijn for generous support to publish this work.

References

- (1) Knudsen, K. G.; Cooper, B. H.; Topsoe, H. *Applied Catalysis A-General*, **1999**, 189, 205.
- (2) Laredo, G. C.; los Reyes, J. A.; Cano, J. L.; Castillo, J. J. *Applied Catalysis A-General*, **2001**, 207, 103.
- (3) Quinlan, J. R. *Machine Learning*, **1986**, 1(1), 81.
- (4) Araki, Kojima *Jinkou Chinou Gakkaishi*, **1992**, 7(6), 992.
- (5) Gerritsen, L. A.; Vogt, K.; Huismans, A. Quinlan, *Summary At the ERTC in Berlin*, in November **1998**.
- (6) Whitehurst, D. D.; Knudsen, K.; Nielsen, I. V.; Wiwel, P.; Zeuthen, P. *Abstracts of Papers of the American Chemical Society*, **2000**, 219, 23-PETR.

FISCHER-TROPSCH PRINCIPLES OF CO-HYDROGENATION ON IRON CATALYSTS

Hans Schulz

University of Karlsruhe
Engler-Bunte-Institute
76131 Karlsruhe, Germany

Introduction

The products of Fischer-Tropsch synthesis on iron catalysts can be composed very similarly as those obtained on cobalt catalysts. This similarity requires a common principle of their formation. But amazingly, FT-synthesis on iron catalysts differs in many regards when compared with FT-synthesis on cobalt:

(1) With cobalt increasing the reaction temperature from e.g. 210 to 350 °C, changes the selectivity to methane as for being the dominant product (e.g. 90 C %). With iron even at 350 °C the methane selectivity can remain low (e.g. 7 C %): The FT-regime is stable over a wide range of temperature.

(2) Increasing the H₂/CO-ratio, respectively reducing the CO partial pressure, changes the FT-selectivity to almost pure methane (at low CO partial) whereas with iron, even when reducing the CO-partial pressure to very low values, the selectivity is merely effected. This means that the FT-regime with cobalt can only exist at sufficiently high CO-partial pressure as in contrast to iron.

(3) Increasing H₂O-partial pressure does positively affect FT-synthesis on cobalt; lowering methane selectivity, increasing chain growth probability, increasing syngas conversion (at some circumstances high H₂O-partial pressure can deactivate the catalyst). With iron, H₂O does inhibit the FT-reaction and restricts the degree of conversion.

(4) Alkali is a very efficient and essential promotor for FT-synthesis on iron, having strong effects on reaction rate and selectivity. With cobalt, no or only minor effects of alkali are noticed.

(5) The water-gas-shift reaction and its reverse generally perform fast on (alkalized) iron catalysts but are not (or only poorly) observed with cobalt catalysts.

(6) The byproducts of FT-synthesis, respectively the minor reactions performing additionally to the main stream of non-trivial surface polymerization, are significantly different with iron- as compared with cobalt catalysts. With cobalt, in contrast to iron, secondary olefin reactions of hydrogenation, isomerization and incorporation occur. Also relations to organic complex catalysis (olefin-hydroformylation, olefin-polymerization and carbene reactions) are noticed in contrast to the performance on iron catalysts.

(7) With both the catalyst metals, processes of self-organization and restructuring of the catalyst occur but they are different in principle with iron and with cobalt. With cobalt the interaction of the cobalt metal with the reactants concerns segregation of the surface. With iron it concerns reaction with carbon, being formed from CO-dissociation to produce iron carbide phases and structured or amorphous carbon phases in addition to further compositional catalyst changes.

In this paper, specifically, the processes of self-organization of the Fischer-Tropsch regime with (alkalized) iron as the catalyst are regarded, as in contrast to the behavior of cobalt catalysts.

Results and Discussion

It is seen in Fig. 1 that the Fischer-Tropsch activity - a measure hereof is the yield of FT-products (Y_{FT}) - initially (t_{exp}, ca. 10 min) is about zero in all the three cases. The precipitated catalysts had been reduced with hydrogen and - generalizing - about half of the iron was in the state of metallic iron and the other half in the state of magnetite in the beginning. So it is concluded that iron in its metallic form exhibits "no" Fischer-Tropsch activity. This is in contrast to e.g. cobalt or ruthenium where essentially the metal is the active phase for FT-synthesis.

The catalyst activity develops with time in about 5 episodes, respectively, kinetic regimes. Episode I relates to the very first contact of the synthesis gas with the catalyst when it replaces the inert gas in the reactor and chromatographic effects and reactor residence-time-behavior overlap with the conversion of reactants.

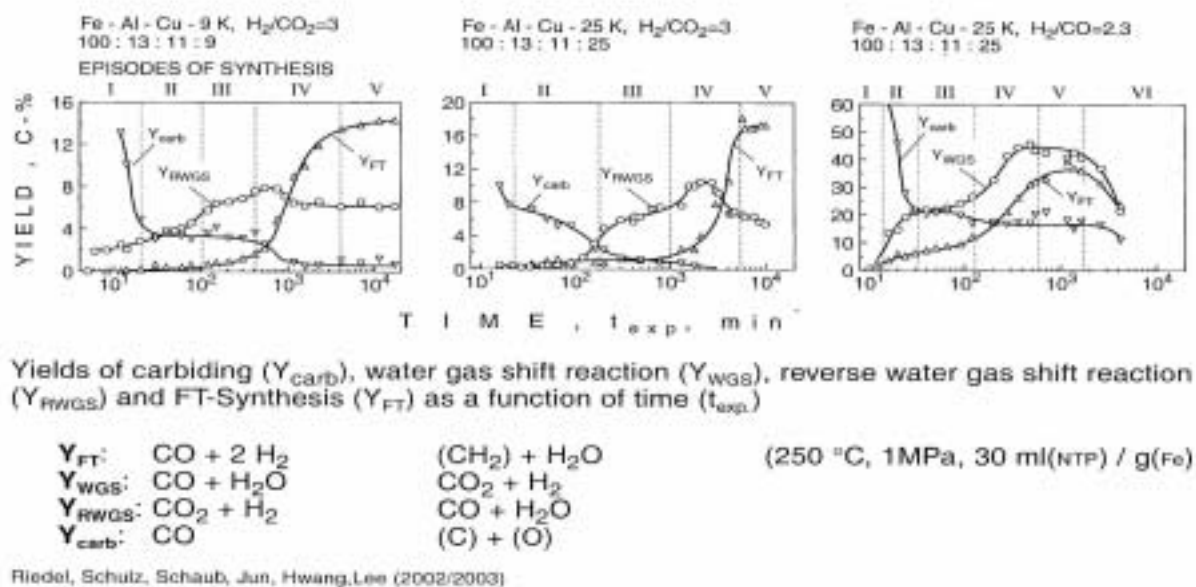


Figure 1. Initial episodes of FT-synthesis with iron as the catalyst.

In Episode II, the main process is the deposition of carbon (Y_{carb}) on the iron catalyst. The carbon yield increases to about 20 C % with the ($\text{H}_2/\text{CO} = 2,3$)-syngas (Fig. 1, right). With the ($\text{H}_2/\text{CO}_2 = 3$)-syngas the carbon yield is less excessive - e.g. 4-6 C % in Episode II (see Fig. 1, middle and left). Here with no CO but only CO_2 in the syngas, the carbon can only be formed as much as CO has been formed by the reverse water-gas-shift reaction. It is seen that also the water-gas-shift activity develops in-situ, prior to FT-activity. But even when in Episode III more CO has been formed from CO_2 plus H_2 (Y_{RWGS}), only marginal FT-activity is noticed (Fig. 1, left and middle). Then, in Episode IV after a number of hours on stream, the Fischer-Tropsch reaction sets in. Obviously, a distinct extent of iron carbiding is necessary for the catalyst to exhibit FT-activity. With the $3\text{H}_2/\text{CO}_2$ -syngas this process of carbiding is slower as compared with the $2\text{H}_2/\text{CO}$ -syngas.

Episode V is the steady-state of FT-synthesis. With the ($2\text{H}_2/\text{CO}$)-syngas a deactivation in Episode VI is noticed as caused by ongoing carbon formation due to high catalyst alkalinization which is favorable at very low CO-partial pressure but too high for a CO-rich syngas.

In Fig. 2 the chain prolongation probability as a function of carbon number is presented for different times on stream and for the same three experiments as in Fig. 1. The result is very remarkable (and in complete contrast to what would be observed with cobalt catalysts). In dependence of time-on-stream only for the initial episodes (up to Episode III) when FT-yields are very low, the curve of growth probability is markedly affected. But during Episode IV when the FT-regime is being established as the FT-yield increases

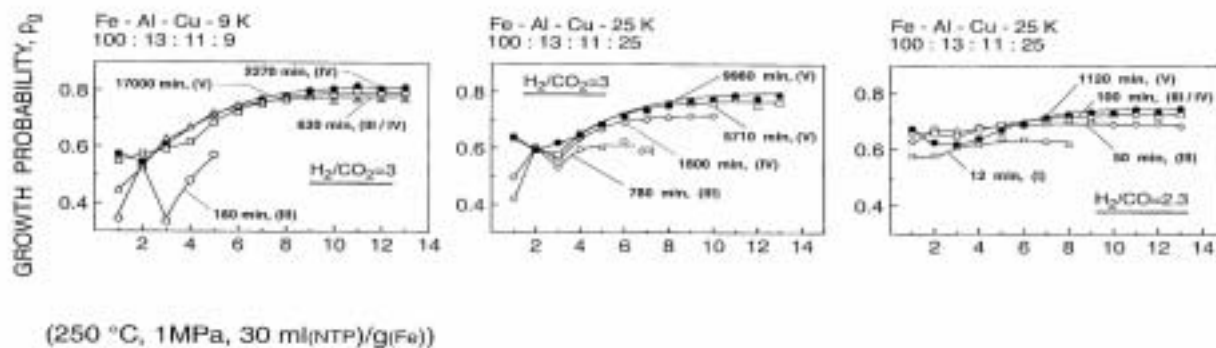
substantially, the curve shape changes only marginally. And even when comparing the steady-state curves for the three experiments the differences are small.

The surprising conclusion is that the FT-chemistry remains much the same, during establishing the FT-regime and even with both the synthesis gases $3\text{H}_2/\text{CO}_2$ and $2,3\text{H}_2/\text{CO}$.

It follows that increasing FT-activity here means an increase of the number of active sites, however, their nature being the same. And as the chemistry (selectivity) is invariant against the partial pressures, specifically of CO, that the sites are not dynamic in nature (in contrast to FT with cobalt).

When now searching for the common FT-principle with iron and cobalt catalysts, it should be a kinetic law, defined more by the sort of involved species than the catalyst composition (iron or cobalt). It is proposed to concern the frustration of the desorption reactions (for paraffins and olefins) thus allowing for the alternative reaction of adding C_1 -species to the adsorbed chain.

In a complementary study of catalyst composition (and structure) as a function of time by XRD, Moessbauer spectroscopy, XPS it was observed that the FT-activity started to develop in correlation to the conversion of the alpha-iron-phase to a Fe_5C_2 -carbide-phase. The carbide-phase is therefore regarded to possess the FT-active sites under reaction conditions and these sites appear to be very stable entities.



At steady state (Episode 5), nearly the same carbon number dependence of growth probability is obtained in all the 3 cases, "no" extra-methane formation is noticed

With CO_2 , olefin readsorption is more pronounced than with CO

Reactions on the FT-sites are very independent on partial pressures of CO and CO_2 , on degree of conversion and on catalyst activity (degree of carbiding)

Figure 2. Chain growth as a function of time (t_{exp})

STUDY ON THE PRODUCT OF FISCHER-TROPSCH SYNTHESIS OVER SKELETON IRON METAL CATALYSTS

Yijun Lu, Peizheng Zhou

R&D Center
Hydrocarbon Technologies, Inc.
1501 New York Ave.
Trenton, NJ 08648

Introduction

Fischer-Tropsch (FT) synthesis can be used to produce either a light syncrude and light olefins or to produce heavy wax hydrocarbons. With its noticeable development of the industrial employed catalysts in SASOL, the iron-based catalysts have been widely studied as commercial FT process catalysts. For the recommended slurry bubble column reactor applied to this process, there exists one critical challenge of difficult solid/wax separation. Skeleton iron (Raney type) catalysts have been initiated years ago and well developed to match this problem solution. This novel iron catalyst has been proved superior CO hydrogenation activity and HC selectivity comparable to conventional precipitated Fe. In the work of optimizing the skeleton catalysts, we realized that the catalysts generation conditions dramatically influence catalyst physical properties and FT synthesis performance. This presentation is to show the effect on FT objective products.

In terms of the synthesis products, Anderson has provided us the thermodynamics reactions of products description in detail¹. Water is a principal primary product. Primary alcohols and /or alpha olefins may also be primary synthesis products. Some researchers have proposed the possible mechanism steps of olefins and oxygenates formation. By far the oxygenates are believed by most people as primary products and sequentially being converted to hydrocarbons². While some authors would accept the point that oxygenates, including normal alcohols, are formed via side reactions. The majority of the oxygenated products are linear with terminal functionality. The amounts and types are highly dependent on the catalyst properties and the reaction conditions. It is reported typically on iron based catalyst and ethanol is the principle oxygenate formed. This presentation provides a chart of the product distribution from novel skeleton iron catalyst, and outlines a rough relationship between the catalyst parameters and product selectivity. Particularly, the significant oxygenates product is addressed and discussed.

Experimental

Making up of skeleton iron catalyst. The patent catalysts were prepared in house and detail procedures can be found elsewhere^{3,4,5}. Several typical catalyst samples were selected for presentation based on following variables.

Table 1. Description of typical skeleton iron catalyst samples

Samples	Components	Alloying (solidification)
1#	Fe/Al	Quenching
2#	Fe/Al/Mn	Q
3#	Fe/Al/Cu	Q
4#	Fe/Al/Zn	Q
5#	Fe/Al	Slow cooling

All catalysts were characterized by X-ray diffraction and demonstrate major phase of metal iron with trace oxides.

Slurry F-T synthesis. The synthesis was conducted in a 1NL continuous stirred tank reactor. Detail operational procedures were reported elsewhere. All above catalyst samples were tested at conditions of : 230-270°C, 2.5 MPa, 2.0 NL/gcat/h, 15wt% catalyst loading. All products samples were collected and only those produced after initial period (~150hours) were analyzed as characteristic data.

Product analysis. HP 6890N series and G1530A GC were used for gas and liquid products analysis. MS-GC was the supplement instrument for verifying plausible components. In respect of the liquid analysis by capillary column, oxygenates were calculated by separated method. Perkin-Elmer CHN element analyzer was applied to ensure the accuracy of oxygenated percent in the liquid.

Results and Discussion

Figure 1 is the XRD data of the as prepared six samples, it indicates that any trace additive element, Zn, Mn, Cu (<5% in the alloy) or the residual Al is not apparently detected by X-ray diffraction. The oxides (Fe₃O₄) were thought formed during the transferring from storage reagent to the instrument monitor.

Brady and Pettit firstly proposed the alkyl mechanism for the Fischer-Tropsch reaction and applied it to explain the similar hydrocarbon product distribution over catalysts such as Ni, Pd, Fe, Co, Ru or Co². Furthermore, almost all researchers accept the conclusion that ethylene as the primary product. Nevertheless, these active FT catalyst components make obvious difference in product composition and distribution. Even for iron base catalysts, there are

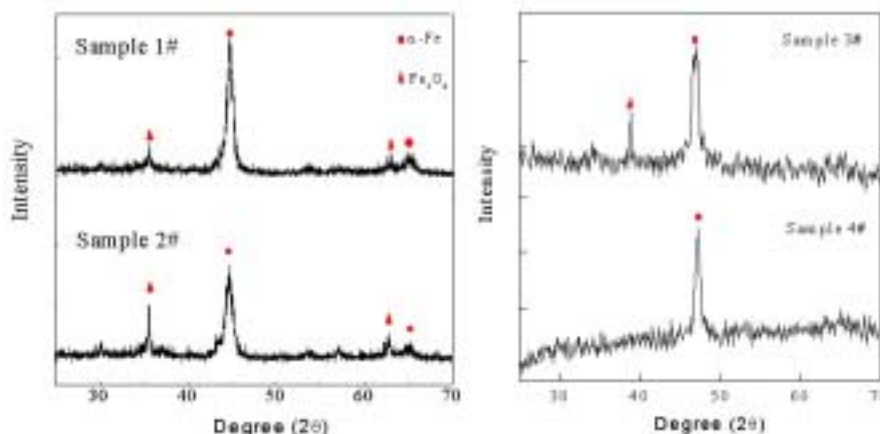


Figure 1. X-ray diffraction spectra of as prepared skeleton iron catalysts

several types catalysts resulted from different precursor material and generation routes (fuse iron, supported iron, precipitated Fe, ultra-fine iron oxide, sinter iron, ferrous alloy etc.). Thus many factors such as active component phase, granule size and combination degree with other components/supports inevitably affect the products quality. And, for each one type of iron base catalysts, say precipitated Fe catalyst, there exists a group of possible active phase comprising α -Fe, Fe_2O_3 , Fe_3O_4 and Fe_xC , which complicated enough to bring up unclear characteristic product distribution¹. Hence the catalytic polymerization mechanism study that extensively concerned by scientists may encounter a potential problem, the complex reaction system gives rise to much similar products over different catalysts (synergetic effect) and hence simplifies the mechanism (acceptable or plausible based on empirical evidence).

This demonstration is purposing on the relationship between lightly altered parameters and FT synthesis products distribution.

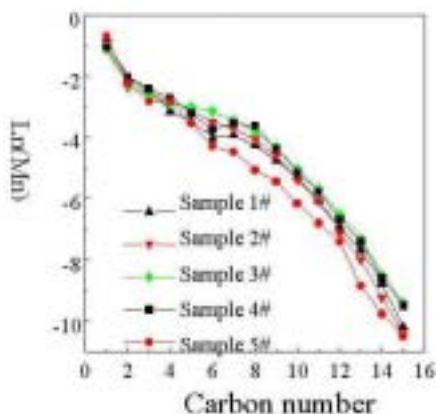


Figure 2. Characteristic carbon number distribution of iron catalysts (skeleton iron here is named as Raney Fe) tested in same reactor

Apparently, the carbon number distribution of HC products (excluded wax) synthesized over skeleton iron catalysts are not severely influenced by trace additives modifying the base catalyst. The exception is the 5# sample, which was characteristic of not-quenching solidification method in the precursor generation, shows a lower chain growth probability ($\alpha \approx -0.63$). To explain this, the metallurgic theory should be referred. Quenching of molten alloy generally results in metal clusters exemplified by $\text{Fe}_{14}\text{Al}_{44}$ (so called frozen eutectic alloy)³. While the slow-cooling way is subjected to yield a simple intermetallic compound such as FeAl_3 . The later one eventually forms to small pores skeleton catalyst (average pore diameter is 15nm, in comparison with the one from former alloy, 22nm).

For all skeleton iron catalyst samples, the related FT products (liquid HC fraction) were almost exclusively linear olefins, alkanes and oxygenates, and methyl-branched was only as minor components of the product distribution. Figure 3 is a typical MS-GC spectrum (from C5 to C13), it is interesting that the normal alcohol is much significant (3rd big peak). It has been stated that the main objective of the synol process was the production of straight chain terminal alcohols of boiling range as high as C_{20} . Thus the skeleton iron catalyst may provide a shortcut to reach this objective. In some case, the amounts of normal alcohols approach 20wt% in the hydrocarbon products. While aqueous product contains about 10% of oxygenates, predominantly methanol and ethanol.

Olefins from the sample catalysts are found in amounts exceeding 50% in each carbon number ($<\text{C}_{18}$). Carbon chains in alcohols are similar to those found in hydrocarbons, and appears

similar carbon number distribution trend. Yields of alcohols on a molar basis are maximal at C_2 and decreasing monotonically with increasing carbon number.

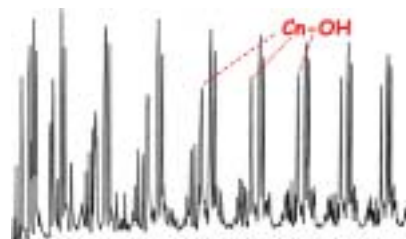


Figure 3. The typical MS-GC spectrum of F-T synthesis products from skeleton iron metal catalyst (Sample 5#)

Some experts offered the explanation that alcohols are the primary products when the synthesis is carried out at low temperatures. They are dehydrated to olefins in a second step. This assumption may find some basis in the fact that the sum total of alcohol plus olefin in synol operation is fairly constant over a wide temperature range. For the skeleton iron catalyst, it was found even at its maximum temperature (280 °C), the oxygenates selectivity did not decrease.

Table 2. Comparison of oxygenates amount in the HC product from different skeleton iron catalysts

Sample	Wt.%	Carbon Range			
		1-2	3-5	6-9	10+
1#	5.11	2.84	2.74	1.86	
2#	2.46	1.51	2.04	1.70	
3#	8.17	3.12	4.90	2.40	
4#	6.60	2.37	3.71	1.73	
5#	8.12	3.06	4.48	2.03	

From Table 2, we knew that copper and zinc added as promoters favored more oxygenates yield than manganese. It must be acknowledged that the aluminum in the skeleton iron catalyst made somehow contribution to the oxygenates formation (aluminum, copper, zinc are the conventional elements for alcohol synthesis catalyst). Nevertheless, as the digesting reaction in the course of alloy leaching step is rigorous and aluminum metal could hardly remain on skeleton surface (except the trace amount of alumina deposition), there is less possibility for aluminum acting as synol synthesis active site. But, it may attribute to any re-crystallization or active sites transfer occurred in the high temperature CO hydrogenation process.

Summary

This paper is to share a viewpoint that FT synthesis products formation mechanism, especially on iron base catalyst, may require study on the isolated active phase. Skeleton iron here exhibits an to some extent ability to produce products without other active phases disturbance.

Acknowledgment. Catalyst characterization work was executed at Material Science Lab, New Jersey Institute of Technology.

References

- Anderson, Robert Bernard, The Fischer-Tropsch Synthesis, Academic Press, Inc., 1984, Orlando, Florida
- Matthew J. Overett, R. Oliver Hill, John R. Moss, Coordination Chemistry Reviews, 206-207 (2000) 581-605
- P.Zhou, L.Lee, J.Zhou and Y.Lu, US Patent 6,277,895 B1, Aug. 21,2001, Appl. No. 09/399,852.
- Y. Lu, P.Zhou and T.Lee, Fuel Chem. Div. Prep., 46(2) (2001) 500-504.
- Y. Lu and P. Zhou, Proceedings of 18th Annu. Intern. Pitts. Coal Conf., Dec. 3-7,2001, Newcastle, Australia
- Devinder Mahajan, P. Vijayaraghavan, Fuel 78(1999) 93-100

DIRECT PARTIAL OXIDATION OF METHANE TO METHANOL: EFFECT OF REACTOR MATERIALS AND CATALYST

Qijian Zhang^{1,2}, Dehua He^{1*}, Qiming Zhu¹

¹State Key Lab of C1 Chemistry and Technology, Department of Chemistry, Tsinghua University, Beijing 100084, China

²Department of Material and Chemical Engineering, Liaoning Institute of Technology, Jinzhou Liaoning 121001, China

Introduction

Direct partial oxidation of methane to methanol (DPOM) is one of the most attractive pathways for the optimization utilization of the abundant natural gas reserves. A great deal of effort have been made on it especially since the promising results reported by Gesser et al.^[1] and Lunsford et al.^[2], respectively, in the early 1980s. Some important results have been obtained, e.g. high pressures and high CH₄/O₂ ratios favor methanol selectivity while high temperatures favor the deep oxidation. However, methanol yield of more than 8% has not been reproducibly achieved till now. Most of the reported methanol yields were about 3~5% and so on. And different researchers always gave different results, and even opposite ones. The discrepancies were attributed to the temperature/heat transfer effects, localized flow patterns in the reactor et al. by Brown and Parkyn^[3] and Srivastava^[4]. In our recent report^[5], methanol yield of ca. 7~8% was obtained in a specially designed quartz lined reactor and the high yield was attributed to the isolation of the reaction mixture from metal surface. And it is believed that the discrepancy in the reported results was due to the difference of such isolation.

In the present work, the effect of the reactor material was further investigated. And the effect of catalysts was also discussed.

Experimental

The experiments of homogeneous partial oxidation of methane were carried out at 380-500°C and 5.0 MPa in a specially designed quartz lined tubular reactor. A quartz line was tightly fixed in a stainless steel line. A Viton O-ring pressed by a locking nut was used to prevent the gas from leaking into the ringed gap between the quartz line and the SS line so as to eliminate the influence of the metal wall. The reactor structure was detailedly described in literature 5.

Catalyst of Mo-V-Cr-Bi-Ox/SiO₂ was prepared by co-precipitation as described in literature 6. The catalytic reaction was performed with 1g catalyst loaded into the reactor.

Results and Discussion

Effect of Reactor Material. The reactor materials have great effect on the performance of the direct partial oxidation of methane to methanol. Three kinds of reactor materials were used for the investigation (see the caption of Figure 1).

In the quartz lined reactor, the methane conversion of ca. 13% and methanol selectivity of more than 60% were obtained (Figure 1, Case-I). The methanol selectivity (Case-I) was the highest among the four cases considered here. The selectivity of completed oxidation product, CO₂, was limited no higher than 5%. And the result obtained in the glass lined reactor (Case-II) was quite similar to the quartz lined reactor; the methanol yield of more than 7% could also be achieved except that the selectivity of CO₂ was a little higher than that in Case-I. And they were both higher than those in the other two cases (Case-III and Case-IV), which indicated that the quartz or glass lined reactor are more favorable for the direct partial oxidation of methane to methanol, especially the quartz lined reactor.

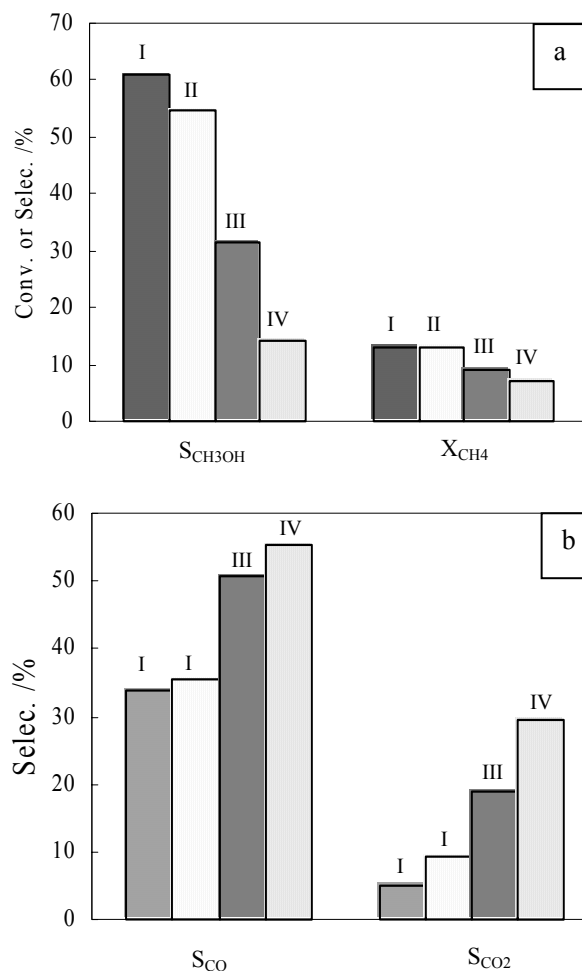


Figure 1. Effect of reactor materials on the homogeneous partial oxidation of methane to methanol

P=5.0MPa, T=440°C, CH₄/O₂/N₂=100/10/10(ml/min)

Case-I: Quartz lined reactor

Case-II: Glass lined reactor

Case-III: Quartz lined reactor without O-ring

Case-IV: Stainless steel reactor

In the stainless steel reactor (Case-IV), methanol selectivity was less than 15%, only about 25% of that in Case-I (Figure 1). But the deep oxidation products, CO and CO₂ were much higher; the selectivity of CO₂ was even raised to 30%. Such results indicated that the SS reactor was not suitable for the direct partial oxidation of methane to methanol because it is too easily to result in the deep oxidation.

It is well known that the iron oxide and other metal oxides are always used as the oxidation or combustion catalysts, because the oxygen in the oxides is very active. But in the direct partial oxidation of methane to methanol, the required product, methanol, is more unstable than methane, and methanol is more easily adsorbed and activated on surface of metals or metal oxides because it is a polar molecular (its dipole moment is 1.70Debyes). Therefore, the surface of metals or metal oxides is not expected to expose under the reaction conditions to cause the deep oxidation of methanol. In other words, it

is necessary to prevent the reaction mixture from contacting the surface of SS reactor during reaction.

The result of Case-III was better than that of Case-IV, but worse than those of Case-I and Case-II, which implied that part of the reactant mixture flow through the inner quartz tube, which did not contact the surface of SS reactor and give higher methanol selectivity, and part of it leaked into the ringed gap between the quartz tube and the SS tube and gave poor methanol selectivity. The methanol selectivity in the effluence was the mean result of the above two parts. It is worth to note that the methane conversion and methanol selectivity were quite similar to those reported in most of the literatures. Researchers have found that the metal surface might cause the deep oxidation of methanol and decrease methanol selectivity. Quartz or Pyrex lined reactors were recommended to be adopted in the direct partial oxidation of methane to methanol. Then how to insure the reactant not to leak into the ringed gap between the inner line and SS tube became a determinant factor, and it might be one of promising explanations for the discrepancy in the reported results.

Effect of catalyst. It is expected that the participation of catalyst could increase methanol selectivity and methane conversion. The catalytic oxidation of methane was investigated over a Mo-V-Cr-Bi-Ox/SiO₂ catalyst.

The increase of oxygen conversion with temperature in catalytic oxidation was not as abrupt as that in homogeneous oxidation, which indicated that the participant of catalyst did take some effect on the reaction. It is worth to note that when temperature was increased above 430°C, the oxygen in the reactants was depleted already. But in the catalytic oxidation, the temperature when oxygen was depleted was higher than 460°C. This result could be attributed to the inhibition of the free radical reaction of the homogeneous oxidation by the catalyst. The participant of catalyst could control the oxidation of methane to some extent.

However, the methanol selectivity in the catalytic oxidation was always less than 50%, which was lower than that in the homogeneous oxidation. And the CO₂ selectivity also increased higher than 10%. The participant of catalyst did not increase the methanol selectivity, but promoted the deep oxidation of methanol. This was mainly because the metal oxides catalyst is very active, and the polar molecular, such as methanol, CO et al. is very easily absorbed on them and activated. The effect of catalyst was to some extent similar to that of the metal reactor surface.

Conclusions

The existence of the metal surface of SS reactor would cause deep oxidation of methanol under the reaction condition, and decrease its selectivity. The reactor should be equipped with the metal-free material, such as quartz or Pyrex glass. And in the quartz (or Pyrex glass) lined tubular reactor, it is important to prevent the reactant mixture from leaking into the ringed gap between the inner tube and the outer SS tube.

Participant of catalyst did affect the homogeneous oxidation, but did not improve the methanol selectivity because it easily causes deep oxidation of methanol.

Acknowledgement. We acknowledge the financial support from the National Key Fundamental Research Project Foundation of the Ministry of Science and Technology of China (G199902240-06) and the Research Foundation of Tsinghua University.

References

- (1) Gesser, H.D., *International Chemical Congress of Pacific Basin Societies*, **1984**, Honolulu, Paper 03002.
- (2) Liu, H.F.; Liu R.S.; Lunsford, J.H., *J. Am. Chem. Soc.*, **1984**, 106, 4117.
- (3) Brown, M.J.; Parkyns, N.D., *Catal. Today*, **1991**, 8, 305.
- (4) Srivastava, R.D.; Zhou, P.; Stiegel, G.J.; Rao, V.U.S.; Cinquegrane, G., *Catalysis*, **1992**, 9,183
- (5) Qijian, Zhang; Dehua, He; Jinlu, Li et al. *Appl. Catal. A: General*, **2002**, 224(1-2), 201
- (6) Zhansheng, Han *Ph.D. thesis*, Department of Chemistry, Tsinghua University, China, **1999**

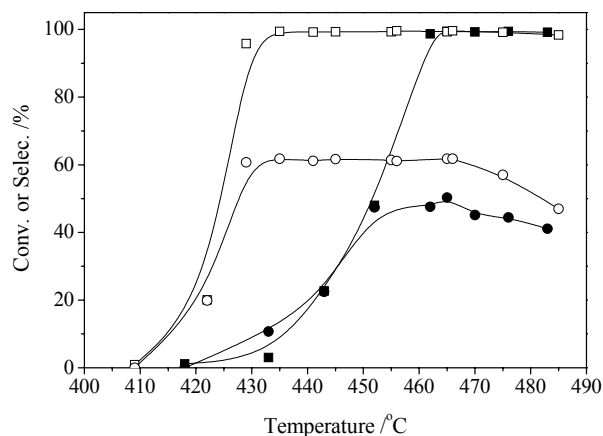


Figure 2. Comparison of homogeneous and catalytic oxidation of methane to methanol.

P=5.0MPa, CH₄/O₂/N₂=100/10/10(ml/min)

- Catalytic oxygen conversion,
- Homogeneous oxygen conversion
- Catalytic methanol selectivity
- Homogeneous methanol selectivity

PREPARATION AND APPLICATION OF Co-Mo MODEL SULFIDE CATALYSTS FOR HYDRODESULFURIZATION

Yasuaki Okamoto

Department of Material Science, Shimane University,
Matsue 690-8504, Japan

Introduction

Hydrotreatings of petroleum feedstocks have recently become more and more crucial not only to protecting the environment but also to efficient utilization of limited natural resources. Development of highly active and selective hydrotreating catalysts, in particular hydrodesulfurization (HDS) catalysts, is one of the most urgent problems in petroleum industries. Sulfided Co-Mo or Ni-Mo(W) based catalysts have been used in industry for HDS reactions. Supported Co(Ni)-Mo sulfide catalysts have been extensively studied to understand the structure and reactivity of catalytically active sites, the microscopic reaction mechanisms of HDS and hydrogenation, the effects of the support and additives and so on.^{1,2} A so-called CoMoS model originally proposed by Topsøe *et al.*¹ for a catalytically active phase, in which Co locates on the edges of highly dispersed MoS₂ clusters, attracts increasing attention to explain many aspects of catalytic and spectroscopic properties. Better characterization and understanding of the nature of Co(Ni)-Mo sulfide catalyst systems in a molecular scale are of great importance to a rational design of highly active HDS catalysts.

One of the promising approaches for these purposes is to utilize model catalysts, such as homogeneous metal sulfide clusters and metal sulfide clusters on a flat surface. In the model catalyst approach for better characterization of hydrotreating catalysts, we tried to fabricate more practical model catalysts than the model catalysts constructed by means of surface science techniques and intrazeolite and homogeneous metal sulfide clusters. In the present study, model catalysts are defined as the catalysts in which all the Co atoms are present as CoMoS phases.

Experimental

Catalyst Preparation. Sulfided MoS₂/Al₂O₃ was exposed to a vapor of Co(CO)₃NO at rt for 5 min (CVD technique), followed by evacuation at rt. Co(CO)₃NO/MoS₂/Al₂O₃ was subsequently sulfided again at 673 K to prepare a Co-Mo/Al₂O₃ catalyst. The resulting catalyst is designated CVD-Co/MoS₂/Al₂O₃. Other supports, TiO₂, ZrO₂ and SiO₂, were also examined.

Characterization and reaction. The amount of NO adsorption was measured by means of a pulse technique. The HDS of thiophene was carried out by using a closed circulation system at 623 K and 20 kPa to evaluate the initial activity of sulfided catalysts.

Results and Discussion

Preparation of Model Catalysts. The addition of Co to MoS₂/Al₂O₃ by means of the CVD technique greatly enhanced the HDS activity of MoS₂/Al₂O₃, irrespective of the Mo loading. In order to examine the location of the Co atoms deposited by the CVD technique, the Co/Mo ratio of CVD-Co/MoS₂/Al₂O₃ was plotted against the NO/Mo ratio of MoS₂/Al₂O₃. When the Mo loading was larger than 9 wt.% (monolayer loading), the Co/Mo ratio was proportional to the NO/Mo ratio. It has been established that NO molecules adsorb on the edge sites of MoS₂ particles rather than on the basal plane. Hence, the linear correlation between the Co/Mo and NO/Mo ratios strongly suggests that Co is located on the edge sites of MoS₂ particles at > 9 wt.% Mo. The Co 2p_{3/2} XPS binding energy for CVD-Co/Al₂O₃ was close to that of Co₉S₈, indicating that Co

sulfide clusters form as expected. However, in the presence of MoS₂ particles, the Co 2p_{3/2} binding energy increased by 0.8 eV, clearly demonstrating that Co species chemically interact with the edges of MoS₂ particles.

When CVD-Co/MoS₂/Al₂O₃ was exposed again to a vapor of Co(CO)₃NO and resulfided, the HDS activity of CVD-Co/MoS₂/Al₂O₃ hardly changed in spite of the increase of the Co content by a factor of 1.7. It is concluded that applying CVD once fills the edge sites of MoS₂ particles with Co atoms, constituting CoMoS phases, and that Co(CO)₃NO molecules adsorbed on the edge sites of Co-MoS₂ particles are transformed into separate Co sulfide clusters. This was also supported by the FTIR spectra of NO adsorption on CVD-Co/MoS₂/Al₂O₃, showing that essentially all the edge sites of MoS₂ particles, that are accessible to NO adsorption, are covered by Co atoms, constituting CoMoS phases.

Evaluation of the Maximum Potential HDS Activity. Figure 1 shows the HDS activity of CVD-Co/Co-Mo/Al₂O₃, which was prepared by exposing sulfided Co-Mo/Al₂O₃ to a vapor of Co(CO)₃NO and subsequent sulfidation, as a function of Co content in Co-Mo/Al₂O₃ impregnation catalysts. The HDS activity of Co-Mo/Al₂O₃ was increased, over the whole range of Co content, by the addition of Co by means of the CVD technique. It is worthy of note that CVD-Co/Co-Mo/Al₂O₃ shows the identical activity with CVD-Co/MoS₂/Al₂O₃, when Co content is lower than 2 wt.% and that the activity of CVD-Co/Co-Mo/Al₂O₃ gradually decreases with increasing Co content at > 2 wt.%. Taking into consideration the fact that the HDS activity of CVD-Co/MoS₂/Al₂O₃ is not changed by the further addition of Co and the FTIR of NO adsorption, it is concluded that the activity increase in Figure 1 results from the increase in the amount of CoMoS phases by the addition of Co(CO)₃NO and that the HDS activity of CVD-Co/MoS₂/Al₂O₃ provides the maximum potential HDS activity for a series of Co-Mo/Al₂O₃ catalysts, as long as the dispersion of MoS₂ particles are not modified by the impregnation of Co.

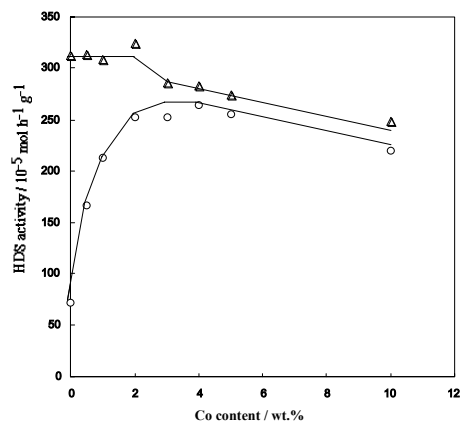


Figure 1. HDS activity of CVD-Co/Co-Mo/Al₂O₃ (triangle) and Co-Mo/Al₂O₃ (circle) as a function of the Co content in Co-Mo/Al₂O₃.

In conjunction with NO adsorption, the decrease in the activity of CVD-Co/Co-Mo/Al₂O₃ (>2 wt.% Co) was ascribed to an increasing extent of blockings of the edges of MoS₂ particles by Co sulfide particles concomitantly formed during the sulfidation of the Co-Mo/Al₂O₃ impregnation catalysts. The maximum HDS activity of Co-Mo/Al₂O₃ attained at 3 wt.% Co was lower than the activity of CVD-Co/MoS₂/Al₂O₃ or CVD-Co/Co-Mo/Al₂O₃ (< 2 wt.% Co). This is obviously caused by the blocking of the edges of MoS₂ particles by Co. It was also shown that the CVD technique can be applied to Ni-Mo catalysts to evaluate the

maximum potential HDS activity as well as Co-Mo catalysts. The evaluation of the maximum potential HDS activity provides a promising guide line for improving catalyst performances.

Effects of the Support. We examined the effect of the support on Co-Mo sulfide catalysts by preparing the catalysts in the same way as the model catalysts. The supports and Mo contents used in the present study were SiO₂ (347 m² g⁻¹, 6.7 and 13 wt.% Mo), ZrO₂ (25 m² g⁻¹, 2.0 wt.%), TiO₂ (50 m² g⁻¹, 4.0 wt.%) and Al₂O₃ (177 m² g⁻¹, 8.7 and 13 wt.%). The Mo content of the catalyst was fixed approximately at or over its monolayer loading. The dispersion of MoS₂ particles was measured by means of NO adsorption.

The supported MoS₂ catalysts were exposed to a vapor of Co(CO)₃NO to prepare CVD-Co/MoS₂/support. The Co 2p_{3/2} binding energies were 779.3±0.1 eV, regardless of the support. These results clearly demonstrate that the Co atoms, introduced by means of the CVD technique, interact with MoS₂ particles on the support.

Figure 2 shows the Co/Mo ratio of CVD-Co/MoS₂/support as a function of the NO/Mo ratio of the MoS₂/support samples. The Co/Mo ratio was proportional to the NO/Mo ratio, showing that Co sulfide species are located on the edge sites of MoS₂ particles. In consequence, we conclude that the Co sulfide species prepared in this way is characteristic of the CoMoS phase proposed by Topsøe *et al.*¹ and that the CoMoS phase is preferentially formed when the CVD technique is applied, irrespective of the support. It is concluded that a Co-Mo model catalyst can be prepared, when the Mo content corresponds to or exceeds a monolayer loading in MoS₂/support.

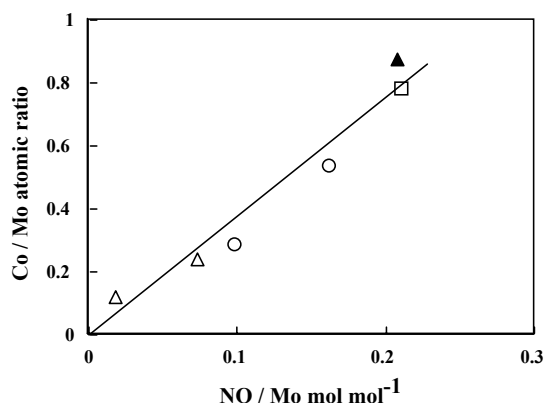


Figure 2. Correlation between the Co/Mo atomic ratio and the NO/Mo ratio for supported CVD-Co/MoS₂/support catalysts. Open triangle: SiO₂, Circle: Al₂O₃, Square: TiO₂ and Closed triangle: ZrO₂.

Figure 3 shows the catalytic activity of CVD-Co/MoS₂/support in the HDS of thiophene as a function of Co loading. A good proportional correlation was obtained for Al₂O₃-, TiO₂- and ZrO₂-supported Co-Mo model catalysts, regardless of the support and the pretreatment (pre-reduced before exposure to Co(CO)₃NO or thermally decomposed after exposure). Since the straight line in Figure 3 passes through the origin, the activity is ascribed to the Co species interacting with MoS₂ or the CoMoS phase and that there are very few unpromoted Mo sites, if any, after the single adsorption of Co(CO)₃NO in agreement with the FTIR of NO adsorption of CVD-Co/MoS₂/Al₂O₃. The TOF of the CoMoS phase (the slope of the line) of the Al₂O₃-, TiO₂- and ZrO₂-supported catalysts are identical. We conclude, therefore, that the support has no significant effects on these catalyst systems. The HDS activity of Co-Mo/Al₂O₃, prepared by an impregnation, was somewhat lower than that of CVD-Co/MoS₂/Al₂O₃ with similar Co and Mo loadings (Figure 3). This is obviously due to the formation of less active Co species such as Co₉S₈ clusters and Co²⁺ in the Al₂O₃ sublayer in addition to the CoMoS phases, in line with the Co 2p XPS results.

Figure 3 shows that the specific activity of the Co species supported on SiO₂ is 1.7 times higher than the activity on the other supports. Taking into account the difference in activity between CoMoS Type I and Type II, CoMoS Type I probably forms on the Al₂O₃, TiO₂ and ZrO₂ supports under the present sulfidation conditions (673 K, atmospheric H₂S/H₂), while CoMoS Type II on SiO₂. The difference is attributed to the difference in the stacking number of MoS₂ particles on the basis of the TEM observations, in agreement with others.

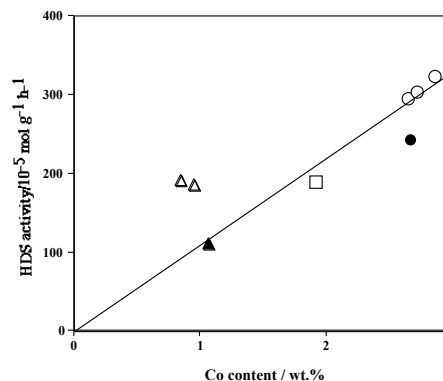


Figure 3. Correlation between thiophene HDS activity and the Co loading of supported CVD-Co/MoS₂ catalysts. See the captions in Fig.2 for the symbols. Closed circle: a Co-Mo/Al₂O₃ impregnation catalyst.

Conclusions

It has been found that the selective preparation of CoMoS phases supported on refractory oxides provides promising model catalysts to understand the nature of practical HDS catalysts. Effects of the support were understood in terms of the TOF of the CoMoS phases. Furthermore, the information on the maximum potential HDS activity of Co(Ni)-Mo(W) catalysts is very unique and will be helpful in the design of highly active HDS catalysts. It is shown in our study that the model catalyst approaches provide important information on the effects of the catalyst preparation and additives, the catalyst structure and the fundamental aspects of HDS catalysts such as microscopic reaction mechanisms and structure-reactivity relationships.

Acknowledgement. The present author expresses his gratitude to Dr. Takeshi Kubota (Shimane University) for useful discussions. This work has been entrusted by the New Energy and Industrial Technology Development Organization under a subsidy of the Ministry of Economy, Trade and Industry.

References

- (1) Topsøe, H., Clausen, B.S., Massoth, F.E., *Catalysis Science and Technology*, eds. Anderson, J.R., Boudard, M., Springer, Berlin, 1996, Vol.11.
- (2) Whitehurst, D.D., Isoda, T., Mochida, I., *Adv. Catal.*, **42**, 345 (1998).Ed.; Plenum Press: New York, 1992; pp. 255-274.

RELATIONSHIP BETWEEN CATALYST STRUCTURE AND HDS REACTION MECHANISM

Narinobu Kagami¹, Bas M. Vogelaar, A. Dick van Langeveld²,
and Jacob A. Moulijn*

Reactor & Catalysis Engineering Group, Faculty of Applied Sciences,
Delft University of Technology, Julianalaan 136, 2628 BL Delft,
The Netherlands

¹Manufacturing Department, Idemitsu Kosan Co., Ltd.

26, Anesakikaigan Ichihara-city, Chiba, 299-0107, Japan

²Particle Optics Group, Faculty of Applied Sciences, Delft
University of Technology, Lorentzweg 1, 2628CJ Delft,
The Netherlands

Introduction

The hydrodesulfurization (HDS) process is receiving more and more attention, because the legislative requirements on transportation fuels are becoming more severe. Therefore, it is very important to elucidate the effect on the relationship between catalyst structure and reaction mechanism of the sulfur compounds.

CoMo/Al₂O₃ and NiMo/Al₂O₃ catalysts are the work-horses in HDS processes. The so-called type II CoMoS phase has a higher activity for thiophene HDS than the so-called type I. For catalyst design such a conclusion is of crucial importance. However, this has not been unequivocally proven to hold for dibenzothiophene (DBT) HDS¹. It should be noted that DBT is a better model compound than thiophene to represent diesel fuel liquid phase HDS.

It is widely accepted that DBT desulfurizes via both direct desulfurization (DDS) and hydrogenation followed by desulfurization (HG-HDS) of benzene ring. This work focuses on the structure type I and type II catalyst structure and the possible relationship with the different routes of DBT HDS.

Experimental

Catalysts

NiO-MoO₃/Al₂O₃ catalysts (type I and type II) were prepared via liquid phase pore volume impregnation. A high purity γ -Al₂O₃ in the form of 1.5 mm cylindrical extrudates was impregnated using aqueous solutions containing the required amounts of Ni and Mo, according to the literature².

Activity measurement

The activity for liquid-phase DBT HDS was determined in a batch reactor. Details on the experimental procedure can be found in the literature¹. Before the reaction catalysts, they were presulfided at 370 °C. Subsequently, the activity tests were carried out at 350 °C and 5 MPa hydrogen pressure. The feed consisted of 0.2wt% DBT in hexadecane (n-C₁₆).

The inhibiting effect of H₂S is quite large on DBT HDS³. In order to mimic the realistic conditions of the commercial reactor bottom, dimethyldisulfide (DMDS) was added to adjust the H₂S partial pressure to 1.4bar.

Results and Discussion

In Fig. 1 a simplified reaction scheme for DBT HDS is shown. Under the applied reaction conditions the main products are cyclohexylbenzene (CHB) and biphenyl (BP). From the yields of

these two products between the direct HDS (DDS) and the hydrogenation route can be discriminated.

In all cases, the time dependency of the DBT concentration followed first order kinetics.

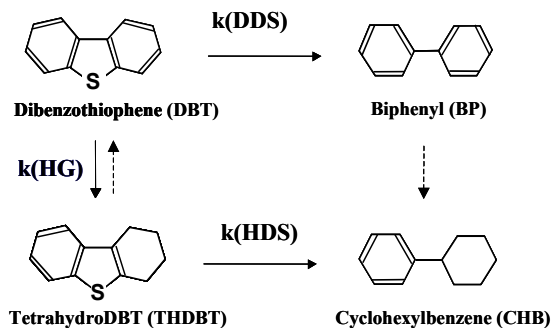


Figure 1. Simplified reaction scheme for DBT HDS

In Fig. 2, the effect of active metals loading on the DBT HDS activity for both NiMo type I and type II catalysts is shown. At increasing loading, type I catalyst did not show higher activity, probably due to formation of MoO₃ crystals, in agreement with literature. Diaz and Bussell reported that at a metal loading above 4.2 atoms Mo per nm², three-dimensional MoO₃ particles are formed⁴. In contrast, type II catalyst showed higher activity at increasing loading.

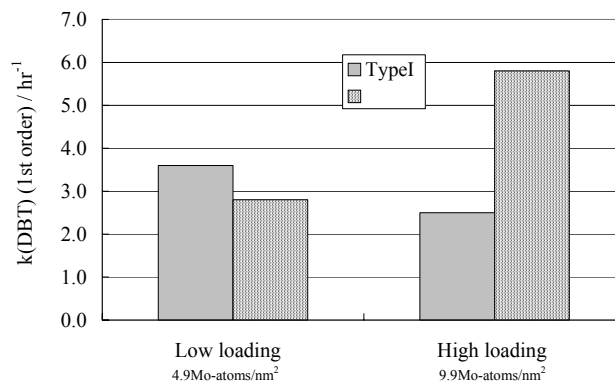


Figure 2. The effect of metal loading for DBT HDS

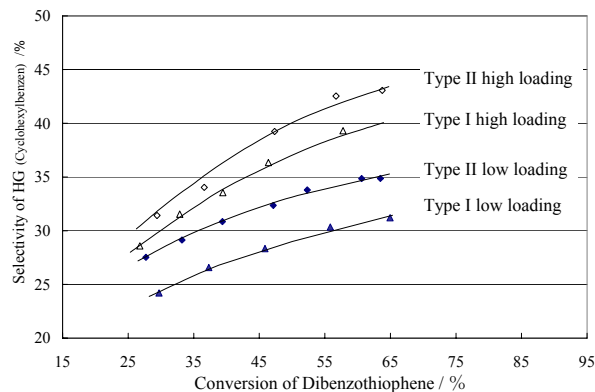


Figure 3. The effect of metal loading for hydrogenation selectivity

* Corresponding author, email: J.A.Moulijn@tnw.tudelft.nl

In Fig.3, the selectivity of cyclohexylbenzene, representative for the hydrogenated route is shown. Note that type II catalysts have a higher selectivity for cyclohexylbenzene. Therefore, it can be concluded that the reaction rate of hydrogenated route on type II catalyst is higher than on type I. Moreover, the higher loading catalysts show higher selectivity for cyclohexylbenzene.

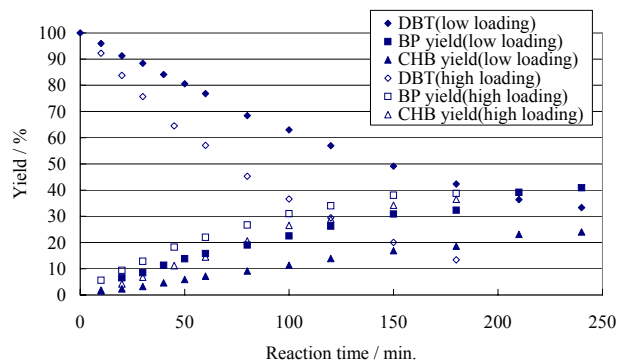


Figure 4. The yield of products HDS DBT on type II NiMo catalysts

In Fig.4, the yields of the products of high and low loading type II catalysts are shown. Time yields of cyclohexylbenzene and biphenyl became higher at increasing loading, but the former increased most. Therefore, the higher HDS activity of type II high loading catalysts is mostly dependent on an acceleration of the hydrogenation route.

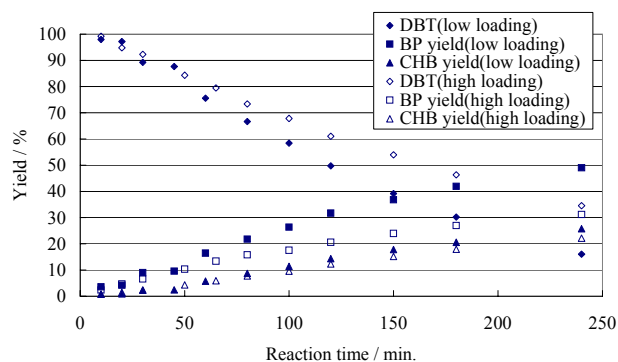


Figure 5. The yield of products HDS DBT over type I NiMo catalysts

In Fig.5, the yields of the products of high and low loading type I catalysts are shown. Time yields of cyclohexylbenzene and biphenyl decrease with increasing loading, but the former becomes much lower. Therefore, it is concluded that due to the formation of MoO_3 crystals, the direct desulfurization reaction rate decreases while hydrogenation route does not change significantly.

To unravel the reaction scheme described in Fig.1, the rate constant of each step was determined numerically by fitting the data to the kinetic model. The inverse reaction of THDBT to DBT, and the hydrogenation reaction of BP to CHB could be neglected because the rate constants were very low.

Table 1. The Rate Constants of Each Reaction Step

	kDBT	k(DDS)	k(HG)	k(HDS)	k(HG)/k(DDS)	k(HDS)/k(DDS)
TypeI Low loading	3.6	2.2	1.4	14.0	0.65	6.5
TypeI High loading	2.5	1.3	1.2	10.9	0.91	8.4
TypeII Low loading	2.9	1.7	1.2	15.9	0.69	9.4
TypeII High loading	5.9	3.0	2.9	27.5	0.99	9.3

In Table 1, the rate constants of each reaction step are given. All data show higher k (HDS) than k (DDS). Therefore, THDBT is supposed to desulfurize easier than DBT. Moreover, type II high loading had a higher k (HG)/ k (DDS) than type II low loading. Therefore, the higher HDS activity of type II high loading catalysts mainly originates from the acceleration of hydrogenation route activity.

These results can contribute to a more rational catalyst design in hydrosulfurization. Work in that direction is in progress.

Conclusions

The various DBT HDS routes significantly depend on the catalyst structure (type I, type II). The higher HDS activity of the high loading type II catalysts mainly originates from the increased hydrogenation activity.

Acknowledgement.

We thank Dr. S. Eijssbouts (Akzo-Nobel, P.O.Box 37650, 1030 BE Amsterdam, The Netherlands) for the stimulating discussions.

References

- (1) Reinhoudt, H.R.; Boons, C.H.; Van Langeveld, A.D.; Van Veen, J.A.R.; Sie, S.T.; and Moulijn, J.A., *Appl. Catal. A*. **2001**, *207*, 25.
- (2) Van Veen, J.A.R.; Gerkema, E.; Van der Kraan, A.M.; and Knoester, A. *J. Chem. Soc., Chem. Commun.* **1987**, 1684.
- (3) Kabe, T.; Aoyama, Y.; Wang, D.; Ishihara, A.; Qian, W.; Hosoya, M.; and Zhang, Q., *Appl. Catal. A*. **2001**, *209*, 237.
- (4) Diaz, A.L.; and Bussell, M.E.; *J. Phys. Chem.* **1993**, *97*, 470.

INTRINSIC KINETICS OF THIOPHENE HDS OVER A NiMo/SiO₂ MODEL CATALYST

A. Borgna, E.J.M. Hensen, J.A.R. van Veen
and J.W. Niemantsverdriet

Schuit Institute of Catalysis, Eindhoven University of Technology,
PO Box 513, 5600 MB Eindhoven, The Netherlands

Introduction

Supported mixed transition metal sulfide catalysts play a pivotal role in refineries for the production of clean motor fuels. They are employed not only to hydrotreat the final products like gasoline and diesel, but also to pretreat fluid catalytic cracking or reformer feed [1]. Furthermore, they provide the hydrogenation functionality in most hydrocracking catalysts that upgrade vacuum residue to more valuable products. Two major drivers for the development of more active hydrotreating catalysts are (i) dwindling oil supplies forcing refiners to use heavier feedstock and (ii) ever-tightening motor fuel specifications (for instance, the EU Auto Oil programme II [2]). Noteworthy is that mostly the use of an improved catalyst is more economic than modifications to the process.

While research on hydrotreating catalysts has been extensive over the last 50 years [3-5], it has proven very difficult to relate catalyst structure to catalyst activity and selectivity on the molecular level. In recent years, we have employed the model catalyst approach to heterogeneous catalysis. The essential point is to prepare planar model catalysts by spin-coating which mimics the industrial pore volume impregnation method. In this way, realistic models can be obtained which are easily amenable to high-resolution spectroscopic studies. We have shown before [6,7] that the strong tandem-mix of characterization and reactivity evaluation enables detailed insight into the influence of active phase formation on the activity. Here, we will show how these well-defined models can be used to obtain intrinsic kinetics of thiophene hydrodesulfurization.

Experimental

Model catalyst preparation NiMo/SiO₂ planar model catalysts consisting of a Si(100) wafer covered by a thin layer of SiO₂ as support were prepared by spin-coating as extensively described before [6,7]. Planar SiO₂ model supports were prepared by oxidizing a Si(100) single-crystal wafer in air at 1023 K for 24h. After calcination the wafers were cleaned in a H₂O₂/NH₄OH solution at 338 K. Subsequently, the surface was hydroxylated in boiling water for 20-30 min. As a typical example, we describe here the preparation of NiMo/SiO₂. A model silica support was spin-coated in nitrogen atmosphere at 2800 rpm with an aqueous solution containing Ni(NO₃)₂·6H₂O (Merck, p.a.) and (NH₄)₆Mo₇O₂₄·4H₂O (Merck, purity >97%) with an atomic ratio of 1:3, respectively. The concentration of the precursor solution was adjusted to result in the required metal loadings (2 Ni at/nm² and 6 Mo at/nm²). Prior to characterization or catalytic testing, a model catalyst was sulfided at a rate of 5 K/min to 673 K + 1 h in a mixture of 10 vol.% H₂S in H₂.

Reactivity evaluation. Atmospheric thiophene HDS reactions were carried out in a batch-type reactor. After sulfidation, the reactor was flushed with the reactant mixture for 5 min at the desired reaction temperature. The reaction was then carried out in batch mode by closing the reactor inlet and outlet. This was marked as zero reaction time. After a reaction time of 1 h a gas-phase sample was taken from the reactor using a precision sampling gas syringe which was injected on a DB-1 column to analyze the main products: 1-butene, n-butane, trans-2-butene, cis-2-butene, thiophene and small

amounts of C₁-C₃ hydrocarbons. The HDS activities are expressed as thiophene conversion after 1 h of reaction time and per 5 cm² of model catalyst. These values were corrected for blank thiophene conversion measured using an empty reactor. Between two experiments the catalyst was resulfided at 673 K for 1 h.

Results and Discussion

Because diffusion limitations are absent, the use of planar model catalysts offers great advantages in kinetic studies. Catalytic data were obtained at different temperatures varying the partial pressures of hydrogen, thiophene and H₂S, respectively. The kinetic data were analyzed considering both power-law and Langmuir-Hinshelwood (L-H) kinetics. Between 573 and 673 K, positive orders in thiophene and hydrogen and moderately negative orders in H₂S were obtained. Moreover, while the reaction order in thiophene significantly decreased as the reaction temperature decreases, the order in hydrogen was nearly constant and close to 1. The lower reaction order of thiophene as compared to the reaction order in hydrogen clearly indicates that thiophene adsorbs much stronger than hydrogen. The negative order in H₂S indicates that the HDS reaction is inhibited by H₂S, probably due to competition with thiophene for sulfur-defect sites. The trends in the reaction orders are in agreement with the literature [8,9]. Heats of adsorption and activation energies can be derived once a kinetic model has been adopted. Several mechanisms and associated kinetic models for the hydrodesulfurization of thiophene have been proposed in the literature [10-14].

Although the precise mechanism of thiophene HDS reaction is still under debate, we have chosen an often-used simplified reaction network consisting of elementary steps, in which thiophene exclusively adsorbs on sulfur vacancies and H₂ adsorbs dissociatively on different sites to form butadiene (B) and H₂S. Assuming that the surface reaction between adsorbed thiophene and H₂ is the rate-limiting step and the H₂S adsorption takes place on sulfur vacancies exclusively, in competition with thiophene adsorption, the following Langmuir-Hinshelwood rate expression can be obtained:

$$r = \frac{k K_T K_{H_2} P_T P_{H_2}}{(1 + K_T P_T + K_{H_2S} P_{H_2S} / P_{H_2}) (1 + K_{H_2}^{1/2} P_{H_2}^{1/2})^2}$$

where k is the rate constant of the rate-determining step and K_T , K_{H_2} , K_{H_2S} are the adsorption constants of thiophene, H₂ and H₂S, respectively. **Figure 1** shows that the experimental data measured at constant thiophene and H₂S partial pressures and varying the H₂ partial pressure can be satisfactorily fitted using the L-H equation, giving an estimation of the adsorption equilibrium constants of hydrogen at different temperatures. The optimized values indicate that the adsorption equilibrium constant is statistically non-different from zero under our experimental conditions. Therefore, the hydrogen adsorption term in the denominator can be ignored. The optimized values for the adsorption equilibrium constants at 673 K of thiophene and H₂S are $3.5 \pm 0.7 \text{ bar}^{-1}$ and 28.9 ± 1.8 , respectively. The intrinsic kinetic parameters, the activation energy of the rate determining step and the heat of adsorptions, can be derived by fitting the kinetic data measured at different temperatures using non-linear multivariable fittings. **Figure 2** shows the quality of this fitting and the intrinsic parameters are summarized in **Table 1**.

The estimated value for the heat of adsorption of thiophene and H₂S are $-57.8 \pm 10.9 \text{ kJ/mol}$ and $-117.1 \pm 11.3 \text{ kJ/mol}$, respectively. A broad range of values for the heats of adsorption of both thiophene and H₂S have been reported in the literature [11,12]. Theoretical values vary between -62 and -137 kJ/mol, whereas the values for the heat of adsorption of H₂S vary between -75 and -93 kJ/mol [15].

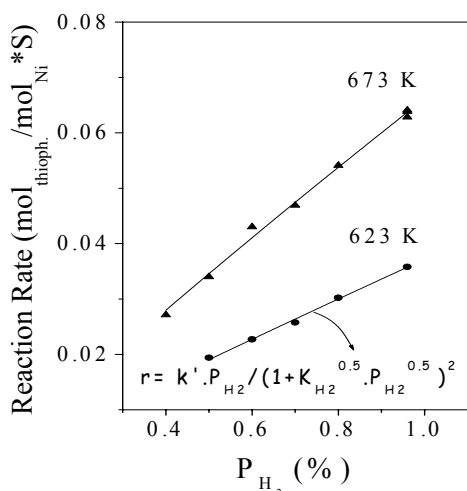


Figure 1. Dependence of the rate of thiophene HDS on the partial pressure of H₂ at different temperatures, along with data fit according to the *L-H* kinetic model. P_{thioph.} = 4 vol% and P_{H₂S} = 0 vol%.

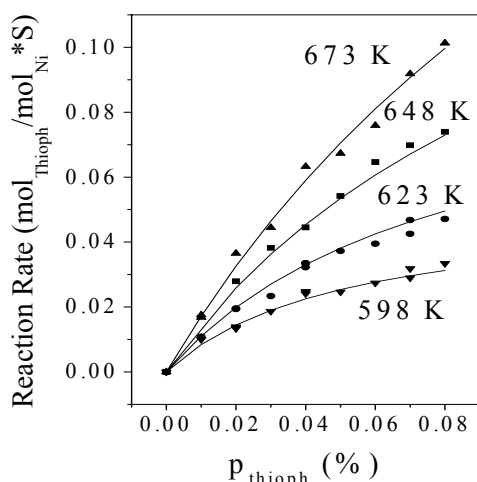


Figure 2. Dependence of the rate of thiophene HDS on the thiophene partial pressure along with a non-linear multi-variable fitting according to the *L-H* model. P_{H₂} = 90 vol% and P_{H₂S} = 0 vol%.

To summarize, the values of the heat of adsorption reported in this contribution indicate a relatively strong adsorption of both thiophene and H₂S.

The activation energy is about 85 kJ/mol, in line with theoretical calculations [15], which predict overall reaction enthalpies for C-S scission and sulfur removal of 70 kJ/mol and 73 kJ/mol, respectively. It is important to mention that much lower activation energies, usually obtained from Arrhenius plots, have been reported in the literature [16-18]. However, the activation energy derived from Arrhenius plots represents the apparent activation energy and not the real activation energy of the rate-determining step. Moreover, a decrease in apparent activation energy with increasing temperature has been frequently observed [16-18]. Such a decrease of the apparent activation energy has been often attributed to a decrease of the surface coverage of the reactants as temperature increases [17, 18]. The relation between apparent and real activation energy is:

$$E_{act}^{app} = E_{act}^{rds} + (1 - \Theta_T^{\#}) \cdot \Delta H_{ads}^T + (1 - \Theta_H^{\#}) \cdot \Delta H_{ads}^{H_2} - \Theta_{H_2S}^{\#} \cdot \Delta H_{ads}^{H_2S}$$

Table 1: Intrinsic kinetic parameters obtained from non-linear multivariable fittings on a sulfided NiMo/SiO₂ model catalyst.

Parameter	Value
k^0 (mol _{thioph} /mol _{Ni} *S)	0.0967
E_{act}^{rds} (kJ/mol)	83.5
K_{thioph}^0 (bar ⁻¹)	8.7
$-\Delta H_{ads}^{thioph}$ (kJ/mol)	-57.8
$K_{H_2S}^0$ (bar ⁻¹)	138.9
$-\Delta H_{ads}^{H_2S}$ (kJ/mol)	-117.1

At high temperatures, the coverages become lower and in the limit of an empty surface, we find

$$E_{act}^{app} = E_{act}^{rds} + \Delta H_{ads}^T + \Delta H_{ads}^{H_2}$$

Therefore, a negative apparent activation energy may be obtained when the adsorption energies of thiophene and hydrogen are large enough. This then explains the *Volcano*-type curve recently reported by Borgna et al. [18].

Conclusion

Planar model catalysts can be applied to obtain intrinsic kinetic parameters for the relatively simple thiophene hydrodesulfurization reaction, offering an excellent opportunity to study reaction mechanism and kinetics without under diffusion-free conditions.

References

- Gosselink, W., *CatTech*, **1998**, 4, 127.
- Auto-Oil II Programme, Com. EU, Com 626, **2000**.
- Prins, R., De Beer, V.H.J., Somorjai, G.A., *Catal. Rev. Sci. Eng.*, **1989**, 31, 1.
- Topsoe, H., Clausen, B.S. Massoth, F.E., *Hydrotreating catalysis*, Springer, Berlin, **1996**.
- Eijsbouts, S., *Appl. Catal. A*, **1997**, 158, 53.
- Kishan, G, Coulier, L., de Beer, V.H.J, van Veen, J.A.R., Niemantsverdriet, J.W, *J. Catal.*, **2000**, 196, 180.
- Coulier, L., de Beer, V.H.J, van Veen, J.A.R., Niemantsverdriet, J.W, *J. Catal.*, **2001**, 197, 26.
- Hensen, E.J.M., Brans, H.J.A., Lardinois, G.M.H.J., de Beer, V.H.J., van Veen J.A.R., van Santen, R.A., *J. Catal.*, **2000**, 192, 98.
- Leliveld, R.G., van Dillen, A.J., Geus J.W, Koningsberger, D.C., *J. Catal.*, **1998**, 175, 108.
- Massoth F.E., Chung, K.S., Proc. 7th ICC, Tokyo, **1980**, p. 629.
- Satterfield, C.N., Roberts, G.W., *AIChE Journal*, **1968**, 14, 159.
- H.C. Lee, Butt, J.B., *J. Catal.*, **1977**, 49, 320.
- Vrinat, M.L., *Appl. Catal.*, **1983**, 6, 137.
- Girgis, M.J., Gates, B.C., *Ind. Eng. Chem. Res.*, **1991**, 30, 2021.
- Neurock, M., Van Santen, R.A., *J. Am. Chem. Soc.*, **1994**, 116, 4427.
- Leglise, J., van Gestel J., Duchet, J.C., Symp. Adv. Hydrotreating Catalysts, ACS, Washington, 533, **1994**.
- Hensen, E.J.M., Vissenberg, M.J., de Beer, V.H.J., van Veen J.A.R., Van Santen, R.A., *J. Catal.*, **1996**, 163, 429.
- Borgna, A., Hensen, E.J.M., Coulier, L., de Croon, M.H.J.M., Schouten, J.C., van Veen, J.A.R. Niemantsverdriet, J.W., Submitted to *Cat. Lett.* (2003).

THIOPHENE HYDRODESULFURIZATION ACTIVITIES AND MICROSTRUCTURE OF SULFIDED NiW/ γ -Al₂O₃ CATALYSTS

Jinye Wang, Dadong Li, Hong Nie, Yahua Shi,

Zeming Jin, Xiaohong Kang

Research Institute of Petroleum Processing, SINOPEC

No. 18 Xueyuan Road, Beijing, China

Postal Code 100083

Introduction

From the recent environmental point of view, hydrotreatment of petroleum fractions to produce clean and high quality transportation fuels is becoming more and more important. Alumina supported Mo (W) catalysts, promoted by Co(Ni), are widely used in the oil industry for these purposes. There is growing need for improvements in the performance of these catalysts. There is a general agreement that the active Co–Mo–S phase is MoS₂ slab with Co atoms decorating the edge plane. The studies of the Ni–W system show that the structure of the Ni–W–S active phase is similar to that of Co–Mo–S phase¹. It is well established that WS₂ is layered compound consisting of stacks of S–W–S layers held together by van der Waals interactions¹. For bulk WS₂ compound, it is known that it has two kinds of structure, i.e. 2H-WS₂ and 3R-WS₂. Whether the tiny WS₂-like crystallite on the surface of sulfided NiW/ γ -Al₂O₃ catalyst is of 2H-WS₂ structure or 3R-WS₂ is unclear. For promoted catalysts, the atomic ratio of Ni/(Ni+W) is an important factor that affects the hydrodesulfurization(HDS) activity of NiW/ γ -Al₂O₃ catalyst. However, the optimal ratio is different in the literature. In this presentation we offer an evidence that the tiny WS₂-like crystallite is of 3R-WS₂ type structure. The reason is given for the explanation why the optimal ratio is 0.23 for catalysts sulfided at higher temperature.

Experimental

Catalyst preparation. γ -Al₂O₃ were used as support. Catalysts were prepared by wetness impregnation of support with an aqueous solution containing nickel nitrate and ammonium tungstate, followed by drying at 120 °C for 4 h and at 500 °C for 4 h. All the catalysts contained 0.19 mole atom per 100 gram of support with different Ni/(Ni+W) ratio. Catalysts were sulfided at 400 °C for 4 h in a flow of 15 % H₂S+H₂ before reaction and characterization. The bulk WS₂ were prepared by the sulfidation of ammonium tungstate at the same conditions.

Catalytic activity. The activities of catalysts for thiophene hydrodesulfurization were measured by using a continuous flow reactor with on-line gas chromatography system. 1 gram of catalyst with 1 gram of silicon carbide particles were packed in the reactor. Catalysts were sulfided, and then feed with 25% thiophene+hexane at LHSV=6 h⁻¹, 275 °C and 310 °C, a hydrogen pressure of 4.14 MPa, and H₂/oil ratio of 2000 v/v. Reaction rate constant *k* were calculated according to first-order kinetics².

Catalyst characterization. XRD patterns were collected on a Simens diffractometer D5005(Cu-K α radiation). Extended X-ray adsorption fine structure(EXAFS) spectra of catalysts were recorded at Beijing Synchrotron Radiation Laboratory, Institute of High Energy Physics, Chinese Academy of Sciences. laser Raman spectra(LRS) were measured on Bruker RFS—100 instrument.

Results and Discussion

Preparation parameters, such as: metal loading; atomic Ni/(Ni+W) ratio; impregnation procedure; calcination temperature; activation procedure, may strongly affect the HDS activity of supported NiW/ γ -Al₂O₃ catalysts. At the general preparation conditions, atomic Ni/(Ni+W) ratio is one of the most important factors, since the addition of nickel has been one of the main routes to prepare improved catalysts. The ratio determines the amounts of active sites, promotion behaviors, and catalyst cost. The optimal Ni/(Ni+W) ratio for alumina supported Ni-W catalysts varied in the wide range from 0.375 to 0.6, and is much higher than the well-known optimal ratio of 0.23 ~0.33 for Co-Mo and Ni-Mo hydrotreating catalysts³. The results obtained in this work are arranged in figure 1, which gives the reaction rate constant of thiophene HDS vs the composition of NiW/ γ -Al₂O₃ catalysts.

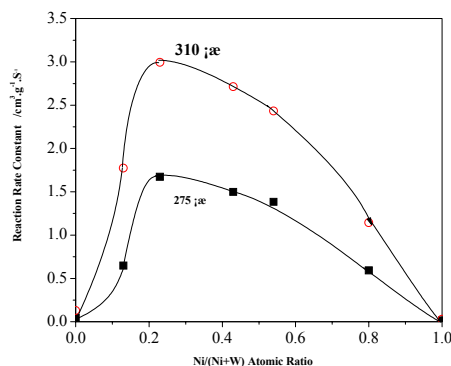


Figure 1. Thiophene HDS reactivity over sulfided NiW/ γ -Al₂O₃ catalysts.

The feature of the results is the marked increase in the catalytic activity with addition of nickel atoms, the activity increases significantly and pass through a maximum at Ni/(Ni+W) ratio of 0.23.

EXAFS was carried out to explain the above results. Figure 2 shows the Fourier transforms of tungsten EXAFS spectra for prepared WS₂ and the sulfided NiW/ γ -Al₂O₃ catalysts.

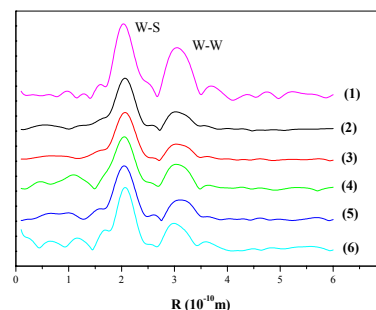


Figure 2. Fourier transforms of tungsten EXAFS spectra for sulfided NiW/ γ -Al₂O₃ catalysts. (1) prepared WS₂; (2) NiW-0.13*; (3) NiW-0.23; (4) NiW-0.43; (5) NiW-0.54; (6) NiW-0.80. *: the number denotes the atomic Ni/(Ni+W) ratio.

For each of the catalysts, there are two main peaks, which correspond to the first W-S and W-W coordinations in WS₂ crystallites, respectively. The highest intensities of the W-S and W-W

peaks were for the prepared WS₂, since the bulk WS₂ compound is complete crystal. EXAFS patterns of sulfided NiW/ γ -Al₂O₃ catalysts is very similar to the pattern of the prepared WS₂, which means that the state of W existence is WS₂-like crystallite.

The structural parameters resulting from the fit of the EXAFS data of sulfided catalysts are listed in table 1.

Table 1. Structural parameters of the W-S and W-W coordinations for sulfided NiW/ γ -Al₂O₃ catalysts.

Catalyst	W-S		W-W	
	N_{W-S}	R_{W-S} (nm)	N_{W-W}	R_{W-W} (nm)
NiW-0.13	4.90	0.241	1.97	0.315
NiW-0.23	4.58	0.241	1.72	0.315
NiW-0.43	5.95	0.241	2.43	0.315
NiW-0.54	5.62	0.241	2.02	0.315
NiW-0.80	4.79	0.241	2.45	0.315

As discussed afterwards, W-S coordinations of bulk WS₂ compound is 6.0. W-S coordinations of all sulfided NiW/ γ -Al₂O₃ catalyst are smaller than 6.0, which means that the WS₂ crystallite on the surface of catalysts is not complete one. The W-S and W-W coordinations of sulfided NiW-0.23 catalyst are the smallest of all sulfided NiW/ γ -Al₂O₃ catalyst, which implies that the size of WS₂-like crystallite is the smallest.

Being similar to Co-Mo-S model, Ni-W-S phase is WS₂-like structures with the Ni atoms located at edges(or corners) of WS₂-like crystallite. The smaller the WS₂-like crystallite, the more the edges(or corners) of WS₂-like crystallite for Ni atoms to occupy. The smaller WS₂-like crystallites on the surface of Catalysts is beneficial to the formation of Ni-W-S phases. Thus, the sulfided NiW-0.23 catalyst with smaller WS₂-like crystallite, has higher HDS activity.

The loadings used in industrial applications are usually governed by the desire to achieve as a high activity as possible with as small amounts of the expensive metals as possible¹. The tungsten loading used is typically in the range of 15~23 wt% W. This corresponds to approximately a monolayer coverage for an alumina support with a typical surface area of about 230 m²/g. The tungsten loadings in this work is all less than a monolayer coverage. Thus, tiny WS₂-like crystallite on the surface of sulfided NiW/ γ -Al₂O₃ can not be detected by XRD method, as only bulk compound of crystallite can be detected by the method. Laser Raman spectroscopy can be used for the investigation of bulk compound as well as dispersed phases⁴. By combination of these two methods, the microstructure of WS₂-like crystallite on the surface of sulfided NiW/ γ -Al₂O₃ can also be identified. The Raman spectra of commercial WS₂, prepared WS₂ and sulfided NiW/ γ -Al₂O₃ catalyst were shown in figure 3.

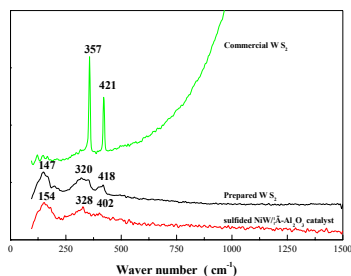


Figure 3. Raman spectra of the sulfided NiW/ γ -Al₂O₃ catalyst and bulk WS₂.

For bulk commercial WS₂, two peaks at 357 and 421 cm⁻¹ attribute to the typical peaks of 2H-WS₂. Thus, commercial WS₂ exists as 2H-WS₂ structure. 2H-WS₂ is an example of a six-fold coordinated layer structure in which the coordination is not octahedral⁵. The crystal is hexagonal with the elongated bimolecular units: $a_0=0.318$ nm, $c_0=1.25$ nm.

The sulfur atoms around the metallic atom are at the corners of right equilateral trigonal prisms which share vertical edges with one another to build up WS₂ layers normal to the c_0 axis. The crystal is built up by repeating these complete layers one above another according to the alternating requirements of hexagonal close-packing. Parallel to c_0 axis, the sulfur anion repeats in the order of AA, BB, AA Because the spectra of commercial WS₂ is different from others, prepared WS₂ and sulfided NiW/ γ -Al₂O₃ catalyst are not of 2H-WS₂ structure.

The structure of prepared bulk WS₂ can be identified by XRD. Its XRD pattern was given in figure 4.

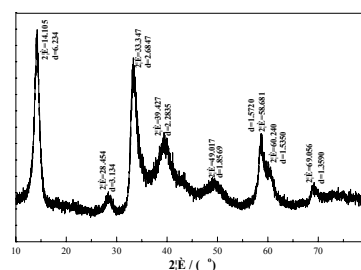


Figure 4. XRD patterns of prepared WS₂.

It is found that prepared WS₂ is mainly in the state of 3R-WS₂ structure by compared data shown in figure 2 with data from the card 35-651 and card 8-237 of JCPDS(the Joint Committee on Powder Diffraction Standards). The form of 3R-WS₂ is rhombohedral and bears the same kind of relation to hexagonal MoS₂. However, the sulfur anion repeats in the order of AA, BB, CC, AA Its trimolecular hexagonal cell has the dimensions⁵:

$$a_0' = 0.318 \text{ nm}, c_0' = 1.875 \text{ nm}.$$

As shown in figure 1, the Raman spectra of prepared WS₂ is very similar to that of sulfided NiW/ γ -Al₂O₃ catalyst. It is inferred that tiny WS₂-like crystallite on the surface of sulfided NiW/ γ -Al₂O₃ catalyst is also mainly in the state of 3R-WS₂ structure, as the two samples sulfided at the same conditions. The tiny WS₂-like crystallite on the surface is incomplete crystal, for it just contains several units.

Acknowledgment. This work was supported by the Key Basic Research Program of Science and Technology of China(Grant No. G2000048003).

References

1. Topsøe H, Clausen B S, and Massoth F E. Hydrotreating Catalysis, eds. Anderson J R and Boudart M, Springer, Berlin, 1996
2. Choong Hyon Kim, Wang Lae Yoon, In Chul lee et al. *Appl Catal A: General*, 1996, 144, 159
3. Vradman L and Landau M V. *Catal Lett*, 2001, 77, 47
4. Payen E, Kasztelan S, Grimblot J, et al. *Catal Today*, 1988, 4, 57
5. Wyckoff Ralph W G. Crystal Structures, Second Edition, Volume I. a Division of John Wiley, New York, London, Sydney, 1963

ELUCIDATION OF SULFUR BEHAVIOR FOR MOLYBDENUM SULFIDE CATALYSTS SUPPORTED ON TITANIA USING ^{35}S TRACER METHODS

Atsushi Ishihara, Dahong Wang, Weihua Qian, Toshiaki Kabe

Tokyo University of Agriculture and Technology
2-24-16 Nakacho, Koganei, Tokyo 184-8588, Japan

Introduction

The need for better hydrodesulfurization catalysts to fulfill the more strict environmental restrictions imposed on the sulfur content of transport fuels has prompted the researchers in the field to look for more active and selective catalyst formulations.¹ Several studies suggested that changing the support into titania² or alumina-titania mixed oxides³ would show promising results. However, despite all the previous studies, no explanation for the substantial difference in HDS activity between alumina- and titania-supported catalysts has yet been elucidated.

In the previous work, the authors showed that the sulfidation states and behavior of sulfur on working hydrodesulfurization catalysts could be determined using ^{35}S tracer methods.^{4,8} The object of the present work is to determine the sulfur behavior for TiO_2 -supported molybdenum catalysts using ^{35}S tracer methods. A ^{35}S radioisotope pulse tracer method using ^{35}S -labeled H_2S , which can exactly determine the sulfidation state of the catalyst,^{4,7} was used to investigate the sulfidation and reduction states of Mo/TiO_2 catalyst. Moreover, a ^{35}S radioisotope tracer method using ^{35}S -labeled dibenzothiophene (^{35}S]DBT), which can give information about the behavior of sulfur on the working catalyst,^{4,8} was used to elucidate the sulfur mobility on the sulfided Mo/TiO_2 catalyst under the reaction conditions.

Experimental

Catalysts. TiO_2 support used in this study is a reference catalyst with a surface area of $70 \text{ m}^2/\text{g}$ supplied from the Catalysis Society of Japan. The Mo/TiO_2 catalysts were prepared by the incipient wetness impregnation of TiO_2 support with an aqueous solution of ammonium heptamolybdate as required. This was followed by drying at 120°C for 3h and calcination in air at 500°C for 3h. The catalysts were denoted as MT(2), MT(3.5), MT(5), MT(6), and MT(12) where the values in parentheses represent MoO_3 contents, corresponding to 2.0, 3.5, 5.0, 6.0, 12.3 wt% MoO_3 , respectively.

Sulfidation of Mo/TiO_2 catalyst using ^{35}S -labeled H_2S . A ^{35}S -radioisotope pulse sulfiding method was developed to investigate the sulfidation process. The pulse tracer apparatus is reported elsewhere.⁷ A pulse of 30 vol% ^{35}S]H $_2\text{S}$ in hydrogen was introduced in the fixed-bed reactor with a gas sampler (2.46 ml) every 10 min under N_2 carrier gas (0.5 MPa, 40 ml min^{-1}). The radioactivity of unreacted ^{35}S]H $_2\text{S}$ absorbed by a commercially available basic scintillation solvent every 10 min was measured by a liquid scintillation counter (LSC).

HDS of ^{35}S]DBT. The HDS experiments were carried out with a fixed-bed reactor. The catalyst was presulfided with a mixture of 5 vol% H_2S in H_2 flowing at 5 l h^{-1} , 0.1 MPa. After presulfiding, the reactor was cooled to room temperature and then pressurized with hydrogen. A decalin solution of ^{32}S]DBT was fed into the reactor at the reaction temperature by a high-pressure liquid pump. Typical reaction conditions were as follows: H_2 flow rate 25 l h^{-1} , WHSV 28 h^{-1} , reaction pressure 5 MPa, concentration of DBT in decalin 1.0 wt%. The liquid products were collected every 15 min and analyzed by gas chromatography with an FID detector and a commercial capillary column. The radioactivity was

measured by LSC. The feed was changed from ^{32}S]DBT to ^{35}S]DBT, neat decalin, ^{32}S]DBT successively after a reaction in each period reached a steady state. A typical operation procedure using ^{35}S]DBT radioisotope tracer method has been described in detail elsewhere.^{4,8}

Results and Discussion

Sulfidation of Mo/TiO_2 catalyst using ^{35}S -labeled H_2S . Figure 1 shows the change in radioactivity of ^{35}S]H $_2\text{S}$ eluted during the sulfidation of MT(2) and MT(6) catalysts at various temperatures. For each catalyst, the radioactivity of unreacted ^{35}S]H $_2\text{S}$ at 100 and 200°C approached a constant value, equal to the radioactivity of the pulse introduced, while at 300 and 400°C , ^{35}S]H $_2\text{S}$ seemed to accumulate on the catalysts slowly; thus the radioactivity of unreacted ^{35}S]H $_2\text{S}$ found it difficult to approach the radioactivity in the introduced pulse. The amount of sulfur incorporated into the catalyst could be calculated by subtracting the radioactivity of released ^{35}S]H $_2\text{S}$ from the total radioactivity introduced (the shaded area).⁷ For MT(2) and MT(6) catalysts, the total sulfur were calculated to be 9.7 and 29.1 mg-S/g-cat respectively when all MoO_3 species were present as MoS_2 . It is reported in our previous study⁷ that MoO_3 supported on Al_2O_3 can be almost sulfided to MoS_2 at 400°C . Therefore, it is supposed here that at 400°C all MoO_3 species on TiO_2 support were present as MoS_2 , and that a part of TiO_2 support could still be sulfided when MoO_3 was supported on it. Such results suggested that the sulfide TiS_2 should play an important role on the HDS activity under the reaction conditions.

Behavior of sulfur on the sulfided Mo/TiO_2 catalyst. HDS of ^{35}S]DBT was performed to investigate the behavior of sulfur on MT(6) catalyst in the steady state. Figure 2 shows a typical operation procedure of ^{35}S tracer method. The HDS reaction of ^{35}S]DBT was carried out on a sulfided MT(6) catalyst at 360°C . Initially, a decalin solution of 1wt% ^{32}S]DBT was pumped into the reactor until the conversion of DBT became constant. A decalin solution of 1wt% ^{35}S]DBT was then substituted for the ^{32}S]DBT and reacted until the formation amount of ^{35}S]H $_2\text{S}$ became constant. After ^{35}S]DBT was introduced, the radioactivity of unreacted ^{35}S]DBT in the liquid product increased and approached a steady state immediately. However, it took ca. 75 min to achieve a steady state in the radioactivity of ^{35}S]H $_2\text{S}$ produced. In order to determine the behaviour of sulfur more accurately, the ^{35}S]DBT solution was subsequently replaced by decalin solvent. It was observed that a portion of ^{35}S , which is represented by the shaded area A in Figure 2,

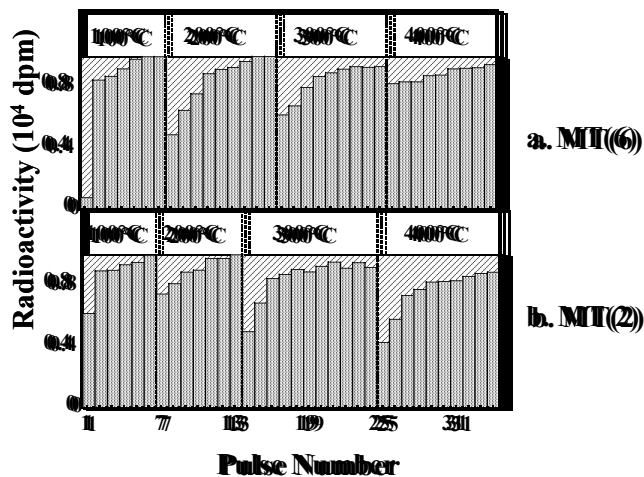


Figure 1 Sulfidation of 6% $\text{MoO}_3/\text{TiO}_2$ catalyst with ^{35}S]H $_2\text{S}$ pulse at various temperatures.

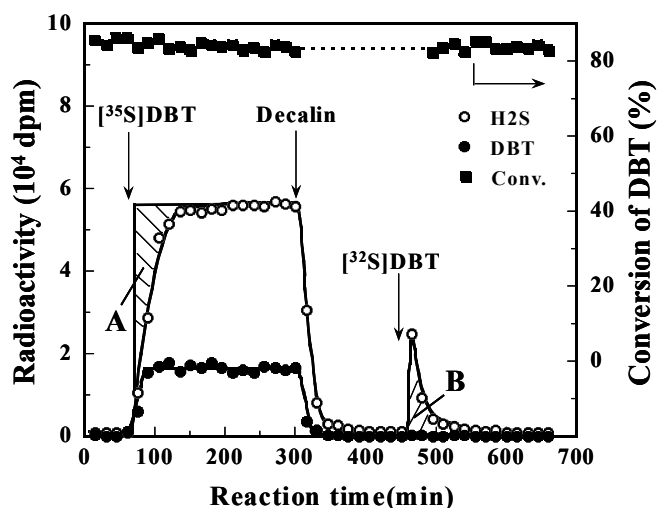


Figure 2. Changes in Radioactivities of Unreacted $[^{35}\text{S}]\text{DBT}$ and Formed $[^{35}\text{S}]\text{H}_2\text{S}$ and DBT Conversion with Reaction Time (360°C)

remained on the catalyst. When decalin and H_2 were used to purge the catalyst, less release of $[^{35}\text{S}]\text{H}_2\text{S}$ was detected. When the reactant solution was replaced by $[^{32}\text{S}]\text{DBT}$ again, a portion of ^{35}S can be released again as $[^{35}\text{S}]\text{H}_2\text{S}$, as shown in **Figure 2** (shaded area B). This portion of ^{35}S was approximately equal to shaded area A, which represented the total amount of labile sulfur on the catalyst under this reaction condition. According to a method reported in reference 17, the amount of labile sulfur can be calculated from the total radioactivity of the $[^{35}\text{S}]\text{H}_2\text{S}$ released after $[^{32}\text{S}]\text{DBT}$ was reintroduced, *i.e.*, shaded area B. To discuss the release process of $[^{35}\text{S}]\text{H}_2\text{S}$ more accurately, the rate constant of $[^{35}\text{S}]\text{H}_2\text{S}$ release from ^{35}S -labeled catalyst was determined. As reported previously,⁸ the release of $[^{35}\text{S}]\text{H}_2\text{S}$ in the range of area B shown in **Figure 2** can be explained with respect to a first-order reaction and the rate constant of $[^{35}\text{S}]\text{H}_2\text{S}$ release, k_{RE} was determined.

In order to understand the promoting effect of TiO_2 support on Mo species under reaction conditions, the amount of labile sulfur (S_0) and the rate constant of H_2S release (k_{RE}) for 6% $\text{MoO}_3/\text{TiO}_2$, 6% $\text{MoO}_3/\text{Al}_2\text{O}_3$ ⁸ and TiO_2 support⁴ are given in **Table 1**. TiO_2 support presents less labile sulfur, although it was active in HDS of DBT, which clearly indicates that the HDS mechanism on TiO_2 support is different from that on Mo-based catalyst. It is suggested that the sulfur vacancies on the reduced sulfided TiO_2 support would act as the active sites for HDS reaction without sulfur accumulation.⁴ Compared with the $\text{Mo}/\text{Al}_2\text{O}_3$ catalyst, the Mo/TiO_2 catalyst shows a little higher amount of labile sulfur (S_0); it is most important that about 2 times higher rate constant of H_2S release (k_{RE}) is obtained on the Mo/TiO_2 catalyst. The amount of labile sulfur (S_0) represents the number of active sites and the rate constant of H_2S release (k_{RE}) represents the mobility of active sites on the surface of the catalyst. Therefore, the results indicate that the presence of TiO_2 makes the sulfur on the sulfided Mo/TiO_2 catalyst more mobile rather than increasing the number of the active sites. In a recent study, we have proposed that the promoting effect of cobalt for molybdenum catalyst was due to increased mobility of the sulfur in the so-called “CoMoS” phase where the strength of the Mo-S bond was considered to be weakened.¹ Similarly, the promoting effect of TiO_2 on Mo catalyst is supposed to bring about the decrease in the strength of Mo-S bond, since the sulfur mobility on the catalyst is dependent on the bond strength of the metal sulfide. The strength of the Mo-S bond on TiO_2 -supported catalyst is assumed to be

Table 1. Amount of sulfur, release constant of $[^{35}\text{S}]\text{H}_2\text{S}$ and HDS activity on MT(6), MA(6) catalysts and TiO_2 support

Catalyst	Temp. ($^\circ\text{C}$)	Conv. (%)	S_{CHB} (%)	S_0 (mg g-cat ⁻¹)	k_{RE} (10^{-2} min ⁻¹)	r_{HDS} (mg g-cat ⁻¹)
MT(6)	360	83.2	44.4	6.51	8.93	0.68
MA(6)	360	36.9	10.6	5.98	4.61	0.30
TiO_2	390	19.6	43.7	0.52	—	0.16

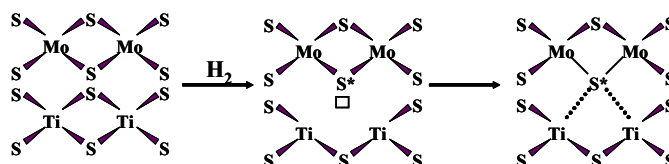


Figure 3. TiMoS phase structure for a Mo/ TiO_2 catalyst

weaker than that on Al_2O_3 -supported catalyst. As shown in **Figure 3**, under H_2 atmosphere the sulfided Ti species can be reduced to Ti^{3+} and sulfur vacancies with electrons trapped in are formed. Sulfur in MoS_2 coordinates the sulfur vacancies in the sulfided Ti species and the so-called “TiMoS” phase is generated. The injection of electrons from Ti to Mo through sulfur will decrease the Mo-S bond energy. Therefore, it is suggested that the role of TiO_2 in Mo catalyst is not only to act as a conventional support but also to act as an electronic promoter of the molybdenum sulfide phase.

Conclusions

When MoO_3 were supported on TiO_2 support, the sulfidation of TiO_2 support would also occur. Compared with $\text{Mo}/\text{Al}_2\text{O}_3$ catalyst, Mo/TiO_2 catalyst shows a little higher amount of labile sulfur (S_0) and about 2 times higher release rate constant of H_2S (k_{RE}). It was suggested that TiMoS phase structure generated for a Mo/TiO_2 catalyst weakens Mo-S bond to increase the rate of H_2S release and the HDS activity.

Acknowledgement

This work has been entrusted by the New Energy and Industrial Technology Development Organization under a subsidy of the Ministry of Economy, Trade and Industry.

References

1. Kabe, T.; Ishihara, A.; W. Qian, *Hydrodesulfurization and Hydrodenitrogenation*, Kodansha, Tokyo, and Wiley-VCH, New York, 1999.
- 2) Ramirez, J.; Fuentes, S.; Diaz, G.; Vrinat, M.; Breyse, M.; Lacroix, M. *Appl. Catal.*, **1989**, 52, 211.
- 3) Yoshinaka, S.; Segawa, K., *Catal. Today*, **1998**, 45, 293.
- 4) D. H. Wang, W. Qian, A. Ishihara, T. Kabe, *J. Catal.*, **2001**, 203, 322-328.
- 5) Ishihara, A.; Lee, J.; Franck, D.; Higashi, R.; Wang, A.; Qian, W.; Kabe, T., *J. Catal.*, **2003** in press.
- 6) Kabe, T.; Qian, W.; Ishihara, A., *J. Phys. Chem.*, **1994**, 98, 912.
- 7) Kabe, T.; Qian, W.; Tanihata, K.; Ishihara, A.; Godo, M., *J. Chem. Soc. Faraday Trans.*, **1997**, 93, 3709.
- 8) Qian, W.; Zhang, Q.; Okoshi, Y.; Ishihara, A.; Kabe, T., *J. Chem. Soc. Faraday Trans.*, **1997**, 93, 1821.

LOW-TEMPERATURE HYDROGENATION OF AROMATICS OVER NOBLE METAL CATALYSTS IN THE PRESENCE OF SULFUR COMPOUND

J.Abe^{1,2}, X.Ma¹, C.Song^{1}*

(1) Clean Fuels and Catalysis Program, The Energy Institute, and Department of Energy and Geo-Environmental Engineering Pennsylvania State University, 209 Academic Projects Building, University Park, PA, 16802

*E-mail: csong@psu.edu

(2) JGC Corporation, Technology Development Department 2205 Narita-cho, Oarai-machi, Ibaraki Pref. 311-1313, Japan
E-mail: abe.jun@jgc.co.jp

Introduction

In recent years, there is a growing interest in the demand of high quality transportation fuels with lower contents of sulfur and aromatics. In order to reduce the aromatics and to raise the cetane number of diesel fuel, deep hydrogenation of diesel fuel may become necessary in the future. Deep hydrogenation of jet fuel feedstock is also important for producing advanced thermally stable jet fuels.

Typical conventional hydroprocessing for diesel is operated at 330-360 °C, and typical catalysts are Co-Mo and Ni-Mo supported on alumina. Since the hydrogenation of aromatics is highly exothermic, there is an equilibrium limitation for the hydrogenation at high temperature. On the other hand, conventional Co-Mo and Ni-Mo catalysts have to be used at higher temperature due to relatively low activity of them at low temperature. Noble metal catalysts are potential candidates for deep hydrogenation of diesel fuel at low temperature because of their high hydrogenation activity. However, it is well known that the noble metal catalysts are easily deactivated by sulfur compounds. Therefore, a two-stage hydroprocessing is adopted for deep hydrogenation. At the first stage, sulfur content is reduced to less than 5 ppmw by ultra deep hydrodesulfurization, and after hydrogen sulfide stripping, deep hydrogenation of aromatics is conducted in the second stage by using noble metal catalysts. The reduction of the sulfur contents in diesel fuel to less than 5 ppmw by hydrodesulfurization process is difficult and requires large investment.¹

Some approaches to developing sulfur-resistant hydrogenation catalysts have been reported.²⁻⁵ At Penn State, we have been exploring the noble metal catalysts with higher sulfur-resistance.⁶⁻¹³ We reported Pd catalysts supported on zeolites tend to show higher tolerance in the batch tests. In the present study, a continuous flow fixed-bed reactor was used for the hydrogenation of tetralin to decalins in the presence of benzothiophene as a model reaction for saturation of aromatics in diesel and jet fuel feedstock. As noble

metal catalysts, Pd and Pt supported on alumina, titania and some zeolites were prepared and examined.

Experimental

Preparation of catalysts. Pt supported on alumina and Y zeolite (HY) catalysts were prepared by incipient wetness impregnation of an aqueous solution of H₂PtCl₆ · xH₂O (Aldrich) with a nominal metal concentration of 2 wt %. Pd catalysts were prepared by incipient wetness impregnation of either PdCl₂ (Aldrich) dissolved in dilute hydrochloric acid (sufficient to form soluble PdCl₄²⁻) or (CH₃CO₂)₂Pd (Aldrich) dissolved in acetone with a nominal metal concentration of 2wt %. The details for metal salts and type of supports are listed in Table 1.

After drying, the catalysts were calcined in air at 450 °C for 3 hrs. Before use, the catalysts were reduced in a continuous flow reactor at 350 °C under H₂ flow at atmospheric pressure for 1 hr.

Reaction system and procedure. Catalytic reaction tests were conducted at 220 °C and 1,000 psig (7 MPa) hydrogen pressure in a continuous-flow fixed-bed stainless steel tubular reactor. In the fixed bed, 3.3 ml of catalysts (2.0 - 0.5mm particles) were loaded, and α-alumina was loaded over and under the catalyst.

Feed used in the present study is 20 wt % tetralin (1,2,3,4-tetrahydronaphthalene, Aldrich 99%) in hexadecane (Aldrich, 99+%, anhydrous) in the absence or in the presence of benzothiophene (BT, Aldrich, 99%) with 500 ppmw based on sulfur. The liquid feed space velocity LHSV = 2.0 hr⁻¹, and H₂/oil ratio is 800 Nml-gas/ml-liquid. The liquid product samples were collected periodically and analyzed quantitatively by GC-FID (HP 5890).

Results and Discussion

Table 2 and Figure 1 show the results for the hydrogenation of tetralin over various supported Pd and Pt catalysts in the presence of BT. The hydrogenation activity of Pt catalysts supported on alumina and Y zeolite was drastically decreased in the first three hours. The activity of Pd catalyst supported on alumina also declined. However, through comparison of these catalysts, Pd catalysts supported on titania and zeolites appear to be relatively more resistant to sulfur poisoning and more stable than the other catalysts after sulfur poisoning.

However, as can be seen from Table 2, the loading density of Pd supported on titania is higher than that of other catalysts. The advantages of zeolite-supported Pd catalysts are more apparent in terms of higher conversion event at lower catalyst loading compared to the case with alumina-supported Pd catalyst.

Table 1. Properties of supports and the supported Pd and Pt catalysts

Catalyst	Support Type	Support Code	Surface Area m ² /g	SiO ₂ /Al ₂ O ₃ Molar ratio	Precursor Metal Salt	Metal Loading Wt%
Pd/HY(5)	Y zeolite	CBV600	660	5.2	(CH ₃ CO ₂) ₂ Pd	2.0
Pd/HY(46)	Y zeolite	CBV740	840	46	(CH ₃ CO ₂) ₂ Pd	2.0
Pd/HM	Mordenite	CBV30A	512	37.5	(CH ₃ CO ₂) ₂ Pd	2.0
Pd/MCM-41	Al-MCM-41	Al-MCM41(50)	1289	50	PdCl ₂	2.0
Pd/Al ₂ O ₃	γ-Alumina	LaRoche	155	Not applicable	(CH ₃ CO ₂) ₂ Pd	2.0
Pd/TiO ₂	Titania	Degussa P25	71	Not applicable	PdCl ₂	2.0
Pt/HY(5)	Y zeolite	CBV600	660	5.2	H ₂ PtCl ₆ · xH ₂ O	2.0
Pt/Al ₂ O ₃	γ-Alumina	LaRoche	155	Not applicable	H ₂ PtCl ₆ · xH ₂ O	2.0

Table 2. Hydrogenation of tetralin over supported Pt and Pd catalysts at 220 °C in a flow reactor

Catalysts	Pt/Al ₂ O ₃				Pt/HY(5)			Pd/Al ₂ O ₃			Pd/HY(5)		
Loading density, g/ml	0.550				0.486			0.520			0.474		
Sulfur content, ppmw	0	500			0	500		0	500		500		
Reaction time, hrs	4	2	4	6	4	2	4	4	2	4	2	4	6
S / Metal, by atom	n/a	0.89	1.78	2.67	n/a	1.01	2.02	n/a	0.51	1.03	0.56	1.13	1.69
Conversion, %	98.2	88.5	30.5	5.7	99.4	52.7	5.3	94.7	78.7	5.3	75.7	55.5	48.3

Catalysts	Pd/HY(46)				Pd/TiO ₂				Pd/MCM-41			Pd/HM		
Loading density, g/ml	0.363				1.010				0.345			0.473		
Sulfur content, ppmw	500				500				500			500		
Reaction time, hrs	2	4	6	2	4	6	7	2	4	6	2	4	6	
S / Metal, by atom	0.736	1.47	2.21	0.26	0.53	0.79	0.93	0.78	1.55	2.33	0.57	1.13	1.70	
Conversion, %	67.4	45.2	46.4	91.3	88.9	36.4	20.7	39.9	19.5	19.1	59.4	54.2	42.6	

□ Reactions were conducted at 220□ and 1,000psig hydrogen pressure in a continuous fixed bed stainless steel tubular reactor.

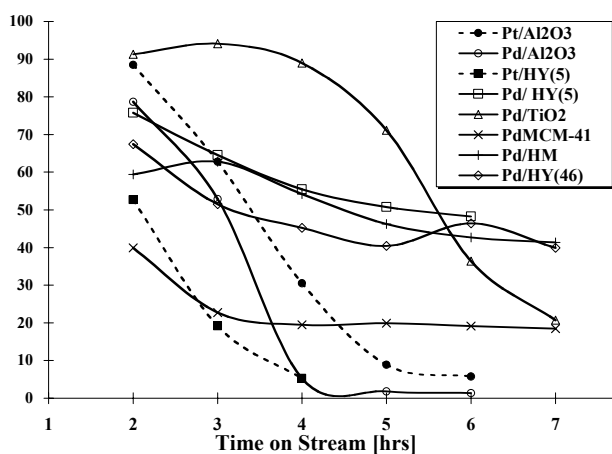


Figure 1. Hydrogenation of tetralin over noble metal catalysts at 220°C and 1,000 psig of hydrogen pressure in the presence of 500 ppm sulfur.

Figure 2 compares the hydrogenation activity versus the atomic ratio of sulfur to metal loading on the support. Pd catalysts supported on Y zeolites, Mordenite and MCM-41 are more sulfur-resistant and stable than other Pd catalysts when the sulfur-to-metal ratio is higher than 1.0.

Addition of BT into the feed decreased the hydrogenation activity of all the noble metal catalysts. However, it appears that zeolite supporters improve significantly the sulfur resistance of Pd catalysts. In other words, zeolite-supported Pd catalysts are clearly superior to zeolite-supported Pt catalysts under the conditions used.

For the Pd catalysts supported on zeolites, the difference between Y zeolite and mordenite supported cases in Figure 2 is not very large. However, they both are superior to the mesoporous aluminosilicate molecular sieve Al-MCM-41.

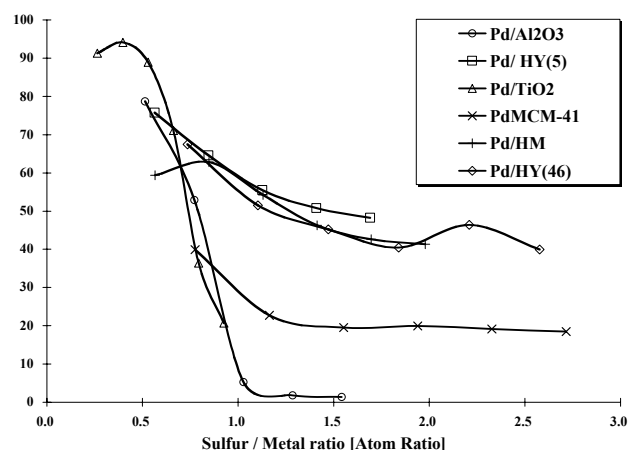


Figure 2. The hydrogenation activity over Pd catalysts as a function of the atomic ratio of sulfur and metal.

After the hydrogenation conversion decreased to 50% on for Y zeolite supported Pd catalyst, when the feed with sulfur was changed to the feed without sulfur it was observed that the hydrogenation conversion was recovered in a few hours, indicating the deactivation of the Y zeolite supported Pd catalyst by sulfur poison is reversible and recoverable.

These flow-reactor results support our proposed design concept^{9,10} of sulfur-resistant noble-metal catalysts, which is based on shape selective exclusion with molecular sieve structure, hydrogen spillover and two types of sulfur resistance that was developed based on our earlier batch tests.⁶⁻⁸

Conclusions

On the basis of the hydrogenation of tetralin over different catalysts in the presence of benzothiophene, 1) Pd catalysts show less sensitive to sulfur compounds than Pt catalysts; 2) Pd and Pt supported on zeolites are superior to Pd and Pt supported on alumina and titania in their sulfur-resistant performance; 3) The deactivation

of Pd catalysts supported on zeolites by the sulfur compound is not permanent, but reversible.

Acknowledgment

We thank our colleagues in the Clean Fuels and Catalysis Program of Energy Institute at PSU (particularly Dr. Xiaochun Xu, Dr. S. Velu, Dr. Jian Zheng) for providing support samples and for assistance in the laboratory. CS is grateful to US AFOSR for providing partial financial support to CS for project work in this area, and to Prof. Harold Schobert for helpful discussions on aromatics hydrogenation related to jet fuel research.

References

- (1) B. H. Cooper, B. B.L. Donnis, *Appl. Catal. A*, **1996**, 137, 203.
- (2) A. Corma, A. Martinez, V.M. Soria, *J of Catal*, **1997**, 169, 480.
- (3) Y.Yoshimura, H. Yasuda, T. Sato, N. Kijima, T. Kameoka *Applied Catalysis*, **2001**, 207, 303.
- (4) V.L. Barrio, P.L. Arias, J.F. Cambra, M.B. Guemez, B. Pawelec, J.L.G. Fierro, *Fuel*, **2003**, 82, 501.
- (5) K.C. Park, D.J. Yim, S.K. Ihm, *Catalysis Today*, **2002**, 74, 281.
- (6) S. D. Lin, C. Song, *Catalysis Today*, **1996**, 31, 93.
- (7) K. M. Reddy, C. Song, *Catalysis Today*, **1996**, 31, 137.
- (8) C. Song, A.D. Schmitz, *Energy & Fuel*, **1997**, 11 (3), 657.
- (9) C. Song, *Chemtech*, **1999**, 29 (3), 26
- (10) C. Song, *Am. Chem. Soc. Symp. Ser.*, **2000**. 738, 381.
- (11) J. Zheng, M. Sprague, C. Song . *Am. Chem. Soc. Div. Petrol. Chem. Prep.*, **2002**, 47 (2), 100.
- (12) M. Sprague, J. Zheng., and C. Song. *Am. Chem. Soc. Div. Petrol. Chem. Prep.*, **2002**, 47 (2), 103.
- (13) C. Song and X. Ma. *Applied Catalysis B: Environmental*, **2003**, 41 (1-2), 207.

PERCEPTION ON THE NATURE OF THE PERFORMANCE OF NI-BASED CATALYST FOR DIESEL CLEANING

Qi Sun, Wayne Turbeville, Jurgen R. Ladebeck

Süd-Chemie Inc, P. O. Box 32370, Louisville, KY 40232, USA, e-mail: gsun@sud-chemieinc.com

Introduction

Catalytic deep hydrogenation of aromatics and desulfurization of diesel is playing a more and more important role in providing environment-friendly fuels. Supported noble metal catalysts on various supports have been proved being superior catalysts for low-temperature hydrogenation of aromatic [1,2] and hydrodesulfurization at high temperatures [3]. However, they are sensitive to sulfur. A trace of them can poison the catalysts. High content Ni/SiO₂ or Ni/Al₂O₃ are practical catalysts to hydrogenate aromatic and remove tough sulfur species from diesel and other fuel oils. In the present work, the performances of different Ni-based catalysts were described and the nature of hydrogenation of aromatic and desulfurization was investigated.

Experimental

Catalyst: Ni/SiO₂ and Ni/Al₂O₃ catalyst with Ni content of 60% were prepared by co-precipitation method, followed by calcinations and extrusion.

Catalytic test: The catalytic performance of Ni/SiO₂ and Ni/Al₂O₃ catalysts for aromatic hydrogenation and desulfurization were tested on a pressurized fixed-bed continuous flowing stainless steel reactor (i.d. 1") packed with extruded catalyst (diameter of 1/16"). The test condition simulated industrial operating process: LHSV of 3h⁻¹; pressure of 450psig and temperature of 190°C. An excess of H₂ was co-supplied to the reactor with diesel feedstock, which consists of 25.5% of aromatic, 4.2% of poly-aromatic and 55ppm of sulfur organic (benzothiophene, dibenzothiophene etc sulfur poly-aromatic).

Product analysis: The quantitative analysis of aromatic and sulfur in the products were carried out using an aromatic analyzer with FID detector and sulfur analyzer (ANTEK 7400), respectively. A HP 6890 GC with FID detector was used to detect cracking hydrocarbon product in the gas phase.

Results and Discussion

Ni/SiO₂ and Ni/Al₂O₃ show excellent activity for aromatic hydrogenation using a sulfur-free feed. 100% aromatic conversion can be achieved on these two catalysts at desired temperatures. However, the S-containing feed leads to the deactivation of the catalysts because the sulfur compounds may deposit on the catalyst surface and poison the active sites. With the time on stream, aromatic conversion decreases (or aromatic leakage increases) and sulfur leakage in the liquid product increases.

Hydrogenation activity relates to the Ni particle size, but sulfur tolerance depends on several different factors. High Ni specific area in the Ni/Al₂O₃ and Ni/SiO₂ catalysts is crucial for a high performance catalyst. For the same type Ni-based catalyst, sulfur tolerance increases with the increase of Ni specific surface area. A linear relationship between Ni specific surface area and sulfur tolerance was observed, as shown in Figure 1. However, the linear relationships for different Ni-based catalyst, i.e. Ni/SiO₂ and Ni/Al₂O₃, show significant difference. It is not the same type of linear relationship between sulfur tolerance and Ni surface area of different type catalysts (Ni/SiO₂ and Ni/Al₂O₃), indicating different intrinsic catalytic capacity per unit Ni surface on Ni/SiO₂ and Ni/Al₂O₃

catalysts. The results strongly demonstrate that, except for Ni surface area, the support has significant effect on the performance of aromatic hydrogenation and sulfur tolerance.

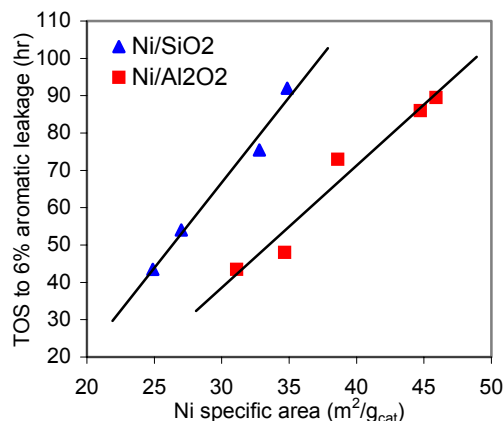


Figure.1: Correlation between sulfur tolerance and Ni specific surface area of different Ni-based catalysts.

Figure 2 illustrates the difference of the performance of Ni/SiO₂ and Ni/Al₂O₃ catalysts for aromatic hydrogenation and sulfur tolerance. Their deactivation behaviors are very different. Although Ni surface area of Ni/SiO₂ is lower than Ni/Al₂O₃, the deactivation rate at beginning hours on Ni/SiO₂ is much lower than that on Ni/Al₂O₃; after 48hours' run on Ni/SiO₂, aromatic shows up in the product and the deactivation rate increases and becomes higher than that on Ni/Al₂O₃. In another word, Ni/SiO₂ catalyst exhibits two different deactivation rates.

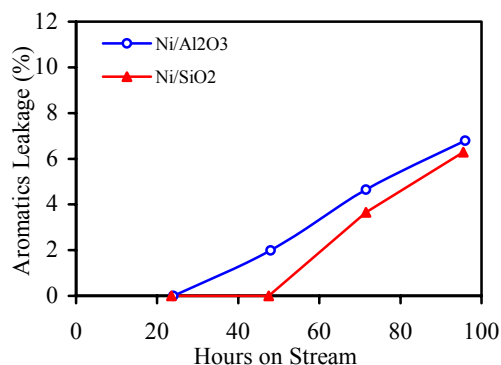


Figure 2: Comparison of the performance of Ni/SiO₂ and Ni/Al₂O₃ catalysts for aromatic hydrogenation and sulfur tolerance. Ni surface area, Ni/SiO₂ : 34.9m²/g_{cat}, Ni/Al₂O₃ : 42.0m²/g_{cat}.

The results indicate the pore structures of Ni/Al₂O₃ and Ni/SiO₂ catalysts play an important role. As shown in Figure 3, the mean maximum pore diameter of Ni/Al₂O₃ catalyst is much bigger than that of Ni/SiO₂ and there is almost no small pore (<20 Å). Ni/SiO₂ catalyst shows a bi-model pore structure. The smaller pore size is between 6~25Å and bigger pore diameter is in a very narrow range of 30~40Å. Since the sizes of sulfur compound in the diesel fuel might be bigger than the smaller pores in Ni/SiO₂, the diffusion adsorption of sulfur species on the active Ni sites in small-pore would be prohibited by the pore size. Aromatic/poly-aromatic and benzothiophene/ ploy-ditheophene molecules would easily enter into those big pores and are hydrogenated or deposited on active Ni surface in big pores, resulting in the deactivation. However, H₂

molecules can readily diffuse into both big and small pores and dissociatively adsorb on the active Ni surface. Those dissociatively adsorbed hydrogen might migrate from small pore to big pore by surface diffusion or spillover, which is much faster and more efficient than direct gas molecule transportation in pore channels. The spillover hydrogen has extra-high reactivity and could partially regenerate the poisoned metallic active sites by surface hydrogenation of organic sulfur compound to H₂S. H₂S can be purged away by the stream; or some of them can further bond with metallic Ni to form NiS_n clusters, resulting in the second deactivation. Since the small pore could not stop the diffusion of H₂S to small pore, the active Ni sites in the small pore would be finally poisoned by H₂S. As a result, the deactivation behavior of Ni/SiO₂ would become similar to that of Ni/Al₂O₃. Since the Ni surface area of Ni/Al₂O₃ is higher than that of Ni/SiO₂, the deactivation rate of Ni/SiO₂ after 48 hours' run becomes higher than that of Ni/Al₂O₃. If the Ni surface areas of Ni/SiO₂ and Ni/Al₂O₃ are the same or similar, it is found that the deactivation rate of Ni/SiO₂ after 48 hours' run is slightly lower than that of Ni/Al₂O₃ (the results not shown).

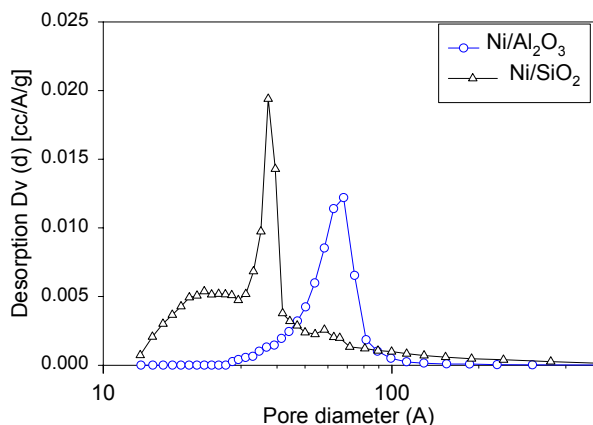


Figure 3: Pore diameter distribution of Ni/SiO₂ and Ni/Al₂O₃ catalysts

Therefore, the combination of bi-model pore structure makes the Ni metal sites exhibit higher sulfur resistance than that on the Ni in single-model pore channels. As a result, it shows higher intrinsic catalytic capacity for deep aromatic hydrogenation and desulfurization. The deactivation of the catalyst, however, cannot be overcome by this combination because H₂S can also diffuse into small pores, poison the metallic Ni sites and leads further deactivation. This observation and conclusion are in agreement with the results on zeolites [4].

Conclusion

High Ni specific area is crucial for hydrogenation and sulfur tolerance. Activity and sulfur tolerance increase with increasing Ni surface area. A linear relationship exists between Ni surface area and hydrogenation and sulfur tolerance performance. Ni/SiO₂ and Ni/Al₂O₃ show significant difference in aromatic hydrogenation and sulfur tolerance; Ni/SiO₂ has higher intrinsic activity than Ni/Al₂O₃ due to 'combination effect'. Shape selectivity and hydrogen spillover (surface diffusion) significantly promote catalyst performance for deep aromatic hydrogenation and sulfur tolerance.

References

1. C. Song, CHEMTECH, 29(1997) 26
2. J. Barbier, E. Lamy-Pitara, P. Marecot, et al., Adv. Catal., 37 (1990) 279
3. D. Huang, P. Jerus and W. Faris, U. S. patent, 06462244
4. C. Song, in "Shape-Selective Catalysis: Chemicals Synthesis and Hydrocarbon Processing", (C. Song, J. M. Garces and Y. Sugi Ed.), ACS Sym. series 738, p383

SYNTHESIS OF POROUS CARBON MATERIALS BY CARBONIZATION IN NATURAL ZEOLITE NANOCANNELS

Billur Sakintuna¹, Zeki Aktaş² and Yuda Yürüm¹

¹Faculty of Engineering and Natural Sciences
Sabanci University
Tuzla, 34956 Istanbul, Turkey

²Department of Chemical Engineering
Ankara University
Tandoğan, 06100 Ankara, Turkey

Introduction

Porous carbons are commonly used as catalysis and adsorbents and catalyst supports. Because of the presence of the three-dimensional channels, zeolites have molecular-sieve property used in adsorption and catalytic purposes. The zeolite-templated carbons has large surface areas and micropore volumes, without activation that is required to open new accessible microporous structures¹⁻². It should be noted that macropores, mesopores and micropores are defined here as pores of the width above 50 nm, between, 2 and 50 nm, and below 2 nm, respectively³.

Carbon framework formed in narrow pores of zeolites retained to templated carbon particles exhibited the morphology of the zeolite template particles. On the basis of this concept, there were few studies on the carbon formation in the zeolite nanoscale pores. Poly furfuryl alcohol¹ and polyacrylonitrile⁴ was carbonized in the zeolite channels and then the resultant carbon was obtained by washing with HF. In addition to zeolite frames, mesoporous silica molecular sieves^{5,6} were also used.

In the present study new porous carbon materials were synthesized by using a natural Turkish zeolite as template. The structure and morphology of zeolite-carbon composite and resulted carbon material was characterized by several means.

Experimental

Zeolite Samples as a Template

Zeolite samples were obtained from Enli Mining Company, Gördes, Manisa, Turkey. The major mineral present in the samples were reported to be clinoptilolite. Four different particle sizes of the zeolite sample (-30 μm , -0.1, -0.5 and -1.0 mm) were used in this study. Their BET surface areas, (m^2/g), pore volume and pore diameters were given in Table 1.

Synthesis Procedure

The zeolite templates was impregnated with aqueous solution of sucrose containing sulfuric acid as described in a previous study⁶. 1 g of zeolite was added to a solution obtained by dissolving 1.25 g of sucrose and 0.14 g of H_2SO_4 in 5 g of H_2O . the mixture was dried at 100 °C, 6 hours and at 160°C additional 6 hours. After adding again sucrose and H_2SO_4 , the same procedure was repeated. The carbonization was carried out at different temperatures, 700, 800 and 900 °C. The zeolite-carbon composite material was then washed with concentrated HF for removing the silica template.

The replication of zeolite using phenol-formaldehyde resin was also studied. The zeolites were ion exchanged with excess 1M NH_4Cl for a total of 3 days. The zeolite samples dried under vacuum at 125°C for 5 hours. Solid phenol was added to the flask and incubated with the zeolite at 65 °C under reduced pressure overnight. Excess formaldehyde was heated to 120 °C to liberate its monomer to produce zeolite-phenol-formaldehyde-resin composite. The samples were heated to 125 °C at 1 °C/min for 5 hours and carbonized at 700,

800 and 900°C for 14 hours in inert atmosphere². Figure 1 illustrates the polymerization of phenol-formaldehyde resin.

Table 1. BET surface area, pore volume and pore diameter of zeolites templates.

Zeolite Type	BET surface area, m^2/g	BJH method cumulative desorption pore volume, cc/g	BJH method desorption pore diameter, Å
- 30 μm	59.44	0.1323	39.39
-0.1 mm	50.18	0.1126	39.37
-0.5 mm	51.20	0.1125	39.33
-1.0 mm	47.15	0.1027	39.24

FTIR Analysis

FT-IR spectra of carbonized and activated samples were measured with a Bruker EQUINOX 55 FT-IR spectrometer. Coal samples were dried under a nitrogen atmosphere at 110°C for 24 hours. KBr pellets were prepared by grinding 2.5 mg of dry coal sample with 200 mg of dried KBr. Spectra were obtained with 200 scans at a resolution 2 cm^{-1} .

Surface Analysis

Surface areas of activated carbons were determined by a Quantachrome NOVA 2200 Series volumetric gas adsorption instrument. Surface area of the samples were determined by using BET equation in the relative pressure range of 0.05 to 0.30, over five adsorption points.

X-Ray Diffraction Measurements

X-ray diffractograms of the samples of carbonized and activated products were measured with a Bruker axs advance powder diffractometer fitted with a Siemens X-ray gun and equipped with Bruker axs Diffrac PLUS software. The sample was rotated (15 rpm) and swept from $2\theta = 10^\circ$ through to 90° using default parameters of the program. The X-ray generator was set to 40kV at 40 mA.

Furthermore, after carbonization of the samples 57% weight loss was also examined via thermogravimetric analysis (TGA). TGA using a Netzsch STA 449C instrument were undertaken upon both the zeolite-carbon complexes and carbon, which was obtained after treatment with HF.

NMR Measurements

Samples were probed further by ^{13}C CPMAS, ^{29}Si CPMAS and ^{27}Al MAS NMR using an Inova 500MHz Varian system. ^{13}C CPMAS, ^{29}Si CPMAS and ^{27}Al MAS NMR spectra were acquired at 125 MHz, 100 MHz and 130 MHz fields respectively, using Si_3N_4 rotors set to 6 Hz. Pulses were separated by a 1s delay in the case of carbon, 2s delay in the case of silicon and 0.25s delay in the case of aluminum.

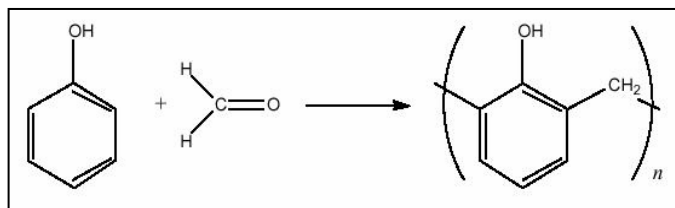


Figure1. Schematic representation of the phenol-formaldehyde resin.

Results and Discussion

BET surface area and adsorption-desorption analysis of zeolite templates were performed and represented in Figure 2 and 3. As expected with increasing particle diameter, surface area was decreased.

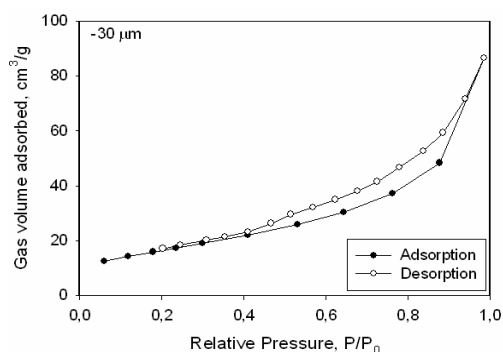


Figure 2. Gas adsorption/desorption isotherms of N₂ at 77K for the zeolite template of the -30 μm size fraction

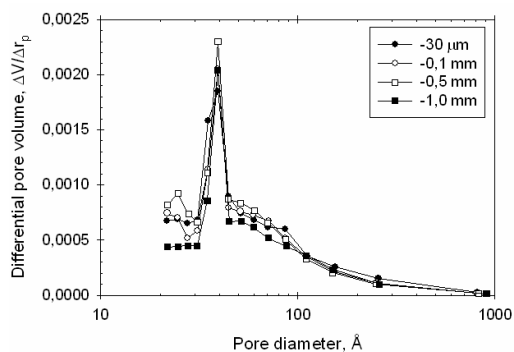


Figure 3. Pore size distributions for the samples (according to the BJH method⁸)

In the nitrogen adsorption there is initially uptake, followed by a rapid approach to equilibrium, and so the most reasonable explanation for this behavior is that there is significant adsorption capacity and very high diffusion resistance within the nanopores. The nanopore surface equilibrates rapidly in the first instances. This is followed by diffusion into the micropores. The adsorption isotherms of resultant carbon materials were also analysed. The surface areas and volumes of replicas produced by HF etching of zeolites were showed that almost all pores of the zeolite templates were filled with carbon material.

Nitrogen adsorption isotherms of the zeolite-carbon composites and carbon provide the confirmation that the resulted carbons were nanoporous. Because of the zeolite templates have nanoscale pore size, all zeolite-carbon samples showed low-pressure hysteresis. This suggest that the nanopores may have constrictions of the width comparable to the size of the nitrogen molecule. And also there is a possibility that not all the pores are in the exterior region⁷. In the adsorption isotherms of the zeolite-carbon composites, no steps were observed as in the previous studies⁷, which indicates that the almost all pores were deposited with carbon. BET areas of resulted carbons have large surface areas.

The percentage of carbon in the zeolite-carbon composites was estimated from the termogravimetric weight loss in air between 100

and 800 °C. Major weight loss was observed between 700 and 800 °C for both sucrose and resin case, indicating that carbon was burned in this range.

Zeolite-sucrose and zeolite-resin carbonized samples have distinct diffraction patterns consisting of narrow Bragg peaks. The zeolite-carbon composites have the almost the same XRD patterns with the zeolite template used for their preparations with lower intensities. After removing the silica template by washing with HF, carbon structure was examined in the XRD. Broad diffraction features were observed at 25 ° and 41° 2θ which was represented of (002) and (10) reflections of graphitized carbon, corresponding to the stacking of carbon sheets, that found in turbostratic structure of carbon. FTIR studies of synthesized carbons also showed that porous carbon material have characteristic bands near 3500 cm⁻¹, and 1450 cm⁻¹ are due to OH stretching and aromatic C-H absorption due to the aromatic structure of resultant carbon. Further evidence of the presence of the zeolite-polymer composite was obtained. by FTIR spectroscopy. Characteristic bands for poly (phenol-formaldehyde) resin at 3500 cm⁻¹ were assigned to OH stretching modes and several sharp bands at 1500 cm⁻¹ were attributed to C-O, C-C groups similar to those found for the bulk poly (phenolformaldehyde).

Further work is being carried out to give an explanation the mechanism of formation of carbon materials and affects of synthesis conditions to the resultant porous carbon properties.

References

1. Kyotani, T., Nagai, T., Inoue, S., Tmita, A., *Chem. Mater.*, **1997**, 9, 609-615.
2. Johnson, S.A., Brigham, E.S., Ollivier, P.J., Mallouk, T.E., *Chem. Mater.*, **1997**, 9, 2448-2458.
3. Sing, K.S.W., Everett, D.H., Haul, R.A.W., Moscou, L., Pierotti, R.A., Rouquerol, J., Siemieniewska, T., *Pure Appl. Chem.*, **1985**, 57, 603.
4. Enzel, P., Bein, T., *Chem Mater.*, **1992**, 4, 819.
5. Jun, S., Joo, S.H., Ryoo, R., Kruk, M., Jaroniec, M., Liu Z., Ohsuna, T., Terasaki, O., *J. Am. Chem. Soc.*, **2000**, 122, 10712-10713.
6. Ryoo, R., Joo, S.H., Jun, S., *J. Phys. Chem. B.*, **1999**, 103, 37, 7743-7746.
7. Kruk, M., Jaroniec, M., Ryoo, R., Joo, S.H., *J. Phys. Chem. B.*, **2000**, 104, 7960-7968.
8. BJH* method : Barrett, E.P., Joyner, L.G., Halenda, P.H., **1951**, *Journal of American Chemical Society*, 73, 373-380.

HRTEM, Synchrotron, and Simulation Techniques Applied to Activity and Selectivity Correlation in Hydrodesulfurization Catalysts

Russell R. Chianelli¹, Gilles Berhault², Miguel José Yácaman³, Apurva Mehta⁴, Sergio Fuentes⁵, Gabriel Alonso⁶, and Myriam De la Rosa¹.

- (1) Materials Research and Technology Institute, University of Texas at El Paso, Burges Hall Room 321, El Paso, TX 79968-0685,
- (2) LACCO-CNRS, Poitiers, France.
- (3) Chemical Engineering, University of Texas at Austin,
- (4) Stanford Synchrotron Radiation Laboratory, Menlo Park, California.
- (5) Centro de Ciencias de la Material Condensada, Enseñada, Mexico.
- (6) CIMAV, Chihuahua, Chihuahua, Mexico.

Introduction

Faced with heavier crudes and increasingly strict regulations regarding sulfur content of fuels, better HDS, HDN and HDM catalysts are sought requiring a deeper understanding of the structure and function of transition metal sulfide based catalysts. Basic functions that describe catalyst activity such as the role of promoters (Co, Ni) and the role of carbon are becoming better understood¹. However, the disordered state of the catalytically stable active phases has hindered complete understanding and “idealized catalysts” that yield specific information do not exist under reactor conditions. In this report small angle scattering (SAXS), wide-angle scattering (WAXS), high resolution transmission electron microscopy (HRTEM) and simulation techniques using CERIOUS² software (ACCELRYN Corp.) are applied to commercial alumina supported and unsupported CoMo catalysts stabilized in real feeds. Through application of these multiple techniques new information regarding structure/function relations in these catalysts are reported.

Background

The first report of the periodic effect in catalysis by TMS (transition metal sulfides) emphasized the importance of determining the “stable catalytic state”². The SCS (stable catalytic state) is the solid-state phase that is stable in the catalytic environment. For example the SCS for Mo under standard HDS (hydrodesulfurization) conditions is MoS₂ and for Ru is RuS₂. Much of the literature that purports to describe the fundamental origin of catalytic effects ignores the importance of the SCS and report results on catalyst precursors that change under catalytic conditions.

The Role of Carbon

Further work after the original paper describing the SCS discusses periodic relations between the SCS and their ability to catalyze the HDS and other reactions. However, these papers only describe the relation between the bulk crystalline SCS and their catalytic properties. Recent results indicate that the surfaces of the SCS contain carbon directly bonded to the catalytic metals³. Thus, the TMS catalysts are properly described as sulfide supported transition metal carbides (SSTMC). Therefore, the complete SCS for Mo is MoS_{2-x}C_x and for Ru is RuS_{2-x}C_x. A similar situation exists for Mo and W catalysts that are promoted with Co or Ni. A description of

TMS catalysts that fails to take into account the important role of carbon in stabilized HDS catalyst cannot give an accurate description of the fundamental origin of catalytic properties in these catalysts. It is also true that promotion must be described as a symmetrical synergism rather than promotion of one phase by another in order to understand the true nature of the effect; for example promotion of Mo by Co and symmetrically promotion of Co by Mo⁴.

Although the role of carbon in TMS catalytic materials has been largely ignored due to the difficulty in characterizing carbon on stabilized catalysts, refinery operators have for many years recognized the existence of “hard carbon” (carbide carbon) and “soft carbon” (coke) in hydrotreating catalysts. In this paper the importance of carbon in understanding the fundamental origins of catalytic behavior in TMS is discussed. Recent evidence for the TMS to form stable carbide surface phases is shown in figure 1. Figure 1 shows the carbon edge Auger electron yield for a tested HDS MoS₂ catalyst compared with Mo₂C. Since the Auger electrons only come from very close to the surface it is concluded that both surfaces are identical and that the Mo in both cases is bound to carbon.

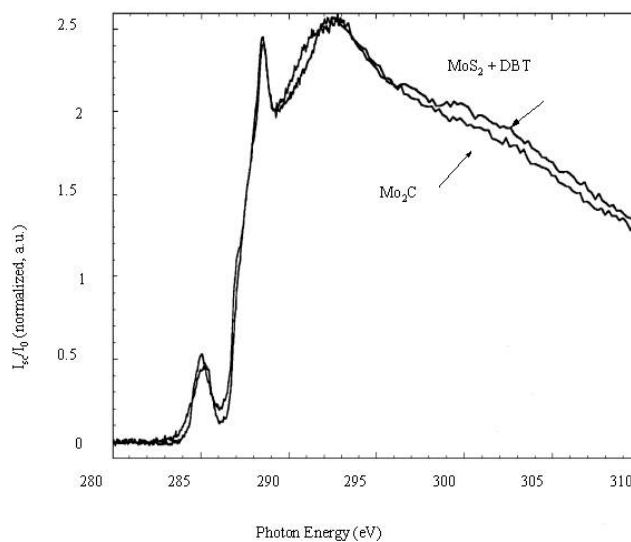


Figure 1: Auger Spectra of Carbon on Catalysts

These studies refer to catalysts that have been pretreated and then exposed to the catalytic feed. These catalysts become the sulfide supported carbides (SCS) described above. However, carbon can be incorporated into the catalyst before pretreatment and this leads to highly active catalysts with unusual pore distributions⁵. For example some catalysts with surface areas greater than 250 m²/gm had most of the surface area in the 40 - 45Å region. We have termed these catalysts “amorphous zeolitic sulfides” because pore distributions can be very narrow around 4nm. They also have an unusual “sponge-like” appearance as shown in Figure 2. This may lead to a fractal description of these catalysts in the future. Associated with these properties are unusual selectivity properties.

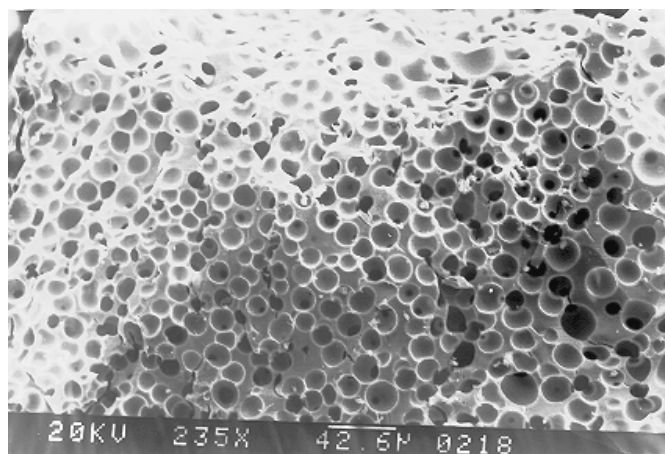


Figure 2: SEM of Amorphous Zeolitic MoS₂ Catalyst

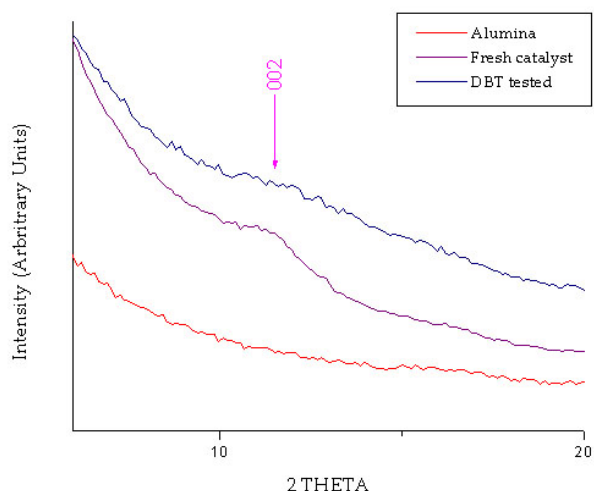


Figure 3: Low angle scattering region for supported catalysts.

Supported Commercial Catalysts:

The fundamental advances described above have been made on unsupported pure catalytic phase such as MoS₂ and promoted MoS₂. Although unsupported catalysts are finding new commercial application because of their high volumetric activity, working commercial catalysts are still predominately alumina supported of the type Co(Ni)MoAl₂O₃. Although catalytic functions measured on unsupported catalysts generally extrapolate to supported catalysts, direct structural information has been hard to obtain due to the disordered state of the active phases.

In the later part of this report SAXS, WAXS, HRTEM and simulation techniques using CERIUSt² software are applied to commercial alumina supported CoMo catalysts that have been tested on real feeds and to non-commercial alumina and silica supported CoMo catalysts. By combining this data with HRTEM and simulation data the following conclusions are reported:

- Scattering from the active phases is easily obtained by subtraction of the alumina support.
- Analysis of the active phase scattering indicates that the catalyst consists of mainly single layers of MoS₂ in contrast to HRTEM studies that “see” only stacked layers (See figure 3).
- Catalysts that have been run for long periods of time under high-pressure conditions tend to “destack”.

In addition scattering results from catalyst run for extended periods in high pressure real feed reactors showed the presence of three phases: MoS_{2-x}C_x, Co₉S₈ and Co metal. This result is surprising in view of the accepted theories of Co promotion and underlines the necessity of determining the SCS for operating catalysts as a basis for understanding activity and selectivity correlations.

References

- ¹ Chianelli, R.R., Daage, M., and Ledoux, M. J., “Fundamental Studies of Transition Metal Sulfide Catalytic Materials”, *Advances in Catalysis*, **1994**, 40, 177.
- ² T. A. Pecoraro and R. R. Chianelli, “Hydrodesulfurization Catalysis by Transition Metals”, *J. Catal.* **1981**, 67(2), 430.
- ³ Gilles Berhault, Apurva Mehta, Alexandru Pavel, Jianzhong Yang, Luis Rendon, Miguel Jose Yacaman, Leonel Cota Araiza, Alberto Moller, and Russell R. Chianelli, “The Role of Structural Carbon in Transition Metal sulfide Hydrotreating Catalysts” *J. Catalysis*, **2001**, 198, 9.
- ⁴ Gilles Berhault, Leonel Cota Araiza, Alberto Duarte Moller, Apurva Mehta, Russell R. Chianelli, “Modifications of Unpromoted and Cobalt-promoted MoS₂ during thermal treatment by Dimethylsulfide”, *Catalysis Letters*, **2002**, 78, 81.
- ⁵ Characterization and HDS Activity of Mesoporous MoS₂ Catalysts Prepared by in situ Activation of Tetraalkylammonium Thiomolybdates. G. Alonso, G. Berhault, A. Aguilar, V. Collins, C. Ornelas, S. Fuentes and R. R. Chianelli. *Journal of Catalysis* **2002**, 208, 359.

POSSIBLE WAYS TO ACHIEVE DEEP HDS OF LIGHT CYCLE OIL

Ki-Hyouk Choi, Yozo Korai, Isao Mochida

Institute of Material Chemistry and Engineering, Kyushu University
Kasuga-Koen, Kasuga, Fukuoka 816-8580 JAPAN

INTRODUCTION

It has been known that light cycle oil(LCO) from fluid catalytic cracker(FCC) is hard to be desulfurized due to its much higher aromatic content than straight run gas oil. Aromatic species in LCO inhibit HDS by occupying the active site for hydrogenation with their higher adsorption energy than sulfur species. Removal of aromatic species prior to HDS by hydrogenation looks not practical because of high hydrogen consumption and presence of strong inhibitor, sulfur and nitrogen species. Furthermore, hydrogenation of aromatic species prefer the low reaction temperature due to equilibrium limitation, meaning the low reaction rate.

We presented already the effect of aromatic and nitrogen contents on the HDS of LCO to indicate that the aromatic inhibition is more distinct in HDS of refractory sulfur species, such as 4,6-DMDBT and such inhibition can not be avoided by using very acidic catalyst which contains zeolite and higher reaction temperature(360 °C)[1].

In the present study, we examined possible ways to achieve deep desulfurization of LCO, such as

- splitting of LCO and desulfurization of each fractions.
- lowering the cut point of LCO below boiling point of 4,6-DMDBT
- blending the low boiling point LCO into LGO

As indicated in the previous presentation, 4,6-DMDBT and other di- and tri-alky DBT suffer strong inhibition by aromatic species. Hence, LCO containing the least amount of 4,6-DMDBT and other alky DBT having higher BP than 4,6-DMDBT is anticipated to achieve deep desulfurization even with abundant aromatic species in itself. LGO can be postulated to dilute LCO to reduce the inhibition by aromatic species. But the beneficial effect may depend on the characteristics of LCO and its blending ratio. Such points are studied by using conventional catalysts and reaction conditions.

EXPERIMENTS

LCO, HCO, fractionated LCO were used as feed oil. As-distilled straight run gas oil, LGO was also used. The basic properties of feed oils are listed in **Table 1**. Cut point of the fractionated LCO was not clear as shown in carbon and sulfur chromatograms in **Fig. 1**.

Commercially available CoMo/alumina and NiMo/alumina were used after grinding and sieving with 380 mesh nylon sieve. NiMo catalyst was characterized to have higher acidity than CoMo catalyst by NH₃ TPD. Hydrodesulfurization experiments were conducted by using autoclave-type reactor(100 ml internal volume) at 340 or 360 °C. Initial hydrogen pressure was adjusted to 50 kg/cm². 10 g of feed oil and 1 g of pre-sulfided catalyst at 360 °C for 2 hours under 5% H₂S/H₂ stream, were charged into the reactor. Reaction time was 2 hour. Feed and products were analyzed by GC-AED(HP5890Plus and G2350A).

RESULTS AND DISCUSSION

LCO 300- didn't contain 4-MDBT, 4,6-DMDBT and other alkylated DBTs. In contrast, LCO 340- contains small amount of those species as shown in Fig. 1. After 2 hour reaction at 360 °C over NiMo catalyst, HDS of LCO 300- was nearly completed to give less

than 5 ppmS. LCO 340- gave also the very low level of sulfur, less than 5 ppmS. However, LCO 300+ and LCO 340+, which contained larger amount of 4-MDBT, 4,6-DMDBT and other alkylated DBTs, provided 109 and 278 ppmS in HDS product, which were 4.1 and 17.4 % of total sulfur content of feed oils, respectively. Reaction temperature was higher(360 °C) than conventional HDS condition(340 °C). These observations indicated the possible way to achieve deep desulfurization of LCO feed by fractionation followed by conventional HDS of low boiling point fraction.

LGO blended with small amount of LCO(1 wt% and 10 wt%) was examined at 340 °C for 2 hour reaction as shown in **Table 2** in order to examine the possibility of diluting LCO with LGO for improvement of HDS reactivity of LCO. Inhibition of aromatic compounds on HDS was anticipated to be alleviated by diluting it in LGO, which had less amount of aromatic compounds.

However, blended LGOs showed higher remaining total sulfur contents than both of LCO and LGO over both of CoMo and NiMo catalysts. Remaining content of 4-MDBT and 4,6-DMDBT were also slightly higher than those of LCO and LGO. Over CoMo catalyst, LGO containing 10% LCO was less active than that containing 1% LCO. In contrast, NiMo showed reverse reactivity order, LGO-1%LCO was less active than LGO-10%LCO over NiMo catalyst. NiMo catalyst was suggested to have higher activity in HDS of LGO in the presence of LCO due to its higher hydrogenation activity and acidity than CoMo catalyst. Remaining content of 4-MDBT and 4,6-DMDBT followed the same trends with those of remaining total sulfur contents. The above observation means that HDS of LGO was strongly inhibited by adding small amount of LCO, even 1%, while LCO could be much more easily desulfurized than LGO. LCO can be noted by its higher aromatic content than LGO. Hence, small amount of aromatic compounds could strongly inhibit HDS of LGO.

LCO and HCO, which had different FBP, 322 and 463 °C, respectively, were compared by hydrotreating at 340 °C over CoMo and NiMo catalysts. Carbon and sulfur chromatograms are plotted in **Fig. 2**. Feed LCO contained 41 ppmS 4,6-DMDBT, which was 0.84% of total sulfur species in LCO. In contrast, Feed HCO contained 162 ppmS 4,6-DMDBT, 1.26% of total sulfur species in HCO. HDS results on those feed oils were listed in **Table. 2**. LCO leaved only 1.5 - 1.8% of total sulfur content after HDS, while HDS product of HCO contained 21.5 - 27.5 % of original sulfur content. Such difference between LCO and HCO was more distinct in remaining content of 4,6-DMDBT. 12.8 - 21.3% and 79.0 - 81.3% of 4,6-DMDBT contained in feed oil were remained after HDS of LCO and HCO, respectively. These findings indicated again the importance of cutting point of LCO to attain deep desulfurization.

NiMo catalyst was more active than CoMo one in HDS of LCO. 4,6-DMDBT in LCO was also more removed over NiMo catalyst than CoMo catalyst. In contrast CoMo catalyst showed better activity in HDS of HCO than NiMo catalyst, while the latter catalyst provided slightly lower content of 4,6-DMDBT in HDS product than the former catalyst. Superiority of NiMo catalyst in HDS of LCO is believed to be from its higher hydrogenation activity and acidity, which is effective to remove the strongly adsorbed aromatic species and refractory sulfur species. However, such activity was disappeared in HDS of HCO, suggested to be due to inhibition of high boiling point aromatics compounds and more refractory sulfur species. The extent of desulfurization was limited by such inhibitors and, hence remaining sulfur content was decided by the content of reactive sulfur species, resulting higher activity over CoMo catalyst, which has been believed to be more active in HDS of reactive sulfur species than NiMo catalyst, although CoMo catalyst also suffered inhibition by aromatic and refractory sulfur species.

CONCLUSIONS

First of all, deep desulfurization of LCO could be achieved by splitting LCO and followed HDS of lower boiling point fraction over conventional catalyst. LCOs fractionated under 300 °C and 340 °C were successfully desulfurized to less than 5 ppmS. However, high boiling point fraction(300 °C+ and 340 °C+) showed very limited HDS reactivity.

Blending of LCO into LGO retarded HDS even with small amount, in particular over CoMo catalyst. NiMo catalyst showed better activity in HDS of LGO, LCO and blended LGO than CoMo catalyst. HDS of HCO was much difficult compared with LGO and LCO. CoMo provided higher sulfur removal than NiMo catalyst in HDS of HCO.

Acknowledgement. This work was supported by the New Energy and Industrial Technology Development Organization (NEDO) through Petroleum Energy Center(PEC) under a subsidy from the Ministry of Economy, Trade and Industry.

REFERENCES

- (1) Choi, K.-H.; Korai Y.; Mochida, I. *Prepr. Am. Chem. Soc., Div. Fuel Chem.*, 2003, 48(1), 101.

Table 1. Basic Properties of LCOs

Name	IBP(°C)	FBP(°C)	Sulfur Content(ppm)
LGO	-	-	13800
HCO	134	463	12900
LCO	168.5	322.0	4800
LCO 300+	LCO Cut fraction over 300 °C		2640
LCO 300-	LCO Cut fraction under 300 °C		450
LCO 340+	LCO Cut fraction over 340 °C		1596
LCO 340-	LCO Cut fraction under 340 °C		301

Table 2. Remaining content(ppmS) of sulfur species in HDS products.

Over CoMo Catalyst				
	Total Sulfur	DBT	4-MDBT	4,6-DMDBT
LGO	523(3.8%)	0(0.0%)	11(10.2%)	19(51.3%)
LCO-1 ^{*1}	688(5.0%)	1(0.5%)	14(12.9%)	20(51.5%)
LCO-10 ^{*2}	669(5.2%)	1(0.4%)	13(12.2%)	20(52.6%)
LCO	86(1.8%)	0(0.0%)	4(4.0%)	9(23.1%)
HCO	2776(21.5%)	2(0.8%)	143(35.8%)	132(81.3%)

Over NiMo Catalyst				
	Total Sulfur	DBT	4-MDBT	4,6-DMDBT
LGO	444(3.2%)	1(1.0%)	14(12.5%)	11(29.7%)
LCO-1 ^{*1}	462(3.4%)	1(1.0%)	14(12.5%)	13(33.4%)
LCO-10 ^{*2}	367(2.8%)	1(0.7%)	12(10.9%)	11(28.9%)
LCO	72(1.5%)	0(0.0%)	4(4.1%)	5(12.8%)
HCO	3551(27.5%)	21(7.6%)	21(52.7%)	128(79.0%)

*1 : 1 wt% LCO blended LGO, *2 : 10 wt% LCO blended LGO

* Values in parenthesis are ratio of remaining content and original content.

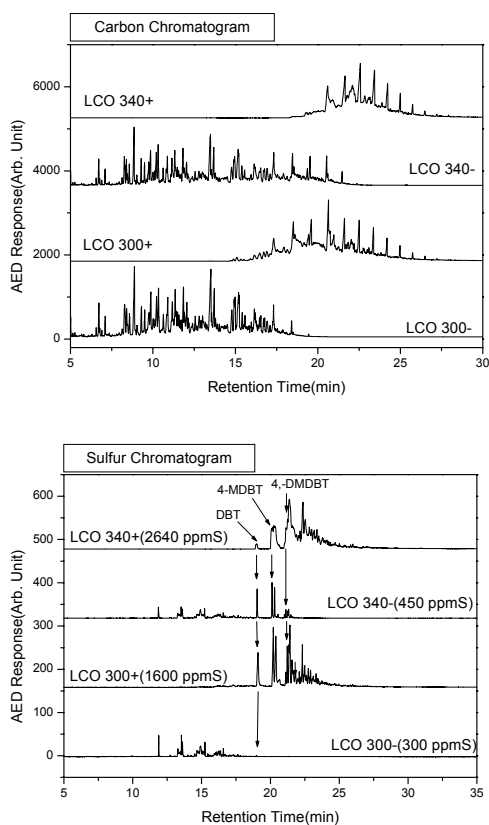


Fig. 1. Carbon and sulfur-specific chromatograms of fractionated LCOs.

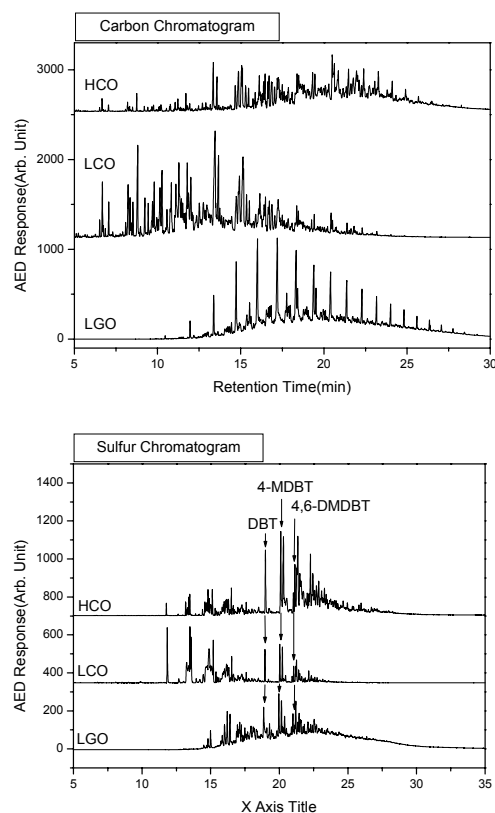


Fig. 2. Carbon and sulfur-specific chromatograms of LGO, LCO, HCO.

Effect of Feed Quality on Deep Desulfurization of Diesel

A. Stanislaus, A. Al-Barood and H. Qabazard

Petroleum Refining Department,
Petroleum Research and Studies Center,
Kuwait Institute for Scientific Research,
P. O. Box 24885, Safat, Kuwait.

INTRODUCTION

The specifications and demand of petroleum based fuels have been changing continuously in the international fuels market. During the 1990s a series of regulations on the specifications of gasoline and diesel were introduced in many countries to reduce harmful emissions from transportation vehicles. For example, in the USA and Europe sulfur content of diesel was first reduced from 2000 ppm to 500 ppm and it is currently set at 350 ppm. Further reductions in sulfur limits to 50 ppm have been proposed in Europe with tighter specifications on other properties such as density, poly aromatic hydrocarbons, cetane number, etc. Germany has introduced 10 ppm sulfur limit for diesel from January 1, 2003, and the U.S. will impose a 15 ppm sulfur cap in 2006. Similar low sulfur specifications are also targeted in many other countries, and most probably will be predominant worldwide during the next decade.

Although the new environmental regulations that limit the sulfur levels of diesel and other transportation fuels to very low levels are beneficial from environmental point of view, meeting the required stringent specifications represent a major operational and economic challenge for the petroleum refining industry. The tightening of sulfur specifications of diesel fuel to very low levels requires deep desulfurization of diesel feedstocks. The shift from normal to deep desulfurization is a very complicated technical problem. Many factors such as the catalysts, process parameters, and the nature of sulfur compounds present in the feed can have a significant influence on the degree of desulfurization of diesel feeds[1-3]. Among these, the feedstock quality plays an important role on deep desulfurization since the types of sulfur, nitrogen and aromatic compounds and their concentrations in different feedstocks are different. In the present work, a comparative study of the degree of desulfurization of two different feedstocks, namely coker gas oil (CGO) and straight run gas oil (SRGO) and their blends under different operating severities was made. The kinetics of desulfurization of both feeds under deep desulfurization conditions were also studied.

EXPERIMENTAL

Two feedstocks, namely, SRGO (density@15 °C, 0.846 g/ml; sulfur, 1.47 wt%; Nitrogen, 60 ppm; aromatics, 27 wt%; T_{95} = 368 °C) and CGO (density@15 °C, 0.876 g/ml; sulfur, 0.76 wt%; Nitrogen, 1020 ppm; aromatics, 46 wt%; T_{95} = 380 °C) were used in the present studies. Hydrotreating experiments were conducted in a fixed bed reactor unit using a commercial Co-Mo/Al₂O₃ catalyst (surface area = 200 m²/g; pore volume = 0.6ml/g). 75 ml of the catalyst diluted with an equal volume of carborundum was charged into the reactor in such a way that the catalyst section was in the middle section of the reactor. Coarse carborundum and inert alumina balls were loaded above and below the catalyst bed. After the catalyst was loaded, the reactor was placed in position inside a vertical electrically heated furnace. Five thermocouples into a thermowell at the center of the reactor tube were used to monitor the reactor temperature at various points. Before the introduction of the feed, the catalyst was presulfided with 3 wt% dimethyl disulfide in straight run

gas oil using a standard procedure [4]. When presulfiding was completed, the gas oil feed was introduced and the reactor temperature and other conditions were adjusted to the desired levels. During the run, the temperature was changed in the sequence 320 → 340 → 360 → 380 °C and back to 320 °C. After maintaining each temperature condition stabilized for 24 hours, three samples were collected at each temperature at 8 h intervals. The sulfur contents of the feed and hydrotreated products were determined using a Coulmax sulfur analyzer. Before sulfur analysis, the hydrotreated product was stripped with nitrogen gas in an ultrasonic water bath to remove the residual H₂S from the product oil. The individual sulfur compound distributions in the feed and product oils were determined with a high resolution gas chromatograph equipped with a 30m x 0.32mm x 0.4μ SPD-1 capillary column and a sulfur chemiluminescence detector (SCD).

RESULTS AND DISCUSSION

Fig. 1 shows the residual sulfur content in the hydrotreated products as function of the operating temperature for the SRGO feed at two different LHSV. It is seen that the total sulfur in the hydrotreated product steadily decreases with increasing reactor temperature. The LHSV also has a remarkable effect on the degree of desulfurization. The results indicate that the LHSV has to be reduced to 2 and the reactor temperature has to be increased to 365 °C to achieve the desired 350 ppm sulfur in the product oil. In the case of CGO feed, a higher temperature (377 °C) is required to reach the same sulfur target indicating that CGO is more resistant to desulfurization than SRGO (Fig. 2).

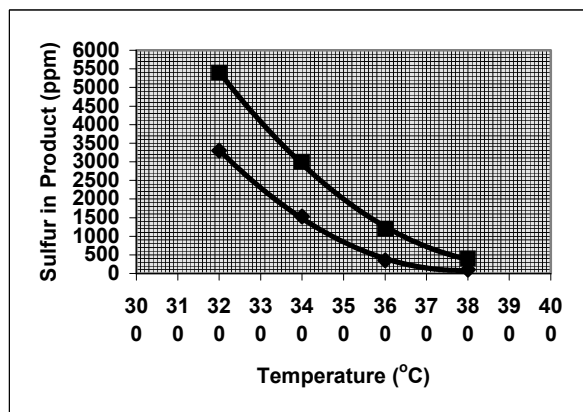


Fig 1. Sulfur in Product vs. Reactor Temperature for SRGO.

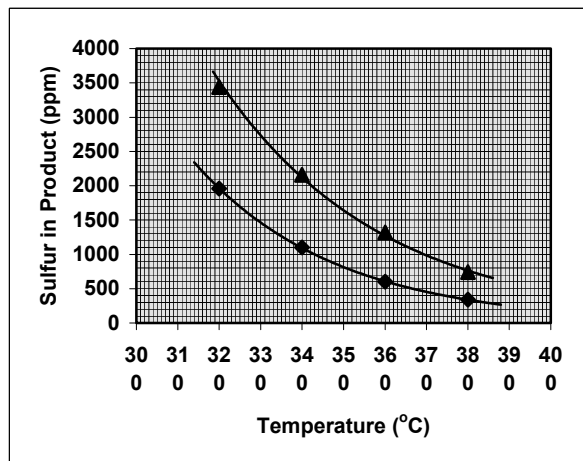


Fig 2. Sulfur in Product vs. Reactor Temperature for CGO.

Blends of SRGO and CGO were evaluated for deep HDS and the results showed that inclusion of CGO in the SRGO feedstock required higher severity operation to obtain the desired low sulfur level in the product (Fig. 3).

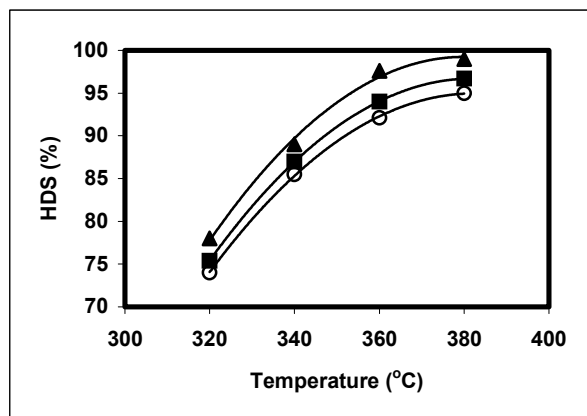


Fig 3. Effect of Blending CGO with SRGO on the degree of desulfurization.

With a view to understand the low reactivity of CGO compared with SRGO, the types of sulfur compounds and their distribution in both feeds were analyzed by a high resolution gas chromatograph equipped with a 30m x 0.32mm x 0.4 μ SPD-1 capillary column and a sulfur chemiluminescence detector. Fig. 4 shows the sulfur compounds distribution in CGO and SRGO

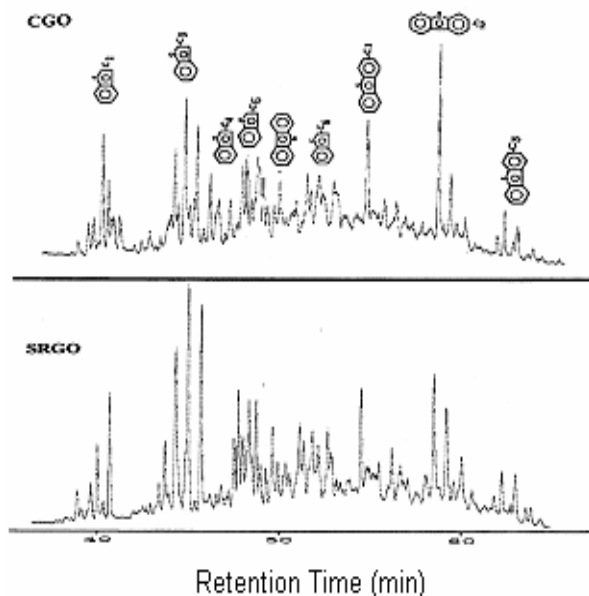


Fig 4. Sulfur Compounds distribution in CGO and SRGO

It is seen that both feeds contain a complex mixture of sulfur compounds that can be classified into two major groups: (i) alkyl benzothiophenes (BT); (ii) dibenzothiophene (DBT) and its alkyl DBTs. The HDS reactivities of these sulfur containing species are considerably different. Benzothiophene and its alkyl derivatives are more easily desulfurized than dibenzothiophene and its alkyl derivatives. Studies have shown that dibenzothiophene with alkyl substituents at 4 or 6 or 4 & 6 positions are more resistant to desulfurization under normal hydrotreating conditions [5-7]. Steric

hinderance by the alkyl groups restricts the access of the sulfur atom to the active sites of the catalyst.

The results presented in Fig. 4 show that the concentration of the refractory sulfur compounds are slightly higher in the CGO feed. The low reactivity of the sulfur compounds could be partly attributed to this. However, this may not be the only reason for the low reactivity of CGO. A closer examination of the composition of the two feedstocks shows that the nitrogen content of the CGO is 17 times higher than that of SRGO. The aromatic content of the CGO is also substantially larger than that of SRGO. Model compound studies conducted in this laboratories on the inhibiting effects of nitrogen and poly nuclear aromatic (PNA) compounds showed that nitrogen compounds are stronger inhibitors of HDS than the PNAs. In a recent study, Knudsen et al., [8] found that nitrogen containing molecules and in particular basic nitrogen compounds strongly inhibited the HDS reaction. The inhibition by nitrogen compounds could be a major cause for the lower HDS of CGO compared with SRGO.

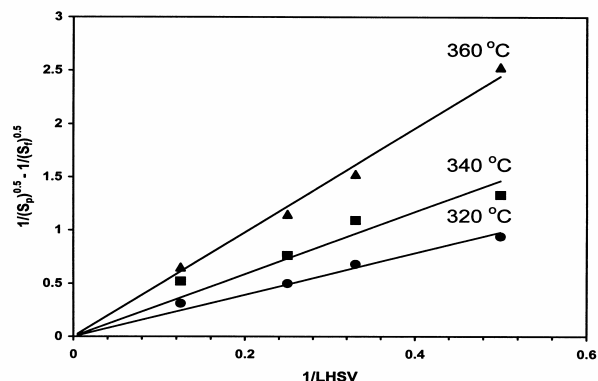


Fig 5. 1.5 order plot of kinetic data for HDS of CGO

Tests conducted at various LHSV were used to for kinetic data analysis and for determining the apparent order for deep HDS of both types of gas oils. The results presented in Fig. 5 clearly show that a reaction order of 1.5 fits the kinetic data even under deep desulfurization conditions. Reaction orders varying between 1.4 and 2 have been reported in the literature for gas oil desulfurization (9-11). The activation energies calculated from the Arrhenius plots (Fig. 6) were 24 kcal/mole and 30 kcal/mole for SRGO and CGO feeds, respectively.

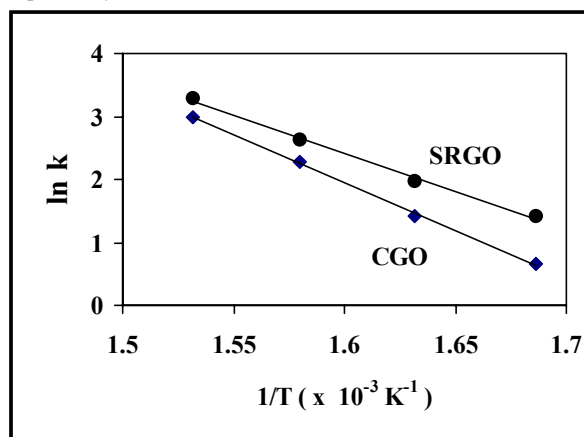


Fig. 6. Arrhenius plots for sulfur removal from straight run and coker gas oils

The higher activation energy observed for deep HDS of CGO is consistent with the key role played by the nitrogen species in inhibiting HDS reaction. The adsorption of nitrogen species on the active sites and their poisoning effect usually decreases with increasing temperature leading to a higher temperature sensitivity for HDS reaction and thereby resulting in higher activation energy for the nitrogen-rich CGO feed.

REFERENCES

1. Song, C., and Ma, X., Applied Catalysis B: Environmental, 41, 207 (2003).
2. Whitehurst, D. D., Isoda, T., and Mochida, T., Advances in Catalysis, 42, 345 (1998).
3. Landau, M. V., Catalysis Today, 36, 393 (1996).
4. Qabazard, H., Abu-Seedo, F., Stanislaus, A., Andari, M., Absi-Halabi, M., Fuel Science and Technology International, 13, 1135 (1995).
5. Knudsen, K.G., Cooper, B. H., and Topsoe, H., Applied Catalysis A:General, 189, 205 (1999).
6. Houalla, M., Broderik, D. H., Spare, A. V., Nag, N.K., De Beer, V. H. J., Gates, B. C., and Kwart, H., Journal of Catalysis, 61, 523 (1980).
7. Machaud, P., Lambertson, J. L., Perot, G., Applied catalysis A:General, 169, 343 (1998).
8. Knudsen, K.G., Whitehurst, D.D., and Zeuthen, P., A detailed understanding of the inhibition effect of organic nitrogen compounds for ultra deep HDS and the consequences for choice of catalyst., Presented at the 3rd International Conference on Refinery Processing., AIChE Spring National Meeting, Atlanta GA, March 5-9 (2000).
9. Sie, S.T., Fuel Processing Technology, 61, 273(1999).
10. Bej, S.K., Dalai, A.K., and Adjaye, J., Petroleum Science and Technology, 20, 887 (2002).
11. Shiflett, W.K., A Users Guide to the Chemistry, Kinetics and Basic Reactor Engineering of Hydro Processing, Presented at the 5th International Conference on Refinery Processing., AIChE Spring National Meeting, New Orleans, March 11-14 (2002).

Selection and Further Activation of Activated Carbons for Removal of Nitrogen Species in Gas Oil as a Pre-Treatment for Deep Desulfurization

YOSUKE SANO, KI-HYOUK CHOI,
YOZO KORAI and ISAO MOCHIDA

Institute of Material Chemistry and Engineering,
Kyushu University, Kasuga, Fukuoka 816-8580, Japan

INTRODUCTION

World refining industry is facing new and stricter challenges on the heteroatom content in their major products, such as diesel fuel and gasoline. The sulfur content of diesel fuel must be lowered to 15 ppmS from current 500 ppmS and even further regulations may be implemented with accelerated concerns on the atmospheric pollution[1]. Several kinds of new ideas have been proposed and some of them were practically examined to achieve the ultra deep desulfurization. However, more efficient and economic process is still required in spite of various efforts. Critical barriers in obtaining ultra deep desulfurization are refractory sulfur species, which have very low reactivity under conventional hydrotreating conditions, and are strongly inhibited by H₂S, NH₃ and nitrogen species. The inhibitors retard the desulfurization reaction, very markedly in ultra deep region [2, 3]. In our previous study, we intended to improve the HDS-reactivity by reducing the nitrogen and sulfur species in the feed oil. Sulfur and nitrogen species were adsorptively removed by activated carbon. Activated carbon and activated carbon fiber have been recognized to be versatile absorbents of gaseous and liquid molecules. Its surface and properties can be easily controlled.

In spite of various advantages in such technology, material cost may limit its practical application. Hence, more adsorption capacity and low cost are still wanted with activated carbon.

In the previous study, we examined a number of adsorbents to find the best one and their reasons.

We attempted to improve the performance of activated carbon and carbon fiber by modifying its surface property and discovered the functional groups that are effective for the adsorption.

EXPERIMENTAL

I Activated carbon materials

The activated carbon was treated by HNO₃, H₂SO₄ and H₂O₂ and dried at respective appropriate temperature. The activated carbon was analyzed by TPD to measure its functional groups

II. Adsorption

Straight run gas oil (11,780 ppmS and 260 ppmN) used in this study was provided by a Japanese commercial refinery. Carbon materials (activated carbons and activated carbon fibers), which were dried at 110 °C under vacuum oven prior to adsorption experiment, were packed into the stainless steel tube of 50mm length and 6 mm diameter. Key properties of carbon materials were listed in Table 1. SRGO was fed into the tube by a HPLC pump at the rate of 0.1 ml/min and at the pressure of 20psi. The temperature of the adsorption reactor was maintained at 10~40°C by water bath. The eluted oil was sampled at every 60min for 30 sec and analyzed by GC-AED (Atomic Emission Detector, HP5890P, and G2350A).

Results and Discussion

Fig.1 showed the breakthrough profiles of nitrogen species over various adsorbents. The activated carbons had larger adsorption capacity than silica gel which practically treated in the refinery. In this figure, MAXSORB-II of largest surface area and highest oxygen

content showed the best adsorption capacity. And, MAXSORB-III showed much lower adsorption capacity than that of MAXSORB-II. However, heating at 600°C under H₂ atmosphere reduced adsorption capacity of nitrogen species of MAXSORB-II.

Fig.2 compared the TPD profiles of MAXSORB-II and MAXSORB-III. The activated carbon produced CO₂ at 200-400°C and CO at 600-800°C. MAXSORB-II showed a particular large CO desorption while another did smaller desorption.

Fig.3 and Fig.4 showed the nitrogen breakthrough profiles by treated MGC-B and OG-20A series. H₂O₂-, H₂SO₄, HNO₃-treated activated carbons, which dried at 180°C, 400°C and 600°C respectively, showed better adsorption than those of as received ones. However, HNO₃-treated, which dried at 350°C, showed worse adsorption than those of as received.

Fig.5 and Fig.6 showed the TPD spectrums of these activated carbons. As you can see, activated carbon of larger adsorption capacity for nitrogen species has distinct CO peak at 600-800°C. MGC-HNO₃, of low adsorption capacity for nitrogen species showed CO₂-peak at 200-400°C. After heated at 600°C and these functional group was removed, the breakthrough profile showed better one.

These findings indicated that surface species responsible for CO evolution during TPD is more effective than those for CO₂. The latter groups may inhibit for the Nitrogen adsorption.

The present study clarified that CO producing functional groups are responsible for adsorptive removal of nitrogen species. Hence introduction of such group through the surface oxidation appeared to be very effective to enlarge the adsorption. Basic nature of C=O may be responsible to adsorb the acidic and neutral -NH- groups. Carboxyl group on the surface of activated carbon appeared to reduce the adsorption of nitrogen species, probably through with COO groups.

Conclusion

Adsorption capacity of carbon materials depended on the textural and surface properties of them.

The most important functional group of activated carbon is C=O group and carbonyl group maybe inhibit the Nitrogen species adsorption.

References

1. T. R. Halbert, G. B. Brignac, R. A. Demmin, and E. M. Roundtree, *Hydrocarbon Engineering*, June, (2000)2.
2. D. D. Whitehurst, T. Isoda, and I. Mochida, *Adv. Catal.*, **42**(1998)345.
3. D. D. Whitehurst, H. Farag, T. Nagamatsu, K. Sakanishi, and I. Mochida, *Catal. Today*, **45** (1998)299.

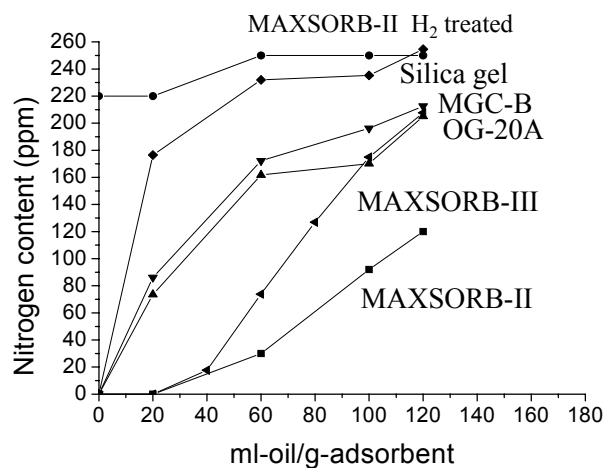


Figure 1. Breakthrough profiles of various materials

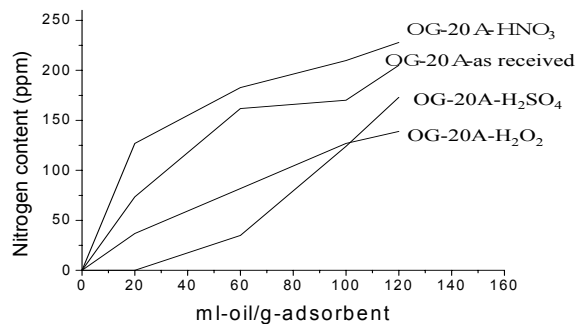


Figure 4 Breakthrough profiles of OG-20A series

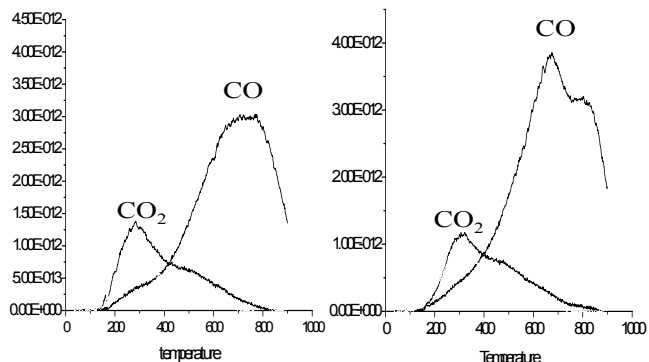


Figure.2 TPD results of MAXSORB-II and MASORB-III

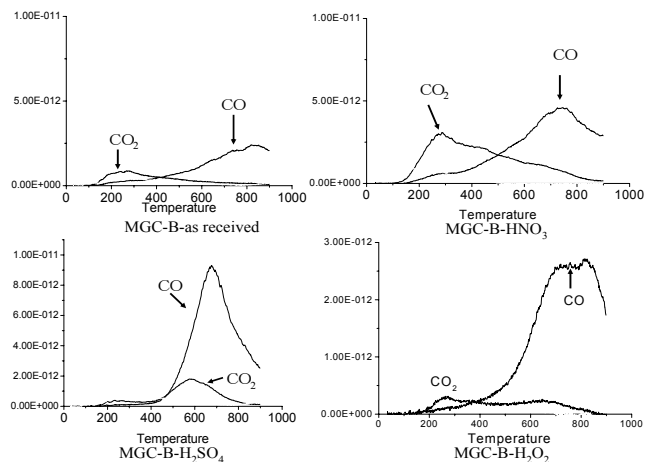


Figure.5 TPD results of MGC-B series

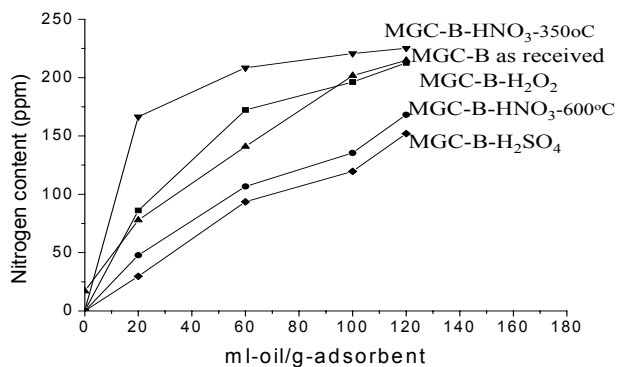


Figure.3 Breakthrough profiles of MGC-B series

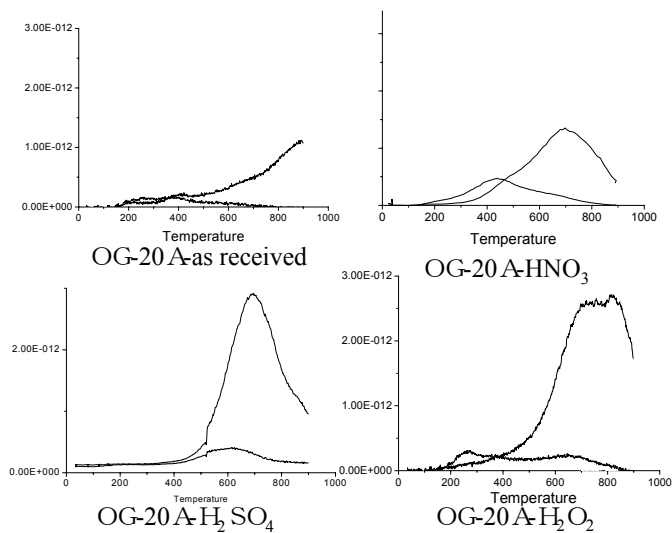


Figure.6 TPD results of OG-20A series

STATISTICAL MODEL FOR BENZENE PREDICTION IN CATALYTIC REFORMING

Qamar Zafar, Börje Gevert*² and Margareta von Sivers*¹

Materials and Surface Chemistry, Chalmers University of Technology, Göteborg, S-412 96, Sweden *¹Scanraff, s-453 81 Lysekil. *²Corresponding and presenting author gevert@surfchem.chalmers.se

Introduction

The maximum limit of benzene content in gasoline is set or will be 1 % in many areas. Scanraff is producing gasoline with 1 % benzene content according to the specifications. Major contributor to the gasoline pool is reformat (more than 80 %). So benzene reduction in the reformat has a major effect in meeting the specification imposed. Due to this reason Scanraff interested in a model, which can predict and control benzene in the reformat. There has been some interest in predicting benzene production in catalytic reforming in the recent years (1-3). The reactions can be studied with kinetic modeling when the content of different molecule types are known in the feed. The objective of this paper is to present a statistical model which will be able to predict benzene in the reformat. Multivariate data analysis (MVDA) was used to develop this prediction model (4). The study was done as a Master of Science thesis between Chalmers and Scanraff (5)

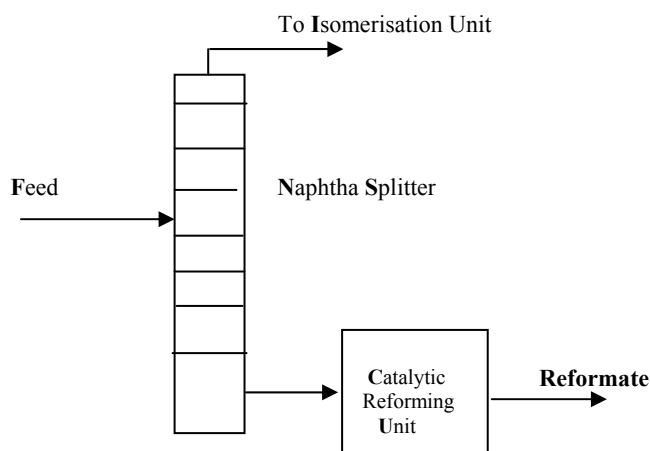


Figure 1. Blockdiagram of the reformer

Straight run naphtha is mixed with naphtha from conversion processes and the mixture is hydrodesulfurised (Figure 1). After this the naphtha is split into two streams, the light part to the isomerisation plant and the heavier part to the Platformer. The feed to the Platformer is preheated before it enters the first fired heater followed by the first reactor. The volume in the first reactor is 20 % of the total reactor volume, the volume in the second reactor is 30 % and the volume in the last reactor is 50 %. Since the reactions are endothermic, the stream leaving the first reactor has to be heated up before it enters the second reactor, and so on. The aim of the Platformer is to produce aromatic hydrocarbons from the naphtha by catalytic reforming. The naphthenes are easily converted to aromatics but the paraffins are more difficult to convert. There is a need for hydrogen for the reactions, which is added before the first reactor. Hydrogen is produced in the reactions and a compressor circulates the hydrogen. A low level of hydrogen increases the formation of coke. The catalyst in the reactors is circulated continuously through

the CCR (Continuous Catalyst Regeneration) where the coke on the catalyst is combusted at low oxygen level. By this procedure, the catalyst activity and thereby the yield is kept constant in the reactor. The reformat is pumped to a stabilizer column where the LPG is stripped. The product quality of the reformat varies depending on which gasoline blend Scanraff wishes to sell at the moment. The normal parameters (that the operators are able to control) are:

MON	90-91	(controlled by the feed rate and the temperature in the Platformer)
Benzene	1.4-1.5% by volume	(controlled by the separation in the naphtha splitter)
Vapor pressure	15-30 kPa	(controlled by the separation in the reformat stabilizer)

Collection of data

A set of 16 process variables was identified as potential importance. The available collection of data was also important for the selection. As a response variable the benzene content in the stabilized reformat was chosen. From the process computer the 8000 sets of values on process parameters and online analysis result were loaded to the statistical program, see Table 1. The computer software used was Simpc 8, Umetrics (www.umetrics.com).

Table 1. Used Process Parameters

No.	Explanation	Abbr.	Units
1	Feed to the naphtha splitter	Feed	m ³ /hr
2	Feed to the catalytic reformer	Capacity	m ³ /hr
3	Pressure at top of naphtha splitter	Top Pres.	bar (g)
4	Temp. at top of naphtha splitter	Top Temp.	°C
5	Reflux ratio in naphtha splitter	Reflux ratio	ratio
6	Steam fed in to naphtha splitter	Steam	m ³ /hr
7	Temperature in catalytic reformer	WAIT	°C
8	Pressure in catalytic reformer	Pressure	bar (g)
9	H ₂ to hydrocarbon ratio in reformer	H2/HC	m ³ /m ³
10	Temperature diff. through 1 st reactor in reforming unit	DT1	°C
11	C6-naphthene in the feed to the reformer	C6-naphth.	Vol. %
12	C7-paraffins in the feed to the reformer	C7-paraf.	Vol. %
13	Density of the feed to reformer	Density	kg / m ³
14	C7-aromatics in the feed to the reformer	C7-roma.	Vol. %
15	Naphthenes in the feed to the reformer	Naphthenes	Vol. %
16	Aromatics in the feed to the reformer	Aromatic	Vol. %

Results and Discussion

PLS analysis results in model coefficients for the variables called PLS weights. In PLS loading plot (Figure 2), the weights for the X-variables (variables with black color in fig 2) denoted W indicates the importance of these variables in the modeling of Y (Benzene). Here we have an indication which variables from table 1 that are important. It can be seen that the C6-naphthenes lies far from the center in the same side of plot, where benzene lies so we can say that C6-naphthenes is highly positively correlated with benzene. In other words, higher C6-naphthenes content in the feed, higher will be the benzene in the product. Aromatic lies in opposite direction of benzene that is why it is negatively correlated with benzene in the product, higher the aromatics content in the feed lower will be the benzene in the product. So we can interpret that variables lying on right side of vertical line in the plot are positively correlated with benzene and variables lying on left of side are negatively correlated with benzene in the product Due to the holdup time in the distillation

HYDRODESULFURIZATION OF FLUID CATALYTIC CRACKED NAPHTHA OVER BIFUNCTIONAL Ni-Mo/HZSM-5 CATALYST

Changlong Yin, Ruiyu Zhao and Chenguang Liu

Key Laboratory of Catalysis, CNPC
State Key Laboratory of Heavy Oil Processing,
College of Chemistry & Chemical Engineering
University of Petroleum, Dongying, Shandong 257061, China

Introduction

Fluid catalytic cracked (FCC) naphtha currently contributes 80–85% of the total gasoline product pool in China, and it provides more than 95% of the sulfur in the gasoline. In order to comply with product specifications or to ensure compliance with environmental regulations, the sulfur compounds may require removal, which are expected to become more stringent in the future. Combined with sulfur reduction in fuel, the content of olefin in gasoline is limited to as low as 10% in the near future. It is well known that olefinic components account for about 40% in the cracked naphtha, which contribute a relatively high octane number for the cracked naphtha.

An obvious approach is isomerization of paraffins in naphtha to offset the loss of olefin, but the octane value of isomerized paraffin is less than that of equivalent olefin, octane number loss is still distinct in practice operation. Alternatively, another way is to increase the content of other components with high octane value, such as aromatics. At present, the content of aromatics in FCC naphtha is 15–20% and the maximum content in gasoline pool is limited to 35%, so there is quite big space to increase of aromatics. It would be desirable to develop an efficient process, with which can not only remove sulfur, but also aromatize paraffin and olefin to minimize loss of octane value from olefin containing naphtha feedstock. This can be implemented by using a bifunctional catalyst with an inexpensive procedure.

It has been shown that HZSM-5 zeolite can be modified by incorporation of metal or metal oxides in order to obtain catalysts for selective hydrocarbon conversions (1-3). Activity, selectivity and stability of the catalysts for those shape selective reactions depend not only on the porous structure of the zeolite but also on the density of acid sites and their strength distribution, as well as on metal sites distribution and metal support interaction(4). The catalyst systems prepared in this way operate bifunctionally. Nickel on HZSM-5 has been found to be active in the aromatization, hydrocracking and isomerization of hydrocarbon(5-7).

In the present paper, a series of zeolite supported Ni-Mo catalysts were prepared by impregnation method, the activities of hydrogenation and aromatization of the catalysts as well as hydrodesulfurization were investigated.

Experimental

Preparation of catalyst. The mixture of commercially available NaZSM-5 (Si/Al atomic ratio=35) and alumina (zsm-5/alumina mass ratio = 50) were mixed with dilute nitric acid and extruded into diameter 1.5mm sticks. The sample was dried in air at 110 °C for 20h, and the supports containing ZSM-5 were obtained by calcination of above dry sticks at 500 °C for 6h. For sodium removal, the supports were treated with a solution of 1.0 M ammonium nitrate and then calcined at 500 °C for 4h. The ZSM-5 supported Ni-Mo catalysts were prepared using incipient wet

impregnation method. The precursors of the active components Ni-Mo were nickel nitrate and ammonium molybdate. All catalysts were dried at 110 °C overnight, and then were calcined at 500 °C for 4 hr.

Characterization of the catalysts. X-ray powder diffraction analysis was carried out with a Rigaku D/max- \square A diffractometer using a graphite-filter CuK α radiation at a scan rate of 2 degrees per minute. BET sorption was used for measuring surface of the catalysts. The final Na content in the catalyst after ammonium nitrate treatment and the Ni and Mo contents in the catalysts were determined with atomic absorption spectrometry method.

Catalyst activity. Catalytic activity measurements were carried out in a high pressure micro-reactor unit of 24 mm I.D., 100cm in length. 100 ml of the catalyst extrudates were loaded in the reactor. Presulfiding is carried out before the reaction at 200 °C for 1 hour, and 300 °C for 2 hours and 360 °C for 3 hours with a liquid stream containing 3w% CS₂ in cyclohexane. FCC naphtha is then admitted at test temperature. The H₂/feed ratio is 150 and LHSV is 3h⁻¹. The reaction product was cooled and separated into gaseous and liquid products in a high-pressure separator. The average hydrodesulfurization activity was calculated as the % conversion of total sulfur in feed and in units of % HDS. The PIONA composition of the feed and hydrotreated naphtha was analyzed by gas chromatography, using a Varian 3800 chromatograph and a 100m PONA capillary column. Two kinds of FCC naphtha produced from two refineries of China were used as the feedstock. The main characteristics of the feed naphthas were shown in table 1. Aromatization activity and hydrogenation activity were measured as the percentages in the increase of aromatics and the decrease of olefin in the hydrotreated naphtha compared with the feed naphtha. Research octane number of the samples was calculated from PIONA composition.

Results and Discussion

Physico-chemical properties

The X-ray diffraction patterns of the supports with different content of HZSM-5 (50%) are completely matched with that of the pure HZSM-5, the Ni-Mo/HZSM-5 catalysts' XRD patterns exhibit almost identical intensity of the peaks with HZSM-5 except some NiO and MoO₃ peaks occurring in the latter's. The BET surface area and metal content of the catalysts were shown in table 2. The decrease in surface area after metal loading may be due to the channel occupation of nickel and molybdenum.

Table 1. Characteristics of the Feed Naphtha.

	Feed 1	Feed 2
Total sulfur, ppm	719.6	1235.6
RON	94.18	92.37
Composition (wt%)		
Aromatics	21.02	16.31
Isoparaffin	29.81	30.54
Naphthene	11.55	11.50
Olefin	26.90	31.52
Paraffin	5.26	4.38
Unidentified	5.46	5.74

Table 2. BET Area and Metal Contents in Catalysts.

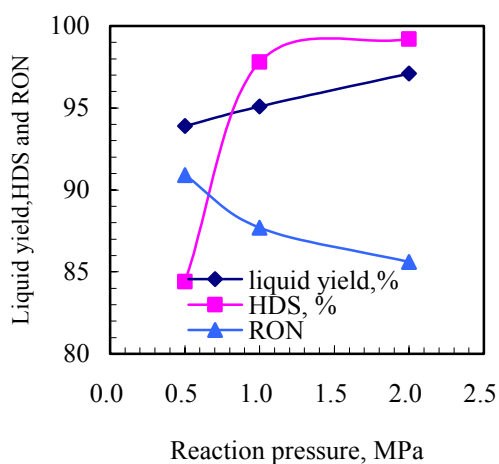
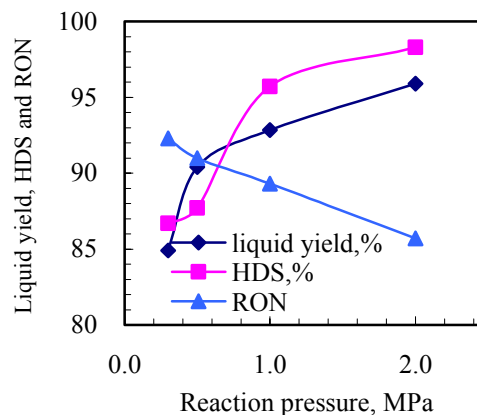
	HZSM-5	Ni-Mo (a)	Ni-Mo (b)
BET area, m ² /g	313.8	246.4	274.2
Na content, %	0.066	0.081	0.086
Ni content, %	--	2.1	1.1
Mo content, %	--	7.6	3.6

Effect of reaction pressure on the catalyst's activity. Figure 1 shows the effect of reaction pressure on the liquid yield, HDS and the RON of the hydrotreated products over Ni-Mo/HZSM-5(a) and table 3 lists the detailed composition of the products. The liquid yield and HDS% of the products increase with the enhancement of reaction pressure, while the RON of the products decreases with the raising of pressure. From the composition of the hydrotreated products over Ni-Mo/HZSM-5(a) it can be found that at low pressure the content of aromatics in the product increased, while at high pressure aromatics is hydrogenated, which contributes to the increase of naphthene. We can find from figure 1 that the HDS% of the product is very sensitive to the reaction pressure, especially at 0.5~1.0MPa. The low liquid yield at low reaction pressure reveals that cracking of the naphtha was carried out on the catalyst because of the acidity of the HZSM-5. Figure 2 shows the effect of reaction pressure on the liquid yield, HDS and the RON of the hydrotreated products over Ni-Mo/HZSM-5(b). The similar trends of the liquid yield, HDS and the RON of the hydrotreated products were obtained.

Table 3. Composition of the hydrotreated products over Ni-Mo/HZSM-5(a) (wt%).

Pressure, MPa	0.5	1.0	2.0
Aromatics	21.89	20.96	18.33
Isoparaffin	32.11	37.57	40.18
Naphthene	12.03	12.72	15.99
Olefin	23.01	14.24	8.84
Paraffin	8.54	12.83	15.45
Unidentified	2.41	1.62	1.44

Feed 1, reaction temperature, 360°C.

**Figure 1.** Effect of reaction pressure on the liquid yield, HDS and the RON of the hydrotreated products over Ni-Mo/HZSM-5(a). Temperature, 360°C.**Figure 2.** Effect of reaction pressure on the liquid yield, HDS and the RON of the hydrotreated products over Ni-Mo/HZSM-5(b). Temperature, 400°C

Effect of Reaction Temperature. Effect of reaction temperature on the liquid yield, HDS and the RON of the hydrotreated products over Ni-Mo/HZSM-5(a) at 2.0MPa was shown in figure 3. It is well known that temperature enhancement can favor the hydrogenation and HDS reactions in the process of naphtha hydrotreatment, which can be testified with the results shown in table 4. The decrease of the liquid yield must be the result of more cracking occurring over the catalyst with the increase of the temperature. About 25 percent of aromatics in feed were hydrogenated at 380°C, which led to the RON fall of the product. A little of the naphtha was probably aromatized at 400°C according to the data in table 4, but the adding of the aromatics can't offset the part that was hydrogenated, so the content of aromatics in the product was still depressed. Figure 4 gives the effect of reaction temperature on the liquid yield, HDS and the RON of the hydrotreated products over Ni-Mo/HZSM-5(b) at 0.5MPa and table 5 lists the composition of the hydrotreated products. The increase of HDS% and the decrease of the liquid yield maybe due to the same reasons as before, while the gain of RON in the hydrotreated products does owe to the raising in aromatics content. It can be concluded from the above results that at high pressure the main reactions in the process of naphtha hydrotreatment are hydrogenation of olefin and aromatics, and the hydrogenation degree increase with the enhancement of the temperature; while aromatization is dominated at low pressure, and the aromatization degree increases with the temperature enhancement, which contributes to the increase of RON.

Table 4. Composition of the Hydrotreated Products over Ni-Mo/HZSM-5(a) (wt%).

Reaction Temp. °C	360	380	400
Aromatics	19.81	15.67	18.72
Isoparaffin	40.77	42.26	40.75
Naphthene	14.08	15.55	15.22
Olefin	8.93	8.78	8.80
Paraffin	14.89	15.25	13.69
Unidentified	1.46	2.48	2.79

Feed 1, pressure, 2.0MPa.

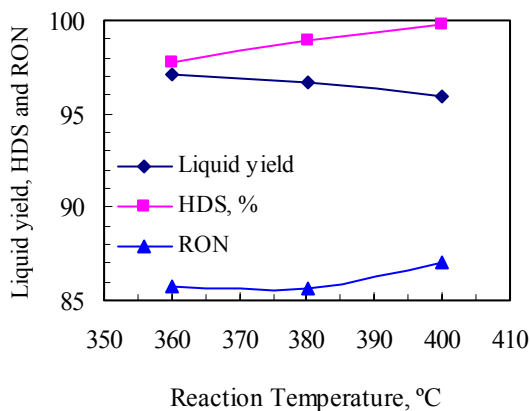


Figure 3. Effect of reaction temperature on the liquid yield, HDS and the RON of the hydrotreated products over Ni-Mo/HZSM-5(a). Feed 1, pressure, 2.0MPa.

Table 5. Composition of the Hydrotreated Products over Ni-Mo/HZSM-5(b) (wt%).

Reaction Temp. °C	280	380	400
Aromatics	17.35	20.71	24.61
Isoparaffin	32.66	34.82	32.15
Naphthene	12.06	13.59	13.10
Olefin	28.15	17.68	16.42
Paraffin	6.93	9.40	8.35
Unidentified	2.83	3.79	5.32

Feed 2, pressure, 0.5MPa.

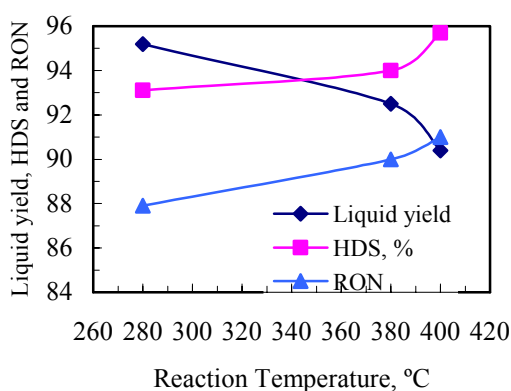


Figure 4. Effect of reaction temperature on the liquid yield, HDS and the RON of the hydrotreated products over Ni-Mo/HZSM-5(b). Feed 2, pressure, 0.5MPa.

Conclusions

Experimental results show that Ni-Mo/HZSM-5 bifunctional catalyst has excellent HDS and hydrogenation properties. The liquid yield and HDS% of the products increase with the enhancement of reaction pressure, while the RON of the products decreases with the raising of pressure. Elevation of reaction temperature can promote the HDS and the aromatization process, but leads to the loss of liquid yield at the same time. The main reactions at high reaction pressure in the process of naphtha hydrotreatment are hydrogenation of olefin and aromatics, and the hydrogenation degree increase with the enhancement of the temperature; while at low pressure aromatization is dominated in the process, and the degree increases with the temperature enhancement, which contributes to the increase of RON in the products.

Acknowledgement. Financial support from PetroChina Corporation Limited is greatly appreciated.

References

- (1) D. Seddon, *Catal. Today* **1990**, 6(3), 351
- (2) Y. Ono, *Catal. Rev. -Sci. Eng.* **1992**, 34(3), 179
- (3) M. Guisnet; N. S. Gnep; F. Alario. *Appl. Catal. A* **1992**, 89, 1
- (4) S. Uemiya; I. Koike; E. Kikuchi, *Appl. Catal.* **1990**, 65, 143
- (5) D. Sun; Z. Zhao, *Ind. Eng. Chem. Res.* **1991**, 76, 171
- (6) C.V.V. Satyanarayana; D. K. Chakrabarty, *Appl. Catal.* **1990**, 66, 1
- (7) T. Inui; Y. Makino; F. Okazumi; S. Nagano; A. Miyamoto, *Ind. Eng. Chem. Res.* **1987**, 26,647

A STUDY ON REMOVAL OF HYDROGEN SULFIDE FROM LIGHT OIL WITH SOLID BASE

Yongfeng Duan Yuzhi Xiang Daohong Xia

(College of Chemistry & Chemical Engineering, University of Petroleum, Dongying, 257061, China)

Abstract: For removal hydrogen sulfide from light oils, a novel solid base, with activated carbon as supporter and alkali or earth-alkali compound as active component, has excellent adsorption capacity for hydrogen sulfide and advantages of simple preparation and inexpensive cost of raw material has been developed. In addition, an additive can promote significantly the removal of hydrogen sulfide by the solid base was also studied.

Keywords: hydrogen sulfide, solid base, removal, adsorption, additive

1, INTRODUCTION

Sulfur compounds exist in various light oils made from petroleum. Such as mercaptan, hydrogen sulfide, which cause foul odors and deteriorate the finished products. In addition, due to their acidity, they are corrosive to metals, which is harmful for storage and usage of oil products. Therefore, it is necessary to remove them.

In the refining industry, an aqueous base such as sodium hydroxide or ammonia is employed fulfilling the purpose. Although its effectiveness and the low cost of fresh caustic are the reasons for its widespread use, the aqueous base especially sodium hydroxide always causes some problems. Such as spending many caustic materials, and discarding lots of hazardous waste. So environmental agencies around the world have tightened the regulations aimed at controlling its disposal. Solid bases merge as an ideal alternative to the aqueous bases to overcome the environmental and economic problems. The report concerning solid base is mostly concentrate in mercaptan oxidation, these solid bases selected from the group consisting of magnesium, nickel, zinc, copper, aluminum, iron oxides and mixtures thereof^[1-4]. However the report concerning solid base on removal of hydrogen sulfide was hardly consulted.

This paper reports the effect of factors of preparation for the solid base on removal of hydrogen sulfide at ambient temperature. Thus selecting the optimum factor of preparation for the solid base on

the removal of hydrogen sulfide in light oil.

2, EXPERIMENTAL

2.1 Preparation of solid base

Activated carbon marked by DV-01 was used as supporter in this study. Physical properties of the activated carbon is listed in Table 1.

Table 1 physical property of activated carbon

BET surface area /m ² .g ⁻¹	945.8
Bulk density /g.mL ⁻¹	0.519
Intensity, %	95.0
Pore volume /mL.g ⁻¹	0.72
Particle size/mesh	6—16

The activated carbon was calcined at high temperature for 6h, then impregnated with a aqueous solution of some alkalic materials at ambient temperature. The saturated activated carbon was filtrated in vacuum for period of time, then dried period of time at special temperature.

2.2 Experimental Oil

Petroleum ether(boiling point 90—120°C) was used as experimental oil with 800—1000µg/g hydrogen sulfide concentration.

2.3 Capability test of solid base for the removal of hydrogen sulfide

1g solid base was loaded in a 200ml flask, to this flask 100ml experimental oil was added, then the solution was electromagnetism stirred at ambient temperature with protection of nitrogen, the stirred speed was 350rpm. The hydrogen sulfide concentration in light oil was analyzed with period by the method of GB/T1792-88.

2.4 Materials calculation

The adsorption quantity of solid base for hydrogen sulfide as follows:

$$X_g = (C_0 - C_t) \cdot \rho \cdot V \cdot 10^{-3} / M$$

where

X_g : the adsorption quantity of the solid base for hydrogen sulfide mg/g

C_0 : Preliminary concentration of hydrogen sulfide µg/g

C_t : concentration of hydrogen sulfide at t hour µg/g

ρ 、 V : density, vol. of oil g/ml, ml

M : the quality of the used solid base g

3、RESULTS AND DISCUSSION

3.1 The effect of different chemical components of solid base on the removal of H₂S

With different alkalic materials, six kinds of solid base were prepared and the removal capacities for H₂S were tested. The results are shown in Fig.1.

As can be seen from Fig.1, the SB15 solid base for adsorption of hydrogen sulfide has the highest capacity.

The solid base adsorption for hydrogen sulfide has a competitive between physical adsorption and chemical adsorption. The removal capacity for hydrogen sulfide of the solid base was the sum of physical adsorption and chemical adsorption. Different solid base has different surface area and chemical center, so the capacity for hydrogen sulfide removal is alternatively. SB15 has the best chemical components.

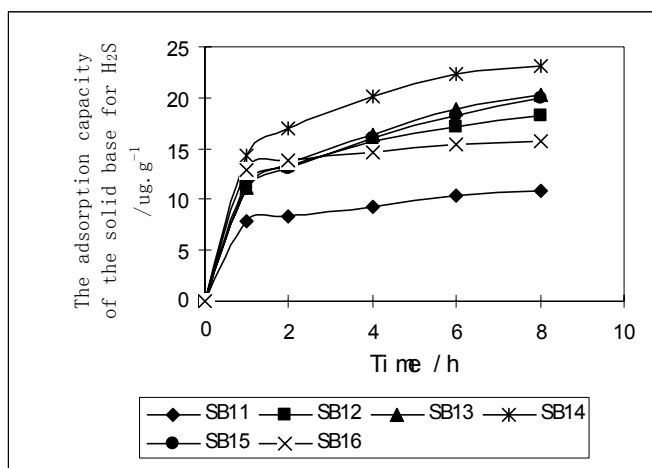


Fig.1 The adsorption capacity of different solid base

3.2 The effect of solid base vacuum filtration time on the removal of H₂S

Experiments examine the effect of time of vacuum filtration during preparation of the solid base for the removal of hydrogen sulfide. The activated carbon was impregnated with the optimum concentration of aqueous, then the loaded activated carbon was vacuum filtrated by different time, thereby making A series of solid bases. The removal of hydrogen sulfide were tested and the results are demonstrated in Fig.2.

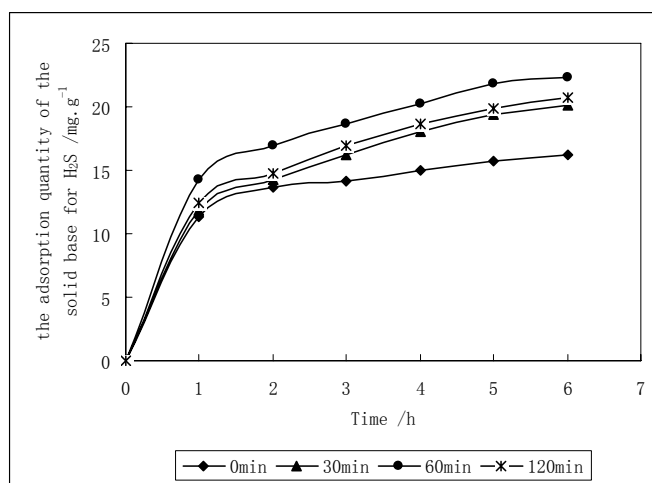


Fig.2 The adsorption capacity of the solid base by different time of vacuum filtration

Fig.2 shows that the adsorption capacity of the solid base for hydrogen sulfide firstly increased and then decreased with the increase of the vacuum filtration time during the preparation of the solid base. As a result, the time of vacuum filtration is a major factor for the solid base on removal of hydrogen sulfide, the optimum time of vacuum filtration should be 60 min.

3.3 The effect of solid base drying time on the removal of H₂S

A series of solid bases were made with different time of drying from short to long. And the removal of hydrogen sulfide of these solid bases were examined. The experimental results are shown in Fig.3.

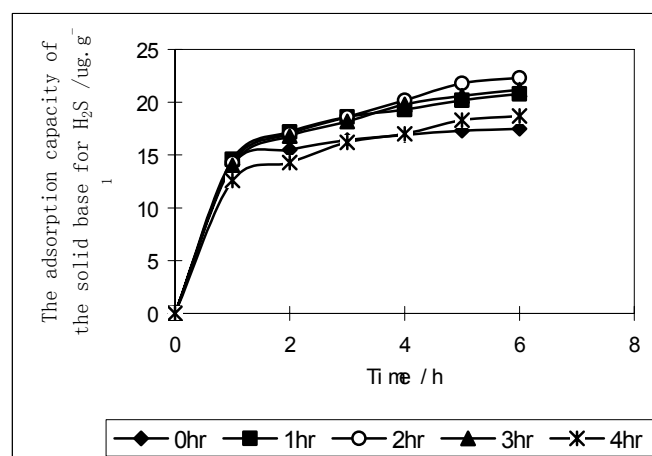


Fig.3 The adsorption capacity of the solid base by different time of drying

Fig.3 shows the adsorption quantity of the solid base for hydrogen sulfide firstly increased then decreased with the time of drying prolonged in the preparation of the solid base. The shorter the time of drying is, the higher the water content of the solid base is, the higher water content of the solid base reduced the physical adsorption of the solid base for hydrogen sulfide. With the further drying, the water is so less in the solid base that can not provide the polar environment for the chemical adsorption. consequently the chemical adsorption quantity of hydrogen sulfide in the solid base was decreased greatly.

It was found that the optimum time of drying for the solid base with good properties should be 2 hr.

3.4 The effect of additive on the removal of H₂S

It is believed that the function of polar compound is to serve as a proton transfer medium in the chemical reaction. Specially the compounds are selected from the group consisting of water, alcohols, esters, ketones, diols and mixtures thereof^[5]. A group of polar compounds was chosen as the additive for the solid base for removal of H₂S. Experiments were carried out for measuring the adsorption capacity of the solid base with different quantity of the additive.

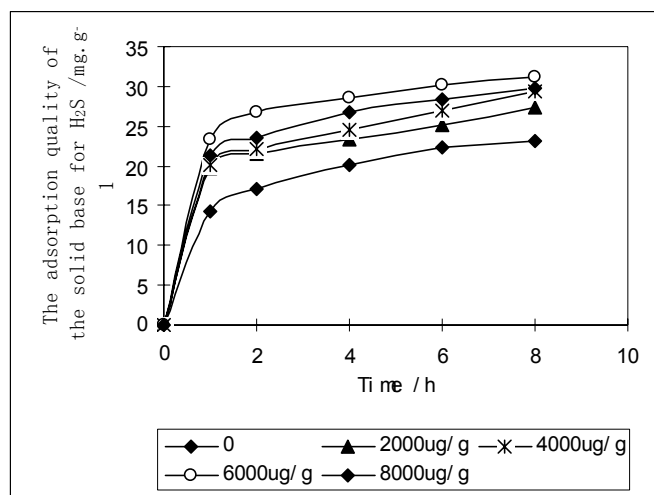


Fig.4 The adsorption capacity of the solid base for H₂S with different amount of additive

Fig.4 shows the adsorption capacity of the solid base for hydrogen sulfide has greatly increased after the additive was added. The adsorption ability of the solid base for hydrogen sulfide firstly increased and then decreased with the increase of the quantity of additive. The adsorption capacity of the solid base was enhanced after

the additive was added, thus the adsorption of the solid base for hydrogen sulfide has greatly increased.

4. CONCLUSIONS

1、 Preparation factors of the solid base play an important role for the solid base on removal of hydrogen sulfide. The preparation factors include the components of solid base, the time of vacuum filtration and the time of drying.

2、 The adsorption capacity of the solid base for hydrogen sulfide was the sum of physical adsorption and chemical adsorption.

3、 Adding a group of polar compounds can promote significantly the removal of hydrogen sulfide by the solid base. The optimum quantity of the additive is 6000 μg/g.

REFERENCES

1. F. Cavani, F. Trifiro, *Catalysis Today*. 1991,11:173
2. P. Ansquer, J. M. Orgebin, US Patent 5,382,354(1995).
3. J. J. Alcaraz, B. J. Arena, R. D. Gillespie, et al. *Catalysis Today*. 1998, 43(1-2):89-99.
4. Jiang De-en, Pan G, Zhao B, et al. *Applied Catalysis A:General*. 2000,201(2):169-176.
5. Arena, J. Blaise, Holmgren, et al. US Patent 5,232,887(1993).

HIGH CONVERSION SLURRY BED HYDROCRACKING PROCESS FOR PRODUCING HIGH OCTANE GASOLINE AND HIGH CETANE DIESEL SIMULTANEOUSLY FROM VACUUM GAS OIL

Jiashun Zhou

College of Chemistry and Chemical Engineering, University of Petroleum, Dongying, Shandong, P.R. China 257061

Introduction

Fluid catalytic cracking process (FCC) is one of the most important processes for producing high octane gasoline. Thermal cracking and isomerization reactions were the main reactions in FCC process. As more isomerized fractions, olefins and aromatic fractions contained in liquid products, the octane number RON of FCC gasoline is generally higher than 90, and the cetane number of diesel is about 30. The percentage of liquid yields in FCC process was usually within the range from 75% to 80%.

High cetane diesel was usually obtained from fixed-bed hydrocracking process. In the process, sulfur and nitrogen contained in feed, olefins generated while cracking reaction taking place and part of the aromatic fractions were hydrogenated. As a result, the octane number RON of gasoline fraction was only about 70, and the cetane number of diesel was usually more than 50.

We could get high octane gasoline from FCC process, and we also could get high cetane diesel from fixed-bed hydrocracking process. It is hard to obtain both of them from a single process up to now.

Slurry bed hydrocracking process is a kind of thermal cracking process in the presence of hydrogen and dispersed catalyst. In this process there were less isomerization and less hydrogenation. The so called dispersed catalyst were such substance as powder of natural ore, powder of coal, water or oil soluble salt which might contain Co, Mo, Ni, Fe, W, Mn, etc.^[1-2] The characteristics of the liquid yields of the process were that the octane number of gasoline was not too low, usually in the range of 70 to 80; the cetane number of diesel was usually over 40. If same measure was applied to raise the octane number of gasoline fraction from 70 to 90, we could obtain high octane gasoline and high cetane diesel from slurry bed hydrocracking process simultaneously.

Methanol can react with olefins and produce oxygen containing compounds, which have a higher than 110 octane number. These kind compounds usually used as the additives to raise the octane number of gasoline. When the feedstock was blend with methanol, hydrogen, dispersed catalyst, the above reactions take place accompany with cracking reactions and hydrogenation reactions. In some cases if the dispersed catalyst can solve in methanol, the mixing procedure of feed with catalyst was simplify and the catalyst become more active and efficient, and as a result, more feed was converted to gasoline and diesel. This was what we dealt with, the high conversion slurry bed hydrocracking process for producing high octane gasoline and high cetane diesel simultaneously from vacuum gas oil. We named this process as HHH process^[3].

Experimental

The Catalyst. The dispersed catalyst used in slurry process was normally the metal elements of Mo, Ni, Fe, Co etc., which were usually used in fixed-bed hydrocracking process. These kinds of catalyst can be used in mild slurry bed hydrocracking process also, whereas less free radical occurs in the reaction environment. If used in critical process, such as with a temperature 440 to 480°C, whereas

more thermal cracking reaction occurs, the radical cracking reaction would be restrained. The macro behavior was that once the catalyst was added, the conversion of the feed lowered down.

The catalyst used in HHH process differed much from the most commonly used catalyst in slurry bed hydrocracking process as shown above. It was the solution of copper nitrate solved in methanol. Since methanol contained in it, when the catalyst was dispersed in the feed and used to promote the cracking and hydrogenation reactions, methanol acted as a kind of reactant and reacted with the olefins yielded while hydrocarbon cracking. Thus, oxygen containing hydrocarbons were produced. As we know, these hydrocarbons have high octane number, which was usually more the 110(RON). When the boil point of these compounds fit the ranges of gasoline, it could raise the octane number of gasoline fraction. While used as a diesel fraction, it can increase the oxygen containing of diesel, and as a result, decrease the discharge of particulates from the engines.

Pilot Plant Experiments. The pilot plant has a capacity of 2.8L/hour of liquid feed. The feed and catalyst mixed in a preheating unit, and hydrocracked in a slurry reactor, and then separated into gasoline, diesel and bottom oil using a distilling unit. The average temperature of the reactor was controlled at 430°C, 440°C and 450°C. System pressure was 11MPa and the volume space hour velocity was 0.6h⁻¹.

Feed Composition. The feed of pilot plant was consisted of 97.42% of vacuum gas oil of Xinjiang crude oil and 2.58% of the dispersed catalyst. The properties of the vacuum gas oil were presented in Table 1. The dispersed catalyst was the methanol solution of copper nitrate. In the catalyst, there were about 3m% to 4m% of copper, 10m% of water and 5m% of carbon disulfide.

Table 1. The Properties of Feed Vacuum Gas Oil

Boil Point Range, °C	360~520
Specific gravity, g/cm ³	0.9182
H/C Atomic Ratio	1.73
Sulfur, m%	0.079
Saturate, m%	75.8
Aromatic, m%	17.1
Resin, m%	7.1

Results and Discussion

Products Distribution. Pilot plant experiments results were illustrated in Table 2. All the data listed was excluded the quantity of methanol added as the solvent of dispersed catalyst. When the reaction temperature was 450°C, the conversion of the feed vacuum gas oil was over 95%. In which, more than 90% was gasoline and diesel.

Table 2. Production Distribution

Reaction Temperature, °C	430	440	450
Gas(C ₁ ~C ₄), m%	5.63	5.90	5.95
Gasoline(C ₅ ~180°C), m%	20.45	27.31	31.73
Diesel(180~350°C), m%	46.46	53.11	58.57
Bottom Oil(>350°C), m%	27.91	14.14	4.23
Conversion of Feed, m%	71.35	85.49	95.66

Properties of Gasoline and Diesel. As illustrated in Table 3. The gasoline fraction contains less aromatics, less olefin, more paraffin, more isoparaffin, and more oxygen containing compounds. The octane number (RON) was 89. It was just a little below than the FCC process. And also, the sulfur containing of the gasoline fraction was only 0.0181m%. The total sulfur contained in gasoline fraction occupied 7.5m% of the total sulfur contained in feed gas oil. This

kind of gasoline can be simply used as clean gasoline. If blending with other high octane fraction and raising the RON to 95~97, more profit could be obtained from this HHH process.

The properties of diesel fraction were presented in Table 4. The obvious characteristics of diesel were low sulfur containing (0.0135m%), low condensation point (-38°C), and a much higher cetane index than the FCC diesel. The total sulfur contained in diesel occupied 10.3m% of the total sulfur contained in feed. Like the gasoline fraction, this kind of diesel can be used as clean diesel also. It would get better effect if blend it with the diesel from fixed-bed hydrocracking process, and raise the cetane number to 45.

Table 3. Properties of Gasoline

Aromatics, m%	17.6
Paraffin, m%	15.4
Isoparaffin, m%	19.5
Cyclane, m%	11.8
Olefin, m%	14.3
Methanol, m%	0.024
Oxygen Containing Compounds, m%	10.0
Octane Number, RON	89
Sulfur, m%	0.0181

Table 4. Properties of Diesel

Specipic Gravity, g·cm ⁻³	0.8824
Aniline Point, °C	55
Sulfur, m%	0.0135
Cetane Index	41
Condensation Point, °C	-38

Characteristics of Catalyst. The concentration of dispersed catalyst copper in reaction system was only 800~1000ppm. As shown above, the HHH process had high conversion and high liquid recovery ratio. One of the reasons was that the catalyst was very finely dispersed in the gas oil. And as a result, the catalyst had high activity to prompt the cracking, hydrogenation and etherification reactions. Figure 1 showed the relative percentage of catalyst particle number and volume of different diameter. These particles were separated from the bottom oil. In the preheating unit or reaction unit, the particles should be much fine. Although the total volume of the catalyst particle, which had less than 1µm diameter, was only about 17%, the number of them was over 80%. Another reason might be the formal electronic configuration of copper. At high temperature copper(I) was the most stable state. It has a 3d¹⁰4s⁰ outer electron, and low valence state. The copper(I) might be hydrogenated to copper(0), and copper(0) might react with hydrogen sulfide changing the formal oxidation state to 2. Copper(II) changed to copper(I) again. During the changing of oxidation state, the free radical reaction might be accelerated.

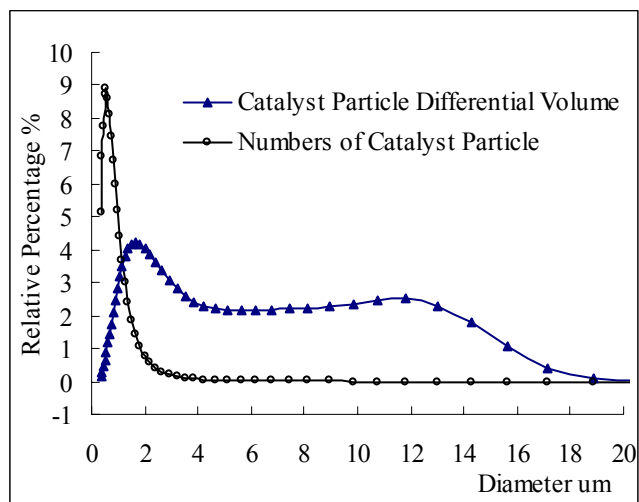


Figure 1. Distribution of Catalyst Particle

Conclusions

By using slurry bed hydrocracking process and using the copper-based methanol solution as dispersed catalyst, high octane number gasoline and high cetane number diesel can be obtained simultaneously from vacuum gas oil. At 450°C, the conversion of the feed gas oil was over 95%, in which, more than 90% was gasoline and diesel. The octane and cetane number of gasoline and diesel were 89 and 41.

References

- (1) Cooke, W.S. et al.; *Prepr. Pap. -Am. Chem. Soc., Div. Fuel Chem.* **1995**, 40(3), 599-603.
- (2) Strausz, O.P. et al.; *Prepr. Pap. -Am. Chem. Soc., Div. Pet. Chem.* **1995**, 40(4), 741-742.
- (3) Zhou, J. et al.; *CN Patent 031120997*.

Progress of FCC Technology in Improving Product Distribution and Quality

Chao-He Yang, Hong-Hong Shan, Jun-Sheng Zheng,
Gen-Lin Niu, Jian-Fang Zhang

State Key Laboratory of Heavy Oil Processing,
University of Petroleum,
271 North 2nd road, Dongying, Shandong 257061, P.R. China

Introduction

In China, the fluid catalytic cracking (FCC) process is one of the most important refining processes, it affords about 80% of gasoline and 30% of diesel oil in market, but now it is faced with a baptism to satisfy the need for producing environmentally-cleaner gasoline and diesel fuels. During the recent decade, almost all the FCC processes became the RFCC (residue fluid catalytic cracking) processes by revamping for processing the heavier feedstock, and RFCC technology got great development around the reaction system, including the feeding atomization, quick separation of oil vapor and spent catalyst, steam stripping of high efficiency, temperature control of reaction, as well as the innovation of riser reactor^[1-3].

In order to improve the product distribution, as well as reduce the olefin content and increase the octane number of FCC gasoline, and raise the cetane number of FCC diesel fuel, many technology innovations were proposed and tested in China. In this article, four new processes, including Maximizing Iso-Paraffins technology, Two-Stage Riser FCC technology, Flexible-Double Function FCC technology and Assistant Gasoline Riser Technology were introduced from their principles of technology and results of experiment or industrial test.

The shortage of the traditional RFCC riser

Although the feedstock of RFCC is different from that of distillate FCC because of its high boiling point, high resin and asphaltene content, and high contaminant concentration, the reactor, riser, is the same for RFCC and FCC process yet. In general, the distillate FCC is thought to be a gas-solid catalytic reaction, but gas, liquid, and solid exist simultaneously in reactor for RFCC. The studies on product distribution along the riser of RFCC show that the main conversion of feedstock to gasoline and diesel distillates is completed in the front stage of riser^[4]. Figure 1 gives the variation of product distribution along the riser length of RFCC unit in a Sinopec Petrochemical Factory. It means that the riser is too long to result in an ideal product distribution at the exit of riser^[5-6].

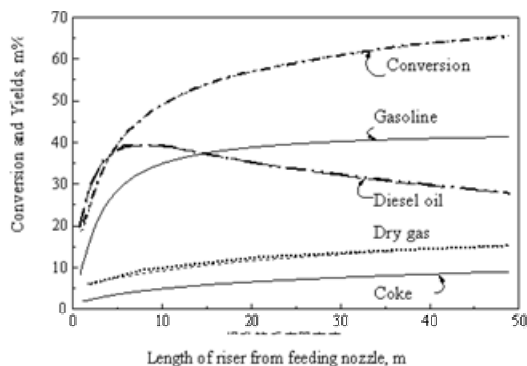


Figure 1. Conversion of feedstock and yields of products versus the length of riser (Simulated result of commercial RFCC unit)

The high olefin content of RFCC gasoline is another problem, it may be close to 60% for residual feedstock from paraffin crude. Although the many special catalysts were developed to reduce the olefin content, it is difficult to seek for a good compromise of operation conditions with the traditional RFCC for improving product quality as well as the product distribution. Therefore, the new reaction technologies of RFCC were proposed.

Maximizing Iso-Paraffins technology (MIP)

The MIP technology^[7] was developed by the Research Institute of Petroleum Processing (RIPP), Sinopec, and was put into commercial use in Gaoqiao refinery. Its advantage is able to respectively create the favorable reaction conditions for heavy feedstock cracking into intermediate products and for upgrading the desired products. The theoretical foundation is that the high temperature and short reaction time is favorable to heavy feedstock cracking, but the isomerization and hydrogen transfer for improving product quality requires low temperature and long reaction time. As shown in figure 2 the most important innovation in MIP is the revamp for the traditional riser.

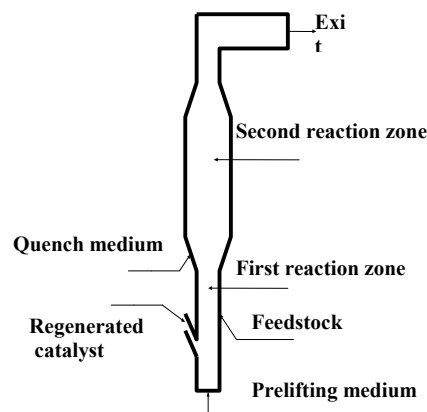


Figure 2. The riser reactor of MIP

The riser was classified into two reaction zones, and varies in diameter for different zones. The first reaction zone with a small diameter at the initial stage of riser is responsible for the cracking of heavy feedstock. This zone can provide the high temperature and short reaction time by controlling the catalyst recycle and the proper design. The second reaction zone with a larger diameter at the downstream section of riser is responsible for the completion of hydrogen transfer and isomerization. A quench medium, such as raw gasoline, LCO, water, or spent catalyst, is introduced into the starting section of this zone to decrease the temperature of the fluid come from the first zone. It is thought that the gasoline produced in the first zone were upgraded by improving the hydrogen transfer and isomerization and restraining the secondary cracking. The observation in pilot unit obviously shows that the conversion of feedstock was increased and the olefin content of gasoline decreased. Under the similar conversions, the yields of dry gas and coke for MIP is similar with the traditional FCC technology, the yield of gasoline increases by 1.37 percents (from 43.07% of traditional FCC to 45.07% of MIP), the yield of diesel oil has a slight increase too. The olefin content of FCC gasoline is 27.2% for MIP, compared with the traditional FCC technology, it drops by 12.4 percents, the aromatic content increases by 6.4 percents, MON increases by 1.3 units and RON has no obvious change. In addition, the sulfur content of gasoline has a notable decrease.

Two-Stage Riser FCC technology (TSRFCC)

In 1994, the TSRFCC technology^[8-10] was proposed by the State Key Laboratory of Heavy Oil Processing, University of Petroleum (East China), and was put into industrial test in 2002 at a revamped unit of 10 thousand ton/year capacity. This year there are four RFCC units to be modified by the TSRFCC technology in China. The TSRFCC aiming at the disadvantage that the activity of catalyst and the selectivity to ideal products fall greatly at the anaphase of reaction in the traditional one-stage riser FCC (OSRFCC) replaces the present single riser reactor by two riser reactors, has two catalyst cycling system. A series of TSRFCC technologies have been developed for various product schemes. TSRFCC-I technology is suitable for enhancing the yield of light oil, especially the ratio of diesel to gasoline. Figure 3 shows the flowsheet of TSRFCC-I technology.

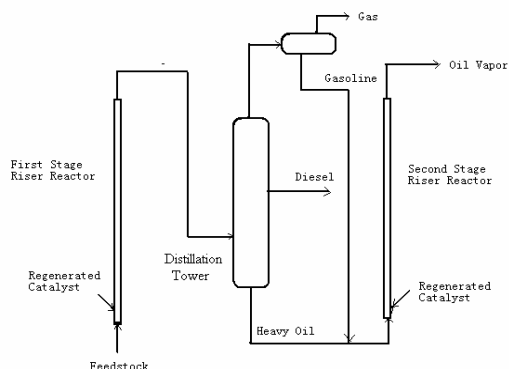


Figure 3. flowsheet of TSRFCC-I technology.

After the first stage cracking reaction to a proper extent, diesel distillate as a part of the final product is separated, while heavy oil (or heavy oil and gasoline when olefin reduction of gasoline is needed) enters the second stage riser reactor, contacts with the regenerated catalysts and reacts simultaneously. Therefore, diesel is well protected from non-desired second cracking since it does not take part in the reaction in the second stage after the separation, which increases the yield of diesel. On the other hand, the partial pressure of diesel at the second stage is effectively lowered, so it is optimal for the large molecules of heavy oil breaking down to generate more light oil. The two risers in TSRFCC-I technology are designed to keep the total reaction time less than 2 seconds, this affords a favorable condition for high temperature and short time operation. Compared with the recycle oil, the residue is easier to cracking, but more difficult to atomize, vaporize, and diffuse into the pores of catalyst, so the recycle oil will firstly vaporize and diffuse into the pores of catalyst and cover the active sites when both together enters the riser at the same time, this does affect the effective conversion of residue. The residue and recycle oil entering the two different risers respectively is reasonable for improving the product distribution.

The industrial test shows that the TSRFCC can enhance the conversion of feedstock and ameliorate product distribution greatly. Light oil and liquid product yields increase by 4 percents and 3 percents respectively, the ratio of diesel to gasoline rises obviously, and yield of dry gas and coke decreases by 2 percents, the capacity of FCC unit raises by 20%~30%. The olefin content of FCC gasoline was reduced by 6-8 percents without recycle of FCC naphtha. When the FCC naphtha is partly recycled to the second riser, the olefin content of FCC gasoline could be dropped by 15-20 percents without

the deteriorating of product distribution relative to the traditional RFCC technology.

DFCC and Assistant Gasoline Riser Technology

Flexible-Double Function FCC technology^[11-12] (DFCC) was developed by Luoyang Petrochemical Engineering Corporation, Sinopec. Assistant Gasoline Riser Technology^[13] was proposed by University of Petroleum (Beijing). These two technologies are mainly used in the FCC gasoline upgrading, especially the reduction of olefin content. In these two technologies, another riser reactor is added to process the FCC gasoline based on the traditional RFCC technology. For Assistant Gasoline Riser Technology, the gasoline reactor consists of a riser and a reaction bed followed, it assures to afford the low temperature and long reaction time for hydrogen transfer and isomerization.

The industrial test for DFCC was completed in 2002, it can reduce the olefin content of FCC gasoline by 20-30 percents, raise the RON by 1-2 units, lower sulfur content 15-20%, and increase the ratio of diesel oil to gasoline. But the yield of dry gas and coke increases obviously for DFCC technology. As to the Assistant Gasoline Riser Technology, observation in pilot unit shown that the olefin content of gasoline was reduced by 15-20 percents, the conversion of olefin in gasoline is close to 60%, only about 1.5% of gasoline was converted into dry gas and coke, and RON of gasoline has a slight increase.

Conclusion

In China, the key problem of RFCC process is to reduce the olefin content of gasoline and to keep the product distribution and gasoline octane number from dropping at least. Based on the different understandings to the chemical mechanism of isomerization, hydrogen transfer, and cracking of olefin component, as well as their relationship, many new RFCC technologies were developed, but the TSRFCC technology gives a better result.

References

- (1) Hou Fusheng. *Petroleum Processing and Petrochemicals*. **2001**, 32(1):1-6
- (2) Miao Yi, Guan Minghua, Luo Yibin. *Petroleum Processing and Petrochemicals*. **2000**, 31(8):1-7
- (3) Xie Chaogang, Zhong Xiaoxiang, and Yang Yinan. *Petroleum Processing and Petrochemicals*. **2001**, 32(1):26-30
- (4) Niu Genlin, Yang Chaohe. *Journal of Fuel Chemistry and Technology*. **2002**, 30(3):249-253
- (5) Dong Wei. *Doctoral thesis, University of Petroleum*. **2001**
- (6) Dong Wei, Xu Chunming, Gao Jinsen. *Journal of the University of Petroleum, China*. **2000**, 24(6):4-7
- (7) Xu Youhao, Zhang Jiushun, and Long Jun. *Petroleum Processing and Petrochemicals*. **2001**, 32(8):1-5
- (8) Zhang Jianfang, Shan Honghong, and Yang Chaohe. *US Patent*, **2002**, Application Number: 0108887A1
- (9) Zhang Jianfang, Shan Honghong, and Yang Chaohe. *Chinese Patent*, **2002**, Application Number: 00134054.9
- (10) Zhang Jianfang, Shan Honghong, and Yang Chaohe. Ninth Annual Conference of Catalytic Cracking. **2002.11**, Guangzhou
- (11) Zhang Fuyi, Zhang Lixin, Li Zhanbao. *Chinese Patent, CN96212360.9*
- (12) Tang Haitao, Wang Longyan, Wei Jialu. Ninth Annual Conference of Catalytic Cracking. **2002.11**, Guangzhou
- (13) Gao Jinsen, Xu Chunming, Bai Yaohua. Ninth Annual Conference of Catalytic Cracking. **2002.11**, Guangzhou

Study on Product Distribution along the Riser Reactor in RFCC Unit

Jun-Sheng Zheng, Chao-He Yang, Gen-Lin Niu, Feng Du,
Hong-Hong Shan, and Jian-Fang Zhang

State Key Laboratory of Heavy Oil Processing, University of
Petroleum, 271 North Second Road, Dongying 257061 China

Introduction

In China, nearly 70% of gasoline pool and 30% of diesel oil are produced by the fluidized catalytic cracking processing (FCC) which is one of the most important processes for converting heavy distillates into light fuels. But the FCC feedstock becomes heavier and heavier for the reason that the decrease of the conventional crude and the increase of demand for light fuels. Since the residuum have a high content of resin, asphaltene, high contaminant concentration and high boiling point, the residuum fluidized catalytic cracking (RFCC) technology has been got a great development in technology scheme, such as catalyst, feed nozzle type, etc^[1-2]. But the key of the RFCC process, the riser reactor, is the same for RFCC and FCC process yet, and the study on the product distribution and composition changes of products along the commercial RFCC riser is very important, but quite scarce. The present paper gives a primary but detail understanding on the product distribution and composition changes of products along the riser reactor of a commercial RFCC unit.

Experimental

In order to make out the true reaction behavior, product distribution and composition changes of products along the riser in RFCC process, a new sampling system which can gain satisfied samples from commercial RFCC riser was developed by the State Key Laboratory of Heavy Oil Processing. Details about this sampling system refer to the previously published papers^[3-4]. With the modified sampling system, the gases, the oil samples and the oily catalyst were obtained at the different positions along the commercial riser in the RFCC unit, Qingdao Petrochemical Factory, SINOPEC. Figure 1 described the sampling position distribution in the commercial riser.

The gaseous products, the PIONA and the RON/MON of gasoline were analyzed by a HP5890II GC with an UP-3000 workstation, developed by the Analysis Centre of University of Petroleum. In order to remove the absorbed oil, the oily catalysts were first extracted with n-C₅H₁₂ as solvent in Soxhlet apparatus, and then stripped by steam at 515°C for 20min, finally analyzed with a combustion-GC method to determine the coke yield. The boiling point distribution of the liquid products and the dissolved oil were determined by a Simulated Distillation GC. The sulfur content of the gasoline distilled from the liquid product was measured by the Micro-Coulomb method.

The RFCC feedstock in Qingdao Petrochemical Factory is the atmospheric residuum of the mix of Shengli, Cabinda and Far East crude. The sulfur, carbon residue, saturate, aromatics, resin, and asphaltene contents of the feedstock is 3400ug/g, 4.29wt%, 52.06wt%, 24.08wt%, 22.60wt%, and 1.26wt% respectively.

Whether the representative samples were got from commercial riser is the key for the present work to be successful. From the obtained samples including gas, liquid and oily catalyst, the material balance can be made at each sampling point. In order to verify the veracity of the data, comparison was made between the sampling point and the product distribution of RFCC unit. The yields of gasoline and diesel oil of the RFCC unit are 42m% and 23m%, respectively. The ratio of recycle is 0.137 in commercial production,

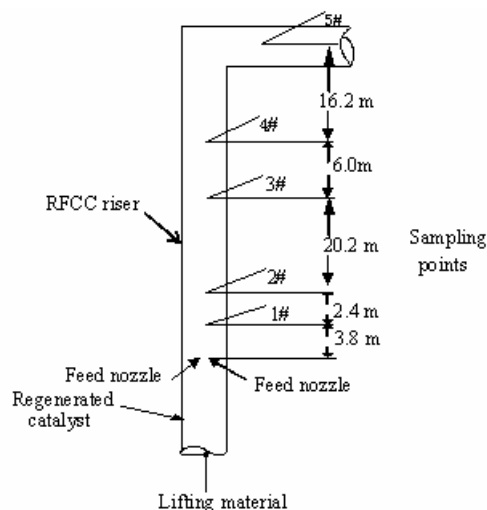


Figure 1. Illustration of sampling points on RFCC riser

so the single-through yields of gasoline and diesel oil is $42 \times (100 - 13.7)$ m% and $23 \times (100 - 13.7)$ m%, that is, 36.3 m% and 19.8m%, respectively, which is similar with the gasoline and diesel oil yield from material balance at the 4# sampling point. And also, the quality of gasoline at 5# sampling point close to the exit of riser, such as sulfur content, olefin content, is similar with the raw gasoline of the commercial RFCC unit.

Results and Discussion

Product distribution along commercial riser. The total amount in every sampling point for making material balance is the sum of gases and liquid products collected in sampling process, as well as the oil absorbed in oily catalysts. The product weight and yield are calculated as follows:

- Coke yield = coke in catalyst \times the ratio of catalyst to oil;
- The weight of gas and oil = the weight of gases + the weight of liquid products + the weight of oil absorbed in oily catalyst;
- Gasoline yield = (the weight of gasoline in liquid products + the weight of C₅⁺ in gases + the weight of gasoline in oily catalyst)/the weight of gas and oil \times (100-coke yield);
- Diesel oil yield = (the weight of diesel oil in liquid products + the weight of diesel oil in oily catalyst)/the weight of gas and oil \times (100-coke yield);
- Heavy oil yield = (the weight of heavy oil in liquid products + the weight of heavy oil in oily catalyst)/the weight of gas and oil \times (100-coke yield);

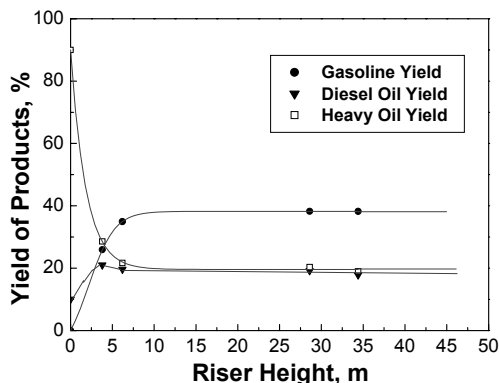
Analysis and calculated results for gaseous composition and product distribution from different sampling positions were listed in table 1 and table 2 respectively.

Table 1. Analysis Result of Gases along RFCC Riser

Sample No.	1#	2#	3#	4#	5#
C ₁ +C ₂ , m%	18.55	11.48	8.52	12.39	18.55
C ₃ +C ₄ , m%	57.37	59.21	62.83	63.22	65.38
C ₃ ⁼ +C ₄ ⁼ , m%	45.75	48.51	49.42	49.22	49.99
(C ₁ +C ₂)/(C ₃ +C ₄)	0.32	0.19	0.14	0.20	0.28
(C ₃ ⁼ +C ₄ ⁼)/(C ₃ +C ₄)	0.80	0.82	0.79	0.79	0.77

Table 2. Product Distribution along RFCC Riser

Sample No.	1#	2#	3#	4#
Gasoline, m%	25.92	34.93	38.23	38.21
Diesel Oil, m%	21.00	19.65	19.18	19.62
Heavy Oil, m%	28.56	21.65	20.35	17.19

**Figure 2.** Product yields Vs. riser height

It is shown from table 1 that the ratio of (C_1+C_2) to (C_3+C_4) , which means the relative capacity of thermal cracking and catalytic cracking, gets its minimum value in the middle of the riser and then increases. This phenomenon is consistent to the change of catalyst activity along the RFCC riser^[5]. At the mix zone of catalyst and feedstock close to the position of feedstock nozzles, the higher contact temperature of oil gas and catalyst (560°C) and the adsorption of high-boiling point components on catalyst surface make the thermal cracking reactions take a more important role relative to catalytic reaction. At the tail of riser, the obvious formation of catalytic coke on the catalyst leads to the same result. Although the content of (C_3+C_4) and $(C_3^-+C_4^-)$ in gases increase along the riser, the ratio of $(C_3^-+C_4^-)$ to (C_3+C_4) , which is the hydro-transfer behavior index of catalytic catalyst, arrives at its top point at the middle of riser and then decreases. This means that the hydro-transfer behavior of catalyst depends on the activity of catalyst and the effective reaction time.

Table 2 and figure 2 described the change of product yield along the RFCC riser. The gasoline yield reaches its maximum point at the middle of riser, but the yield of diesel oil reaches its maximum point at the initial stage of riser. The yield of heavy oil ($>350^\circ\text{C}$) decreased along the riser, but the trend of diminution shrinks quickly; there is no notable change at the later half of riser. In another words, the change of product distribution is drastic in the initial stage of riser and tempered at the later half of riser. In the initial stage of riser, the heavy oil yield decreases from 90m% in feedstock to 28.9m% at the first sampling point, and nearly 60m% of feedstock are converted into gasoline, diesel oil, gaseous product and coke. This points again that the initial stage play a very important role in RFCC processing, and improving the contacting situation of feedstock with regenerated catalyst is a key method to get satisfied product distribution and maximum refinery profit.

Composition and Properties Changes in Gasoline. Table 3 lists the composition and properties in gasoline at different sampling points. The naphthene content in gasoline has no notable change for the reason that the naphthene is relative stable in FCC process^[6]. The olefin content of gasoline first increases to its maximum at the

middle of riser and then decreases. Based on the change analysis of catalyst activity along the riser^[5], the thermal cracking plays a more important role in the conversion of feedstock to gasoline and diesel distillates, the olefin content of gasoline increases firstly with its rapid formation in the initial stage of RFCC riser. At the top of olefin content in gasoline, the yield of gasoline reaches a stable number, and then the olefin in gasoline will be reduced gradually with the reaction proceeding in the later section of RFCC riser. There is no significant change in RON, MON and anti-knock index of gasoline. This may be explained by the corresponding increase of aromatics with the decrease of olefin in gasoline.

Table 3. Properties of Gasoline along Commercial Riser

Sample No.	1#	2#	3#	4#	5#
Paraffin, m%	32.6	27.0	29.2	30.0	29.9
Naphthene, m%	9.4	8.5	9.0	9.5	9.7
Aromatics, m%	19.9	18.1	14.7	16.8	22.2
Olefin, m%	37.8	46.2	47.0	43.5	37.9
RON	92.6	92.3	93.0	92.6	92.3
MON	79.4	79.2	79.8	79.4	79.2
Anti-knock index	86.0	85.8	86.4	86.0	85.8
Sulfur content, $\mu\text{g/g}$	430	382	264	251	230

The sulfur content of gasoline decreases along the riser, but the tendency of decrease shrinks quickly. The sulfide is one type of L-bases, and the cracking of sulfide should first be absorbed in catalyst and then be cracked to H_2S or other sulfides^[7]. At the rear of riser, the cracking centre of catalyst was covered with coke, and the cracking activity decreasing, so the tendency of sulfur content decreasing become slowly.

Conclusions

This work gives the changes of product distribution and properties of products along riser in commercial RFCC unit. The present studies will be favorable to the progress of RFCC technology.

Acknowledgement. This work was supported by the PetroChina, the Ministry of Education and the Qingdao Petrochemical Factory, SINOPEC. Thanks Guo-qing Fu and Tong-peng Mo for their help in sampling process and Zhong-xiang Han, Jin-you Wang, Bin Luo and Jian-wen Wang for their work in analysis of products.

References

- (1) Yan Ran-zhao. *Oil and gas processing*. **1997**, 7(3), 40-44.
- (2) Hou Fu-sheng. *Petroleum processing and petrochemicals*. **2001**, 31(1), 1-6.
- (3) Xu Chun-ming, Lin Shi-xiong, Lu Liang-gong. *Petroleum refinery engineering*. **1997**, 27(3), 39-42.
- (4) Xu Chun-ming, Lu Liang-gong, Lin Shi-xiong. *Journal of the University of Petroleum, China*. **1997**, 21(2), 72-75.
- (5) Shan Honghong, Yang Chaohe, Niu Genlin. Preprints, Division of Petroleum Chemistry, ACS. **2002**, 47(3):321-322
- (6) Chen Junwu, Cao Hanchang, *Catalytic Cracking Technology and Engineering*, China Petrochemical Press: Beijing, 1995; pp.130-132.
- (7) Zheng JunSheng, Li ChunYi, Yuan Q-Min, Li Min, Yang ChaoHe Shan HongHong, Zhang JianFang, *Journal of the University of Petroleum, China*. **2002**, 26(1), 88-90.

Studies on the Interactions between ZnO and USY

Qimin Yuan, Chunyi Li, Hongyan Yang, Honghong Shan, Chaohe Yang, and Jianfang Zhang

State Key Laboratory of Heavy Oil Processing, College of Chemistry and Chemical Engineering, University of Petroleum, Dongying, Shandong Province, P.R. China 257061

Introduction

USY/ZnO/Al₂O₃ additive has excellent sulfur removal activity for FCC gasoline^{1,2}. However, it deactivates very quickly under hydrothermal conditions at 800°C. In the additive USY and Al₂O₃ are two main components and the deactivation is impossible to be caused by the interaction between the two components. So, the destruction can only be due to ZnO. In the paper, XRD technique was used to investigate the interactions between USY and ZnO.

Experimental

The impregnation method was used to prepare the USY/ZnO samples with various ratios. These samples were calcined at different temperatures and then measured by a D/MAX-III A X-ray diffractometer.

Results and Discussion

Effect of ZnO contents and preparation The XRD patterns of the samples calcined for 6 hours at 500°C were shown in figure 1. When ZnO content is 40%, the characteristic peaks of ZnO ($2\theta=31.8, 34.5, \text{ and } 36.2^\circ$) are stronger, of which 36.2° is the strongest peak, and 34.5° is the weakest; the peaks of USY also can be detected though they are very faint. However, the order of the peak intensities change with the decrease of ZnO content. For 30% ZnO, the order is still $31.8^\circ > 36.2^\circ > 34.5^\circ$, while, for 20% ZnO it is $31.8^\circ > 34.5^\circ > 36.2^\circ$ and the peak at 36.2° is very weak. When the ZnO content decreases to 10%, the peaks of 31.8° and 34.5° can also be detected clearly, but the one at 36.2° almost disappears.

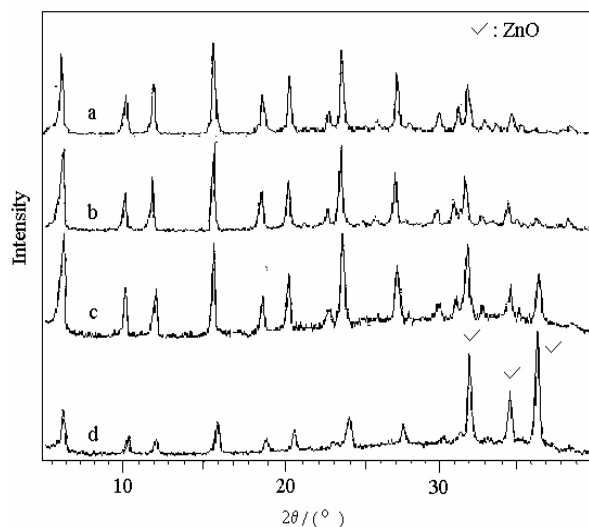


Figure 1. XRD patterns of USY/ZnO with different ratios. The contents of ZnO: a, 10%(wt); b, 20%(wt); c, 30%(wt); d, 40%(wt).

It is well known that the diffraction intensity mainly depends on the kind, number and arrangement of the atoms forming the crystal cells. In X-ray diffraction of polycrystalline, the relative peak

intensity may vary with crystal surface orientation³. If we mixed USY and ZnO with the ratio of 9/1(wt), the sequence of the characteristic peak intensity of ZnO also changes after being calcined (Fig.2). The peak intensities of 31.8° and 36.2° are very similar in the XRD pattern of sample before being calcined; however, after being calcined, the peak at 36.2° is lower than the one at 31.8° . Obviously, it is unreasonable to attribute the change to the crystal surface orientation. In our opinion, this may be caused by the strong interaction between USY and ZnO.

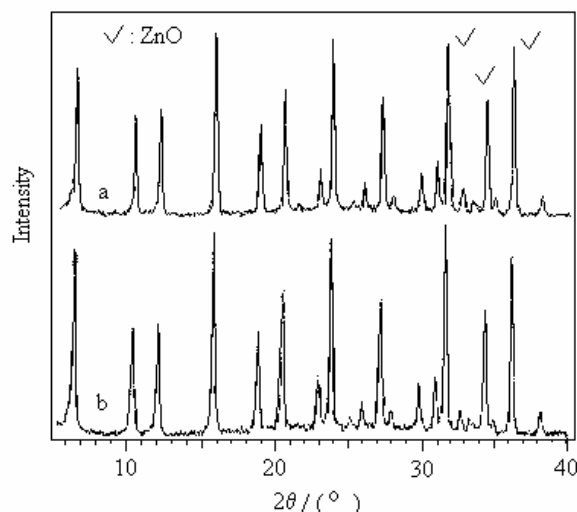


Figure 2. XRD patterns of USY/ZnO (9/1, wt.): a, mixed directly; b, sample further calcined at 500°C for 6h.

For those prepared by impregnation method, ZnO can dispersed uniformly on the USY surface, that is to say they can contact intimately. So the diffraction peaks of ZnO affected by USY seriously. At low ZnO content, there may be no large crystal particles of ZnO. Therefore, the characteristic peaks of ZnO are not the same as that of pure ZnO.

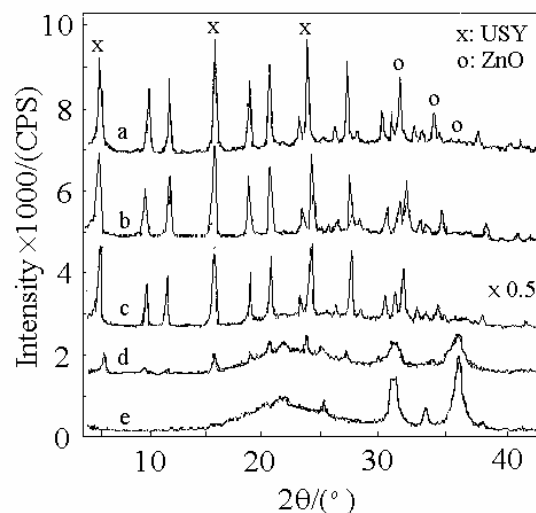


Figure 3. XRD patterns of USY/ZnO (ZnO content: 15wt%) calcined at various temperatures: a: 400°C, b: 600°C, c: 700°C, 750°C, and 800°C.

Effect of calcining temperature The XRD patterns of the ZnO/USY samples contained 15% (wt) ZnO calcined for 6 h at various temperatures were shown in **Figure.3**. Zn in the samples calcined at 400 and 600°C is present as ZnO. The characteristic peaks of ZnO weaken with temperature, and disappears completely with those of USY together in the one calcined at 800°C. This shows that some reactions between USY and ZnO take place, otherwise the crystal structure of USY is impossible to be destroyed and converts to amorphous state. We plot the peak intensities of USY (15.7°) and ZnO (31.6°) vs. calcining temperature and obtain fig.4, from which we see that USY and ZnO change according to the same trend with temperature. This proves again that the destruction of USY is caused by ZnO. In fig.4 we can also find that ZnO can not destroy USY significantly when the temperature is lower than 600°C. However, when it is higher than 650°C, the destructive effect gets more and more serious. When the temperature rises to 800°C, the peak intensity of both USY and ZnO drops to zero.

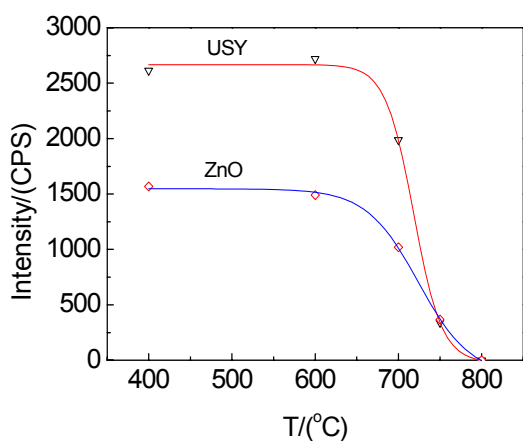


Figure 4. Trends of peak intensity of USY ($2\theta=15.7^\circ$) and ZnO ($2\theta=31.6^\circ$) with temperature.

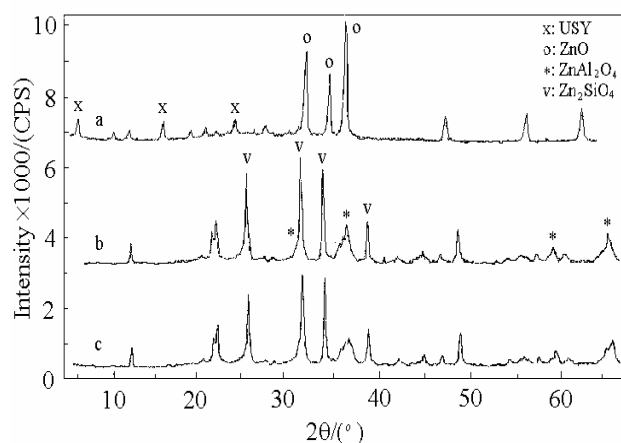


Figure 5. XRD patterns of 3/2 (wt) USY/ZnO samples. a: calcined at 700°C for 6 h, b: sample "a" further calcined at 800°C for 4 h, c: sample "a" further treated in 100% steam at 800°C for 4 h.

Destruction of ZnO to USY How ZnO to destroy the USY crystal structure has two possibilities. One is that a kind of solid-melting material forms between USY and ZnO, just like the destruction of

V_2O_5 to USY under high temperature; another is that ZnO can react with Si and/or Al of USY framework via solid phase reactions, and thus destroys the USY crystal structure. Unlike V_2O_5 , However, the melting-point of ZnO is far more 1000°C, so the possibility of form solid-melting material is very small. Thus, the destruction of ZnO to USY can only attribute to solid phase reactions between ZnO and USY.

Formation of $ZnAl_2O_4$ spinel and Zn_2SiO_4 willemite The XRD patterns of the 3/2(wt) ZnO/USY samples calcined for 6 h at various temperatures were shown in **Figure.5**. The XRD patterns of sample "a" shows USY crystal structure is not seriously destroyed under 700°C. However, sample "b" shows the characteristic peaks of USY and ZnO have been replaced by the strong peaks of Zn_2SiO_4 willemite ($2\theta=25.3,31.5,34^\circ$) and the weak peaks of $ZnAl_2O_4$ spinel ($2\theta=31.2,37.0,59.2^\circ$). In **Figure.5**, the broad peak at 31° , and the two weak peaks at 25.2° and 34° correspond to the characteristic peaks of Zn_2SiO_4 willemite; while the two broad peaks at 31° and 36.5° correspond to the characteristic peaks of $ZnAl_2O_4$ spinel, which shows that the structures of Zn_2SiO_4 willemite and $ZnAl_2O_4$ spinel have been formed in the samples calcined at 750 °C and 800°C. However the samples were calcined at 750 °C or 800°C, the peak intensity of $ZnAl_2O_4$ spinel at 36.5° is always stronger than the one of Zn_2SiO_4 willemite at 31° . Meanwhile, the peak of Zn_2SiO_4 willemite at 34° is very weak. Thus, it can be concluded that ZnO reacts preferentially with the framework Al of USY to form $ZnAl_2O_4$ spinel, and cause the collapse of the USY crystal structure. For the Si/Al ratio of USY is very high, the peak intensities of Zn_2SiO_4 willemite and are stronger than that of $ZnAl_2O_4$ spinel. Furthermore, the XRD patterns of the samples calcined and treated with steam at 800°C are all almost the same, so the interactions between ZnO and USY have no relations with the steam.

In addition, XPS results show that ZnO can react with surface of HZSM-5 zeolite, and then form $[ZnOH]^+$ ^{4,5,6}. The mechanism of the interaction between ZnO and USY maybe similar to that, ie. ZnO firstly reacts with the oxygen of Bronsted acid of USY, and formed $[ZnOH]^+$. Through the dehydration between $[ZnOH]^+$ and adjoining aluminum hydroxy at high temperature, Zn and Al can be connected by oxygen to form spinel structure. Certainly, this is just a guess, and the detailed explanations need further research.

Conclusions

Temperature is the determined factor and steam does not play a great role in the destruction of ZnO to USY. The results shows that in the USY/ZnO ZnO can capture the framework Al of USY at high temperature to form $ZnAl_2O_4$ spinel to cause the collapse of the framework of the USY zeolite, and the USY then converts to amorphous state. The alumina and silica can further react with ZnO, if it is enough, to form $ZnAl_2O_4$ spinel and Zn_2SiO_4 willemite.

Acknowledgement. The project is supported by China Petroleum and Natural Gas Stock Corporation(Contract No: 01030206)

References

- (1) Chun, Y.Li; Hong, H.S.; Bo, Y. Zhao; Chao, H. Y.; Jian, F.Z. *Acta Physico Chimica Sinica*, **2001**, 17(7), 641.
- (2) Hong, H.S.; Chun, Y.Li; Qi, M. Y.; Jun, S.Z.; Chao, H. Y.; Jian, F.Z. *Chinese J. Catal.*, **2002**, accepted.
- (3) Wan, J.Z. *Petrochemical Technology*, **2001**, 30(7), 571.
- (4) Erndt, H.; Lietz, G.; Volter, J. *Appl. Catal. A*, **1996**, 146(2), 351.
- (5) Erndt, H.; Lietz, G.; Volter, J. *Appl. Catal. A*, **1996**, 146(2), 365.
- (6) Jun, C.; Fu, X.D. *Chinese J. Catal.*, **2001**, 22(3): 229.

Evaluation of Sulfur Removal Additive for FCC Gasoline in a Recycling Fluidized-Bed Apparatus

Li Chun-Yi, Du Feng, Yuan Qi-Min, Shan Hong-Hong, Yang Chao-He, Zhang Jian-Fang

State Key Laboratory Heavy Oil Processing, College of Chemistry and Chemical Engineering, University of Petroleum, Dongying, Shandong Province, 257061 P.R. China

Introduction

SO_x is one of the most important pollutants of air. With the increase of automobile number, its pollution is more and more serious. So the developed countries promulgated rules to limit the sulfur content of gasoline stringently. In China, the sulfur content of gasoline must be equal to or less than 800 μg/g, and will be reduced greatly in the near future. Therefore, developing effective and cheap sulfur removal technologies is a very important thing.

FCC is the leading process for transforming heavy oil to light fuels. In China about 80% commercial gasoline is from FCC. Because most of FCC feeds are not pretreated, the sulfur content of FCC gasoline is far higher than catalytic reforming, isomerization and alkylation gasoline components. That is to say, the sulfur in commercial gasoline is mainly from FCC gasoline. Therefore, almost all the sulfur removal routines of gasoline, such as hydrotreating of FCC feed, hydrodesulfurization of FCC gasoline, adsorption desulfurization, etc. are aiming at FCC gasoline. In these technologies, hydrotreating of FCC feed, which operates under high temperature and pressure, is a very effective way to desulfurize, but it is also very costive; hydrodesulfurization of FCC gasoline can operate under relatively mild conditions, however, how to avoid the decrease of octane number is a difficult problem; the process of adsorption desulfurization is quite complex, and H₂ is needed to restrain coke formation in sulfide adsorption step and to regenerate the adsorbent¹⁻³.

In fact, if the sulfur content of FCC gasoline can be reduced *in situ* FCC process, it is no doubt that this will be the most convenient and cheapest technology for sulfur removal. Wormsbecher and Kim⁴⁻⁶ invented the additive for sulfur reduction of FCC gasoline which can be added into the reaction-regeneration system of FCC expediently based on the real situation to promote the cracking of sulfur compounds in the gasoline range. The maximum of sulfur reduction is about 40% compared to the sulfur content of gasoline produced without adding the additive if the additive is combined with the specially developed FCC catalyst⁷. Although the sulfur reduction percent is quite high, the highest absolute amount of sulfur removed is only about 200 μg/g. In China, the sulfur content of FCC gasoline is often higher than 1000 μg/g. Obviously, if only less than 200 μg/g sulfur can be reduced, then the technology seems useless. Therefore, we aim at the situation in China to develop the technology of sulfur removal additive of FCC gasoline.

In our previous work, we have designed the additive which includes selective adsorption site of sulfides and sulfide cracking site⁸. According to the idea we prepared USY/ZnO/Al₂O₃ additive and evaluated it in a confined fluidized bed unit for catalytic cracking experiments with VGO as the feed. The results show that the additive has excellent sulfur removal performance, and no marked effect on the product distribution was observed except for a little increase in coke yield⁹. In the paper, we will introduce the evaluation results of the additive in recycling fluidized bed reactor.

Experimental

The VGO feed was provided by Shenghua refinery. The properties of the feed have been introduced somewhere⁹.

The FCC catalyst used in the experiments is Vector 60 SL regenerated catalyst. The USY/ZnO/Al₂O₃ additive was prepared with semi-synthesis method. Firstly we mixed the Zn(NO₃)₂ and Al(NO₃)₃ solutions together, and then dripped NH₃·H₂O solution into the mixed solution with continuous stirring till to all the solution to be deposit. After filtration and washing, we dried the deposit at 120°C for 10 h, and then calcined it in a muffle at 700°C for 6 h. Crashing and screening the solid, we obtained the additive with the size 0.078~0.18mm. The BET area was determined by Nitrogen adsorption-desorption on an ASAP 2010 surface area analyzer and is 206 m²/g.

The evaluation of the additive was conducted in the recycling fluidized-bed apparatus for catalytic cracking experiments (fig. 1). The pure FCC catalyst or the mixed catalyst (the FCC catalyst/the sulfur removal additive = 7/3 (wt./wt.)) is firstly added into the system before experiments. When the temperatures of all the controlled points reach the set values and the catalyst impelled by steam can recycle normally, the steam is switched to heated feed. Thus, the catalytic cracking of the feed takes place in the riser and the coked catalyst is regenerated in the regenerator by air. In our experiments, the feeding rate was 4kg/h; the temperatures at the outlet of the riser and the regenerator were 500°C and 680°C, respectively; the catalyst/oil ratio was controlled at 5.9.

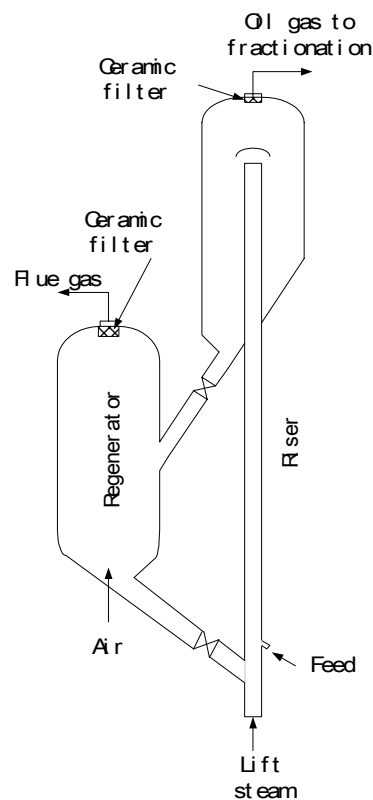


Figure 1. Schematic of FCC apparatus for experiments.

When the reaction proceeded stably, we collected the gas, liquid and flue gas for 1 h to calculate the material balance, analyze the coke, dry gas, and C₃+C₄ yields by chromatography. Gasoline and diesel are separated from the liquid product by distillation. The sulfur

content of the gasoline was determined by Micro-Coulomb method. Hydrocarbon composition and octane number of the gasoline were analyzed by HP5890.

Results and discussion

The USY/ZnO/Al₂O₃ additive was evaluated in a recycling fluidized-bed apparatus for catalytic cracking experiments with the catalyst/oil ratio of 5.9 at 500°C. The results adding 30% the additive and using pure FCC catalyst under the same conditions are listed in table 1. From the table we can see that the conversion adding 30% the additive is about 8 percent points higher than that using pure FCC catalyst because the additive is more active than the FCC catalyst, however, the sulfur content of the gasoline adding the additive is 784.3 µg/g, nearly 32% lower than that using pure FCC catalyst. Compared to the situation using the pure FCC catalyst, adding the additive can improve the yields of C3+C4, gasoline and diesel with almost the same dry gas yield, especially the yield of gasoline increases by more than 5 percent points with almost the same selectivity; the negative effect is that the yield of coke increases by 2.25 percent points.

Table 1. Comparisons of the experimental results in Riser

		30% Additive	FCC Catalyst
Condition	Temperature, °C	500	500
	Catalyst/Oil	5.9	5.9
	Residence time, s	0.90	0.91
Yield wt%	H ₂	0.48	0.26
	Dry gas	2.31	2.21
	C3+C4	14.33	13.95
	Gasoline	44.93	39.51
	Diesel	19.16	18.10
	Coke	7.25	5.01
Conversion, %		68.82	60.68
Yield of light oil, wt%		64.09	57.61
Selectivity %	Dry gas	3.36	3.64
	C3+C4	20.82	22.99
	Gasoline	65.29	65.11
	Diesel	27.84	29.82
	Light Oil	93.13	94.94
	Coke	10.53	8.26
Sulfur content µg/g	Gasoline	784.3	1150
	Coked catalyst	99.81	97.85
Sulfur reduction of gasoline, %		31.8	-

Our previous work shows that in FCC gasoline about 80% sulfides are thiophene and thiophenes with different or different number alkyls¹⁰, and the others are mercaptans, thioethers and di-sulfides. Mercaptans, thioethers and di-sulfides are easier to crack to H₂S and hydrocarbons, thiophenes, however, are relatively more difficult to desulfurize by cracking because of their stable conjugation structure. Thus, to remove thiophenes effectively, the additive must have higher activity besides its selective adsorption ability to sulfides. So that the conversion and the light oil yield are higher is what we have expected.

Moreover, all the sulfides in FCC gasoline can form coke or sulfur contained coke during cracking¹¹, however, thiophenes are

easier to form coke because of their lower H/C ratio. The experiments using pure thiophene as the feed show that thiophene can cracking to hydrocarbons and H₂S, meanwhile coke is unavoidable because the formations of hydrocarbons and H₂S need hydrogen which is from thiophene directly or indirectly¹². Benzothiophenes are even easier to form coke than thiophene for its even lower H/C ratio¹¹. Since the sulfur removal additive we prepared can adsorb and crack sulfides selectively, that the coke yield is higher is not abnormal.

Table 2. Comparisons to the hydrocarbon composition and octane number of the gasoline produced using pure FCC catalyst and adding 30% the additive.

Catalyst	Adding 30% USY/ZnO/Al ₂ O ₃	FCC Catalyst
Alkane, %	25.47	25.62
Naphthene, %	8.20	7.07
Aromatic, %	30.27	29.85
Alkene, %	35.99	37.47
RON	95.9	96.1
MON	82.2	82.4

The hydrocarbon compositions and octane numbers of the gasoline are listed in table 2. Adding the additive, we can see that in the gasoline naphthene and aromatic increase a small amounts and alkene decreases about 1.5 percent points. Obviously, the additive can not change the gasoline composition significantly. Consequently, both the RONs and MONs are almost the same in the two situations of adding and not adding the additive.

Conclusions

The USY/ZnO/Al₂O₃ sulfur removal additive for FCC gasoline has excellent sulfur removal activity. At 500°C and the catalyst/oil ratio of 5.9, the sulfur content of gasoline can be reduced more than 30% when 30% the additive is added compared to the situation using pure FCC regenerated catalyst, and adding the additive can improve the yields of C3+C4, gasoline and diesel except for about 2 percent point increase in coke yield.

Acknowledgment. This work was supported by PetroChina.

The issue number is 010302-06.

References

- Oil & Gas J., Sept. 10, 2001: 8.
- Irvine R L, Benson B A, and Varraveto D M. *NPRA Annual Meeting*, Texas, **1999**. AM-99-42.
- Greenwood G J, Kidd D, and Reed L. *NPRA Annual Meeting*, Texas, **2000**. AM-00-12.
- Wormsbecher R. F., Kim G. US Patent: 5,376,608 (**1994**).
- Wormsbecher R. F., Kim G. US Patent: 5,525,210 (**1996**).
- Cheng W.C., Kim G., Peters A.W., Zhao X., and Rajagopalan K. *Catal. Rev.-Sci. Eng.*, **1998**, **40**(1&2): 39.
- Balko J., Podratz D., Olesen J. *NPRA Meeting*, March 26-28, Texas, **2000**. AM-00-14.
- Li C. Y., Shan H. H., Zhao B. Y., Yang C. H., Zhang J. F. *Acta Physico Chimica Sinica*, **2001**, **17**(7): 641.
- Shan H. H., Li C. Y., Yuan Q. M., Zheng J. S., Yang C. H., Zhang J. F. *Chinese J. Catal.*, **2002**, **23**(3): 245.
- Shan H. H., Li C. Y., Zhao B.Y., Du F., Yang C.H., Zhang J.F. *J. Uni. Petro.*, **2001**, **25**(6): 78.
- Pang X.M., Li C.Y., Shan H.H., Zheng J.S., Yang C.H., Zhang J.F., Li S.B. *J. Uni. Petro.*, **2002**, accepted.
- Shan H.H., Li C.Y., Zhao H., Yang C.H., Zhang J.F. *J. of Fuel Chemistry*, **2001**, **29**(6): 481.

Maximum FCC diesel yield with TSRFCC technology

Hong-Hong Shan, Wei Zhao, Chang-Zheng He, JianFang Zhang, and Chao-He Yang.

State Key Lab of Heavy Oil Processing, University of Petroleum, 271 North Second Road, Dongying 257061 P.R. China

Introduction

After a quite long time exploration, steadily heavier crude oil is becoming one of the toughest frontiers in fluid catalytic cracking (FCC) process. Almost at the same time, stringent environmental constraints also put a big pressure on FCC process to readjust its product distribution and improve its product quality.

In recent years, many upgrades and modification have been done for RFCC units. In terms of process technology, MSCC^[1], Down-Flow FCC^[2], Double-Riser FCC^[3] and Two-Stage Riser FCC^[4,5] (TSRFCC) were developed one by one. Another term is advanced by FCC equipment enhancement such as novel feed nozzle^[6], fast separating system at riser outlet^[7], high-efficiency regenerator, multi-step reactor strippers, and riser terminations, etc. Among these technologies and studies, obviously, most are merely peripheral modification around the FCC riser reactor; quite few touched the very course of FCC reaction except that MSCC and Down-Flow FCC are on the way to real industrialization.

Riser reactor, commonly applied by worldwide FCC (One-Stage Riser, OSRFCC) process, was proved that, in the second half of riser, the activity and selectivity of the catalyst drop dramatically and over-cracking of intermediate products occurs^[8], which deteriorate markedly the product distribution and final products properties. Based on this fact, a novel FCC process named TSRFCC had been invented successfully in china. The features of this new process are attributed to catalyst in relay, subsection reaction, high catalyst/oil (C/O) ratio and short residence time, through which the average activity and selectivity of the catalyst are enhanced and undesirable secondary reaction and thermal reaction are suppressed efficiently. Some former studies proved that TSRFCC process open a fairly good way to maximize gasoline yield. But under the atmosphere of insufficient supply of diesel in the worldwide market, especially in China, how to maximize diesel/gasoline ratio is a very important and urgent task. TESRFCC-I technology, a modified TSRFCC process had been studied on this paper to fulfill the task.

The Configuration and Theory of TSRFCC-I

The primary difference between TSRFCC and TSRFCC-I is that in the latter process the diesel cut produced by the first stage riser is removed from the internal products, then the rest parts of gasoline and heavy oil being injected into the second stage riser instead of overall internal products in series in the original OSRFCC process. Figure 1 shows the principle flow chart of both OSRFCC and TSRFCC processes. In the modification of commercial plants, the internal fractionating tower will be a new one or the former one.

Firstly, TSRFCC-I inherits the original features of catalyst in relay and subsection reaction to ensure oil vapor contact regenerated catalyst in both stages. Secondly, removing internal diesel produced by the first stage avoids its over-cracking in the second stage, thus maximum diesel yield can be achieved. Thirdly, removing internal diesel enhances the heavy oil conversion to light oil in the second stage, illustrated by chemical balance of catalytic cracking reaction.

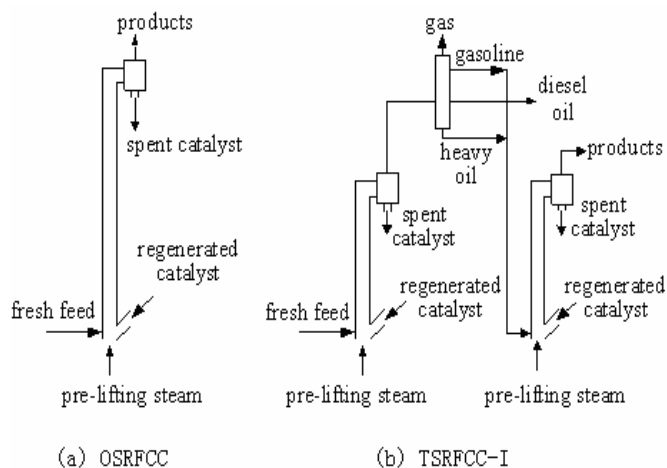


Figure 1 Comparison between OSRFCC and TSRFCC-I

Experimental

The performance of TSRFCC-I was evaluated in a pilot FCC plant^[4]. One mixture of 65wt%VR + 35wt%VGO was employed as feedstock, the properties in Table 1. Catalyst used is commercial equilibrium catalyst ZC-7300, the microactivity is 60. Gaseous products were analyzed in HP5890II and Varian GC-3800C, and liquefied products in HP5880A.

Table 1 Property and composition of FCC feedstock

Density(20°C, g/ml)		0.9205	CCR (wt%)		4.62
Group components (wt%)	saturated	52.37	Metal Content (ppm)	Fe	2.52
	aromatics	30.08		Ni	4.90
	resin	17.47		Cu	/
	asphaltene	0.076		V	0.095
element components (wt%)	H	12.67	Distillation range(°C)	0%	331
	C	85.91		10%	467
	N	0.31		20%	491
	S	0.16		30%	518

The main reaction conditions include temperature 490~520°C, the ratio of catalyst to feedstock 6, and residence time 1.5~2.2 s.

Results and Discussion

Yield Distribution Table 2 shows the product distributions of two different technologies. Compared with OSRFCC, at high conversion, TSRFCC-I showed a 6-7 percent point increase in diesel yield, accompanied by a 1.5-2 percent point increase in light oil while maintaining the same level of liquid product yield. Moreover, a 2 percent point decrease of dry gas yield was achieved. Obviously, reduced effect of thermal cracking had been confirmed as well as the yield distribution of TSRFCC-I had been markedly improved.

Table 2 Product structure of OSRFCC and TSRFCC-I

Pro. Distri. (wt%)	OSRFCC		TSRFCC	
hydrogen	0.19	0.14	0.11	0.15
dry gas	4.27	4.42	2.3	2.68
LPG	19.72	17.84	17.73	18.27
gasoline	50.07	50.47	45.11	44.86
diesel	15.15	14.13	23.44	21.87
heavy oil	4.41	5.84	3.24	3.75
light oil	65.23	64.6	68.56	66.73
coke	6.38	7.30	8.17	8.57
liquid product yield*	84.94	82.44	86.29	85
Conversion**	95.59	94.16	96.75	96.25

* Liquid product yield = LPG + gasoline + diesel

** Conversion = (100 - heavy oil)%

It is commonly believed that dry gas is produced by thermal cracking abiding by free radical mechanism. In the second half of conventional riser with 3 second above residence time, oil vapor can't fully contact acid sites due to deposited coke on the catalyst, so high temperature increases thermal cracking dramatically and quickly, as a result, increasing dry gas yield appears. In the course of TSRFCC-I, at the outlet of first stage riser oil vapor is separated with the deactivation catalyst in time before impending increasing thermal cracking, then injected into the second stage to contact with the regenerated catalyst exhibiting great accessibility of active sites. Consequently, thermal cracking was reduced radically and dry gas yield was minimized accordingly.

In the term of diesel, TSRFCC-I showed a 6-8 percent point increase compared with OSRFCC at similar conversion. It can be explained by two reasons. Firstly, removing internal diesel as final product prevent it from over-cracking in the second stage. Secondly, a great amount of active sites on the catalyst in the second stage cater for the heavy oil cracking well, which make speed of diesel producing surpass cracking. Diesel yield and diesel/gasoline ratio can therefore be maximized, which satisfies the changing trend of marketing structure.

Light oil yield in TSRFCC-I is 1-2 percent point higher than that in OSRFCC at highly extended conversion while keeping sound yield structure. Even though gasoline yield is relatively low in TSRFCC-I via cracking twice, the increase of diesel yield compensate the decrease of light oil for the loss of gasoline yield excessively.

As far as coke is concerned, the relatively high yield may be related to the hydrocarbons entrapped in the pores of the catalyst and carried through the inefficient stripping. This situation will be improved in FCC commercial unit.

To fully utilize TSRFCC-I technology, an optimum internal conversion must be controlled. Inappropriate internal conversion will definitely break the balance of two stages and deteriorate the course of reaction in whichever stage unavoidably, so the overall product structure is doomed to get worse. Numerous experiments proved that an optimum internal conversion must be chosen at the point where the high yield and selectivity of light oil in first stage was obtained and catalysis of catalyst dropped evidently. Only by doing so, two stages can run effectively and intimately.

Product Properties Data concerning the composition of LPG are shown in Table 3. The total yields of propylene and butylenes in TSRFCC-I are 85wt% above, versus 81wt% below in OSRFCC, higher 4 percent point. Higher light olefin yield in FCC unit is compatible with the trend of increasing demand of petrochemical feedstock.

Table 3 C₃ and C₄ olefins contents (wt%) in LPG

Olefin	OSRFCC		TSRFCC	
C ₃	33.56	34.56	40.15	37.70
C ₄	47.27	40.83	47.23	47.49
Total olefin	80.84	75.39	87.38	85.20

Used feedstock, a kind of paraffin-rich oil, is potentially efficient to produce smaller olefins by catalytic cracking leading to higher olefin content in FCC gasoline. This explains why gasoline produced by paraffin-based crude is generally unqualified for the environmental regulations. At the same conversion, gasoline in TSRFCC-I, compared with OSRFCC, gives a similar content of n-paraffins, an increase of i-paraffins, a considerably deduction of olefins as well as an increase of octane number. The composition data of gasoline are present in Table 4.

Table 4 Gasoline composition of OSRFCC and TSRFCC-I (wt%)

Items	OSR1	TSR1	OSR2	TSR2	OSR3
Conversion	80	96.56	76.27	96.75	95.78
n-paraffin	5.58	5.40	5.36	5.42	5.11
i-paraffin	23.65	28.12	25.79	29.90	24.00
naphthene	7.79	8.07	8.00	7.65	6.34
aromatic	18.86	25.45	16.82	18.75	19.02
olefin	44.31	33.13	44.09	38.29	45.47
RON	90.9	94.2	90.9	93.2	93.2
MON	78.0	80.8	78	80.0	80.0
Anti-knock index	84.4	87.5	84.4	86.6	86.6

The feed is nearly converted completely in the present of catalyst via two stages. Employing regenerated catalyst and higher C/O ratio brought by subsection reaction in the second stage increase the amount of accessible active sites, which would lead to more hydrogen transfer, so more gasoline olefins would be saturated, otherwise, the probabilities of isomerization and aromatization also increased, as a result, the gasoline olefinicity went down significantly. Higher octane numbers of increased aromatics and i-paraffins than decreased olefins account for the little enhancement of gasoline octane numbers.

Conclusions

The novel TSRFCC-I process (vs. OSRFCC) has a great impact on yield structure, conversion and products properties. Removing diesel cut from internal products boosts overall conversion, maximizes the production of diesel and diesel/oil ratio, minimizes the content of olefins in gasoline, and improves the qualities of LPG and gasoline. Due to the unique configuration of TSRFCC-I process, maximizing the profitability of FCC units will become possible in the near future.

Acknowledgement. This work was Supported by the PetroChina.

References

- Chang, T., Louisiana Refinery Revamp Takes Advantage of Heavy Sour Margins. *Oil & Gas J.*, **96**(45), 68-72(1998).
- Ren-sheng Deng, Teng-fei Liu, Fei Wei, Yong Jin, Composition of the Process in Riser and Downer Reactors, *Chemical Reaction Engineering and Technology*, **17**(3), 238-243(2001).
- Hai-tao Tang, Research and Development of Flexible Multi-Functional FCC process, *Petroleum Refinery Engineering*, **31**(6), 8-10(2001).
- Jian-fang Zhang, Hong-hong Shan, Zheng Li, Gen-lin Niu, Yu-dong Sun, New Development of FCC Through Two-staged Riser in Series. I. The Reactor of Two-staged Riser, *ACTA PETROLEI SINICA(PETROLEUM PROCESS SECTION)*, **16**(5), 66-69(2000).
- Zheng Li, Jianfang Zhang, Honghong Shan, Zhongxiang Han, Feng Du, Development of Two-stage Riser FCC Technology II. Increase of The Light Fraction Yield and Decrease of The Olefins Content in Gasoline, *ACTA PETROLEI SINICA(PETROLEUM PROCESS SECTION)*, **17**(5), 26-29(2001).
- Zhouping Lai, High-efficiency Feed Nozzle for RFCC unit, *Petro-chemical Equipment Technology*, **17**(5), 15-18(1996).
- Zhanyou Cao, Votex Type Fast Separation System at FCCU Riser Outlet, *Petroleum Refinery Engineering*, **28**(3), 14-18(1999).
- Jun-wu Chen and Han-chang Cao, *Catalytic Cracking Technology and Engineering*, SINOPEC Press, 1991.
- Xiang-yu Li, Market Analysis and Forecast to Diesel, *Shanghai Chemical Industry*, (1), 31-34(2001).

Cracking behavior of MCM-22, ZSM-5 and Beta as FCC catalyst additives

Liu Zhongqing, Fu Jun, He Mingyuan and Li Minggang

Research Institute of Petroleum Processing,
Beijing, China, 100083

1 Introduction

To meet the production of the different commercial and increasingly stringent environmental demands, FCC as an important gasoline producing unit will point to decreased sulfur, to maximize the octane barrel while keeping a good output, and to be flexible enough to increase the production of valuable C₃~C₅ olefins and isobutene, which are desired for producing oxygenates and alkylated gasoline. It is difficult to accomplish all these goals with a simple catalyst formulation, and one may oversee the possibilities of using, besides Y, other zeolites, either as the main active components or as catalyst additives. In order to explore good FCC catalytic materials, other than ZSM-5 and Y, researchers have investigated zeolites, such as, Beta and Omega^[1,2,3] as FCC catalyst additives. MCM-22 zeolite, with nonconnected 10 and 12 member ring channels, may play an important role in the multi-function of FCC catalyst.

It was reported in the open literature^[4,5] that the behavior of MCM-22 in catalytic cracking of pure paraffins is between 10 member ring zeolites, such as ZSM-5, and 12 member ring zeolites, such as Beta. Corma et al^[6] compared the behavior of MCM-22 zeolite with that of ZSM-5 zeolite as FCC catalyst additives. It is found that MCM-22 produces less total gases, as well as less dry gases, with a lower loss of gasoline than ZSM-5, in the line of the claims in Mobil patents^[7,8].

In the present work we have studied the catalytic cracking of a FCC feedstock on a FCC catalyst with MCM-22 as an additive, and the results are compared with those obtained on ZSM-5 and Beta additives respectively. The influence of pore geometry on cracking parameters such as the hydrogen transfer coefficient (HTC), and the cracking mechanism ratio (CMR) is also discussed.

2 Experimental

2.1 Materials

The zeolites used were Beta, ZSM-5 and MCM-22. The former two were provided by RIPP (Research Institute of Petroleum Processing), and the latter was synthesized in the lab^[9]. The parent zeolites were subject to steam treatment at 1 atmosphere of steam and 800°C for 4h. The characteristics of the zeolites used in this work are given in Table 1.

The base FCC catalyst used was CC-16, which used USY as the main active cracking component, and did not contain an additive, a commercial FCC catalyst produced by Changling Catalyst Corporation. The base catalyst was also steamed at 1 atmosphere of steam and 800°C for 4h, then mixed with the steamed zeolites Beta, ZSM-5 and MCM-22, respectively. The percentage of the zeolite over the total catalyst was 8wt%. All catalysts were palletized, crushed, and sieved, a 0.59 to 0.84 mm diameter fraction was taken.

2.2 Reaction procedure

The feedstock, a vacuum gasoil mixed with a vacuum resid by 30wt%, whose characteristics were given in Table 2, has been cracked in a down flow MAT unit, which has been designed to accomplish the ASTM D-3907 standard. Catalyst loading was always

5 grams. All reactions were carried out at 500 °C, and a time-on-stream of 60 seconds. In order to get different conversion levels, different catalyst-to-oil ratios were obtained by changing the amount of feedstock. The liquid products were collected in a glass receiver located at the exit of the reactor, which was refrigerated in a water-ice bath. Meanwhile, the gaseous products were collected in a gas buret by water displacement. Coke was determined in-situ by combustion in an air stream at 600°C for 1h and monitoring the CO₂ formed by means of an IR cell. Gases were analyzed by GC. Liquid products were analyzed by simulated distillation.

3 Results and Discussion

In Fig1 the total conversion and selectivities are given for different catalyst-to-oil ratios and therefore, for different conversion levels, at 500 °C of reaction temperature and 8wt% of steamed additive over the total catalyst. The results (Fig1a) show that, at the same catalyst-to-oil ratios, the catalyst with MCM-22 additive has the lowest activity among all the catalysts, and even lower than the base catalyst which does not contain an additive. The data in Table 1 indicate that MCM-22 is a hydrothermal stable zeolite both in the case of structure and acidity, so the lower activity may be attributed to the limitations of diffusion of the large molecules in the feedstock through the two-dimensional 10 member ring windows in MCM-22 crystal. In Fig1, the results also show that MCM-22 additive yields more gasoline, LCO and coke, less gases comparing with ZSM-5, and less gasoline and LCO, more coke and gases comparing with Beta, in accordance with the open literature^[6,7,8]. These indicate that the cracking behavior of MCM-22, which contains both 10 and 12 member ring channels, is between that of ZSM-5, which only contains 10 member ring channels, and Beta, which only has 12 member ring channels.

The ratio of C₄⁰/C₄⁼ observed in the gas products were defined as the hydrogen transfer coefficient (HTC), which reflects the hydrogen transfer activity of a catalyst^[10]. In Fig2a, the results show that the HTC for MCM-22 is the largest, then, Beta, and ZSM-5 is the smallest among the three zeolites. These indicate that the hydrogen transfer activity of the three zeolites is: MCM-22>Beta>ZSM-5. In addition, the olefinicity of the gas products also can reflect the hydrogen transfer activity of a zeolite. In Fig2b, the C₃⁼/Total C₃ ratio is in the following order: ZSM-5>Beta>MCM-22, in agreement with the conclusion reached from the analysis of the HTC, that is, the hydrogen transfer activity of MCM-22 is even higher than Beta, which has 12 member ring channels. The reason may be that it is ease to occur hydrogen transfer reaction of the molecules of products in the 12 member ring super cages of MCM-22, which have 10 member ring apertures, since the molecules of cracking products are difficult to diffuse through the 10 member ring windows. The results we got are in agreement with that in the Mobil patents^[7,8], but Corma^[6] et al found that the C₃⁼/C₃⁰, C₄⁼/C₄⁰ ratios are higher for MCM-22 than for ZSM-5, and they suggested the reason may be that there is a relatively low amount of framework Al content in the super cages of MCM-22.

The cracking mechanism ratio (CMR), which is defined as the ratio of dry gases (methane, ethane, and ethylene) to isobutane in the gas products, is used to measure the ratio of monomolecular to bimolecular types of cracking, since C₁ and C₂ are typical products from protolytic cracking, while iC₄ is a typical product formed by β-scission of branched products^[11,12]. The results from Fig2c show that the CMR is largest for ZSM-5 among the three additives, the CMR for MCM-22 is little larger than that of Beta, and far smaller than that of ZSM-5. These indicate the ratio of protolytic to β-scission cracking occur on zeolites in the following order:

ZSM-5>MCM-22>Beta, and also indicate that the 12 member ring cavities, which, is half of the supercages of MCM-22, opened to the exterior, at the end of the crystal platelets of MCM-22, play a more important role in the catalytic cracking reaction than the 10 member ring channels of MCM-22.

4 Conclusions

When MCM-22, ZSM-5, and MCM-22 use as FCC catalyst additive respectively, in agreement with their structure, MCM-22 yields more gasoline, LCO and coke, less gases comparing with

ZSM-5, and less gasoline and LCO, more coke and gases comparing with Beta. The hydrogen transfer activity of MCM-22 is higher than that of ZSM-5 and Beta; while the cracking mechanism ratio (CMR) of MCM-22 is much lower than that of ZSM-5, little larger than that of Beta, which means that the 12 member ring cavities on the crystal surface of MCM-22 play an important role in the catalytic cracking reaction. The performance of MCM-22 in catalytic cracking reaction is between that of ZSM-5 and Beta, and close to that of Beta.

Table 1 Physicochemical Characteristics of the Zeolites

Zeolites	S_{BET} / m^2/g	$\text{SiO}_2/$ Al_2O_3	$V_{\text{micro}}/$ ml/g	$\text{NH}_3\text{-TPD}$ acidity / mmol/g	Pyridine adsorbed acidity (200°C) / $\mu\text{mol}/\text{g}$			
					Brönsted	Lewis	B+L	
Fresh Samples	MCM-22	572	27	0.202	1.092	61.0	9.5	70.5
	ZSM-5	397	32	0.162	1.074	91.5	7.1	98.6
	Beta	610	30	0.229	1.220	54.2	20.2	74.4
Steamed Samples	MCM-22(S)	486	27	0.161	0.207	37.3	7.1	44.4
	ZSM-5(S)	350	32	0.150	0.166	13.6	33.3	46.9
	Beta(S)	440	30	0.166	0.120	33.9	57.1	91.0

Table 2 Characteristics of the Feedstock

Density (20°C) / g/cm^3	0.8731	Refractive Index (70°C)	1.4682
Distillation Curve / °C		$v(80^\circ\text{C}) / \text{mm}^2/\text{s}$	17.56
IBP	189	Acid Number / mgKOH/g	0.07
5%	398	Conradson Carbon / wt%	0.7
10%	418	Ash Content / wt%	0.05
30%	457	Sulfur / wt%	0.12
50%	497	Nitrogen / wt%	0.11
70%	549	Carbon / wt%	86.43
90%	73.5%, 560°C	Hydrogen / wt%	13.53

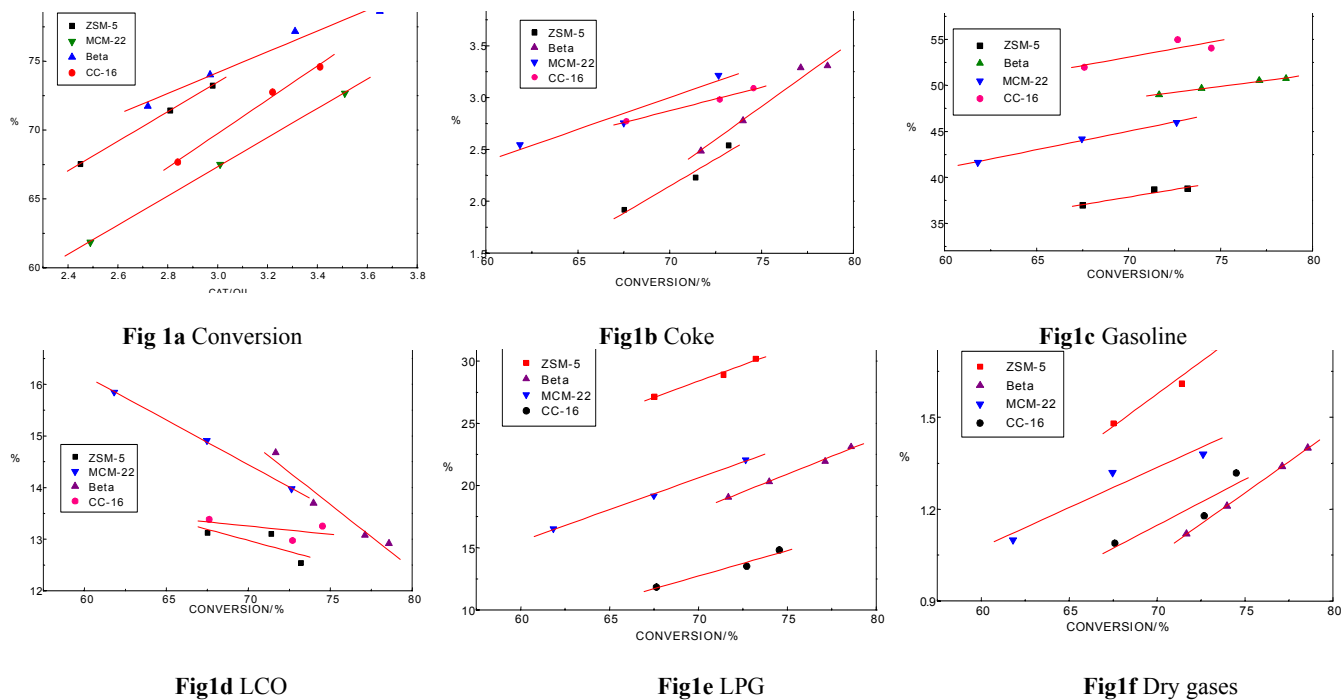


Fig 1 Total conversion and Selectivities of products in the catalytic cracking of feedstock at T=500°C, TOS=60s, and 8wt% of steamed additive

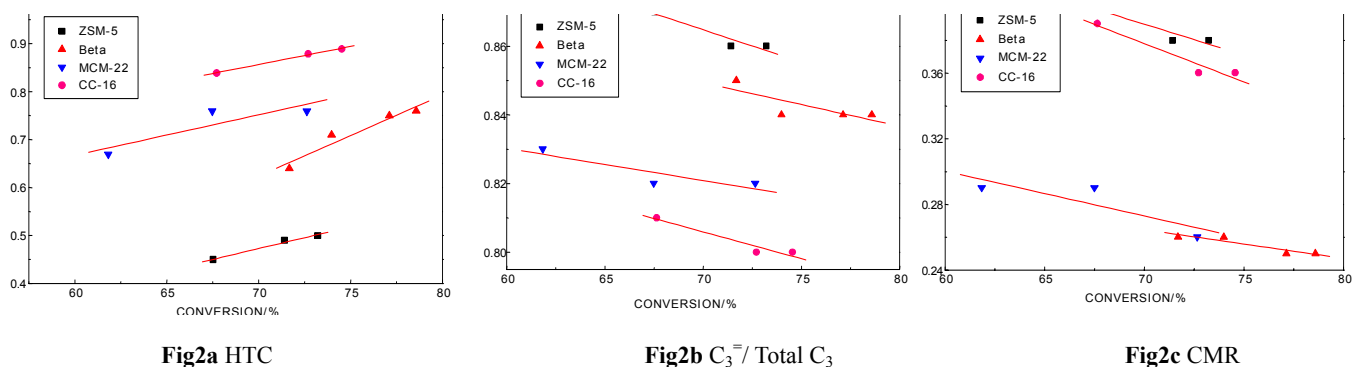


Fig 2 Ratios of interest in the catalytic cracking of feedstock at T=500°C, TOS=60s, and 8wt% of steamed additive

5 References

- Jacquinot, E. J., Raatz, F., and Macedo, A., et al., *Stud. Surf. Sci. Catal.*, **1989**, *46*, 115.
- Bonetto, L., Corma, A., and Cambior, M., et al., *Appl. Catal.*, **1992**, *82*, 37.
- Bonetto, L., Corma, A., and Herrero, E., In Proceedings 9th International Zeolite Conference. Higgins, J. B., and Treacy, M. M. J., eds., Montreal, 1992; Vol 2. pp. 369.
- Corma, A., Davis, M., Fornes, V., et al., *J. Catal.*, **1997**, *167*, 438.
- Corma, A., Alfaro, V. G., Orchilles, A. V., *Appl. Catal. A*, **1995**, *129*, 203.
- Corma, A., Triguero, J. M., *J. Catal.*, **1997**, *65*, 102.
- Absil, R. P. L., Angevine, P. J., Bundens, R. G., et al., *US 4983276*, 1990.
- Absil, R. P. L., Angevine, P. J., Bundens, R. G., et al., *US 5039640*, 1990.
- Liu, Z. Q., Wang, Y. M., Fu, J., He, M. Y., *Chin. J. Catal.*, **2002**, *23(5)*, 439.
- Zhu, H. Y., A Dissertation for Ph. D. of RIPP, Beijing, 2001.
- Wielers A F H, Vaarkamp M, Post M F M, *J. Catal*, **1991**, *127*, 51.
- Yan, L. J., A Dissertation for Ph. D. of RIPP, Beijing, 1999.

TRANSFORMATION OF N-HEPTANE OVER HZSM-5 AND METAL/HZSM-5 CATALYSTS

Changlong Yin, Jingbing Wang, Wenyu Deng and Chenguang Liu

Key Laboratory of Catalysis, CNPC,
State Key Laboratory of Heavy Oil Processing
College of Chemistry & Chemical Engineering
University of Petroleum, Dongying, Shandong 257061, China

Introduction

Light alkanes aromatization over zeolite based catalysts is well known (1,2). It has been shown that HZSM-5 zeolite can be modified by incorporation of metal or metal oxides in order to obtain catalysts for selective hydrocarbon conversions (3-5). Activity, selectivity and stability of the catalysts for those shape selective reactions depend not only on the porous structure of the zeolite but also on the density of acid sites and their strength distribution, as well as on metal sites distribution and metal support interaction (6). The catalyst systems prepared in this way operate bifunctionally. Among the Group VIII metals, platinum and palladium supported on HZSM-5 have been widely and thoroughly investigated (7). Nickel on HZSM-5 has been found to be active in the aromatization, hydrocracking and isomerization of hydrocarbon (8-10).

In the present paper, a series of zeolite supported metal catalysts were prepared by impregnation method, the transformation of n-heptane over the catalysts was investigated

Experimental

Preparation of catalyst. A certain ratio (50:50 in this paper) of commercially available NaZSM-5 (Zhoucun, China, Si/Al atomic ratio=35) and alumina were mixed with dilute nitric acid, the mixture was then extruded into diameter 1.5mm sticks. The sample was dried in air at 110 °C for 20h, and the supports containing ZSM-5 were obtained by calcination of above dry sticks at 500°C for 6h. For sodium removal, the supports were treated with a solution of 1.0 M ammonium nitrate and then calcined at 500 °C for 4h. The ZSM-5 supported nickel catalysts were prepared using incipient wet impregnation method. A series of Ni/HZSM-5, Mo/HZSM-5 and Ni-Mo/HZSM-5 catalysts were prepared according to this method. The active components NiO and MoO₃ were deduced from nickel nitrate and ammonium molybdate, respectively. All catalysts were dried at 110 °C overnight, and then were calcined at 500 °C for 4 hr.

Characterization of the catalysts. X-ray powder diffraction analysis was carried out with a Rigaku D/max- \square A diffractometer using a graphite-filter CuK α radiation at a scan rate of 2 degrees per minute. Temperature programmed desorption (TPD) experiments were conducted on a self-installed TPD/TPR combined apparatus. About 0.1g of sample was placed in a stainless tubular reactor with inner diameter of 6mm. The sample was treated in a flow of ultra-pure nitrogen at a flow rate of 30ml/min at 150°C for 2h to remove the impurity absorbed on the surface of samples. The reactor was cooled down to 50°C and then NH₃ was pulsed into the system until the saturation of adsorption of NH₃ was reached at this temperature. The flow of nitrogen was kept for another 2h at 50°C in order to obtain a high quality base line. Then the reactor was heated from 50°C to 540°C at a rate of 8°C/min, holding at 540°C for 60min. The gas evolved during each TPD run was detected with a thermal conductivity detector (TCD) and recorded by computer. The final Na

content in the catalyst after ammonium nitrate treatment and the Ni and Mo contents in the catalysts were determined with atomic absorption spectrometry method.

Catalyst activity. Catalytic activity measurements were carried out in a high pressure micro-reactor unit of 10 mm I.D., 40cm in length. 10 ml of the catalyst extrudates were loaded in the reactor. For reduction process, the catalyst is reduced in H₂ atmosphere for 3 hours at 360°C (for Ni/HZSM-5) or 500°C (for Mo/HZSM-5 and Ni-Mo/HZSM-5). Pure n-heptane is then fed at test temperature. The reaction conditions are reaction pressure, 0.2~1.0MPa, H₂/feed ratio, 150, and LHSV, 2h⁻¹. The reaction product was cooled and separated into gaseous and liquid products in a high-pressure separator. The gaseous products in this test were not analyzed, and the PIONA compositions of the liquid products were analyzed using a Varian 3800 gas chromatography equipped with a FID detector and a 100m-quartzose PIONA column.

Results and Discussion

Catalysts Characterization. The X-ray diffraction pattern of the support with 50% HZSM-5 content was completely matched with that of the pure HZSM-5, the Ni/HZSM-5, Mo/HZSM-5 and Ni-Mo/HZSM-5 catalysts' XRD patterns exhibit almost identical intensity of the peaks with HZSM-5 except some NiO and MoO₃ peaks occurring in the latter's. The final Na contents in the 50% HZSM-5 support is 0.066%; the Ni content in Ni/HZSM-5 catalyst is 7.1%; the content of Mo in Mo/HZSM-5 is 6.8%; the contents of Ni and Mo in Ni-Mo/HZSM-5 are 7.6% and 2.1%, respectively.

The spectrums of NH₃-TPD from HZSM-5(50%), Mo/HZSM-5 and Ni-Mo/HZSM-5 were shown in figure 1. It was reported (11) that according to the desorption temperature on NH₃-TPD profile, the acid sites were classified as weak (<300°C), medium (300~450°C) and strong (450~550°C). It was indicated from the results that the acid sites distribution of the Mo/HZSM-5 and Ni-Mo/HZSM-5 changed after the metal incorporation in HZSM-5, the medium and strong acid sites in the catalysts weakened due to the effect of Ni and Mo.

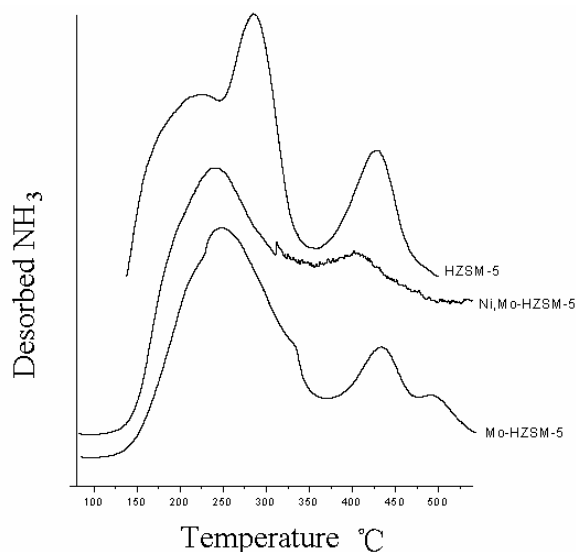


Figure 1. Temperature-programmed desorption spectrums of NH₃ from HZSM-5, Mo/HZSM-5 and Ni-Mo/HZSM-5

Effect of hydrogen pressure and reaction temperature.

Effect of hydrogen pressure on the conversion of n-heptane and aromatics selectivity over Ni/HZSM-5 catalyst was shown in figure 2. The conversion of n-heptane increases with the enhancement of the hydrogen pressure, but the aromatics selectivity of the product decreases with the raising of the hydrogen pressure, which indicating that low hydrogen pressure can promote the production of aromatics. It is well known that low hydrogen pressure is in favor of dehydrogenation, while the dehydrogenation of n-heptane produces the aromatics. Figure 3 illustrates the effect of reaction temperature on the aromatics selectivity over Mo/HZSM-5 and Ni-Mo/HZSM-5 catalysts. Aromatics selectivities of the two catalysts increase with the elevation of the reaction temperature, but Ni-Mo/HZSM-5 catalyst shows higher aromatics selectivity than that of Mo/HZSM-5 at 380~400°C. There is a general acceptance (12) that the major role of the metal in the catalyst is to accelerate the combination of surface hydrogen, which formed from the dehydrogenation and dehydrocyclization process involved as key steps in the conversion of alkanes to aromatics via alkenic intermediates. The Ni-Mo may have a more marked tendency to accelerate the combination of surface hydrogen than the Mo in the catalyst, so the aromatics selectivity of the Ni-Mo/HZSM-5 catalyst is higher than that of Mo/HZSM-5. The relatively less medium and strong acid sites in Ni-Mo/HZSM-5 than in Mo/HZSM-5 is potentially related to the higher aromatization activity of the former.

Effect of metal component. The detailed products selectivity from n-heptane over HZSM-5, Mo/HZSM-5, Ni/HZSM-5 and Ni-Mo/HZSM-5 catalysts was summarized in Table 1. Under the same reaction conditions, Mo/HZSM-5 and Ni-Mo/HZSM-5 show higher conversion of n-heptane than the rest two catalysts. The aromatics selectivity increases with the order of HZSM-5, Mo/HZSM-5, Ni/HZSM-5 and Ni-Mo/HZSM-5. The Ni-Mo catalyst gives the highest aromatics selectivity 54.89, while the aromatics selectivity of the HZSM-5 is only up to 25.53. The relatively high percent ratios of paraffin and iso-paraffin in the products achieved from n-heptane over above four catalysts indicates that cracking of n-heptane occurring in the reactions. From the results it can be found that about 60% of n-heptane was cracked over HZSM-5 and only 20% of the feed was changed into aromatics. While only 30% of n-heptane was

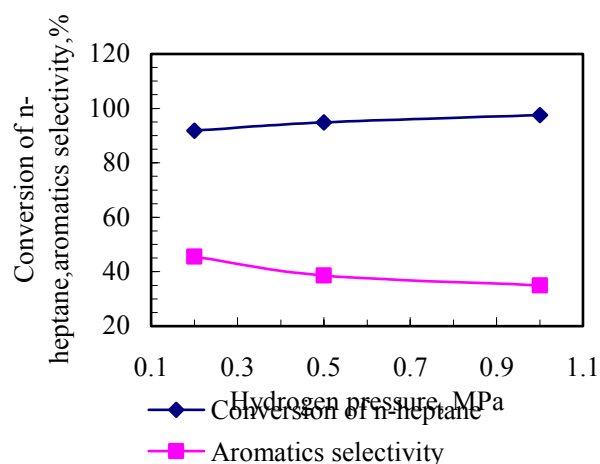


Figure 2. Effect of hydrogen pressure on the conversion of n-heptane and aromatics selectivity over Ni/HZSM-5 catalyst. Temperature 380°C, H₂/feed ratio, 150, and LHSV, 2h⁻¹.

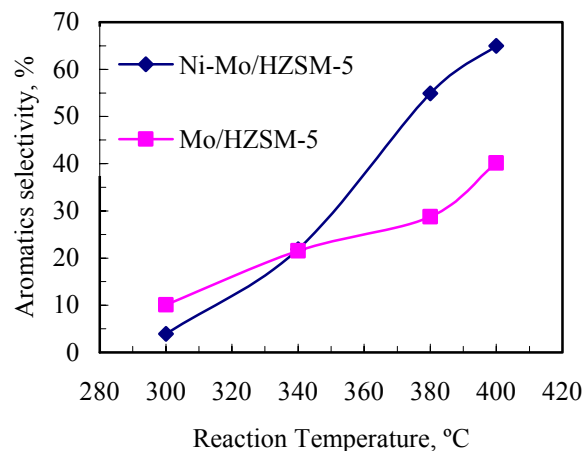


Figure 3. Effect of reaction temperature on the aromatics selectivity over Mo/HZSM-5 and Ni-Mo/HZSM-5 catalysts. Hydrogen pressure, 0.2MPa, H₂/feed ratio, 150, and LHSV, 2h⁻¹.

cracked over Ni-Mo/HZSM-5 and above 50% of the feed was changed into aromatics. The cracking of alkanes is related to the acidic sites on the catalyst; the incorporation of Ni-Mo on the HZSM-5 has weakened the medium and strong acidic sites on the HZSM-5, which depressed the cracking of n-heptane over the catalyst. The cracking of n-heptane over Mo/HZSM-5 and Ni/HZSM-5 was also restrained and the aromatics selectivity of the two catalysts was higher than that of HZSM-5 but lower than that of Ni-Mo/HZSM-5. The group components of the products from n-heptane over Ni-Mo/HZSM-5 with the reaction temperature were illustrated in figure 4. The results reveal that n-heptane was mainly cracked over Ni-Mo/HZSM-5 at low reaction temperature (<300°C), and at high temperature n-heptane was mainly aromatization over the catalyst. A few of olefin and naphthene were detected in the products of n-heptane over above tested catalysts, which can be thought of reasonably as the intermediate products of the dehydrogenation and dehydrocyclization processes.

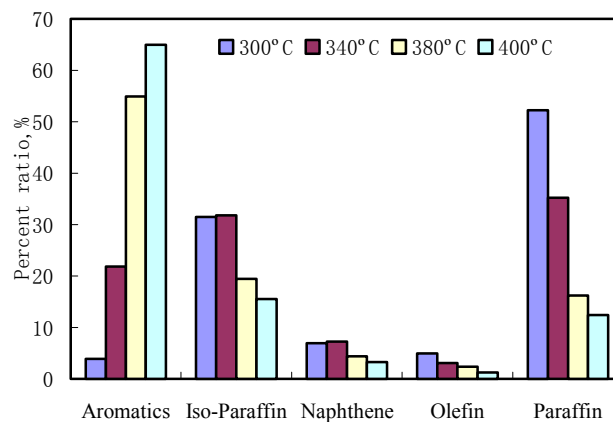


Figure 4. Products distribution from n-heptane over Ni-Mo/HZSM-5 with different reaction temperature. Hydrogen pressure, 0.2MPa, H₂/feed ratio, 150, LHSV, 2h⁻¹.

Table 1. Products Selectivity from n-heptane over Different Catalysts

Catalysts	HZSM-5	Mo	Ni	Ni-Mo
Conversion,%	90.2	95.7	91.8	96.4
Selectivity,%				
Aromatics	25.53	28.71	45.51	54.89
C6	2.44	2.20	4.50	3.88
C7	9.19	10.66	17.67	22.10
C8	9.73	11.30	17.20	21.60
C9	3.50	4.02	4.37	5.55
C10+	0.66	0.54	1.77	1.76
Iso-paraffin	37.22	36.41	27.78	19.43
C4	11.56	6.30	6.33	3.75
C5	17.13	15.05	11.18	7.10
C6	6.23	8.69	5.33	4.63
C7+	2.3	6.38	4.96	3.95
Naphthene	2.67	2.49	2.39	4.39
C6	0.62	0.10	0.40	0.88
C7	1.55	2.19	1.36	2.70
C8	0.12	0.05	0.11	0.24
C9	0.00	0.00	0.00	0.04
C10+	0.38	0.15	0.52	0.53
Olefin	1.23	0.78	1.18	2.39
C4	0.19	0.41	0.09	0.19
C5	0.24	0.32	0.18	0.39
C6	0.34	0.05	0.32	0.85
C7+	0.47	0	0.59	0.97
Paraffin	33.13	29.54	20.15	16.20
C3	2.71	1.39	3.00	2.23
C4	20.63	12.55	10.68	6.91
C5	8.07	12.87	4.89	5.40
C6	1.72	2.73	1.58	1.57
C7+	0.00	0.00	0.00	0.10
Unidentified	0.22	2.06	2.99	2.70

Hydrogen pressure, 0.2MPa, H₂/feed ratio, 150, and LHSV, 2h⁻¹

Conclusions

The reaction of n-heptane over Ni/HZSM-5, Mo/HZSM-5 and Ni-Mo/HZSM-5 bifunctional catalysts was mainly Low hydrogen pressure can reduce the conversion of n-heptane but at the same time accelerate the production of aromatics. Experimental results show that the aromatization activity of the catalysts increases with the elevation of the reaction temperature and the incorporation of metal in HZSM-5 decreases the cracking reaction on the catalysts, while at the same time increases the reactions that may result in the production of aromatics, i.e. dehydrogenation and dehydrocyclization.

Acknowledgement. Financial support from PetroChina Corporation Limited is greatly appreciated.

References

- (1) C. P. Nicolaides; N. P. Sincadu; M. S. Scurrell. *Catal. Today*. **2001**, 71, 429
- (2) J. A. Biscardi; E. Iglesia. *J. Catal.* **1999**, 182, 117
- (3) D. Seddon, *Catal. Today* **1990**, 6(3), 351
- (4) Y. Ono, *Catal. Rev. -Sci. Eng.* **1992**, 34(3), 179
- (5) M. Guisnet; N. S. Gnep; F. Alario. *Appl. Catal. A* **1992**, 89, 1
- (6) R. J. Taylor; R. H. Petty, *Appl. Catal.* **1994**, 119, 121
- (7) S. Uemiya; I. Koike; E. Kikuchi, *Appl. Catal.* **1990**, 65, 143
- (8) D. Sun; Z. Zhao, *Ind. Eng. Chem. Res.* **1991**, 76, 171
- (9) C.V.V. Satyanarayana; D. K. Chakrabarty, *Appl. Catal.* **1990**, 66, 1
- (10) T. Inui; Y. Makino; F. Okazumi; S. Nagano; A. Miyamoto. *Ind. Eng. Chem. Res.* **1987**, 26, 647
- (11) J. R. Grzechowiak; J. Rynkowski, *Catal. Today*. **2001**, 65, 225-231
- (12) J. A. Biscardi; G. D. Meitzner; E. Iglesia. *J. Catal.* **1998**, 179, 192

CHEMICAL STRUCTURE CHANGE OF RECYCLING VACUUM BOTTOM RESIDUE FROM SLURRY-BED HYDROCRACKING OF KARAMAY ATMOSPHERIC RESIDUE IN THE PILOT PLANT

Bin Shi, Guohe Que

State Key Laboratory of Heavy Oil Processing, College of Chemistry & Chemical Engineering, University of Petroleum, Dongying, Shandong 257061, China, shibin@hdpu.edu.cn

INTRODUCTION

Since the early 1980s, slurry-bed hydrocracking of residue has been developed for upgrading poor-quality residue, which may be high content of sulfur, metal and Conrason carbon residue, to produce distillate product(1). Conventionally slurry bed hydrocracking of residue is achieved by once-through heating residue in a high-pressure hydrogen atmosphere in the presence of a dispersed and disposable catalyst (2). However, once-through hydrocracking mode dependent on different reaction conditions can give 60%~80 % conversion (<524°C). To achieve higher conversion of residue and keep coke formation low and the operation successful at the same time, some hydrocracking modes can be adopted such as cracked vacuum residue recycling, cracked atmospheric residue recycling and cracked vacuum gas oil recycling. Generally cracked atmospheric residue recycling model can achieve higher conversion and get more distillate products than the other three models at the same reaction conditions. The objective of this study is to investigate chemical structure change of cracked atmospheric residue recycling from slurry-bed hydrocracking and to evaluate the subfractions change in the cracked atmospheric residue recycling.

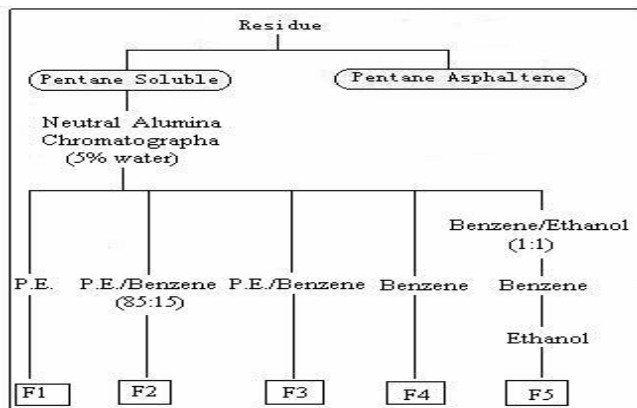
EXPERIMENTAL

The feed was chosen as Karamay atmospheric residue and obtained from Karamay Petrochemical Complex, Xingjiang, China. The property of Karamay atmospheric residue (>360°C) and its vacuum residue (>500°C) was presented in Table 1. Keeping the total VSHL is 1h⁻¹, Karamay atmospheric residue was hydrocracked in the presence of about 1000 ppm multi-metal dispersed catalyst, under 10MPa H₂, 445 °C, in a pilot plant of 120 kg/d and the products were fractionated into gases, naphtha (C₅~180°C), AGO (180~360 °C) and atmospheric bottom residue (>360°C). Some atmospheric bottom residue (about 5wt%) was thrown off, and the other atmospheric bottom residue was pumped back intermittently and mixed with the fresh feed for recycled hydrocracking (the ratio is 1:1). Thus we can obtain non-recycled atmospheric bottom residue, which is the once-through atmospheric bottom residue (ABR#), the first-time recycled atmospheric bottom residue (first-ABR), the second-time recycled atmospheric bottom residue (Sec-ABR), the third-time recycled atmospheric bottom residue (Third-ABR). The atmospheric bottom residues(>360°C) were distilled into the corresponding vacuum bottom residues(>500°C), which include fresh VBR(VBR#), the once-through vacuum bottom residue (VBR#), the first-time recycled vacuum bottom residue(first-VBR), the second -time recycled vacuum bottom residue(Sec-VBR), the third-time recycled vacuum bottom residue(Third-VBR) and these VBRs were precipitated using n-pentane. The pentane-solubles were separated into fraction 1 (mixture of saturates, light and middle aromatics), fraction 2 (heavy aromatics), fraction 3(light resins), fraction 4 (middle resins) and fraction 5 (heavy resins) by the alumina chromatography column with 5% water. The separation scheme is shown in Figure1. The

contents of H, C and average molecular weights of all subfractions were determined by Shimadzu Element Analyzer and Knauer analyzer by VPO, respectively. Structural parameters of fractions for all VBRs were calculated based on Density Method and the calculation program was shown in the appendix (2).

Table 1. Properties of Karamay atmospheric residue and Karamay Vacuum Residue

Sample	AR	VR
Density, d ₄ ²⁰	0.9442	0.9613
Viscosity (100°C), mm ² ·s ⁻¹	109	1115
Molecular weight (VPO)	470	950
CCR, wt%	7.0	11.0
C, wt%	86.6	87.1
H, wt%	12.5	11.9
H/C atomic Ratio	1.73	1.62
N, wt%	0.13	0.63
S, wt%	0.13	0.24
Ni, ug·g ⁻¹	11.8	21.6
V, ug·g ⁻¹	0.35	0.65
Ca, ug·g ⁻¹	346	460
Fe, ug·g ⁻¹	10.2	20.4
Saturate wt%	50.4	35.3
Aromatic	22.2	25.6
Resin	27.2	38.3
n-C ₇ Insoluble	0.2	0.8



Note: P.E.---Petroleum Ether

Figure1 Separation of six subfractions in residue

RESULTS AND DISCUSSION

Change of Six Fraction Yields. From Table2, it is clear that the VGO and vacuum bottom residue yields of AR have been greatly changed after slurry-bed hydrocracking. Before reaction, VGO and VBR in Karamay atmospheric residue were 41.02%, 58.98% and after hydrocracking, they were 61.77%, 38.23%. When cracked atmospheric residue was recycled from slurry bed hydrocracking(recycling ratio 1:1), the decrease of VGO in AR and the increase of VBRs depended on different recycling times. The more recycling times were, the less yields of VGO were and the more yield of VBRs were. It shows that the recycled AR is the more refractory with the recycling times.

Tables 2 yields for different recycle times of VGO and vacuum bottom residue

	VGO(W/%)	VBR(W/%)
ABR	41.02	58.98
ABR#	61.77	38.23
First- recycled ABR	58.31	41.69
Second- recycled ABR	55.71	44.29
Third- recycled ABR	31.92	68.08

Tables 3 Subfractions yields for feed and different times recycled VBRs

	VBR	VBR#	First-VBR	Sec-VBR	Third-VBR
F1(W/%)	54.53	42.58	42.09	41.84	41.47
F2(W/%)	9.98	9.27	9.64	9.10	8.77
F3(W/%)	13.28	13.27	13.76	13.83	12.80
F4(W/%)	7.26	6.13	6.40	7.20	7.29
F5(W/%)	8.42	6.65	5.98	6.95	6.18
F6(W/%)	6.53	22.11	22.12	21.08	18.88
Coke(W/%)	0	1.80	2.45	2.89	4.57
F1+F2(W/%)	61.51	51.85	51.67	50.94	50.24
F3+F4+F5(W/%)	28.96	26.05	26.14	27.98	26.27

From Table3, it is clear that the yields of six sub fractions in fresh vacuum residue and residues from once-through operation and the recycling-operation have been changed, although F1+F2 (saturates and aromatics) was the main fraction of fresh VBR and hydrocracked VBRs. Among six sub fractions, F1 and F6 have considerably changed after slurry-bed hydrocracking. On the one hand, F1 in VBR decreased sharply, while F6 and coke increased sharply. On the other hand, with recycling-operation times increasing, the yields of six fractions in recycled VBRs have changed smooth. It is clear that the biggest change happened in the once-through hydrocracking operation. It is shown that it is in the first time hydrocracking process (the once-through hydrocracking process) that the cracking and condensation reaction of fresh feed was the most obvious in all processes. Although the increasing cracking yields could be achieved through recycling operation of cracked atmospheric residue, increasing degree of that was limited since cracking reaction of ABR had almost been finished. On the contrary, the degree of increasing of condensation reaction was very clear depended on the recycling-operation times.

H/C and average molecular weight of six fraction. From Table 4, H/C of six subfractions for feed and different times recycled VBR show different change. H/C of F1 hardly changed and the H/C of F2, F3, F4 and F5 decreased a little. However, H/C of F6 decreased sharply. Tables 5 give out the average molecular weight (VPO) of six subfractions for feed and different times recycled vacuum bottom residue. It is obvious that average molecular weight of all six subfractions decreased after once-through hydrocracking and different ABR recycling times hydrocracking. Among six subfractions, the decreasing trends of F6, F5 and F4 were very clear, especially for F6. It is shown that in the hydrocracking and different cracked ABR recycling hydrocracking, the moleculars of six subfractions have experienced different degree cracking reactions. On the other hand, the more complex molecular (F6, F5 and F4) have gone through the more considerable cracking reactions. In addition, the de-aggregation reaction of C₅-asphaltene can be important in the

hydrocracking based on the three-time sharp change of average molecular weight before and after once-through reaction.

Tables 4 H/C of fractions for feed and different times recycled VBRs

H/C	VBR	VBR#	First-VBR	Sec-VBR	Third-VBR
F1	1.76	1.75	1.72	1.73	1.76
F2	1.51	1.43	1.31	1.31	1.35
F3	1.49	1.27	1.16	1.17	1.19
F4	1.44	1.28	1.23	1.17	1.19
F5	1.41	1.43	1.34	1.32	1.28
F6	1.38	0.88	0.84	0.83	0.86

Tables 5 Average molecular weight (VPO) of fractions for VBR and different-time recycled VBRs

	VBR	VBR#	First-VBR	Sec-VBR	Third-VBR
F1	730	682	637	614	608
F2	880	718	549	518	550
F3	1160	871	781	708	704
F4	1485	988	894	695	699
F5	1484	791	733	798	909
F6	7879	2545	2247	2330	1684

Structural parameters of subfractions for VBR and different-time recycled VBRs. From Table 6-9, Structural parameters of fractions for VBR and different-time recycled VBR have different degree change in the once-through hydrocracking and recycled hydrocracking process. After once-through hydrocracking, structural parameters including Condensation Index, aromaticity, C_T, C_A, R_A, R_T of six fractions have changed greatly compared to the corresponding of feed. Then after ABR recycling hydrocracking, structural parameters of six fractions have changed smooth deepened on the recycling times and the changing trend show Condensation Index, aromaticity, C_T, C_A, R_A, R_T of six fractions have more change to a smooth limit while more recycling times go on. It is shown that the substantial chemical structure change happened in the first hydrocracking. For F₆, F₅ and F₄, the important change can be more obvious

CONCLUSION:

1. Saturates and aromatics were the main subfractions of fresh VBR and all hydrocracked VBRs
2. Structural parameters of six fractions after once-through hydrocracking have changed greatly compared to the corresponding of feed. It is shown that the substantial chemical structure change happened in the first-time hydrocracking.
3. Structural parameters of six fractions have changed smooth deepened on the recycling times. After different times recycling hydrocracking, the average molecular weights of six subfractions decrease and the content of saturates decreases obviously, while asphaltene and resins increase sharply, C/H, aromaticity and Condensation Index of the asphaltene increase.

REFERENCES:

- [1] Alberto Del Bianco, Nicoletta Panariti and Mario Marchionna, Upgrading heavy oil using slurry processes [J]. Chemtech, 1995, 25.(11):35-43
- [2] Wen Jie Liang Petroleum Chemistry [M]. Press of University of Petroleum (China), 1993

Tables 6 Structural parameters of fractions for VBR and different-time recycled VBRs

		F1	F2	F3	F4	F5	F6
VBR	Conden. Index	0.136	0.217	0.223	0.240	0.242	0.245
	C _T	47.0	63.7	84.4	107.0	104.7	528.6
	C _A	4.9	17.4	24.2	34.5	36.2	198.0
	R _T	4.2	7.9	10	14	14	65.8
	R _A	0.7	3.9	5.6	8.1	8.5	49.0
	R _N	3.5	4.0	4.8	5.5	5.1	16.8
VBR#	Conden. Index	0.140	0.242	0.281	0.278	0.229	0.360
	C _T	49.0	52.8	64.3	71.9	51.7	184.8
	C _A	5.6	17.6	28.6	31.8	17.4	141.1
	R _T	4.4	7.4	10.0	11.0	6.9	34.3
	R _A	0.9	3.9	6.7	7.4	3.8	34.8
	R _N	3.6	3.5	3.4	3.6	3.1	-0.5
First-times recycled VBR	Conden. Index	0.149	0.271	0.308	0.288	0.259	0.371
	C _T	46.0	40.5	57.9	64.7	50.7	166.5
	C _A	6.0	16.8	30.8	30.8	20.5	132
	R _T	4.4	6.5	9.9	10	7.6	31.9
	R _A	1.0	3.7	7.2	7.2	4.6	32.5
	R _N	3.4	2.8	2.7	3.1	2.9	-0.7
Second-times recycled VBR	Conden. Index	0.146	0.273	0.306	0.302	0.265	0.372
	C _T	44.4	38.2	52.6	50.32	56.0	172.3
	C _A	5.5	16.1	27.5	26.4	23.4	138.0
	R _T	4.2	6.2	9.0	8.6	8.4	33.0
	R _A	0.9	3.5	6.4	6.1	5.3	34.0
	R _N	3.4	2.7	2.7	2.5	3.1	-1.0
Third-times recycled VBR	Conden. Index	0.136	0.263	0.302	0.300	0.275	0.368
	C _T	43.7	40.6	52.3	51.1	64.3	125.1
	C _A	4.6	15.8	26.6	26.2	28.6	97.1
	R _T	4.0	6.3	8.9	8.7	9.8	24.0
	R _A	0.6	3.5	6.2	6.0	6.6	23.8
	R _N	3.3	2.9	2.7	2.6	3.2	0.2

Tables 7 Aromaticity of subfractions for VBR and different-time recycled VBRs

f _a (%)	VBR	VBR#	First-VBR	Sec-VBR	Third-VBR
F1	10.37	11.28	12.96	12.41	10.51
F2	27.33	33.34	41.5	42.12	38.97
F3	28.69	44.51	53.24	52.32	50.87
F4	32.19	44.19	47.7	52.6	51.23
F5	34.56	33.6	40.42	41.74	44.56
F6	37.45	76.36	79.34	80.13	77.61

Tables 8 R_T of subfractions for VBR and different-time recycled VBRs

R _T	VBR	VBR#	First-VBR	Sec-VBR	Third-VBR
F1	4.2	4.4	4.4	4.2	4.0
F2	7.9	7.4	6.5	6.2	6.3
F3	10.0	10.0	9.9	9.0	8.9
F4	14.0	11.0	10	8.6	8.7
F5	14.0	6.9	7.6	8.4	9.8
F6	65.8	34.3	31.9	33.0	24.0

Tables9 R_A of subfractions for VBR and different-time recycled VBRs

R _A	VBR	VBR#	First-VBR	Sec-VBR	Third-VBR
F1	0.7	0.9	1.0	0.9	0.6
F2	3.9	3.9	3.7	3.5	3.5
F3	5.6	6.7	7.2	6.4	6.2
F4	8.1	7.4	7.2	6.1	6.0
F5	8.5	3.8	4.6	5.3	6.6
F6	49.0	34.8	32.5	34.0	23.8

Appendix:

Density Method for calculating structural parameters of subfractions in residue is as follows:

- 1.Relative density: $D_4^{20}=1.4673-0.04.31 \times H\%$
- 2.Ratio of H/C atom: $H/C =11.92 \times H\%/C\%$
- 3.Mc/d: $Mc/d=Mc/(D_4^{20} \times C\%)$
- 4.Corrected Mc/d: $(Mc/d)_c= Mc/d-6.0(1- C \% - H\%)/ C \%$
- 5.Aromaticity in an average molecular: $fa=0.09(Mc/d)_c-1.15 H/C +0.77$
- 6.Condensation Index in an average molecular: $C.I=2-H/C-fa$
- 7.Total carbon atom in an average molecular: $C_T=(C \% \times M)/12.01$
- 8.Aromatic carbon atom in an average molecular: $C_a= C_T \times fa$
- 9.Total rings in an average molecular: $R_T=[C_a \times (C.I)/2]+1$
- 10.Aromatic rings in an average molecular: $R_A=(C_a -2)/4$
- 11.naphthenic rings in an average molecular: $R_N=R_T-R_A$

Note: M refers to average molecular weight

Hydrocracking of LiaoHe Vacuum Residue with Oil-Soluble Co-Ni Bimetallic Catalysts and Hydrogen Donor

Bin Shi* Guohe Que

State key laboratory of heavy oil processing University of Petroleum, Dongying, ShanDong, 257061, PRC
E-mail: shibin@hdpu.edu.cn

INTRODUCTION

The use of oil-soluble metal compounds to enhance the distillate yield and to reduce coke formation has been studied extensively in the hydrocracking of poor-quality heavy residue, which often have high contents of sulfur, nitrogen, metal, asphaltene and CCR (1). Such compounds are based on the transition metals, like Mo, Ni, Co, W, Cr, V, Fe, Cu, Zn and so on. It is clear and important that the corresponding metal sulfide, such as MoS₂, Ni₈S₉, CoS, Fe_{1-x}S and so on can be the activation catalysts in the slurry-bed hydrocracking of heavy oil (2). On the other hand, it is well known and of great industrial importance that the addition of a second transition metal Co or Ni to a binary sulfide such as MoS₂ or WS₂ can produce an enhancement of HDS activity (3). Some researchers also transplanted the promoters of Co, Ni or Fe into the dispersed Mo catalytic hydrocracking system of poor-quality heavy residue considering the addition of promoter can decrease the cost of the disposable catalysts and they found that Ni-Mo, Co-Mo and Fe-Mo show very clear enhancement of hydrocracking activity compared to monometallic dispersed catalyst (4-6). The reason is attributed to the better dispersion effect or synergism effect like the supported catalysts such as Mo-Ni (Fe)/Al₂O₃ in the slurry-phase hydrocracking system. As the promoters, we are very interested in the performance of bimetallic catalysts of Co and Ni in the hydrocracking system.

Hydrogen donor in petroleum chemistry can be classified into three kinds in a broad sense. That is the hydrogen donors can produce anionic hydrogen, radical hydrogen and molecular hydrogen, which include complex hydride (such as LiAlH₄ and NaBH₄), poly-ring hydroaromatics and gaseous hydrogen and water gas (CO+H₂+CO₂+H₂O). In a narrow sense, hydrogen donor indicates those poly-ring hydroaromatics that have incompact C-H bondage and the typical hydrogen donors are tetralin, dihydroanthracene and so on. Since these compounds can provide radical hydrogen reacted with hydrogen-acceptors, when heated together with them, thus hydrogen donors have often been applied into coal liquefaction, petroleum residue conversion, transportation fuel and other petroleum chemicals as hydrogen shuttle, hydrogen-transferer and radical scavenger based on their important roles (7).

In the paper we investigated and evaluated the application of bimetallic oil-soluble catalysts and the combination of bimetallic oil-soluble catalysts and hydrogen donors in the slurry-phase catalytic hydrocracking of LiaoHe vacuum residue.

EXPERIMENTAL

The naphthenic-base LiaoHe vacuum residue (LHVR) was upgraded and the main properties were reported in Table 1. The experiments were carried out in a 100ml FDW-01 magnetic-stirred autoclave and LiaoHe vacuum residue was upgraded with two kinds of oil-soluble monometallic catalysts cobalt naphthenic and nickel naphthenic as hydrocracking dispersed catalyst, and tetralin (THN) as hydrogen donor. The experimental procedure was as follows: 34g residue blended with 200μg/g Co-naph or Ni-naph or their mixture

of the Co-naph and Ni-naph and 3.4g tetralin (THN) was placed in the autoclave, pressurized hydrogen to 7.0Mpa, heated to reaction temperature 436 °C and then maintain it smoothly. The autoclave was cooled with water quickly when defined reaction time 1h was achieved. After reaction, the products were recovered with toluene. The toluene-insoluble (TI or coke) was separated from the reaction product by centrifugation. The toluene-soluble was treated to remove toluene and the products were distilled into AGO (160~350 °C), VGO (350 ~450°C) and reacted residue (>450°C). The amounts of naphthalene and tetrahydronaphthalene were analysed by GC.

RESULTS AND DISCUSSION

Comparison of hydrothermal, catalytic hydrocracking system and hydrothermal system with hydrogen donors. In order to make a comparison of catalytic activities between the Ni-based oil-soluble monometallic catalyst and Co-based oil-soluble monometallic catalyst used in LiaoHe vacuum residue hydrocracking processes, the same concentrations of these two kinds of catalysts were separately used in the hydrocracking experiments, while the hydrothermal and hydrothermal in the presence of 10%wt tetralin based on feed were also conducted as comparison, the results are listed in Table 2. Both of the monometallic catalysts and tetralin could suppress coke formation and cracking reactions in comparison with hydrothermal cracking system without adding catalysts and H-donor and the effects of the two oil-soluble catalysts were more clear than that of tetralin. However, the Co-based oil-soluble catalyst gave lower total conversion yield than the Ni-based oil-soluble catalyst did. The former produced higher conversion per unit coke than the latter did. The conversion per unit coke was 23.60% for the Co-based oil-soluble catalyst, 18.02% for Ni-based oil-soluble catalyst and 9.11% for tetralin, 6.66% for hydrothermal cracking.

Table 1 Composition and properties of LHVR

Molecular weight, (VPO)	870	V, μg/g	2.9
Density/g/cm ³ (20°C)	0.9976	Ni, μg/g	123
Saturates	17.4	C, m%	86.9
Aromatics	30.3	H, m%	11.0
Resins	50.2	N, μg/g	10800
C ₇ -asphaltene	2.1	S, μg/g	4300
Total metal content, μg/g	259	CCR, %	14.4

Catalytic hydrocracking of LHVR by using oil-soluble Ni- Co bimetallic catalysts. As shown in Table 3, the combined employment of Ni-based oil-soluble catalyst and Co-based oil-soluble catalyst seems to produce slight synergetic effect on the coke inhibition. With 200μg/g Co-based oil-soluble catalyst and 200 μg/g Ni-based oil-soluble catalyst, the coke yield was 2.39% and 3.34%, respectively; and conversion was 56.40% and 60.21%, respectively. With 100 μg/g Co and 100 μg/g Ni bimetallic catalysts, the coke yield and conversion were 2.71% and 59.00%, which were nearly simple mathematical addition of corresponding yields.

As the promoters of a second transition metal Co or Ni to a binary sulfide such as MoS₂ or WS₂ of HDS catalyst, the addition of the promoters can produce a great enhancement of HDS(3). As the promoters of Co, Ni or Fe in the dispersed Mo catalytic hydrocracking system of residue, the improvement is also considerable(4-6). But the combination effect between Ni and Co was very slight so that it is reasonable that the combination of Ni-Co oil-soluble bimetallic catalysts could produce simple

mathematical addition effect on the coke inhibition, residue conversion and conversion per unit coke in the upgrading residue, which was different from the clear and traditional synergism between Mo and Co or Mo and Ni in the HDS systems.

Catalytic hydrocracking of LHVR by using oil-soluble Ni-Co bimetallic catalysts and Tetralin. The authors have studied the synergism between hydrogen donors and Mo, Ni, Co and Fe dispersed monometallic catalysts in the literature (8,9). The activities of the four pure oil-soluble catalysts were improved based on conversion per unit coke, especially the activity of Mo gave a large leap with a combination with tetralin, however the order of catalyst activities did not change. The combination of monometallic catalysts and tetralin could effectively inhibit coke formation and yield a good upgrading of LHVR (8,9).

The upgrading results of catalytic hydrocracking of LHVR with oil-soluble Ni-Co bimetallic catalysts and tetralin were listed in Table 4, in which the upgrading results with pure Ni-Co bimetallic catalysts or pure tetralin were also listed as comparison. Table 4 shows more coke generated in the cracking of residue with pure H-donor or pure dispersed Ni-Co bimetallic catalysts. However, H-donor combined with dispersed bimetallic catalyst could improve upgrading results of LHVR than with pure H-donor or pure Ni-Co bimetallic catalysts. The synergism between hydrogen donor and dispersed Ni-Co bimetallic catalyst in hydrocracking conversion of LHVR was the same clear as that between dispersed monometallic catalysts and H-donors according to the value of conversion per unit coke. It is clear that synergism between hydrogen donor and dispersed Ni-Co bimetallic catalysts was important to upgrading of heavy residue.

CONCLUSION

1. Compared with hydrothermal cracking, the addition of dispersed monometallic catalysts or hydrogen donor can improve upgrading of vacuum residue.

2. The combination of Ni-Co oil-soluble bimetallic catalysts produces simple mathematical addition effect on the coke inhibition and residue conversion in the upgrading residue, which was different from the clear and traditional synergism Mo and Co or Mo and Ni in the HDS systems.

3. It is clear that there is synergism between dispersed Ni-Co bimetallic catalyst and hydrogen donor in LHVR cracking conversion and the synergism helped to effectively inhibit coke

Acknowledgment. The authors thank Mr. Bin Huang for his helpful and laborative experimental work.

REFERENCES:

1. Alberto Del Bianco and Nicoleta Panariti. Thermocatalytic hydro conversion of heavy petroleum cuts with dispersed catalyst [J] Appl.Catal, 1993,(94):1-16
2. Chengguang Liu. Hydrocracking of Gudao vacuum residue in the presence of dispersed catalysts [D] University of petroleum: 1991
3. Petroleum Chemistry [M] edited by WenJie Liang. Press of University of Petroleum (China), 1993
4. Ruihua Sheng Hydrocracking of LHVR with bimetallic oil-soluble catalysts [D] University of petroleum: 1997.
5. Zongxian Wang, Hongyu Zhang, Aijun Guo, Guohe Que Catalytic hydrocracking of petroleum vacuum residue by using a combination of molybdenum based oil-soluble and iron-based water-soluble catalysts Preprints, Div. Fuel Chem. ACS. 1998.43. (2). 486-489..
6. Pradhan V.R., Herrick D.E., Tierney J.W. et al. Finely dispersed iron, iron-molybdenum and sulfated iron oxides as catalysts for coprocessing reactions [J] Energy & Fuels, 1991, 5: 712
7. Bin Shi, Guohe Que. Hydrogen Donor (personal communication to Dr.Oona Schmid and Dr.J.G.Speight).
8. Bin Shi, Guohe Que Effects of additives and H-donors on catalytic hydrocracking of residue Preprints American Chemistry Society Petroleum Division. 2002.47(2). 113-116
9. Bin Shi, D.L.Lin, L.Q.Wang, G.H.Que. Synergism between hydrogen donors and dispersed catalysts in LHVR hydrocracking. Preprints American Chemistry Society Petroleum Division. 2001.46.(4).325-328

Table 2 Hydrocracking of LHVR with oil-soluble monometallic catalysts or tetralin

Reaction system	Product distribution /wt%				Conversion wt%	Conversion per unit coke
	<350°C	350-450°C	>450°C	coke		
Blank	45.77	19.43	25.61	9.79	65.20	6.66
THN (10%wt)	41.54	22.36	29.06	7.02	63.92	9.11
Ninaph (200µg/g)	35.25	25.96	35.45	3.34	60.21	18.02
Conaph (200µg/g)	26.70	29.70	41.21	2.39	56.40	23.60

Table 3 Catalytic hydrocracking of LHVR by using oil-soluble Ni-Co bimetallic catalysts

Catalysts, µg/g		Product distribution/wt%				Conversion wt%	Conversion per unit coke
Conaph	Ninaph	<350°C	350-450°C	>450°C	coke		
200	0	26.70	29.70	41.21	2.39	56.40	23.60
180	20	28.36	28.94	40.50	2.40	57.30	23.87
160	40	30.95	27.25	39.29	2.51	58.20	23.19
100	100	32.80	26.21	38.09	2.71	59.00	22.60
40	160	33.18	26.32	37.51	2.99	59.50	19.90
0	200	35.25	25.96	35.45	3.34	60.21	18.02

Table 4 Catalytic hydrocracking of LHVR by using oil-soluble Ni-Co bimetallic catalysts and tetralin

Catalysts, µg/g		Tetralin	Coke /wt%	Conversion /wt%	Conversion per unit coke	Donating yield of tetralin /wt%
Conaph	Ninaph					
0	0	0	9.79	65.20	6.66	---
		10	7.02	63.92	9.11	84.23
200	0	0	2.39	56.40	23.60	--
		10	1.39	54.98	39.55	25.32
160	40	0	2.51	58.20	23.19	--
		10	1.59	56.00	35.22	27.10
100	100	0	2.61	59.00	22.61	--
		10	1.73	57.42	33.19	29.33
40	160	0	2.99	59.50	19.90	--
		10	1.93	57.91	30.00	32.00
0	200	0	3.34	61.21	18.33	--
		10	2.29	59.35	25.92	34.86